THE UNIVERSITY
of EDINBURGH

Investigating the spatiotemporal dynamics and fate decisions of axial progenitors and the potential of their in vitro counterparts

THE UNIVERSITY *of* EDINBURGH

Yali Huang

Thesis submitted in fulfilment of requirements for the degree of Doctor of Philosophy

Institute for Stem Cell Research, MRC Centre for Regenerative Medicine, School of Biological Sciences, University of Edinburgh

October 2014

Acknowledgments

I would like to express my sincere gratitude to my supervisor, Prof Val Wilson, for her continuous guidance and support during the whole study. I really appreciate that she accepted me as her student and taught me everything from the very beginning of my study. I would also like to thank my PhD committee: Dr. Sally Lowell and Dr. Tilo Kunath for their encouragement and suggestions.

I would like to extend my appreciation to Anestis Tsakiridis who continuously provided cells for my study and inspired me with his passion for science. I am also very grateful for all the help from Ron Wilkie and his company throughout my PhD. Also, I would like to give a big thank you to all the other members of Val's lab: Filip Wymeersch, Frederick Wong, Eleni Karagianni, Amy Pegg and Julia Watson. I thank them for providing such a good studying atmosphere and valuable suggestions in my projects.

Special thanks to Suling Zhao, Valeria Berno and all the staff in the animal unit. My experiments would have not been possible without them. I also really appreciate the help and advices from Guillaume Blin and all the people who attend the developmental group meeting. Big thanks to all my friends in the SCRM for their continuous support and friendship. I am also very grateful to Abcam for supplying antibodies.

A special thank and love goes to my family, especially my mother, for their abiding love and support throughout my life. I would also like to thank my old friends in China for answering those late night phone calls and their encouraging words.

致谢

最要感谢的是我的父母，感谢他们对我无限的爱和支持。也谢谢所有的亲人从小到大对我的陪伴和帮助。感谢所有的好朋友，不可能提到所有人的名字但如果你觉得我烦，那说的就是你咯。谢谢美琴表姐，从小到大都对我很好。谢谢锦培，从高中开始在你面前我一直表现的最差，我很开心。谢谢小肠，便便，高大妈还有韩洁，无聊的时候我最经常去看我的群，无论在哪都希望大家过的开心。非常感谢在厦大器官移植研究所的时光和那里认识的老师同学。也感谢在爱丁堡认识的所有朋友，特别是静静姐在我连菜刀都不怎么会拿的时候每天给我做饭，还有室友孙超，经常帮我买菜的KIMI，一起吃火锅的姐夫和经常陪我聊天的张晖…….还有那些无数个深夜还被我骚扰的朋友。

Abstract

Elongation of the mouse anteroposterior axis depends on stem cell-like axial progenitors including a neuromesodermal (NM) bi-fated population existing in the primitive streak and later in the tail bud. Fate mapping experiments have demonstrated these NM progenitors reside in precise locations of the embryo. At E8.5, these cells are found in the node-streak border (NSB) and anterior epiblast on either side of the primitive streak. At tail bud stages (E10.5-E13.5), these progenitors reside in the chordoneural hinge (CNH). The coexpression of the transcription factors T (brachyury) and Sox2 has been proposed as a good marker to identify NM progenitors in vertebrates. However, this cell signature has never been thoroughly assessed during mouse axis elongation.

In this thesis, I performed T and Sox2 double immunofluorescent stainings on different stages of mouse embryos and reconstructed their expression domains in the 3D images to investigate the spatiotemporal dynamics of NM progenitors during axis elongation. The results show the transient existence of $T^{+}Sox2^{+}$ cells in the posterior progenitor zone, from the headfold stage (E8.0) to the end of axis elongation (E13.5, 65somites). Moreover, the number of $T^{+}Sox2^{+}$ cells increases between E8.5 and E9.5 but gradually declines afterwards. I then investigated the time points for initiation and loss of NM progenitors by performing a series of heterotopic grafting experiments. It has been previously shown that distal epiblast ($Sox2^{+}T^{-}$ cells) at LS-EB stages (E7.5) are fated to become NSB cells in E8.5 embryos. However, when cells from the distal region of LS-EB stage embryos (E7.5) were grafted to E8.5 NSB, these cells contribute extensity to the notochord but not either neural tissues or paraxial mesoderm. This indicates that NM progenitors may be not yet specified before the onset of T and Sox2 coexpression, while the notochord progenitors are already specified at E7.5. The grafting experiments also show the loss of NM progenitors at E14.5 after the end of axis elongation, which coincides with the disappearance of $T^{+}Sox2^{+}$ cells in the tail. Collectively, these results indicate that $T^{+}Sox2^{+}$ cells may represent a distinct cell state that defines NM progenitors.

Wnt/β-catenin signalling has been shown to play an important role in maintaining the posterior progenitor zone. However, due to the wide expression of β-catenin and the early lethality of β-catenin null embryos, the exact effect of losing β-catenin in NM progenitors is still unknown. In this study, I took advantage of the Cre-ER^{T2} system and grafting technique to conditionally delete β-catenin specifically in NM progenitors during ex vivo culture. The results show that Wnt/β-catenin signalling is required cell autonomously for initiating

mesoderm fate choice in NM progenitors. In its absence, mesoderm fated NM progenitors convert their fate and differentiate to neural derivatives. Moreover, the interchangeability between neural and mesodermal fate only exists in NM progenitors, as the loss of β-catenin in mesoderm committed progenitors does not affect their fate choice. Using image analysis and quantification software, I also show that Wnt/β-catenin signalling is crucial for the expansion of $T^{+}Sox2^{+}$ NM progenitors during axis elongation.

Due to difficult access and a limited number of NM progenitors in vivo, in vitro generated NM progenitors from pluripotent cells, such as epiblast stem cells (EpiSCs), can offer an insight into the maintenance and differentiation of NM progenitors. Since the in vivo potential of EpiSCs had never been successfully demonstrated before, I first grafted EpiSCs into postimplantation embryos and cultured them ex vivo for 24-48 hours to assess their cell integration. The results show that EpiSCs can integrate successfully in streak stage embryos (E6.5-E7.5), but not at early somite stages (E8.5), when the epiblast has lost its pluripotency. I then further investigated the in vivo potential of EpiSC derivatives. The results show that increasing Wnt signalling in EpiSCs inhibits their ability to generate anterior neural tissues in vivo, which is consistent with the previous in vitro data. Recently, it has been demonstrated that NM progenitors can be derived from EpiSCs. These in vitro derived NM progenitors can incorporate into E8.5 embryos and give rise to both neural and mesodermal derivatives. In this thesis, I show that these in vitro derived NM progenitors do not incorporate successfully in E7.5 embryos. Collectively, by combining grafting experiments with a chimeric embryo formation assay, I can identify the in vivo stage of the in vitro counterparts of the embryonic cell types.

Table of contents

List of Figures

Chapter 1

Chapter 2

Chapter 3

Chapter 4

Chapter 6

List of Tables

Abbreviations

4-OHT	4-hydroxytamoxifen
	A
AP	Anteroposterior
	B
Bra	Brachyury
BSA	Bovine serum albumin
β-catCKO	*β-catenin* conditional knockout reporter embryo
	C
CNH	Chordoneural hinge
CLE	Caudal lateral epiblast
CHI	CHIRON99021
	D
D	Distal
DAPI	4',6-diamidino-2-phenylindole
DV	Dorsoventral
	E
E	Embryonic day
EB	Early allantoic bud
EMT	Epithelial-to-mesenchymal transition
EpiSCs	Epiblast stem cells
ESCs	Embryonic stem cells
ES	Early-streak stage

F

FGF	Fibroblast growth factor

G

GFP	Green fluorescent protein

H

HH	Hamburger Hamilton Stages
H	Hours

I

ICM	Inner cell mass

K

KOSR	Knockout Serum Replacement

L

L	Caudal lateral epiblast
LVM	Lateral ventral mesoderm
LS	Late-streak
Lef	Lymphoid enhancer-binding factor

M

MA:	Mid-anterior
ME	Mesoendoderm
MP	Mid-posterior
MS	Mid-streak

N

NM	NMP

NSB	Neuromesodermal progenitors
Neuromesodermal	Node-streak border

O

OB	No allantoic bud

P

PGCs	Primordial germ cells
PFA	Paraformaldehyde
PSM	Presomitic mesoderm
PXM	Paraxial mesoderm
PP	Proximal-posterior
PS	Primitive streak or Pre-streak

R

RT	Room temperature

S

sGFP	silent GFP

T

TBM	Tail bud mesoderm
TSA	Tyramide Signal Amplification
TF	Transcription factor
Tcf	T cell-specific transcription factor

V

VT	Vestigial tail

W

WT	Wild type

Chapter 1. Introduction

Summary of early mouse embryo development

After fertilization, the zygote undergoes serial cell division. Before compaction, each cell in the 8-cell stage embryo is totipotent (i.e. able to give rise to all embryonic and extraembryonic cell types). During the blastocyst stage on embryonic days (E)2.5-4.5, the embryo starts to form two distinct cell types: the inner cell mass (ICM) and the trophoblast in the outer layer. The ICM gives rise to the whole foetus, while the trophoblast only contributes to the placenta. At E4.5, the ICM segregates into two lineages: epiblast and primitive endoderm (reviewed in (Gardner, 1998). Implantation occurs at E5.0, after which the morphology of mouse embryos changes dramatically forming a cylindrical shape named egg cylinder. After implantation at E5.5, the embryonic part of the egg cylinder consists of two germ layers: the epiblast and primitive endoderm (Figure 1.1A). The epiblast, a columnar epithelium, is the sole source of all foetal tissues and also contributes to amnion ectoderm and all extraembryonic mesoderm. Primitive endoderm, squamous in shape, gives rise to the extraembryonic endoderm: the visceral and parietal yolk sacs (reviewed in (Lu et al., 2001).

By E6.5, gastrulation starts with the manifestation of the primitive streak (PS), which marks the posterior side of the embryo (Figure 1.1B). During gastrulation, the epiblast cells migrate into the primitive streak, undergo an epithelial-to-mesenchymal transition (EMT) and move away to form mesoderm and definitive endoderm. Cells remaining in the anterior epiblast become ectoderm (Figure 1.1C). A detailed fate map of streak stage embryos (E6.5-E7.5) epiblast has been extensively reviewed by (Kinder et al., 1999; Lu et al., 2001; Tam and Behringer, 1997). At the headfold stage (E8.0), the precursors of broad domains in the anterior part of the embryo have been established. Cells that give rise to the trunk and tail including the posterior nervous system are localised in the primitive streak region.

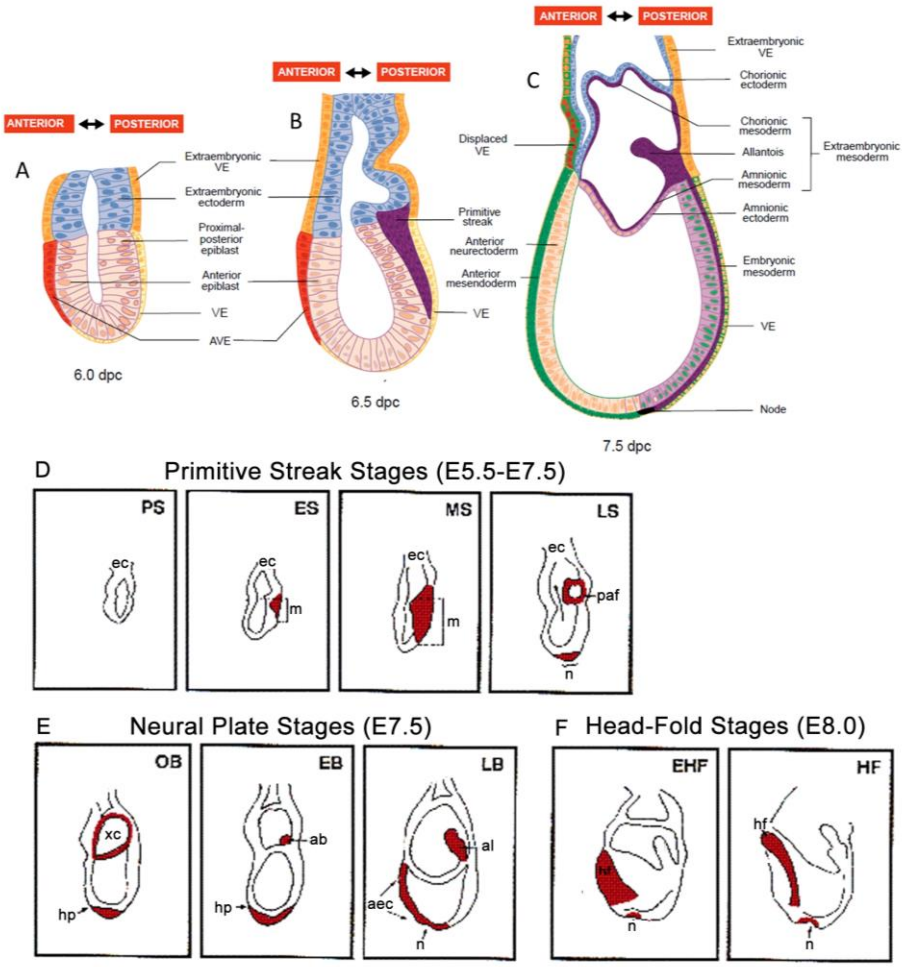

Figure 1. 1 . Morphology of mouse egg cylinder from E5.5 to E8.0

(A-C) Detailed structure of the egg cylinder. (A) After implantation and before gastrulation; (B) mid-streak stage; (C) early bud stage.

(D-F) Staging of gastrulating mouse embryos. Schematic drawings showing morphological landmarks (in red) of gastrulation. (D) Primitive streak stages: Pre-Streak (PS); early-streak (ES); mid-streak (MS) and late-streak (LS). (E) Neural plate stages: no bud (OB); early bud (EB) and late bud (LB). (F) Head-fold stages: early headfold (EHF) and head fold (HF)

Abbreviation: dpc, days post coitum; VE, visceral endoderm; m: embryonic mesoderm; ec: ectoplacental cone; paf, posterior amniotic fold; n: node; xc: exocoelomic cavity; ab: allantoic bud; al: allantois; aec:anterior neurectoderm; hf: headfold; hp: head process.

Images A-C are reprints from Lu et al.,2001; Images D-F are reprints Downs and Davies, 1993

Somite formation and axis elongation

After gastrulation, the longitudinal elongation of the body axis is evident by the increasing number of paired segmental structures called somites. Somites are blocks of mesoderm containing the precursors of vertebrae, cartilage, muscles and dermis. In mice, somites bud off periodically from the anterior end of the presomitic mesoderm (PSM) from E8.0 to E13.5 (Christ et al., 2007). The period when embryos form somites is called somitogenesis. Fate maps have shown that somites are derived from the primitive streak, and later, from the tail bud (Tam, 1986, 1988; Tam and Tan, 1992). The total number of somites is precisely defined for any given species but varies widely from one species to another. For example, mouse embryos have 65 somites and human embryos have 33 somites (Richardson et al., 1998). The termination of somite formation indicates the cessation of axis elongation. Figure 1.2 shows some critical time points during early mouse embryo development, as well as their approximate equivalents in chick.

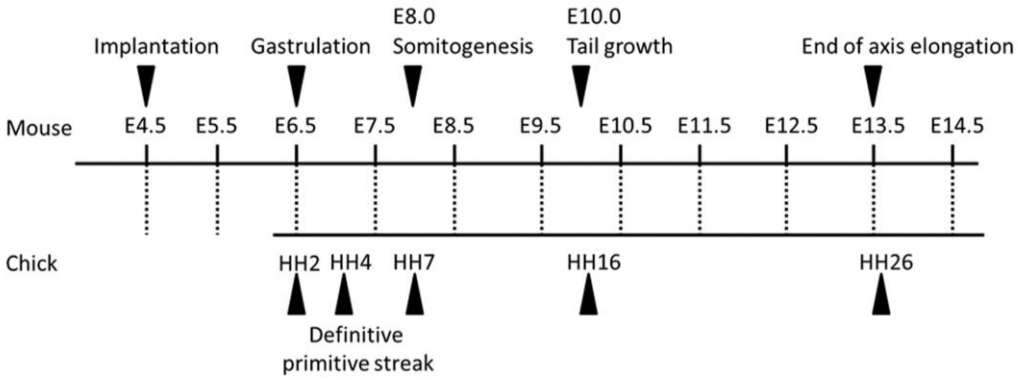

Figure 1. 2 Critical time points during early mouse and chick embryo development mentioned in this thesis.

Abbreviation: E, embryonic days ; HH, Hamburger and Hamilton

In mice, axis elongation was traditionally divided into phases: primary (primitive streak stage) and secondary body formation (tail bud stage). The transition of these two phases is marked by the closure of the posterior neuropore at the 35 somite stage (E10.5), when the primitive streak is replaced by another transient structure named the tail bud in the posterior (Tam and Tan, 1992). However, in current opinion these two phases are considered as a continuum of the same process, because (1) genes known to be important during gastrulation are continuously expressed in the tail bud (Cambray and Wilson, 2007); (2) fate mapping shows that the node and the anterior primitive streak are the precursors of the tail bud (Wilson and Beddington, 1996); (3) chordoneural hinge (CNH) cells in the tail bud are able to incorporate and contribute to the neural tube and mesoderm when grafted into the primitive streak, indicating the developmental equivalence between these two structures (Cambray and Wilson, 2002; McGrew et al., 2008). This will be further discussed below.

Node and notochord in mouse embryos

In mouse embryos, the node is first clearly visualized as a rosette of cells in the distal tip of the egg cylinder at the late bud stage (E7.5) (Figure 1.3B). Later, cells in the node region form a distinctive pit, which is a landmark indicating the most anterior extent of the primitive steak. (Figure 1.3E-G). This prominent morphology persists until the 7-somite stage (late E8.5) before the hindgut extends underneath the primitive streak (Jurand, 1974; Sulik et al., 1994). Upon closer examination, there are two cell layers in the node with distinct morphologies: the dorsal node composed of columnar epithelium and the ventral node containing a small rosette of monociliated cells (Figure 1.3B-D). The two layers of the node are separated by a basement membrane except in the most posterior part where the node is adjacent to the primitive streak (Figure 1.3C-D) (Bellomo et al., 1996; Poelmann, 1981). Besides morphology differences, the proliferation rate is also different in the node between these two layers. Cells in the dorsal node are highly proliferative with a similar cell division rate as that in their contiguous neurectoderm (Figure 1.3D). However, the majority of cells in the ventral node are quiescent until E8.5 (Figure 1.3D) (Bellomo et al., 1996; Ukita et al., 2009). Collectively, these observations suggest that dorsal and ventral node cells are two different populations.

Cell lineage studies also indicate that dorsal and ventral node cells are differently fated. During late-streak to bud stage (E7.5) (Figure 1.1D, E), if only the ventral node was labelled at the same stage, the majority of the fluorescent cells were mainly observed in the

notochord along the axis with some in the foregut after 24 hours in culture (Beddington, 1994). Therefore, it is indicated that ventral node cells are the notochord progenitors. The notochord, also called axial mesoderm, is inserted in the endoderm layer at headfold and early somite stages (E8.0-E8.5), and later forms a slender cylindrical structure between the neural tube and the gut during axis elongation (Jurand, 1974). It is an important structure for the patterning of early embryos, because the notochord produces secreted factors which provide position and fate information to the surrounding tissues (Yamada et al., 1993; Yamada et al., 1991). Although the cylindrical structure starts to deform at E14.5 (Jurand, 1974), lineage tracing experiments show that notochord cells differentiate to the nucleus pulposus of the intervertebral disc in later stages (McCann et al., 2012). When both dorsal and ventral layers of the node were labelled with Dil, their descendants were later detected in the notochord, neural tube and the endoderm (Sulik et al., 1994). Since the ventral node cells contribute extensively to the notochord (Beddington, 1994) and the ventral and dorsal node are likely to represent two different populations as discussed previously, it is highly possible that dorsal node cells are mainly fated to be neuroectoderm. The reason that the labelled cells were also found in the endoderm may be due to accidentally labelling the endoderm fated crown cells surrounding the node (Sulik et al., 1994).

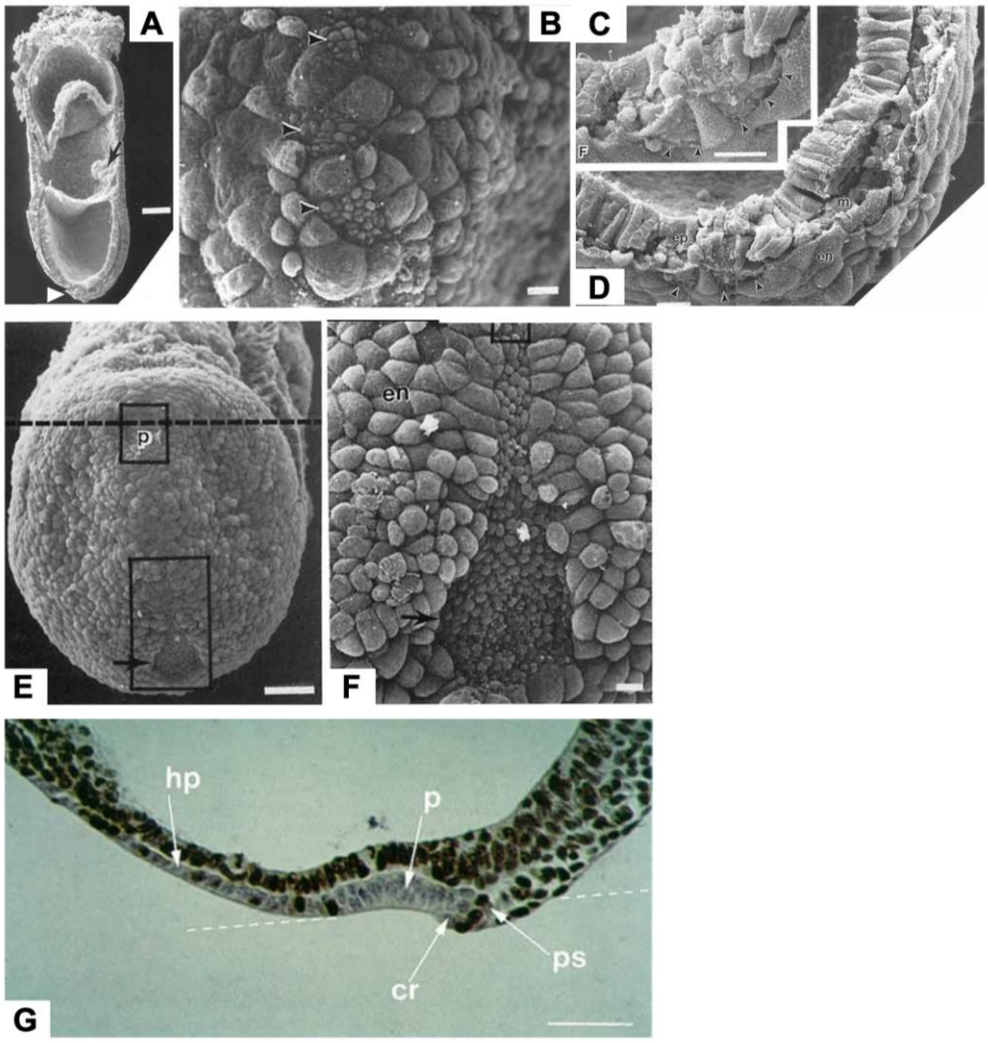

Figure 1.3. Two layers of cells in the node in early mouse embryos (E7.5-E8.0)

(A) Electron microscopy image of an early bud stage embryo (E7.5). Allantois is indicated by the black arrow. The node is indicated by the white arrowhead. (B) Distal view of the embryo shown in A. Small rosette of ventral node cells indicated by the black arrowheads. (C) Higher magnification showing the morphology of the node in specimen A. (D) An enlargement of the central portion of C. The ventral node cells are indicated by the black arrowhead.

(E, F) Distal view of a headfold stage embryo (E8.0) under electron microscopy. Cells comprising the anterior prechordal plate (p) are shown in the small upper box. The ventral node (arrows) is shown in the lower box. (F) An enlargement of lower box in E showing the ventral side of the node.

(G) A mid-sagittal section of the node area in a headfold stage embryo (E8.0). The embryo was cultured with BrdU for 4 hours. Proliferating cells are shown in brown, whereas, non-proliferating cells are shown in blue.

Abbreviation: p, prechordal plate; en, endoderm. ep, epiblast; m, mesoderm; en, endoderm; cr, crown; hp, head process; p, pit; ps, primitive streak. Bar = 100 p.m (A); bar=10µm (B-D and F); bar=50µm (E); bar = 50 pn (G).

Images A-F are reprints from Sulik et al., 1994; Image G is a reprint from Bellomo et al., 1996.

Functions of node and notochord in mice

The organizer is considered to act as a source of signals that induces the patterning of the body axis including anterior-posterior, dorsal-ventral and left-right patterning. It was first discovered in amphibians. When the dorsal lip of the blastopore was transplanted into the ventral margin of the blastopore, it induced the host tissue to form a secondary body axis (Spemann and Mangold, 1924). In mice, the node is considered as an organizer. As seen in the original amphibian experiment, the node tissue (at late-streak to no bud stage, E7.5) grafted to the posterior lateral mesoderm in a stage matched embryo was able to induce adjacent host tissue to form a secondary axis containing neural tube and somites. The grafted node itself predominantly contributed to notochord and endoderm tissues in this secondary axis (Beddington, 1994). Interestingly, grafting only the dorsal layer of the node from the same stage embryos to either anterior or posterior part of embryos could not induce a secondary axis formation (Beddington, 1982). Therefore, these two studies show the indispensable role of the ventral node in organizing axis formation. Also, it appears that the organizing properties of the node either require the ventral layer itself, or the structural integrity of both layers in the node.

Foxa2 is expressed in the node, notochord, floor plate and endoderm in early embryos (Ang and Rossant, 1994; Ruiz i Altaba et al., 1993; Sasaki and Hogan, 1993). Homozygous mutations are lethal and lack a definitive node and notochord. Although *Foxa2*$^{-/-}$ embryos show a rudimentary body axis, the primitive streak is highly truncated. Dorsoventral (DV) patterning of the neural tube is also severely affected (Ang and Rossant, 1994). Their phenotypes indicate that the node and notochord are indispensable for axis elongation and DV patterning of the neural tube but may not be critical for initiating an AP axis.

Noto expression initiates in the node at E7.5 and persists in the posterior notochord until E12.5. *Noto*$^{-/-}$ mutants show vertebral column defects and various sacral and tail truncations, indicating the importance of posterior notochord for axis elongation (Abdelkhalek et al., 2004). It is also known that Wnt/β-catenin signalling is highly activated in the notochord (Galceran et al., 1999; Kelly et al., 2004; Takada et al., 1994). Deletion of β-catenin in Noto expressing cells results in the truncation of posterior notochord and body axis after the lumbar region or the first sacral vertebra (Ukita et al., 2009). This result shows that Wnt/β-catenin is required cell autonomously for posterior notochord extension. Collectively, these studies show that the integrity of the node and notochord is indispensable for axis elongation.

Lim1 is first expressed exclusively in the visceral endoderm before gastrulation (E5.5). During early gastrulation (E6.5-E7.5), it is expressed in the anterior visceral endoderm, primitive streak and mesoderm wings. At E8.0, the transcripts are also detected in a horseshoe-shaped pattern surrounding the node (Barnes et al., 1994; Perea-Gomez et al., 1999). *Lim1*$^{-/-}$ embryos lack anterior head structures (Shawlot and Behringer, 1995). *Lim1*$^{-/-}$ /Foxa2$^{-/-}$ double mutants show severe defects in anterior primitive streak specification and mesoderm patterning (Perea-Gomez et al., 1999).

The node also plays a critical role in the left-right patterning. *Nodal* is expressed in the ventral node at E7.5. At E8.5, it is expressed in both the node and left lateral plate mesoderm (Norris et al., 2002). Conditional removal of Nodal activity in the node disrupts asymmetry gene expression in the left versus right lateral plate mesoderm, indicating morphogens secreted by the node have long range effects on early embryonic patterning (Brennan et al., 2002).

Axis progenitors in the posterior domain

Conventional fate mapping depends on prospective lineage tracing experiments, for example dye labelling and grafting experiments. In these methods, cells in a defined region are labelled and their descendants can be traced by a genetic or fluorescent marker. Another approach for lineage tracing is retrospective clonal analysis, in which the progenitors of a group of cells are inferred by studying the descendants of clonal events that occurred at an earlier time. One example of this approach relies on a rare recombination event to recreate a functional *LacZ* gene from its inactive form (where a truncated protein is encoded due to a duplicated sequence in *LacZ*), the *LaacZ* gene (Bonnerot and Nicolas, 1993). The *LacZ* gene encodes an enzyme called β-galactosidase which can cleave the artificial substrate X-gal (5-bromo-4-chloro-3-indolyl-β-D-galactopyranoside) and convert it to an insoluble blue precipitate (Miller, 1992). Therefore, the descendants of recombined cells can be identified by X-gal staining. The downside of this approach is that because the appearance of recombined *LacZ* cells is random, by itself, it cannot identify the location of the first LacZ expressing cells in the embryos. In fact, this requires information gathered from prospective lineage studies. However, since the frequency of recombination is extremely low, this method allows analysis of the distribution of progeny from a single recombined cell (Tzouanacou et al., 2009). This makes it a powerful tool for *in vivo* lineage tracing. It can

also be used to study the involvement of stem cells in different tissue formation if the *LaacZ* gene is applied under a tissue specific promoter (reviewed in (Petit et al., 2005).

When *LaacZ* is placed under the control of a myotome-specific promoter, the α subunit of the acetylcholine receptor (αAChR), some $LacZ^+$ clones show a long AP dispersal with variable anterior limits but extend as far as the posterior end of the myotome. This pattern fits the profile of clones which are derived from stem-cell like progenitors in the posterior region of embryos (Figure 1.4 A). Although the accurate locations of the precursors of these clones are unknown, it is possible to predict their approximate locations according to their contribution. Grafting experiments have shown that somites are derived from the primitive streak, and later, from the tail bud (Tam, 1986, 1988; Tam and Beddington, 1987; Tam and Tan, 1992). Since these myotome progenitors contribute bilaterally to somites along the axis, they must have persisted in the primitive streak. Moreover, some $LacZ^+$ cells are present in the very anterior somites, suggesting their precursors are already located in the primitive streak in early developmental stages (i.e. E7.5 and/or the anterior primitive streak at E8.5) (Nicolas et al., 1996).

A similar clonal analysis using a neural promoter shows that some long spinal cord clones also extend as far as the posterior end of the neural tube (Roszko et al., 2007). The distribution of $LacZ^+$ cells in these clones also fits the profiles of clones derived from stem cell-like progenitors in the posterior region of embryos. A map of prospective ectodermal tissues conducted on bud stage embryos (E7.5-E8.0) shows that neural progenitors are located in the anterior part of the caudal lateral epiblast (CLE) (Tam, 1989). Another fate map of the subregions in E8.5 embryos shows that cells in the posterior node adjacent to the primitive streak contribute to the neural tube all along the axis until the tail bud (Wilson and Beddington, 1996). Moreover, when chordoneural hinge cells from E10.5 tail bud were grafted to E8.5 embryos, they were able to contribute to the neural tube. Taken together, these results indicate that there are stem cell-like neural progenitors which are present in the anterior of the primitive streak and later in the tail bud.

Collectively, the results from fate mapping experiments and retrospective clonal analysis indicate the existence of stem cell-like myotome and spinal cord progenitors located in the posterior progenitor zone (i.e. the primitive streak, and later, the tail bud). Since these stem cell-like progenitors contribute to axis elongation, they are also named axial progenitors (reviewed in (Wilson et al., 2009).

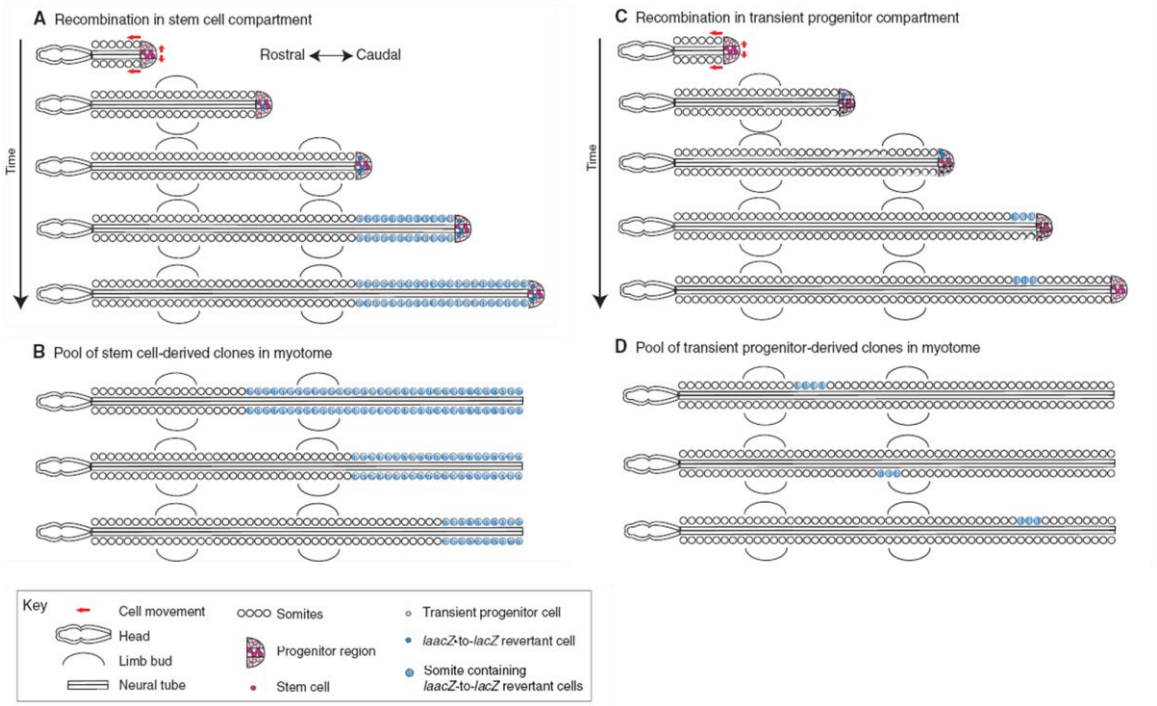

Figure 1.4. Profiles of clones derived from stem cell-like axial progenitors or transient axial progenitors

(A) The recombination event occurs in a stem cell-like axial progenitor in the posterior end of embryos. During axis elongation, the distribution of its descendants in the embryo is shown in (A).

(B) Profiles of clones derived from stem cell-like axial progenitors.

(C) The recombination event occurs in a transient progenitor. During axis elongation, the distribution of its descendants in the embryo is shown in (C).

(D) Profiles of clones derived from transient progenitors.

This is a reprint from Wilson and Storey, 2009.

Existence of NM progenitors in mouse embryos

The conventional paradigm of vertebrate body formation postulated that three germ layers were completely segregated at E7.5 when the primitive streak is fully formed. A retrospective clonal analysis using a ubiquitous promoter demonstrates that endoderm and surface ectoderm segregate during gastrulation (Tzouanacou et al., 2009). Surprisingly, this study shows that neural ectoderm and mesoderm share common progenitors, namely neuromesodermal (NM) progenitors, until the early somitogenesis and very possibly throughout axis elongation (Tzouanacou et al., 2009). In this clonal study, a prominent feature of N-M clones in E8.5 embryos is that although they start from a variable anterior border, most of them extend as far as the posterior neuropore. This pattern meets the profile of clones generated by the stem cell-like population in the posterior region of the embryos (Figure 1.4A). Therefore, it is likely that the NM progenitors are also a stem cell-like population contributing to axis elongation. However, not all N-M clones in E10.5 embryos extend to the tail bud, suggesting that some of these NM clones are not derived from stem cell-like population in the posterior region of the embryos. Therefore, this raises a possibility that there may be two types of NM progenitors: short-term and long-term NM progenitors. In this scenario, only the long-term NM progenitors could be considered as stem cell-like axial progenitors. Interestingly, the N-M clones that extend to the tail bud in E10.5 embryos show extensive mesodermal contribution in both body axis and the tail bud. Their profiles are similar to the previous myotome clones (Nicolas et al., 1996). Therefore, it is likely that long-term NM progenitors are also stem cell-like somite progenitors.

Locations of NM progenitors in mouse embryos

Although clonal analysis shows the existence of NM progenitors, it cannot indicate the precise locations of these cells. A series of population fate maps based on homotopic grafts and Dil labelling has been performed by our group to investigate the possible locations for NM progenitors in early somitogenesis (E8.5) and tail bud stages (E10.5-E12.5) (reviewed in (Wilson et al., 2009). During early (2-5) somite stages (E8.5), population fate maps show that cells in the anterior node and the primitive streak only contribute to axial and non-axial mesoderm, respectively (Cambray and Wilson, 2007). Interestingly, a region containing the posterior node and the anterior 5-10% of the primitive streak termed “node-streak border” (NSB) in E8.5 embryos is fated for neural tube, somites and notochord (Figure 1.5A, B). As

mentioned previously, the ventral layer of NSB exclusively gives rise to notochord (Wilson and Beddington, 1996). Therefore, the dorsal layer of the NSB, and not the ventral layer, is the location of neural tube and somite progenitors. Moreover, a recent homotopic grafting experiment in our group shows that the most anterior region of CLE (L1) on either side of the primitive streak also gives rise to both neural tube and somites (Wilson lab, unpublished data) (Figure 1.5B, C), while other regions do not efficiently produce both tissue types in situ. Thus, the NM fated cells observed in clonal analysis are most likely to reside in the dorsal NSB and L1. However, the relationship between the dorsal NSB and L1 is unknown.

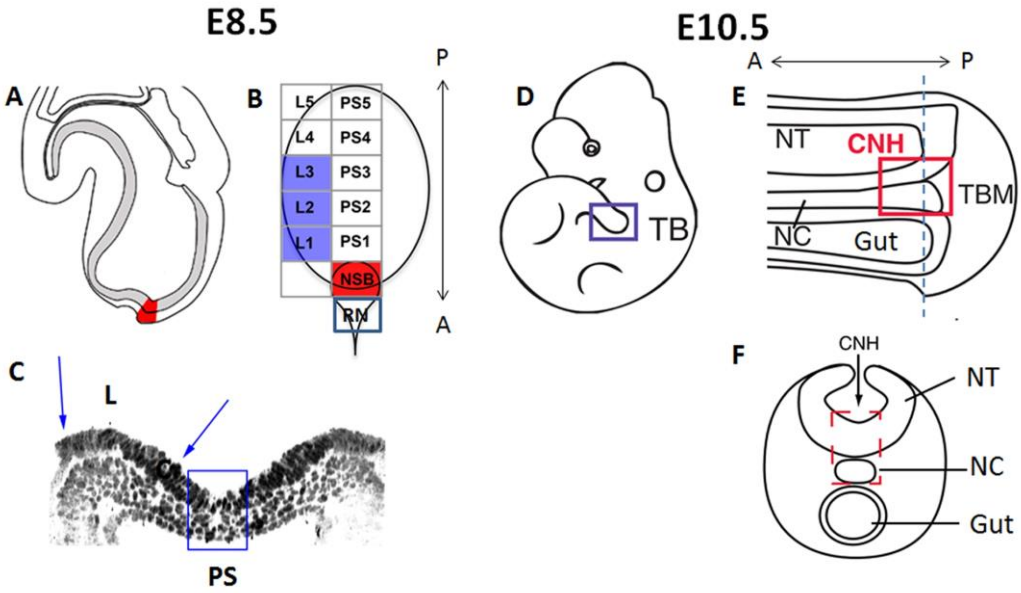

Figure 1.5. Schematic for locations of NM progenitors in mouse embryos

(A) Lateral view of E8.5 embryos. The NSB region is shown in red. (B) Schematic diagram showing subregions in the posterior part of E8.5 embryos. (C) A transverse section through the primitive streak. One side of the caudal lateral epiblast (CLE) is indicated by arrows. The primitive streak (PS) region is shown in the blue box.

(D) Schematic diagrams showing E10.5 embryos. (E) An enlargement showing basic structures in the tail bud (TB) of D; (F) A transverse section through the blue dashed line in E

Abbreviation: ps, primitive streak; L, caudal lateral epiblast; NSB, node streak border; RN, rostal node; CNH, chordoneural hinge; NT, neural tube; NC, notochord; TBM, tail bud mesoderm; A, anterior; P, posterior

Images D-F are reprint from Cambray and Wilson, 2007.

The fate map also shows that the descendants of NSB and L1 cells are located in the chordoneural hinge (CNH) at E10.5, which is composed of the most posterior of ventral neural tube and the notochord (Figure 1.5D, F). Furthermore, CNH cells are able to contribute to both neuroectoderm and mesoderm when grafted back to E8.5 NSB. By contrast, tail bud mesoderm (TBM) which is immediately posterior to the CNH exclusively produces mesoderm in E8.5 embryos (Figure 1.5E). More importantly, CNH cells in both mouse and chick can be serially passaged through three successive generations in young stage embryos without apparent loss of their ability to differentiate and to remain in the tails. In contrast, cells just posterior to this region cannot be serially passaged in this way (Cambray and Wilson, 2002; McGrew et al., 2008). Therefore, the ability of CNH cells to self-renew and differentiate to neural tube and mesoderm indicates that they are stem cell-like long-term NM progenitors in the tail bud.

A series of heterotopic grafting experiments has also been performed to investigate the potency of cells in different regions at E8.5. Cells in the L2-3 region predominantly fated to be mesoderm robustly produce both neurectoderm and mesoderm when grafted to the anterior of the NSB (Wilson lab, unpublished data) (Figure 1.5B). This indicates that L2-3 cells are also NM potent and the fate differences between L2-3 and NSB cells possibly results from their environment rather than their intrinsic properties. Thus, L2-3 cells can also be considered as NM progenitors.

Heterotopic grafting experiments also show that cells in the L1-3 and NSB are highly adaptable when grafted to other regions close to the primitive streak and contribute to similar tissues to the host cells (Cambray and Wilson, 2007) (Wilson lab, unpublished data). However, cells in other regions show a more restricted potency (Cambray and Wilson, 2007); Figure 1.5B). Cells in the rostral node (RN) fated to form notochord give rise to extensive ventral neural tissue with some contribution to the notochord and extremely low contribution to the paraxial mesoderm when grafted to NSB and PS1 (Cambray and Wilson, 2007) (Figure 1.5B). It should be noted that the RN also contains two cell layers. Therefore, it is likely that the ventral part of RN contributes to the notochord and the dorsal region of RN contains cells that can act as neural progenitors, although the neural contribution is not shown in the homotopic grafts (Cambray and Wilson, 2007). The neural contribution (ventral neural tube but not restricted to the floor plate) of the RN may be due to the influences of the graft sites. PS1 cells showed a very poor level of incorporation in the anterior node, indicating that cells in the primitive streak are incompatible with the node environment. When grafted to NSB, PS1 cells still mainly give rise to mesoderm. (Cambray

and Wilson, 2007). Taken together, these results show that NM progenitors are more potent than their adjacent neighbours.

The cell potency in these subregions was further examined by kidney capsule grafting. Although almost all grafted kidneys contain disorganised growth of well-differentiated somatic tissues, there is no evidence of teratocarcinoma formation (Wilson lab, unpublished data). This suggests that no pluripotent somatic cells persist in E8.5 embryos. Anterior node grafts produce mainly neurectoderm and a low proportion of bone. PS1and TBM grafts predominantly give rise to adipocytes. Cells in the most posterior of the primitive streak (L5 and PS5) produce mesoderm and non-neural ectoderm cells. L1-3 grafts mainly give rise to mesoderm with a few neural tissues. Interestingly, NSB and CNH cells produce a range of axial tissues including muscle, bone, cartilage, adipocytes and neural tissues, indicating these cells have the potential to give rise to both neural and mesodermal cells (Wilson lab, unpublished data).

To summarize, cell fate is highly regionalized in the posterior part of the embryos during axis elongation. NM progenitors refer to cells that are potent to give rise to both neural and mesoderm tissues. In E8.5 embryos, both NM bi-fated (NSB and L1) and NM potent (L2-3) cells are considered as NM progenitors. In tail bud stages (E10.5-E12.5), NM progenitors are located in the CNH.

Functions of Hensen's node in chick embryos

In chick embryos, gastrulation starts at Hamburger and Hamilton Stage (HH) 2, the primitive streak is fully extended at HH4, somitogenesis starts at HH6 and the end of axis elongation is about HH26 (Hamburger and Hamilton, 1951) (Figure 1.2). The organizer in chick embryos is known as Hensen's node. It is a bulb-like thickening initiating at the anterior end of the primitive streak during mid-gastrulation stage. It has been shown that when transplanted to the extraembryonic germ cell crescent of chick embryos, a quail Hensen's node is able to induce the host chick tissue to form a secondary axis (reviewed in (Nieuwkoop et al., 1985). Ablation of Hensen's node after HH4 (HH4-HH6) stage results in serious truncation in early embryos, indicating that this structure is vital for axis elongation (Psychoyos and Stern, 1996).

Upon closer examination, Hensen's node at 5-6 somite stages (HH8) shows heterogeneity. Morphologically, it can be divided into three zones in an AP direction (Figure 1.6): zone a, anterior to the median pit; zone b, the median pit; and zone c, the most posterior node, where cells are in close contact with the anterior of the primitive streak (Charrier et al., 1999), which is geographically similar to the NSB in mice. A fate mapping experiment based on quail-chick chimeras shows that zone c cells give rise to the basal plate of the neural tube bilaterally, the medial part of bilaterally paired somites to the tail bud and the CNH (Charrier et al., 1999). Therefore, the cell fates are also similar between zone c in chick and the NSB in mice. Notably, only when zone c is excised is the axis elongation arrested posterior to the thoracic region with massive cell death in the posterior. Moreover, when zone c is replaced by zone b tissues, posterior truncation still occurs (Charrier et al., 1999). These results indicate that in chick embryos axial extension particularly depends on zone c cells.

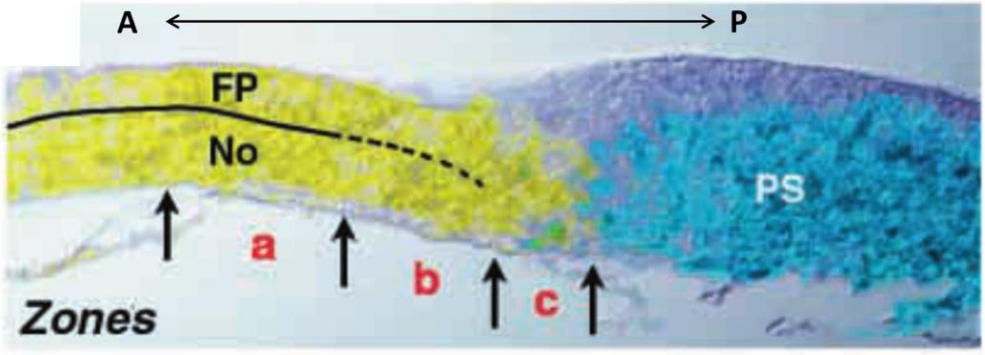

Figure 1.6. Sagittal section showing Hensen's node region in a 5-6 somite stage chick embryo

Cells expressing Foxa2 are labelled in yellow. Cells expressing Ch-Tbx6L are labelled in light blue. Three zones are distinguished in the node: zone a, the anterior one where notochord and floor plate are segregated; zone b, the bulk of the node which corresponds to the median pit; zone c, the caudal node with the anterior tip of the primitive streak.

The floor plate and notochord is clearly separated by basal membrane in the anterior indicated by the black solid line. The separation is not clear when it is close to the primitive streak. Black dotted line indicates the presumptive territories of the floor plate and notochord.

Abbreviation: PS, primitive streak; FP, floor plate; No, notochord; A, anterior; P, posterior

This is a reprint from Charrier et al., 1999

NM progenitors in chick embryos

Similar to mouse embryos, fate mapping studies show that cell fate is highly regionalized in early chick embryos and axis elongation probably also depends on stem cell-like populations which are located in the Hensen's node and the anterior region of the primitive streak (Garcia-Martinez et al., 1993; Garcia-Martinez and Schoenwolf, 1992; Selleck and Stern, 1991; Stern, 1992). Single-cell labelling experiments show that cells in the posterior part of Hensen's node adjacent to the primitive streak at HH4 contribute to the notochord, neural tube and somites. Moreover, there are still common progenitors for notochord and paraxial mesoderm in Hensen's node during early somitogenesis (Selleck and Stern, 1991). Interestingly, another detailed fate mapping study shows a small number of neural and mesoderm polyclones after labelling only 1-3 epiblast cells in the caudal neural plate (CNP) at HH6 (Brown and Storey, 2000). This observation indicates the potential existence of NM progenitors in chick embryos. It has also been shown that Hensen's node contributes to the chordoneural hinge (CNH) in tail bud stages (Catala et al., 1996). Moreover, CNH cells in chick embryos can be serially passaged between host embryos, contributing to both neural tube and mesoderm and repopulating themselves (McGrew et al., 2008). Therefore, it is likely that there are stem cell-like NM progenitors in chick embryos which are located in similar areas to those in mouse embryos (reviewed by (Wilson et al., 2009).

Markers for NM progenitors

Since the only possible locations for NM progenitors are in the dorsal layer of the NSB and the anterior CLE (L1-3), and later, in the CNH, gene expression in these areas has been extensively investigated. Although genes that are important for axial elongation such as *Fgf8*, *Evx1*, *Wnt3a*, *T*, *Cdx2*, *Nkx1.2* and *Hlxb9* are expressed in the NSB and L1-3 and show continuity of expression in the CNH, they are also expressed in the primitive streak, posterior CLE, mesodermal cells underneath the CLE and tail bud mesoderm. Currently, no individual gene expression pattern can distinguish NM progenitors from their adjacent cells (Cambray and Wilson, 2007; Delfino-Machin et al., 2005; Wymeersch, 2011).

A microarray analysis based on precise microdissection of small subregions in the posterior progenitor zone from E8.5 to E13.5 has been performed in our group to investigate the markers and special signalling pathways of NM progenitors. However, no unique marker has yet been identified (Wilson lab, unpublished data). The same conclusion is reached by comparing gene expression of the NSB and its adjacent regions using single cell qPCR

analysis (Jakuba, 2013). Recently, it has been shown that cells coexpressing Sox2 and Brachyury (T) coincide with NM progenitor regions in the dorsal layer of the NSB and L1-3 (Tsakiridis et al., 2014). Similar results are also reported in zebrafish (Martin and Kimelman, 2012), chick and human embryos (Olivera-Martinez et al., 2012). Therefore, although there is no unique single marker for identifying NM progenitors, coexpression of T and Sox2 can be used as a marker for NM progenitors.

Brachyury (T)

T, a T-box transcription factor, is one of the first genes expressed in the primitive streak at the onset of gastrulation (Herrmann, 1991). During gastrulation, T expression is also detected in the posterior epiblast adjacent to the primitive streak, newly formed mesoderm, node and notochord. After the closure of posterior neuralpore (E10.0) T expression continues in the tail bud (Cambray and Wilson, 2007; Wilkinson et al., 1990). Embryos homozygous for the *T* mutation (*T/T*) die around E10 with a severe axis truncation posterior to the first 7 somites, little to no notochord, and a defective allantois (Herrmann, 1991; Rashbass et al., 1994). Heterozygotes for *T* also show a range of abnormalities from shortening of the tail to the malformation of sacral vertebrae (Yanagisawa et al., 1981). A study investigating *T/T* cells in a wild type background shows that in the chimeric embryos *T/T* cells predominantly congregated in the primitive streak, and later, in the tail bud, indicating that the *T* mutation may result in a defect in cell movements (Beddington et al., 1992; Wilson et al., 1995). Collectively, these studies indicate that T expression is important for axis elongation and cell migration in the posterior progenitor zone but is not essential for anterior mesoderm formation.

Sox2

The *Sox* genes, a family of transcription factors, contain a highly conserved HMG (high mobility group) domain. The B1 Sox family, including Sox1, 2, 3 and 19, has been implicated in various processes of embryogenesis due to a variety of expression sites in embryos (reviewed by (Kondoh and Kamachi, 2010). In mice, Sox1, 2 and 3 are expressed in early embryos. Sox2 expression initiates in the ICM at the blastocyst stage. It is detected in the epiblast at the pre-streak stage (E5.5) and becomes restricted in the anterior ectoderm from E7.5. *Sox2*$^{-/-}$ embryos die during implantation (Avilion et al., 2003). The early lethality of *Sox2*$^{-/-}$ embryos prevents the investigation of its role in axis elongation. Sox3 is expressed

in the epiblast immediately after implantation. Its expression pattern is similar to Sox2 but spreads more widely into the posterior epiblast after E7.5 (Wood and Episkopou, 1999). *Sox3*$^{-/-}$ embryos are viable, suggesting B1 *Sox* genes are functionally redundant (Yoshida et al., 2014). A low level of Sox1 becomes detectable after the late bud stage (E8.0) in the anterior neural plate (Wood and Episkopou, 1999).

In mice, five Sox2 enhancers have been identified. Two of them (N1 and N2) have been extensively studied in postimplantation embryos due to their mutually exclusive activation patterns. At E8.5, the N2 enhancer activation is detected in the neural plate, whereas the N1 enhancer is activated in the whole CLE and the primitive streak but is absent in the neural plate and mesoderm (reviewed by (Uchikawa et al., 2011). Since Sox2 is expressed in the neuroectoderm and the anterior CLE at E8.5, the N1 enhancer activation does not correlate well with Sox2 expression. Deletion of the N1 enhancer results in the absence of Sox2 from the anterior CLE but has no effect on the survival of the mutants (Takemoto et al., 2011; Yoshida et al., 2014). This may be because of a functional compensation by Sox3, which is expressed in the neuroectoderm and CLE. A recent study shows that an additional deletion of Sox3 in *Sox2*$^{\triangle N1/\triangle N1}$ mutants results in a thicker primitive streak and larger somites, suggesting an increase in mesoderm progenitors in these mutants (Yoshida et al., 2014). Therefore, it is proposed that the B1 Sox family is required for adjusting the production of mesoderm from the posterior progenitor zone.

Signals for axis elongation

There are three main developmental processes involved in axis elongation: maintenance of posterior progenitor zone, cell fate choice, and segmentation of PSM. Mutations that affect one process normally also have an influence on another (this will be discussed below). Here, I will focus on introducing the Wnt, FGF and Notch signals which are known to be important for axis elongation.

Wnt/β-catenin singalling

The initiation of Wnt signalling requires a Wnt protein to bind to a Frizzled family receptor in the cell membrane. Based on different downstream components three Wnt signalling pathways have been characterized: the Wnt/β-catenin (canonical Wnt) pathway, the non-

canonical planar cell polarity (PCP) pathway and the Wnt/calcium pathway. In this study, I will focus on introducing Wnt/β-catenin signalling in early mouse embryo development (reviewed in (MacDonald et al., 2009). An overview of Wnt/β-catenin signalling is presented in Figure 1.7. In the absence of a Wnt protein, cytoplasmic β-catenin is phosphorylated by a complex consisting of Axin, APC, and the protein kinase GSK-3 and then targeted for proteasomal degradation in order to maintain a low level of cytoplasmic β-catenin (Figure 1.7A). When Wnt proteins bind to Frizzled (Fz) /low density lipoprotein receptor-related protein complex (LRP receptor complex) at the cell surface, Dishevelled (Dsh) is recruited to bind the intracellular parts of Fz leading to LRP complex phosphorylation and Axin recruitment. As a consequence, β-catenin protein molecules are released from the phosphorylation complex and accumulate in the cytoplasm. The excess stabilized β-catenin proteins translocate to the nucleus and interact with transcription factors such as lymphoid enhancer-binding factor /T cell-specific transcription factor (Lef/Tcf) family to activate the transcription of downstream genes (Figure 1.7B) (reviewed in (Logan and Nusse, 2004; MacDonald et al., 2009).

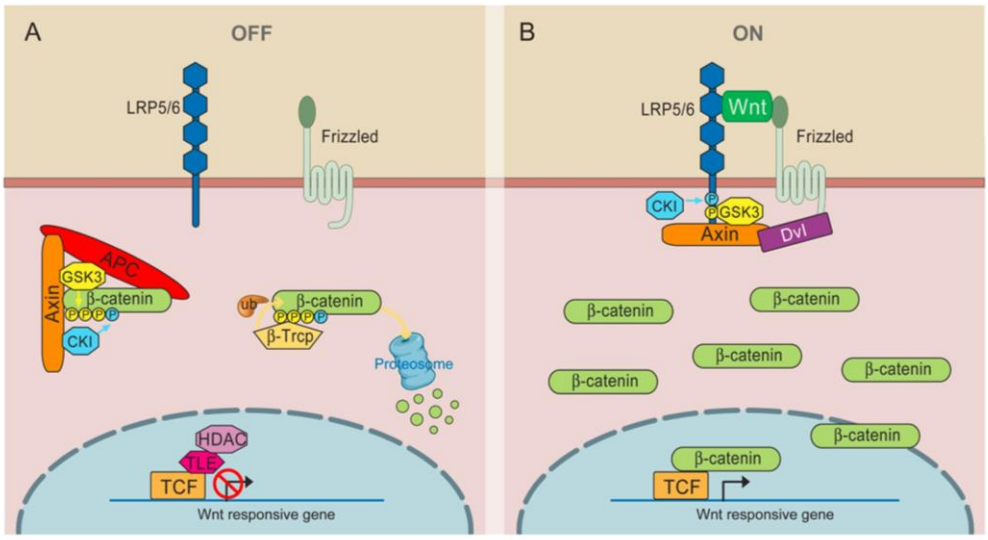

Figure 1.7. Sketch of Wnt/β-catenin signalling pathway

(A) In the absence of Wnt proteins, cytoplasmic β-catenin is phosphorylated by a complex with Axin, APC, GSK3β and CK1. Phosphorylated β-catenin is then degraded by proteasomes. Wnt downstream genes are repressed.

(B) In the presence of Wnt proteins, the complex-mediated phosphorylation is disrupted. β-catenin transfers into the nucleus where it binds to TCF and activates Wnt responsive genes.

This is a reprint from MacDonald et al., 2009

Wnt proteins for axis elongation

Wnt proteins are a large family of secreted glycoproteins. 19 Wnt proteins have been identified in mouse embryos, of which 6 are expressed during early gastrulation: *Wnt2b, Wnt3, Wnt3a, Wnt5a, Wnt5b* and *Wnt8* (Kemp et al., 2005). *Wnt2b* initiates in presumptive posterior epiblast at the pre-streak stage (E5.5). During early gastrulation (E7.5), its expression is detected in the primitive streak, newly formed mesoderm and visceral endoderm (Kemp et al., 2005). However, its expression is restricted in the prosencephalon, future midbrain and foregut during early somitogenesis (E8.5) (Zakin et al., 1998). The expression pattern of *Wnt3* is similar to *Wnt2b* with additional expression in the posterior epiblast during early gastrulation (E7.5) but its expression becomes undetectable at E8.5 (Liu et al., 1999). In chick embryos, *Wnt8* is expressed in the epiblast of the posterior marginal zone before gastrulation and has been proposed to be associated with axis induction. Ectopic expression of *CWnt8C* under *human β-actin* promoter in mouse embryos results in the duplication of primitive streak and anterior neuroectoderm truncation (Popperl et al., 1997). In zebrafish, both *Wnt3a* and *Wnt8* are expressed in the blastoderm margin and later in the tail bud. The combined inhibition of both Wnt3a and Wnt8 results in the loss of tail structure, indicating that Wnt3a and Wnt8 play an important role in the posterior body formation in zebrafish (Shimizu et al., 2005). However, *Wnt8* shows different expression patterns in mouse embryos compared with chick and zebrafish embryos. In mouse embryos, *Wnt8* is detected at E7.5 in the embryonic ectoderm up to the boundary at the base of the developing headfolds with transient expression in the newly formed mesoderm. During early somitogenesis (E8.5), it is expressed in the prospective hindbrain and the caudal region of the neural plate but absent from the posterior progenitor zone (Bouillet et al., 1996; Niederreither et al., 2000). Only Wnt3a, Wnt5a and Wnt5b expression persists in the posterior progenitor zone from the primitive streak stages to the tail bud stages (Cambray and Wilson, 2007; Gofflot et al., 1997; Parr et al., 1993; Roelink and Nusse, 1991; Takada et al., 1994).

Wnt3$^{-/-}$ embryos do not form a primitive streak or mesoderm, suggesting it is required for initiating mesoderm formation (Liu et al., 1999). The early lethality of the mutants makes it difficult to investigate the role of *Wnt3* in axis elongation. All *Wnt2b*$^{-/-}$, *Wnt5b*$^{-/-}$, *Wnt8a*$^{-/-}$ and *Wnt8b*$^{-/-}$ mutants are viable, indicating their functions are redundant during embryo development (reviewed by (van Amerongen and Berns, 2006). Since *Wnt3a* and *Wnt5a* are the only genes left of which the expression persists in the posterior progenitor zone from the

primitive streak stages to the tail bud stages and their homozygous null mutations die due to the axial truncation, I will discuss their role in axis elongation in detail below.

Wnt3a

Wnt3a initiates at the late-streak stage (E7.5) in the entire length of the primitive streak and the adjacent epiblast (Takada et al., 1994). Its expression persists in the posterior progenitor zone until E12.5 (Cambray and Wilson, 2007). *Wnt3a*$^{-/-}$ embryos exhibit a severe axial truncation posterior to the forelimb (first 9 somites). The posterior paraxial mesoderm, notochord and tail bud are absent in the mutants. Notably, ectopic neural tissues are formed in the posterior part of the embryo at the expense of mesodermal derivatives in these mutants (Takada et al., 1994; Yoshikawa et al., 1997). Embryos homozygous for *Wnt3a* hypomorphic allele *vestigial tail (vt)* show a significant reduction of *Wnt3a* in the tail bud and result in the absence of caudal vertebrae. Moreover, the lower doses of *Wnt3a* gene result in more anterior defects in the skeleton (Greco et al., 1996). Overexpressing Wnt3a under the Cdx2 promoter also results in malformations posterior to the forelimb bud. In particular, the posterior neural tube is completely absent in these transgenic mice, suggesting that overexpressing Wnt3a blocks neural differentiation in the posterior progenitor zone (Jurberg et al., 2014). Collectively, these studies show *Wnt3a* regulates axial elongation in a dosage dependent manner.

The phenotype of *Wnt3a*$^{-/-}$ embryos is strikingly similar to that of *T/T* embryos. Moreover, there is no T expression detected posterior to the forelimb level in *Wnt3a*$^{-/-}$ embryos, indicating that Wnt3a may be upstream of T expression. Indeed, two Lef1/Tcf1 binding sites are identified in T promoter and they are essential for T expression in the primitive streak (Yamaguchi et al., 1999b). Since Lef1 and Tcf1 are functionally redundant, null mutations in either do not affect axial elongation in early embryos. However, the phenotype of a *Lef1*$^{-/-}$*; Tcf1*$^{-/-}$ compound mutation is similar to that of *Wnt3a*$^{-/-}$ and *T/T* embryos (Galceran et al., 1999). Furthermore, the phenotype of *Wnt3a*$^{-/-}$ embryos can be rescued by constitutive expression of Lef1 (Galceran et al., 2001). Taken together, these studies indicate that Wnt3a directly mediates T expression via Wnt/β-catenin signalling.

Wnt5a

Wnt5a is expressed in the primitive streak and lateral mesoderm wing from E7.5 to E8.5, with expression gradually decreasing as cells exit the primitive streak region and differentiate (Takada et al., 1994). Expression of Wnt5a is also detected in all three germ

layers of the tail bud. Besides the posterior progenitor zone, Wnt5a is also expressed in the first branchial arch and limbs during early organogenesis (Takada et al., 1994; Yamaguchi et al., 1999a).

During early somitogenesis, *Wnt5a*$^{-/-}$ embryos show a shortened primitive streak and PSM and smaller somites (Yamaguchi et al., 1999a). Since Wnt5a is not expressed in somites, the phenotype of smaller somites is likely to result from a reduction in the number of proliferating mesodermal progenitors in the posterior progenitor zone and/or PSM. Unlike Wnt3a mutants, which are truncated at the forelimb bud level, the tail bud structure is present in *Wnt5a*$^{-/-}$ mutants. By E10.5, somites are found extending to the tail tip and the mutants display a truncation posterior to the hindlimb bud level (Yamaguchi et al., 1999a). Moreover，in *Wnt5a*$^{-/-}$ embryos normal Lef1 expression is detected in the primitive streak and PSM (Yamaguchi et al., 1999a), suggesting that Wnt5a is involved in axis elongation via a non-canonical Wnt pathway (Slusarski et al., 1997). Collectively, these studies indicate that Wnt5a regulates axis elongation by supporting the expansion of axial progenitors via a non-canonical Wnt pathway.

The role of Wnt/β-catenin in axis elongation

β-catenin protein, encoded by the *Ctnnb1* gene, acts both as a transcriptional coactivator of the Wnt signalling pathway, as stated above, but also regulates cell-cell adhesion. β-catenin expression is critical for early embryo development. *β-catenin*$^{del/del}$ embryos die before E9.5 without mesoderm formation (Huelsken et al., 2000). Since intact adherens junctions and desmosomes are observed in the mutants, this early lethality may not result from defects in cell adhesion. Moreover, plakoglobin, the closest relative of β-catenin in the armadillo family, is increased, suggesting it substitutes for β-catenin in adherens junctions in the mutants. To bypass the gastrulation lethality, *β-catenin* was conditionally deleted in nascent mesoderm under the control of the *T* promoter. The mutants show similar phenotypes to *Wnt3a*$^{-/-}$ mutants including a severe axial truncation posterior to the forelimb (Aulehla et al., 2008; Dunty et al., 2008). However, constitutively stabilizing β-catenin in T expressing cells also results in malformations posterior to the heart region with a kinked neural tube and an amorphous mesodermal mass underneath it (Jurberg et al., 2014). Collectively, these studies show β-catenin expression is vital for axial elongation.

The activity of Wnt/β-catenin signalling in the mouse embryo is identified by using transgenic reporter lines such as BAT-LacZ (Maretto et al., 2003), TCF/Lef-LacZ

(Mohamed et al., 2004) and TCF/Lef:H2B-GFP (Ferrer-Vaquer et al., 2010). During gastrulation, Wnt/β-catenin signalling is activated in the primitive streak, its adjacent posterior epiblast, the mesodermal wings, the node and emergent notochord. Wnt/β-catenin signalling is maintained in these domains during early somitogenesis and is also detected in the tail bud in later stages (Ferrer-Vaquer et al., 2010). The persistence of Wnt/β-catenin activity in the posterior progenitor domain during axis elongation indicates it may be involved in the maintenance of axial progenitors.

Fibroblast growth factor (FGF) signalling in axis elongation

There are 23 Fgf proteins identified in mice. They are generally related to cell growth and differentiation. Most Fgfs mediate signal transduction by binding and activating Fgf receptors (Fgfr), a subfamily of cell surface receptor tyrosine kinases (RTKs). There are four known *Fgfr* genes in mice (Fgfr1-4), which code for single spanning transmembrane proteins with an extracellular ligand-binding region and an intracellular domain harbouring tyrosine kinase activity (reviewed in (Itoh and Ornitz, 2008). FGF signal transduction can proceed through the Ras/MAPK (ERK), PI3K/AKT and PLCγ intracellular pathways (reviewed in (Bottcher and Niehrs, 2005). An overview of the FGF signalling pathway is shown in Figure 1.8.

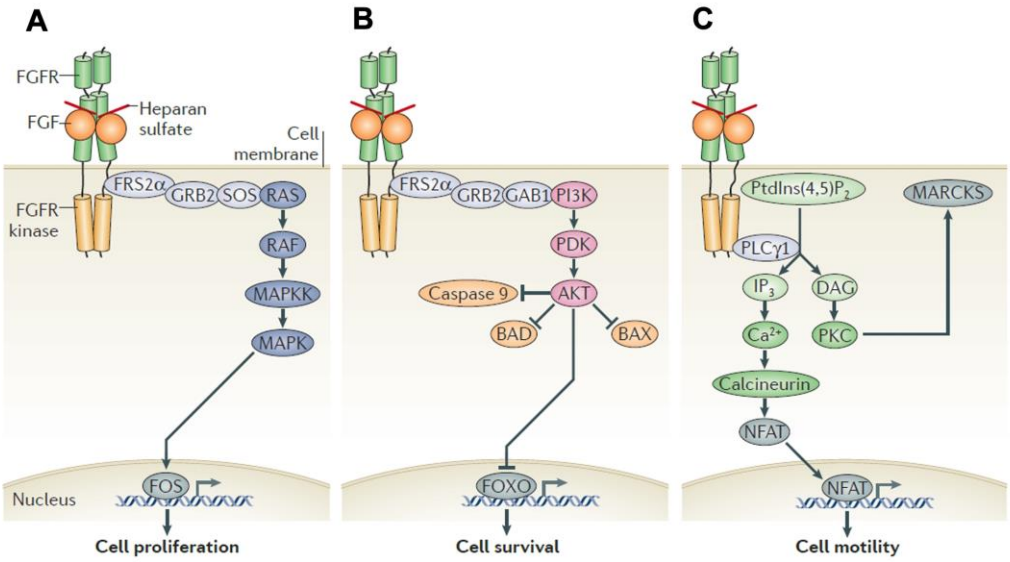

Figure 1.8. Sketch of FGF signalling pathways

(A) Key components of Ras/MAPK pathway. (B) Key components of PI3K/AKT pathway; (C) Key components of PLCγ pathways. This is a reprint from Goetz and Mohammadi, 2013

Although some Fgf proteins (Fgf3, 4, 5, 8, 17 and 18) are expressed in the posterior progenitor zone of mouse embryos (Crossley and Martin, 1995; Hebert et al., 1991; Maruoka et al., 1998; Niswander and Martin, 1992), only *Fgf4* and *Fgf8* knockout mice die during early embryonic stages, indicating they play a key role in early mouse embryo development. The expression of Fgf4 starts in the inside cells at the late morula stage (E2.0). During the blastocyst stage, Fgf4 expression becomes restricted to the epiblast cells of the ICM (Kang et al., 2013). During gastrulation and early somitogenesis, *Fgf4* is detected in the primitive streak and CLE (Niswander and Martin, 1992). *Fgf4* expression persists in the posterior of embryos at E10.5 (Boulet and Capecchi, 2012). However, current data does not clearly show when the expression disappears from the tail bud. *Fgf4*$^{-/-}$ embryos die during implantation due to a lack of primitive endoderm, indicating Fgf4 is required for the formation or maintenance of primitive endoderm (Feldman et al., 1995; Kang et al., 2013). The early lethality of *Fgf4*$^{-/-}$ embryos leaves the role of Fgf4 in gastrulation and axis elongation in question.

Fgf8 is detected in the posterior part of the epiblast during the onset of gastrulation. From E7.5 to E9.5, it is expressed in the primitive streak, CLE and PSM but not in the somites (Maruoka et al., 1998; Perantoni et al., 2005). *Fgf8* expression persists in the tail bud until E12.5 (Cambray and Wilson, 2007). *Fgf8*$^{-/-}$ mutants die due to the defect mesoderm and endoderm formation. The posterior half of the mutant embryos formed a bulge which protruded into the amniotic cavity. The transcripts of T were only detected cells with epithelial morphology in the surface of the bulge but not in the cells with a mesenchymal morphology within the bulge. Moreover, the expression of *Tbx6*, a marker for mesoderm cells exiting from the primitive streak, was undetectable in the mutants. However, the mutants show normal development of extraembryonic mesoderm (Sun et al., 1999). Collectively, these results indicate that Fgf8 may not be required for initiating mesoderm formation but is essential for cell migration away from the primitive streak.

Fgf4 expression is absent in the posterior region of *Fgf8*$^{-/-}$ embryos, indicating that Fgf8 is required for Fgf4 expression during gastrulation. Since *Fgf8* is not expressed in preimplantation embryos, presumably the lack of *Fgf4* expression occurs after implantation. Therefore, the phenotypes of *Fgf8*$^{-/-}$ mutants may result from a deficit of both Fgf8 and Fgf4 during gastrulation. To further investigate the individual roles of Fgf4 and Fgf8 in the primitive streak, *Fgf4* and/or *Fgf8* were conditionally deleted in T expressing cells (Naiche et al., 2011; Perantoni et al., 2005). Conditional deletion in either gene alone does not affect fetal growth. However, deletion of both *Fgf4* and *Fgf8* in T expressing cells results in the

premature differentiation of the PSM and a severe axis truncation after the forelimb (Naiche et al., 2011). Therefore, these studies indicate that Fgf4 and Fgf8 are functionally redundant during gastrulation and they function to maintain the posterior progenitor zone and to suppress PSM differentiation.

In mice, there are four Fgf receptors, of which only Fgfr1 is expressed in the posterior progenitor zone throughout axis elongation (Wahl et al., 2007). From the headfold stage (E8.0) onward, *Fgfr1* is detected in the primitive streak, CLE, posterior neuroectoderm, PSM and the newly formed mesoderm (Yamaguchi et al., 1992). Its expression in these domains continues in tail bud stages (Wahl et al., 2007). *Fgfr1*$^{-/-}$ mutants die between E7.5 to E9.5 and show similar phenotypes to *Fgf8*$^{-/-}$ embryos with an accumulation of cells in the posterior region of the embryo and aberrant mesodermal patterning (Ciruna et al., 1997). To elucidate the cell-autonomous function of Fgfr1, a chimeric analysis was performed by injecting *Fgfr1*$^{\Delta tuk/\Delta tuk}$ ES cells into the wild type embryos. Mutant cells accumulated in the primitive streak and tended to form ectopic neural tubes in the context of wild type embryo development (Ciruna et al., 1997). A later study shows that *Fgfr1*$^{-/-}$ *mesodermal* cells do not display a significant abnormality in general cell migration during *in vitro* culture (Ciruna and Rossant, 2001). However, compared with WT cells, *Fgfr1*$^{\Delta tuk/\Delta tuk}$ cells show defects in traversing the streak and the mutant cells which managed to progress through the primitive streak still maintain high E-cadherin expression, indicating that FGF signalling is involved in EMT at the primitive streak by regulating the expression of E-cadherin (Ciruna and Rossant, 2001). Together, FGF signalling is important for both the morphogenesis and patterning of mesoderm during axis elongation.

The hierarchy of Wnt and FGF signalling in axis elongation

As mentioned above, both Wnt and FGF signalling are involved in the posterior pattering during axis elongation. *Wnt3a*$^{-/-}$ embryos and Fgfr1 chimeric embryos share some common phenotypes such as the posterior truncation and formation of ectopic neural tube (Ciruna and Rossant, 2001; Takada et al., 1994; Yoshikawa et al., 1997). Moreover, T expression is reduced in a similar domain of the primitive streak in both *Wnt3a*$^{-/-}$ and *Fgfr1*$^{-/-}$ embryos, indicating both signalling pathways play a role in mesoderm specification (Ciruna and Rossant, 2001; Yamaguchi et al., 1999b). As mentioned previously, T is a direct target of Wnt/β-catenin signalling pathway (Yamaguchi et al., 1999; Arnold et al., 2000). In *Fgfr1*$^{-/-}$ embryos, *Wnt3a* expression is maintained but T expression is absent at the primitive streak.

It has been suggested that the loss of T expression in *Fgfr1*$^{-/-}$ embryos is due to the attenuation of Wnt signalling at the primitive streak (Ciruna and Rossant, 2001). It has been shown that *Fgfr1*$^{-/-}$ cells retain E-cadherin expression even when they migrate away from the streak (Ciruna and Rossant, 2001) and E-cadherin expression may result in the accumulation of β-catenin in the cell membranes and prevent β-catenin/LEF-1 interaction in the nuclei (Orsulic et al., 1999). Moreover, T expression is restored in the primitive streak of *Fgfr1*$^{-/-}$ explants after blocking E-cadherin functions using anti-E-cadherin antibodies (Ciruna and Rossant, 2001). Therefore, all these results indicate that FGF signalling indirectly regulates T expression at the primitive streak through Wnt/β-catenin signalling. Since the deletion *Fgfr1* attenuates Wnt signalling at the primitive streak and *Fgf8* expression is absent in *Wnt3a*$^{-/-}$ embryos and significantly reduced in tail bud of *Wnt3a* $^{vt/vt}$ embryos (Aulehla et al., 2003; Naiche et al., 2011), it is likely that there is a positive regulatory loop between Wnt and FGF signalling for posterior mesodermal fate specification.

It should be also noted that although *Wnt3a*$^{-/-}$ embryos and *Fgfr1* chimeric embryos display an ectopic neural tube, the reason for their formation differ. As mentioned previously, *Fgfr1*$^{-/-}$ cells cannot successfully undergo EMT (Ciruna and Rossant, 2001), however, *Wnt3a*$^{-/-}$ cells can (Yoshikawa et al., 1997). Therefore, although both signalling pathways are importation for the specification of mesoderm progenitors, it is more likely that Wnt signalling directly regulates the cell fate choice between neural and mesodermal lineages.

Notch signalling in axis elongation

Notch signalling is activated when the membrane-bound Notch ligands (jagged1, jagged2, Dll1, Dll3 and neurogenin2) bind to the single-pass transmembrane Notch receptors (Notch 1-4). The ligand-receptor interactions induce the cleavage and release of the Notch intracellular domain (NICD). NICD enters the nucleus where it binds to the transcriptional repressor, RBP-Jκ and then converts it into an activator, which activates its downstream gene expression such as Hes/Hey family members (Figure 1.9) (Kopan and Ilagan, 2009).

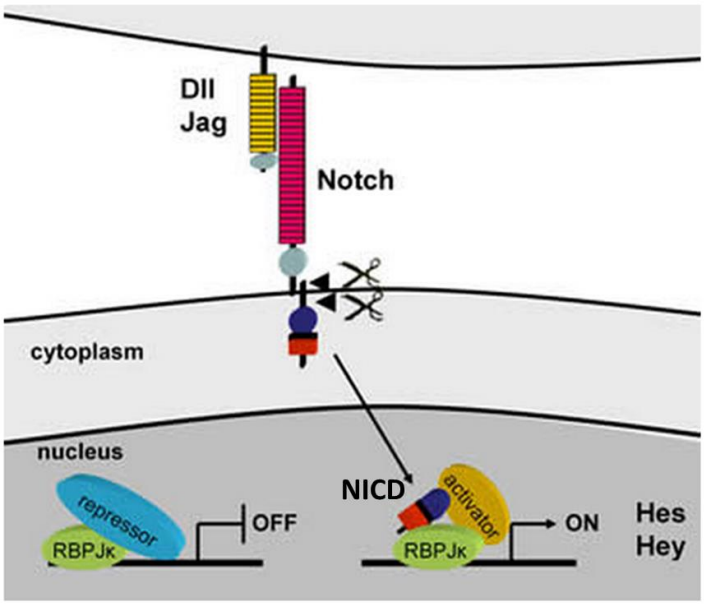

Figure 1.9. Sketch of Notch signalling pathways

This is a reprint from https://neurowiki2012.wikispaces.com/Causes

In mice, Notch1 is expressed in the primitive streak and posterior mesoderm during gastrulation. During somitogenesis, its expression extends to a wide variety of tissues such as the PSM and differentiating endothelial cells (Reaume et al., 1992). *Notch1*$^{-/-}$ embryos are indistinguishable from wild type embryos before E8.5. However, during somitogenesis the mutants show a delay and disorganization in somite formation. All mutants die around E11.0 (Reaume et al., 1992). RBP-Jκ, a transcriptional regulator of Notch signalling, is predominantly expressed in the PSM and developing somites in early mouse embryos. *RBP-Jκ*$^{-/-}$ embryos also die around E9.5 with abnormalities similar to *Notch1*$^{-/-}$ mutants, including premature neuronal differentiation, defective somitogenesis and axial truncation (with 4

somites) (de la Pompa et al., 1997; Oka et al., 1995). Some other Notch related mutants such as *Dll3*$^{-/-}$ and *Lfng*$^{-/-}$ are also lethal and display defects in somite formation and axis elongation (Collu et al., 2014; Dunwoodie et al., 2002; Evrard et al., 1998; Lowell et al., 2000). Collectively, these studies indicate that Notch signalling is important for somite formation and axial elongation. The role of Notch signalling in segmentation has been extensively investigated (reviewed in (Lewis et al., 2009; Pourquie, 2011), however, its role in axial truncation is still unclear. It is possible that defects in Notch signalling result in abnormal somite patterning, which may affect the maintenance of posterior progenitor zone. Alternatively, Notch signalling within the posterior progenitor zone itself may be required for the maintenance of progenitors.

Cessation of axis elongation

In mice, termination of somitogenesis occurs around E13.5 and is one of the most obvious features indicating the end of axis elongation. Many studies have been conducted to reveal the mechanism for termination of axial elongation and several hypotheses are proposed. I will list them below. However, it should be noted that since many events accompany the end of axis elongation, it is still unclear which of these are causative, and which are merely consequences of a key trigger event.

The loss of cyclic gene expression in the PSM

Somitogenesis can be subdivided into three main phases: (1) axial progenitors acquire a paraxial mesoderm progenitor identity and are added to the PSM pool; (2) A group of cyclic genes are expressed periodically as a dynamic wave across the PSM to segment a new pair of somites from the anterior PSM. It has been proposed that the oscillatory expression of these cyclic genes is regulated by a segmentation "clock" acting within the PSM and somite formation is controlled by this clock and wavefront mechanism (reviewed in (Dequeant and Pourquie, 2008); (3) the morphological boundaries are established to separate the newly formed somites from the PSM (reviewed in (Dequeant and Pourquie, 2008). Therefore, in principle the number of somites is linked to the PSM lifetime, which depends on a balance between the speed of somitogenesis, the proliferation rate of PSM cells and the speed of their progenitors emerging from the tail bud. If the speed of somitogenesis was faster than the growth of the PSM, the PSM will gradually shrink until it is exhausted, leading to the end of

somite formation. In this scenario, the arrest of somitogenesis could be due to the exhaustion of the PSM.

It has been shown that the PSM size in the mouse, chicken, zebrafish and corn snake shows a progressive shrinkage of the PSM during late stages of somitogenesis (Gomez et al., 2008). Although a small strip of unsegmented PSM remains in the tail bud after the completion of somitogenesis in chicken and mouse embryos, the cyclic genes are no longer expressed in the remaining unregimented PSM at the end of somitogenesis, indicating that the termination of axis elongation may result from the arrest of cyclic gene expression in the PSM (Tenin et al., 2010). A grafting experiment shows that the mesenchymal cells in the E13.5 tail bud (when somitogenesis had recently ceased) are still capable of contributing to somites when transplanted into a young environment (Tam and Tan, 1992). Therefore, it is possible that the remaining PSM at the end of axis elongation still has the potential to segment. The reason they do not form somites may be due to the cessation of the segmentation clock. However, the clock could be reactivated when these tissues are transplanted to a young environment.

A significant reduction of Wnt and FGF signalling

As mentioned previously, Wnt5a and Fgf8 are expressed in the posterior progenitor zone and their transcript levels gradually reduce in the emergent differentiating cells. Therefore, it has been proposed that progenitor maintenance is driven by high levels of Wnt and FGF signals in the posterior progenitor zone, while low Wnt and FGF activity anterior to the posterior progenitor zone promotes the maturation of axial progenitors on their exit from the posterior progenitor zone (reviewed in (Dequeant and Pourquie, 2008; Wilson et al., 2009). Therefore, it is likely that the exposure of axial progenitors to a certain threshold of Wnt and FGF signals is critical for their maintenance. It has been shown that *Wnt3a, Fgf8, Fgf17, Fgf18* and *T* are expressed broadly in the posterior progenitor zone until E10.5. However, their expression starts to gradually decline in the tail bud from E11.5 and is almost undetectable at E13.5 (Cambray and Wilson, 2007; Wymeersch, 2011). Moreover, *Wnt3a*$^{-/-}$ mutants display severe truncation posterior to the hindlimbs, while embryos heterozygous for mutations in both *Wnt3a* and *T* only show a tail truncation, indicating the dosage of Wnt3a expression is involved in the maintenance of axial progenitors (Greco et al., 1996). Therefore, it is possible that a gradual decrease of Wnt and FGF signals and eventually their disappearance from the posterior progenitor zone causes the extinction of axial progenitors during late tail bud stages. This then leads to the reduction of the PSM and the subsequent end of somite formation after E13.5.

Posterior extension of retinoic acid (RA) signalling

Embryos administered with RA, a vitamin A derivative, at E8.5 display severe malformations including the formation of ectopic neural tubes, a reduction of T and Wnt3a expression in the posterior progenitor zone and axial truncation (Iulianella et al., 1999). Retinaldehyde dehydrogenase type 2 (Raldh-2) is a major RA synthesis enzyme. It is expressed in the mesodermal cells migrating away from the primitive streak during late gastrulation and then in the recently formed somites during somitogenesis (Niederreither et al., 1997). *Raldh2*$^{-/-}$ embryos die at E9.5 with an enlargement of the primitive streak and ectopic expression of mesodermal markers in the anterior CLE (Ribes et al., 2009). This indicates that RA signalling plays a role in inducing the differentiation of axial progenitors (Olivera-Martinez and Storey, 2007; Ribes et al., 2009).

It has been shown that the presence of RA in the PSM and somites represses Fgf8 expression at the anterior border of the posterior progenitor zone and promotes cell differentiation (Diez del Corral et al., 2003; Sirbu and Duester, 2006). Mouse embryos exposed to exogenous RA lose Wnt3a expression in the tail bud (Iulianella et al., 1999). Therefore, RA signalling is generally considered to have inhibitory effects on both FGF and Wnt signals during axis elongation.

It has been shown that retinoid signalling plays an important role in the cessation of axis elongation in chick embryos. The onset of *c-Raldh2* expression and RA activity are associated with localized cell death and repression of Fgfs in the chick tail bud, which further leads to the end of axis elongation (Olivera-Martinez et al., 2012; Tenin et al., 2010). Thus, it has been proposed that the posterior extension of RA signalling causes the gradual extinction of Wnt and FGF signals from the progenitor zone during late tail bud stages, which then leads to the cessation of axis elongation (reviewed in (Wilson et al., 2009).

It should be noted that although Raldh2 transcripts are detected in the mouse tail bud, retinoic acid response element (RARE)-LacZ^{+} cells do not appear in any T^{+}Sox2^{+} regions in the tail bud (E10.5-E13.5) of RA activity reporter mouse embryos. This indicates that there is no endogenous RA activity in mouse the tail bud (Cunningham et al., 2011). This result shows that the presence of *Raldh2* may not always result in RA production. Collectively, unlikely in chick embryos, the role of retinoid signalling in the cessation of axis elongation in mouse embryos is still unknown.

Apoptosis

In chick embryos, a burst of localized apoptotic cells has been observed in the tail bud at the end of axis elongation (Hirata and Hall, 2000). This raises another hypothesis that the cessation of axis elongation is caused by the removal of axial progenitors from the tail bud through apoptosis. To investigate the apoptosis in mouse axial progenitors, a terminal deoxynucleotidyl transferase dUTP nick end labelling (TUNEL) assay which detects DNA fragmentation caused by apoptotic has been previously conducted in our group (Wymeersch, 2011). During early tail bud stages (E10.5-E11.5), few TUNEL-positive cells were detected in the CNH but there was a relatively high incidence of apoptosis in the posterior neuropore and the ventral tail bud. A general increase of apoptotic cells was observed in E12.5 and E13.5 tail buds. However, apoptosis in the CNH is not higher than other regions in the tail bud at the end of axis elongation (Wymeersch, 2011). Therefore, in contrast to chick embryos, no localized apoptotic cells were detected in the mouse tail bud at the end of axis elongation. This leaves in doubt the hypothesis that apoptosis is the causative event for the cessation of axis elongation in mice.

A high cell death rate in the posterior progenitor zone is observed in some mouse mutants showing axial truncations. For example, *T/T* embryos show an increase in cell death in the truncated region (Conlon and Smith, 1999). Extensive cell death is also observed in the posterior region of *Wnt3a*$^{-/-}$ embryos (Takada et al., 1994). The administration of RA to E8.5 mouse embryos results in axis truncation with massive cell death in the posterior region (Shum et al., 1999). Therefore, a high rate of apoptosis in the posterior progenitor zone could cause the premature arrest of axis elongation. However, this situation could conceivably be different from the normal cessation of axis elongation.

The expression of posterior *Hox* genes

In mice, 39 *Hox* genes are found in four clusters that share a common linear order of 13 paralogous group (PG) *Hox* family members. In each cluster, *Hox* genes are arranged sequentially from a 3' to 5' direction, which corresponds to the order in which their expression initiates over time during gastrulation and axis elongation. Moreover, their expression domains in the AP axis roughly reflect their positions in the cluster (Figure 1.10). These characteristics of *Hox* genes are termed temporal and spatial collinearity respectively (reviewed in (Durston et al., 2011). Mutations in *Hox* genes generally cause transformations in the identity of vertebral elements (reviewed by (Mallo et al., 2010). For example, the lumbosacral region in *Hox10* mutants (carrying loss of function mutations in all members of

Hox10) appears to display thoracic-like characteristics (Wellik and Capecchi, 2003). However, *Hoxb13* is unique among all other *Hox* genes analysed to date due to its null mutation resulting in a longer axis. *Hoxb13*$^{-/-}$ embryos show an overall increase in somite size and an overgrowth in the tail with two extra posterior vertebrae (Economides et al., 2003). As far as is known, this is the only single gene mutation that can result in a longer tail. Precocious expression of Hoxb13 under the Cdx2 promoter (Cdx2 is expressed in the posterior progenitor zone from gastrulation to E12.5) causes a tail truncation in homozygous embryos. Loss-of-function mutations in other *PG13 Hox* genes do not affect axis elongation (Dolle et al., 1993; Fromental-Ramain et al., 1996; Godwin and Capecchi, 1998). However, precocious expression of other PG13 Hox genes also causes an axis truncation (Young et al., 2009). Collectively, these studies indicate that the expression of Hox13 is involved in the negative regulation of axis elongation.

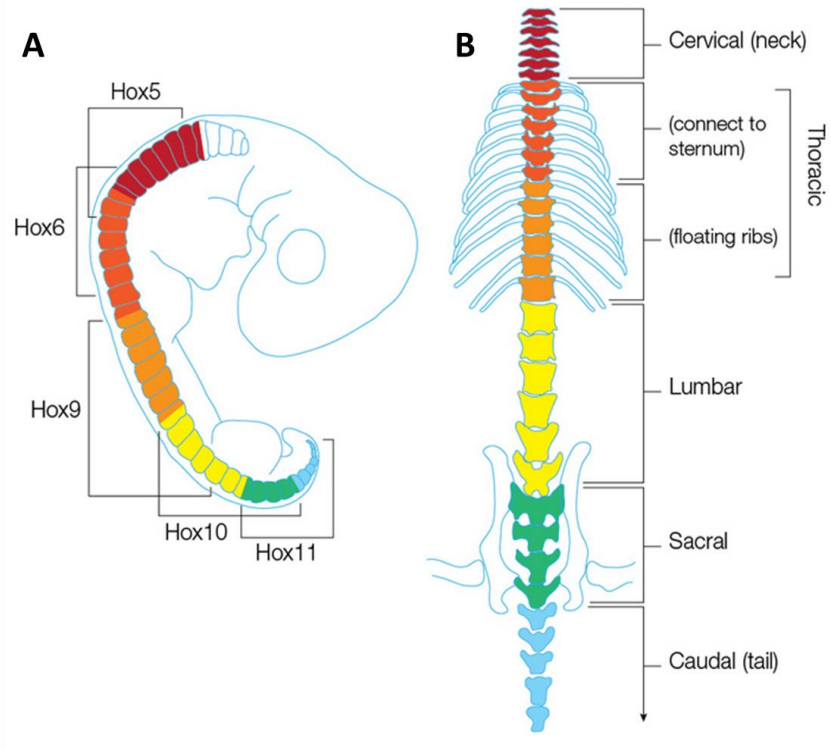

Figure 1.10. Hox patterning in mice

Regions of representative Hox gene activity in the somites of mouse embryos (A) and adult mouse vertebral column (B).

This is a reprint from http://learn.genetics.utah.edu/content/variation/hoxgenes/

Based on images in Wellik, 2007

Mouse embryonic stem cells (mESCs) and epiblast stem cells (EpiSCs)

Mouse ESCs derived from the ICM can integrate into the preimplantation embryo when injected into blastocysts, generating chimeras with a high efficiency (Brook and Gardner, 1997). This critical feature of mESCs demonstrates both their pluripotency, and their functional equivalence between mESCs and preimplantation epiblast in vivo.

Mouse EpiSCs are cell lines derived from the postimplantation epiblast from E5.5 to E8.0 presomite-stage embryos (Brons et al., 2007; Kojima et al., 2014; Osorno et al., 2012; Tesar et al., 2007). They can also be derived in vitro from mESCs (Guo et al., 2009) or directly from E3.5 blastocysts (Najm et al., 2011). As in the postimplantation epiblast (Arnold and Robertson, 2009; Pfister et al., 2007), self-renewing EpiSC populations also express lineage-specific markers such as *Foxa2, Dkk1, Sox17, Cer1, Nodal,* and *Fgf5* (Bernemann et al., 2011; Iwafuchi-Doi et al., 2012; Kojima et al., 2014; Teo et al., 2011; Tesar et al., 2007). Similar to mESCs, EpiSCs express the core pluripotency factors Oct4, Nanog, and Sox2, and are able to form teratocarcinomas and differentiate into multiple lineages in vitro (Brons et al., 2007; Tesar et al., 2007). Clonal sublines of EpiSCs can differentiate into derivatives of all three germ layers, indicating that EpiSCs are pluripotent rather than a heterogeneous population consisting of multiple lineage restricted cells (Brons et al., 2007).

Although both mESCs and EpiSCs are pluripotent cell lines, they still differ in several respects (for reviews, see (Chenoweth et al., 2010; Nichols and Smith, 2009, 2012; Osorno and Chambers, 2011). For example, EpiSCs depend on Activin and FGF2 for self-renewal, whereas mESCs depend on leukaemia inhibitory factor (LIF), while Fgf signalling stimulates differentiation. These two cell types are also distinguished by their morphologies: EpiSCs grow as flat, monolayered colonies, while ES cells form compact domed colonies. They also show different gene expression profiles, for example, *Klf4, Esrrb* and *Tbx3* expression is much lower in EpiSCs compared with that in mESCs. Moreover, female EpiSCs exhibit X chromosome inactivation, whereas mESCs do not. Crucially, unless EpiSCs are selected for rare subpopulations that resemble very early postimplantation epiblast (Han et al., 2010) or are genetically engineered to express a high level of E-cadherin (Ohtsuka et al., 2012), they are unable to contribute to chimeras upon blastocyst injection or morula aggregation.

Although mESCs and EpiSCs are two types of pluripotent cells, some studies show that the two states are interchangeable. When cultured in standard EpiSC medium, mESCs are able to transform into EpiSCs (Guo et al., 2009). However, it is relatively difficult (0.1%–1% efficiency) to generate mESCs by simply culturing EpiSCs in mESC medium (Bernemann et

al., 2011). Some studies have shown that overexpressing a single transcription factor, for example Klf4 or Nanog, can efficiently induce the reversion of EpiSCs (Guo et al., 2009; Silva et al., 2009). A recent study shows that a modified EpiSC culture condition with additional CHIR99021 (CHI), a GSK3β inhibitor, converts EpiSCs to pluripotent stem cells after 7-8 passages which are in an intermediate state between mESCs and EpiSCs. Interestingly, these cells can efficiently generate chimeras by blastocyst injection and contribute to the germline (Tsukiyama and Ohinata, 2014).

Human embryonic stem cells (hESCs), derived from human blastocysts, are also considered as pluripotent cells. They are able to form teratocarcinomas and differentiate into all three germ layers in vitro (Thomson et al., 1998). However, hESCs show some distinctions from mESCs such as their culture condition, clonogenicity, morphology and molecular profile (reviewed in (Nichols and Smith, 2009, 2012). Interestingly, the culture requirements and morphology of hESCs are similar to mouse EpiSCs. Therefore, it has been proposed that hESCs and EpiSCs are in a primed state of pluripotency, while mESCs may represent a naïve ground state of pluripotency. However, it should be noted that the gene expression profiles are different between hESCs and EpiSCs (Chia et al., 2010) and the precise relationship between these two cell types is still unclear. Recently, it has been shown that a short-term expression of Nanog and Klf2 transgenes in hESCs results in resetting them into a naive pluripotent state (Takashima et al., 2014).

Wnt signalling in EpiSCs

It has been suggested that EpiSCs are a heterogeneous population and contain subpopulations with distinct potentials (Han et al., 2010; Hayashi and Surani, 2009). A recent study in our group also demonstrated that there are lineage-biased subpopulations within undifferentiated EpiSCs (Tsakiridis et al., 2014). However, suppressing Wnt signalling in EpiSCs can reduce their heterogeneity (Sumi et al., 2013). These authors showed that that when a Wnt inhibitor (XAV939) is added to the EpiSC culture for 48 hours, the cells exhibit a more homogeneous morphology with a uniform expression of pluripotency markers. Moreover, the lineage specific markers such as *T, Mixl, Sox17* and *Cer1* are absent from XAV939 treated EpiSCs. Similarly, EpiSCs treated with WIF-1 (a Wnt antagonist) for 120 hours results in a significant reduction of the PS-like population and T expression (Tsakiridis et al., 2014). Deletion of β-catenin in EpiSCs also leads to an increase of Oct4, Sox2, and Otx2 expression and the reduction of differentiation markers (Sumi et al.,

2013; Tsakiridis et al., 2014). Although *β-catenin*$^{del/del}$ EpiSCs form smaller colonies, their cell growth is not affected. Therefore, these studies indicate that blocking Wnt signalling in EpiSCs does not affect their self-renewal but reduces their spontaneous differentiation and results in a more homogeneous population.

In contrast, elevation of Wnt signalling has been shown to induce mesoderm and endoderm differentiation in EpiSCs. Adding recombinant Wnt3a protein to EpiSC culture leads to an increase of the PS-like population (Tsakiridis et al., 2014). Similarly, stimulation of Wnt signalling in EpiSCs with CHI for 48 hours results in the upregulation of mesodermal and posterior neural markers but the downregulation of pluripotency genes and anterior neural makers (Sumi et al., 2013; Tsakiridis et al., 2014). However, it should be noted that EpiSCs treated with CHI for a longer period (7-8 passages) become mESCs-like cells (Tsukiyama and Ohinata, 2014) (A. Tsakiridis, personal communication). However, the reason why the different time scale of CHI treatment results in different cell types is still not clear. Since EpiSCs are considered as a heterogeneous population, one possibility could be that a subpopulation of mESCs-like cells in EpiSCs is selected after a longer culture time with additional CHI. Collectively, these results indicate that elevation of Wnt signalling for a short period induces the differentiation of EpiSCs and its inhibition to a more homogeneous population.

Scope of the thesis

As discussed in this chapter, cells in the posterior progenitor zone drive axis elongation. In mouse embryos there are bi-fated NM progenitors, of which some act as stem cell-like axial progenitors during axis elongation. Wnt and FGF signals are important for the maintenance of the posterior progenitor zone and may affect neural versus mesoderm differentiation of axial progenitors. However, many questions about NM progenitors remain unclear, for example, the distribution and number of this population during axis elongation, reasons for their loss and factors for their differentiation decision. The first part of my project was to investigate the characteristics, prevalence and the number of NM progenitors in axis elongation, together with their signalling requirements. In Chapter 2, I study the specification, persistence and loss of NM progenitors during axis elongation. In Chapter 3, I investigate the role of Wnt/β-catenin signalling in the maintenance and differentiation of NM progenitors.

The second part of my thesis will focus on testing the in vivo potential of pluripotent stem cell lines and their derivatives. Although pluripotent stem cell lines and cells differentiated

from them have been widely used for studying developmental biology, many of these studies are focused on characterizing these cells using in vitro methods. How in vitro cultured cells reflect in vivo populations and their behaviour when transplanted in vivo are important questions for stem cell research. Therefore, in Chapter 4 I investigate the potential of in vitro cultured stem cells and their derivatives in vivo using an ex vivo chimeric formation assay.

Chapter 2. The specification, persistence and loss of neuromesodermal progenitors during axis elongation

2.1 Spatiotemporal dynamics of neuromesodermal progenitors during axis elongation

2.1.1 Introduction and Aims

As mentioned in the previous chapter, coexpression of T and Sox2 is a strong candidate for a marker combination to identify NM progenitors in 2-5 somite stage (E8.5) mouse embryos (Tsakiridis et al., 2014). Although cells expressing both transcription factors (TF) have also been detected in the tail bud of zebrafish, chicken, and human embryos (Martin and Kimelman, 2012; Olivera-Martinez et al., 2012), $T^{+}Sox2^{+}$ domains have not been carefully mapped in any vertebrate throughout axial elongation. Here, I performed whole-mount double immunofluorescence for T and Sox2 in mouse embryos and imaged these samples using confocal microscopy to study the spatiotemporal dynamics of T and Sox2 expression during axial elongation. This will first demonstrate whether T/Sox2 coexpression marks NM progenitors over the entire axial elongation period. Secondly, based on the whole-mount confocal images, 3D images can be reconstructed showing the exact locations of $T^{+}Sox2^{+}$ cells and single TF positive cells in the posterior regions of the embryos. Thirdly, by taking advantage of image analysis software, I can quantify the number of $T^{+}Sox2^{+}$ cells and single TF positive cells at different stages.

2.1.2 Results

1. Expression of T and Sox2 during body formation (E8.5-E9.5)

Since T and Sox2 expression patterns have been previously demonstrated in early E8.5 embryos (2-5 somite stage) (Tsakiridis et al., 2014), I performed immunofluorescence staining on late E8.5 embryos (6-8 somite stage). The results showed that the expression of Sox2 was, as expected, strong in the neuroectoderm anteriorly and gradually decreased in the CLE in an AP direction (Figure 2.1B). Sox2 expression stretched posteriorly to L3 and PS3 but was barely detected in the posterior-most part of embryos (L4-5 and PS4-5). Some cells expressing high levels of Sox2 were detected at the base of the allantois and are most likely the primordial germ cells, which have been shown to reside there at this stage in development (Ohinata et al., 2005) (Figure 2.1B).

In E8.5 embryos, T was highly expressed in the notochord and ventral node. T expression was also detected in the CLE, the primitive streak, the nascent mesoderm and the proximal part of the allantois. Published *in situ* hybridisation and immunostaining data have also

confirmed these expression patterns (Cambray and Wilson, 2007; Herrmann, 1991; Inman and Downs, 2006; Tsakiridis et al., 2014). Notably, T expression in the CLE was high posteriorly and gradually decreased from posterior to anterior, in contrast with Sox2 expression in this area (Figure 2.1B).

At E8.5 the anterior limit of T^+Sox2^+ cells was at the anterior limit of the NSB (Figure 2.1B). In the NSB, T^+Sox2^+ cells were mainly restricted to the dorsal layer (Figure 2.1B). T^+Sox2^+ cells spread out laterally from the dorsal NSB to L3, forming a "heart" shape (Figure 2.1C). T^+Sox2^+ domains show extensive overlap with NM potent areas except for a few T^+Sox2^+ cells that appeared in the PS1-3 (Figure 2.1B).

At E9.5 T and Sox2 expression domains remained similar to those at E8.5. T expression was restricted to the posterior part of the neural plate, the notochord, the PSM, the developing tail bud mesoderm and the hindgut (Figure 2.2A-E). Sox2 expression was high in the neural tube fading out posteriorly and absent from the most posterior part of the epiblast which is considered to be equivalent to L4-5 at E8.5 embryos (Figure 2.2C). Sox2 expression was also detected in the hindgut and the CNH (Figure 2.2E, F). T^+Sox2^+ cells were observed in the CNH, the neural plate anterior to the CNH and the dorsal part of the posterior hindgut (Figure 2.2D-F).

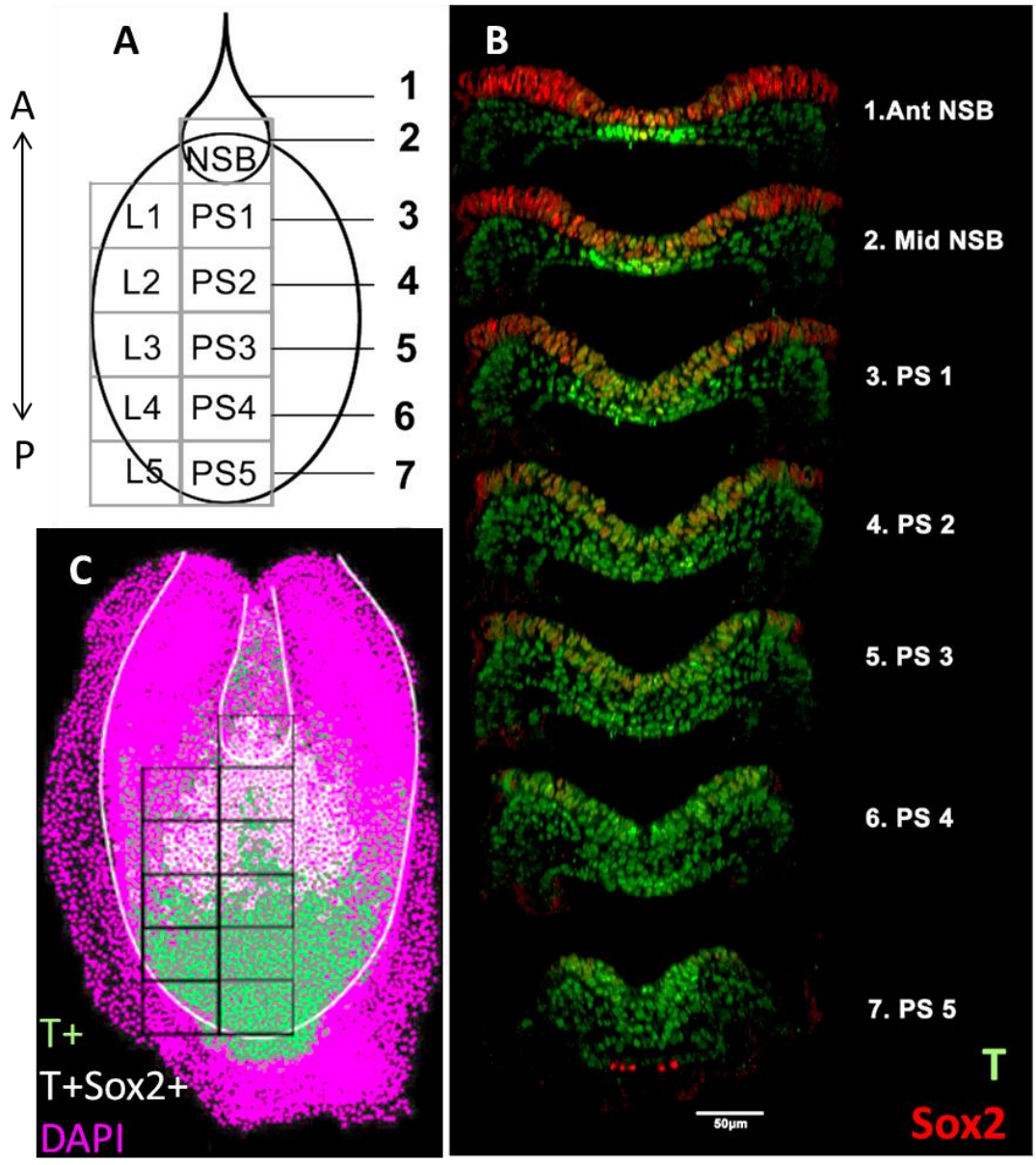

Figure 2. 1 **. T and Sox2 expression in the posterior of E8.5 embryos**

(A) Schematic diagram showing the subregions in the posterior of E8.5 embryos. A: anterior; P: posterior, L: caudal lateral epiblast; PS: primitive streak. The numbers in (A) correspond to those in (C).

(B) Confocal images of whole-mount immunostained E8.5 embryos (6-8 somite stage). Representative transverse sections showing Sox2 (red) and T (green) expression in the subsections indicated in (A)

(C) 3D reconstruction image generated from the sample in shown in (B). The black boxes correspond to those in (A), showing T+Sox2+ cells (white) are located in the NSB and L1-3. T+ cells in green and cells that do not express either T or Sox2 in magenta.

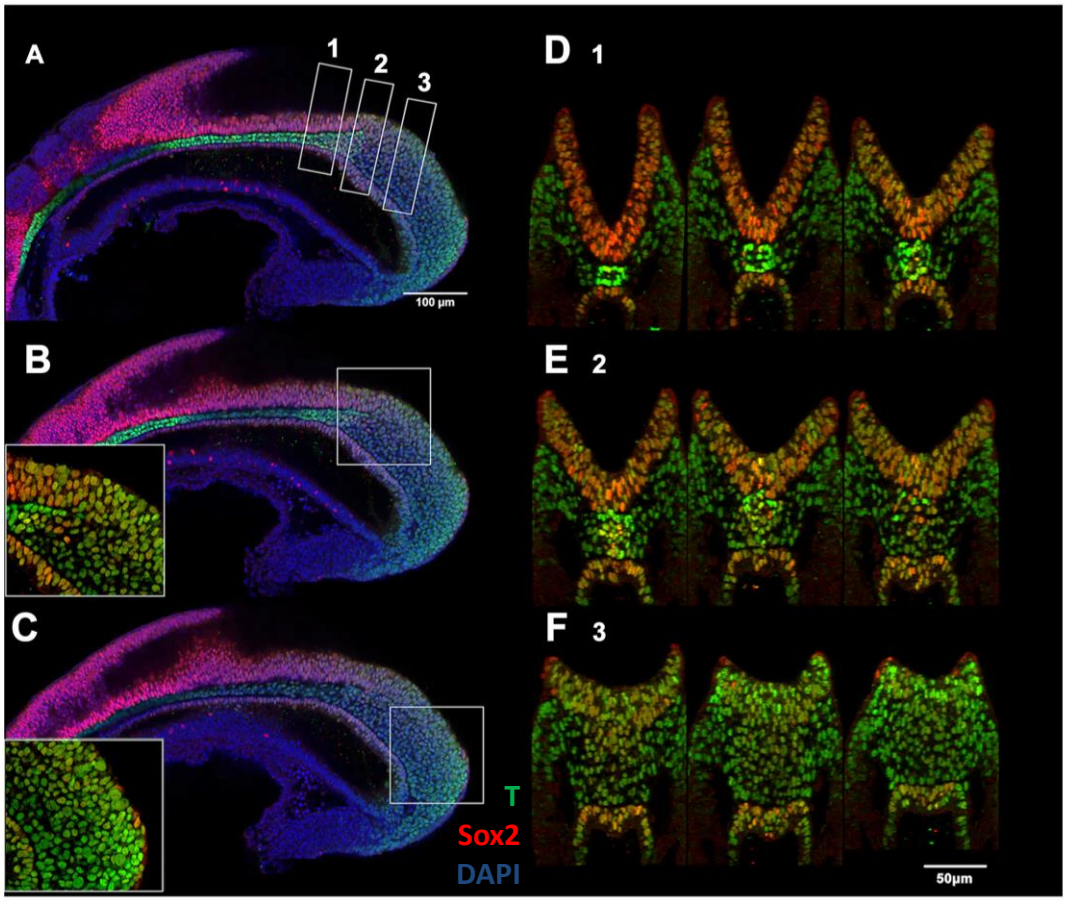

Figure 2. 2 . T and Sox2 expression in the posterior region of E9.5 embryos

Confocal images of whole-mount immunostained E9.5 embryos. Sox2 in red, T in green and DAPI-counterstain in blue.

(A) Representative sagittal section showing the midline of E9.5 embryos. Three small white boxes indicate approximate sectioning planes of the images in (D-F). (B, C) Sagittal section lateral to midline focusing on the ectoderm anterior (B) and posterior (C) to the CNH. Insets: enlargement of the area in the white box with the removal of blue channel.

(D-F)Transvers sections corresponding to the regions indicated by the white boxes in (A). (D) Sections anterior to the CNH. (E) The CNH sections (F) Sections posterior to the CNH.

2. Expression of T and Sox2 during early tail formation (E10.5 to E11.5)

T and Sox2 expression persisted in the tail bud after the closure of posterior neuropore. At E10.5, the strongest Sox2 expression was seen in the neural tube. Sox2 expressing cells were also detected in the tail gut and the CNH (Figure 2.3A, B). Expression of T was present in the tail bud and PSM, posterior neural tube and the tail gut, with the highest level in the notochord (Figure 2.3A.C). Notably, the Sox2 and T opposing gradient was still maintained within the tail bud (Figure 2.3B, C). At E10.5, $T^{+}Sox2^{+}$ cells were detected in the posterior neural tube, the CNH and the tail gut (Figure 2.3A-C). Interestingly, according to the 3D reconstructed image the rostral limit of $T^{+}Sox2^{+}$ cells coincided with T expression in the PSM (Figure 2.7C).

As the tail developed, some morphological changes were observed between E10.5 and E11.5. For example, at E11.5 the diameter of the posterior neural tube was reduced compared with that at E10.5 (Figure 2.3B, C and Figure 2.4B, C). In some E11.5 tails, the posterior of the tail gut was divided into two separate dorsoventrally arranged tubules (Figure 2.4C). This morphology was also observed in developing rat tails (Gajovic et al., 1993). However, the T or Sox2 expression domains remained similar between E10.5 and E11.5, as well as T/Sox2 coexpression domains. At E11.5 $T^{+}Sox2^{+}$ cells were still present in the posterior neural tube, the CNH and the tail gut (Figure 2.4B, C).

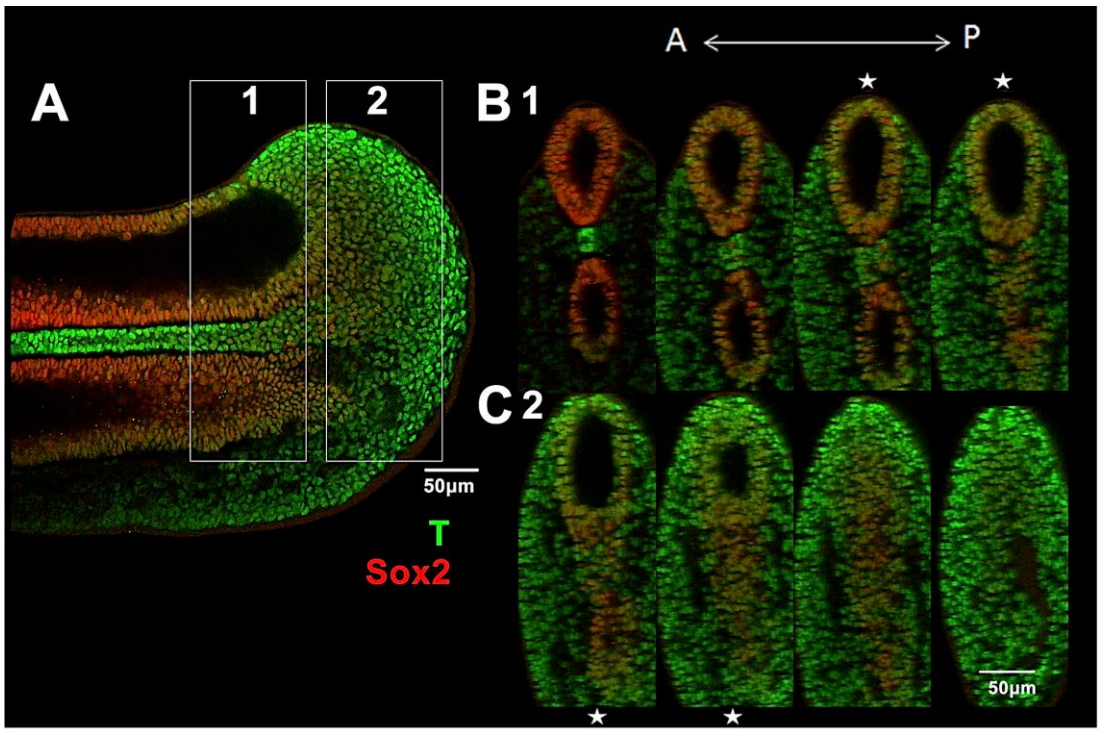

Figure 2. 3 . T and Sox2 expression in E10.5 tails

Confocal images of whole-mount immunostained E10.5 tails. (A) Representative sagittal section showing T (green) and Sox2 (red) expression. Two small white boxes indicate approximate sectioning planes of the images in (B-C). Transverse sections in the CNH are indicated by white stars. A: anterior; P: posterior.

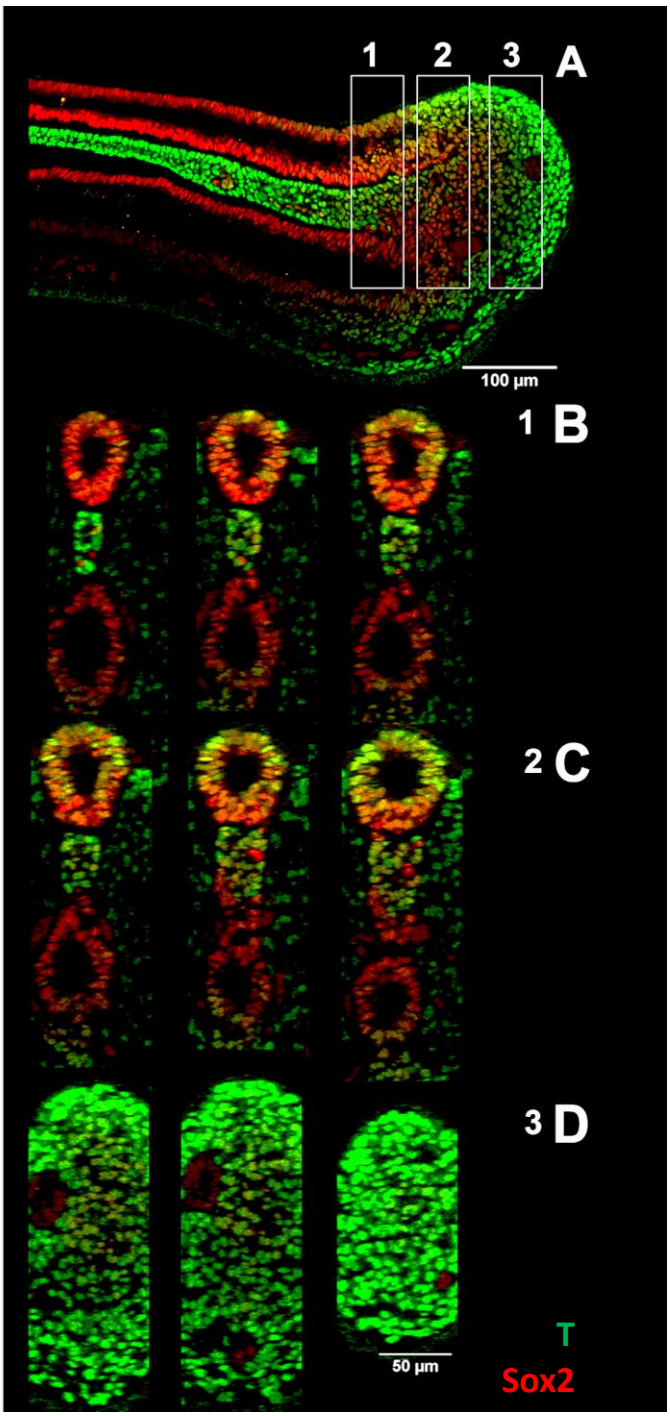

Figure 2. 4 . T and Sox2 expression in E11.5 tails

Confocal images of whole-mount immunostained E11.5 tails. (A) Representative sagittal section showing T (green) and Sox2 (red) expression. Three small white boxes indicate approximate sectioning planes of the images in (B-D). (B) Transverse sections anterior to the CNH. (C) The CNH sections (D) Sections posterior to the CNH.

3. Expression of T and Sox2 during late tail formation (12.5 to E13.5)

The shape and structure of the tail bud alters during late tail formation and has been described before (Wymeersch, 2011). However, the overall tail bud structure is maintained at E12.5. Also, Sox2 or T expression domains were not much different compared to previous tail stages: $Sox2^+$ cells were detected in the neural tube, the CNH and the tail gut; T^+ cells were present in the tail bud, PSM, CNH and tail gut with the highest level in the notochord (Figure 2.5C-D). T^+Sox2^+ cells were situated in the posterior part of the neural tube, the CNH and the tail gut (Figure 2.5C-D).

From E12.5 to E13.5, the overall tail bud dimensions were smaller and cells appeared more condensed (Figure 2.5). As described before (Wymeersch, 2011), one of the most prominent features of the E13.5 tail bud is a flattened neural tube that slightly bends over the notochord, which I also noted in my samples (Figure 2.5F, Figure 2.6A,B and Figure 2.7F). In mouse embryos, axis elongation ends around E13.5 after the formation of 65 somites in total. Therefore, I examined T and Sox2 expression in two different stages at E13.5: just before the end of axis elongation (62-63 somites) and after axis elongation ceases (65 somites).

At 62-63 somites, Sox2 or T expression domains remained similar to those in E12.5 tails and T^+Sox2^+ cells were dispersed in the posterior end of the flattened neural tube and the notochordal plate (Figure 2.5F,G and Figure 2.7F). In embryos that had completed somitogenesis (65 somites), $Sox2^+$ cells were still detected in the neural tube and T^+ cells in the notochord and tail bud mesoderm. However, the size of the tail bud mesoderm was drastically reduced in 65-somite stage tails, as indicated by the shrinkage of the T expression domain in the posterior (Figure 2.6B and Figure 2.7F). Moreover, compared with 62-63-somite stage, the number of T^+Sox2^+ cells was also much reduced in 65-somite stage tails, with only very few T^+Sox2^+ cells located close to the tip of the tail.

Notably, in the previous stages (E9.5 to E13.5 62-63 somites), the end of the neural tube indicated by T^+Sox2^+ or $Sox2^+$ cells was also adjacent to the T expressing mesodermal cells (Figure 2.7B-F). However, after the cessation of the axis elongation (65 somites), the neural tube appeared to separate from the T^+ tail bud mesoderm cells (Figure 2.6A, B), implying that contact between T^+ tail bud mesoderm cells and the neural tube may positively influence the maintenance of T^+Sox2^+ and/ or the axis elongation.

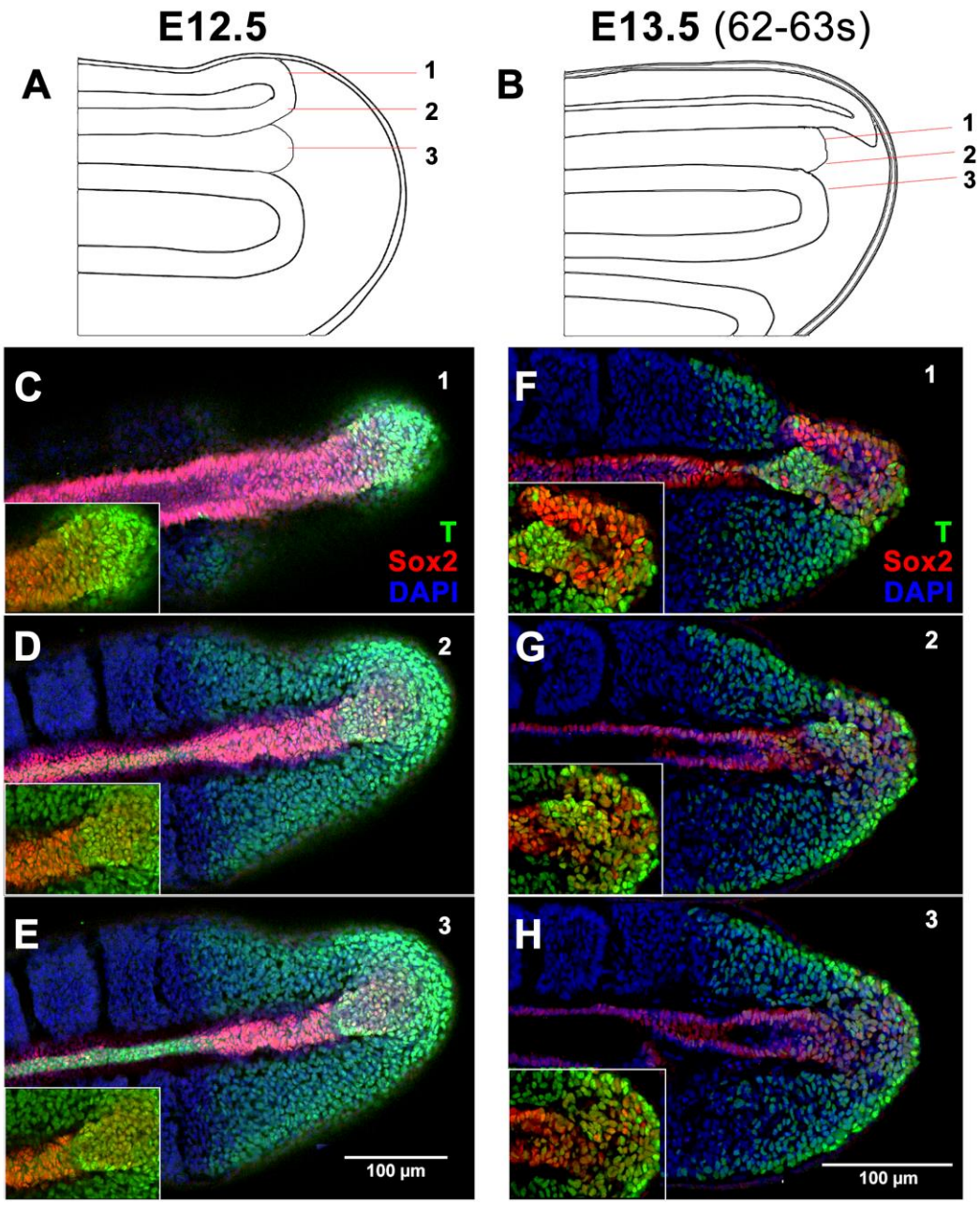

Figure 2. 5 . T and Sox2 expression in E12.5 and E13.5 tails

(A and B) Schematic diagrams showing the morphology of tails at E12.5 and E13.5 (62-63 somite stage. Approximate sectioning planes of the images in (C-H) are indicated by the red lines.

Confocal images of E12.5 (C-E) and E13.5 (F-H) tails. Sox2 in red, T in green and DAPI-counterstain in blue. Insets: enlargement of the area containing $T^{+}Sox2^{+}$ cells. Blue channel was removed for a clearer illustration.

4. Expression of T and Sox2 at the end of axis elongation (E14.5)

At E14.5, the tail bud structure maintained over the previous three days became largely unrecognisable. The neural tube and tail gut were both absent, leaving behind a compacted mesenchymal cell mass, containing the notochord in the middle, and surrounded by a multi-layered surface epithelium (Figure 2.6C, D). In tails, T expression was only detected in the posterior notochord, while Sox2 expression was completely absent, consistent with the absence of the neural tube (Figure 2.6C). Thus, there were no $T^{+}Sox2^{+}$ cells at E14.5.

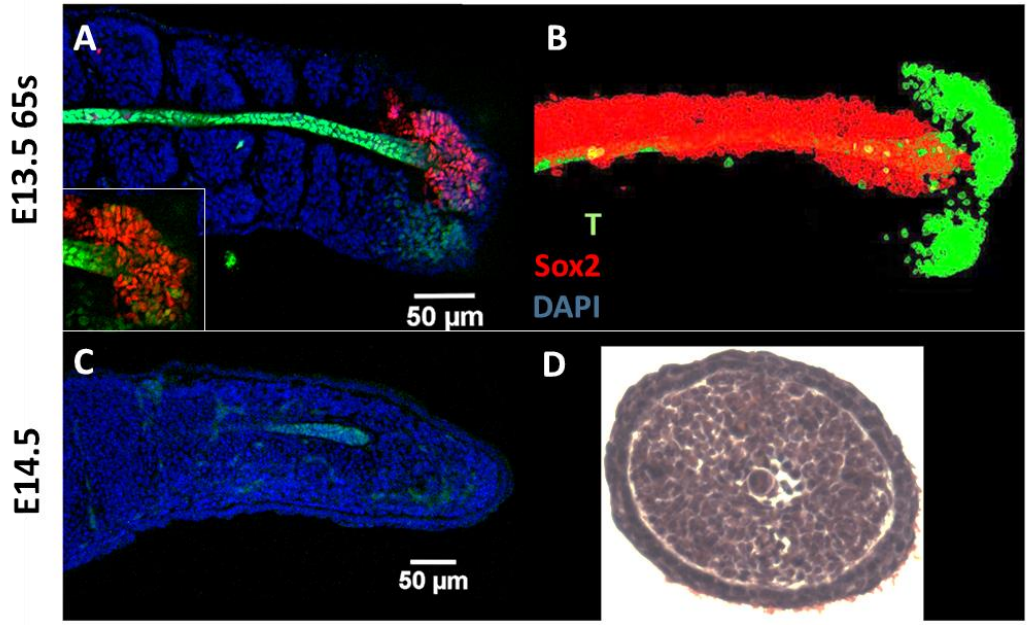

Figure 2. 6 . T and Sox2 expression in E13.5 and E14.5 tails

Confocal images of E13.5 (65-somite stage) (A) and E14.5 (C) tails. Sox2 in red, T in green and DAPI-counterstain in blue. Inset: enlargement of the area containing $T^{+}Sox2^{+}$ cells. Blue channel was removed for clearer illustration.

(B) 3D reconstruction image generated from the same sample in (A). (D) Hematoxylin and eosin staining of an E14.5 transverse section, showing the disappearance of the neural tube at this stage.

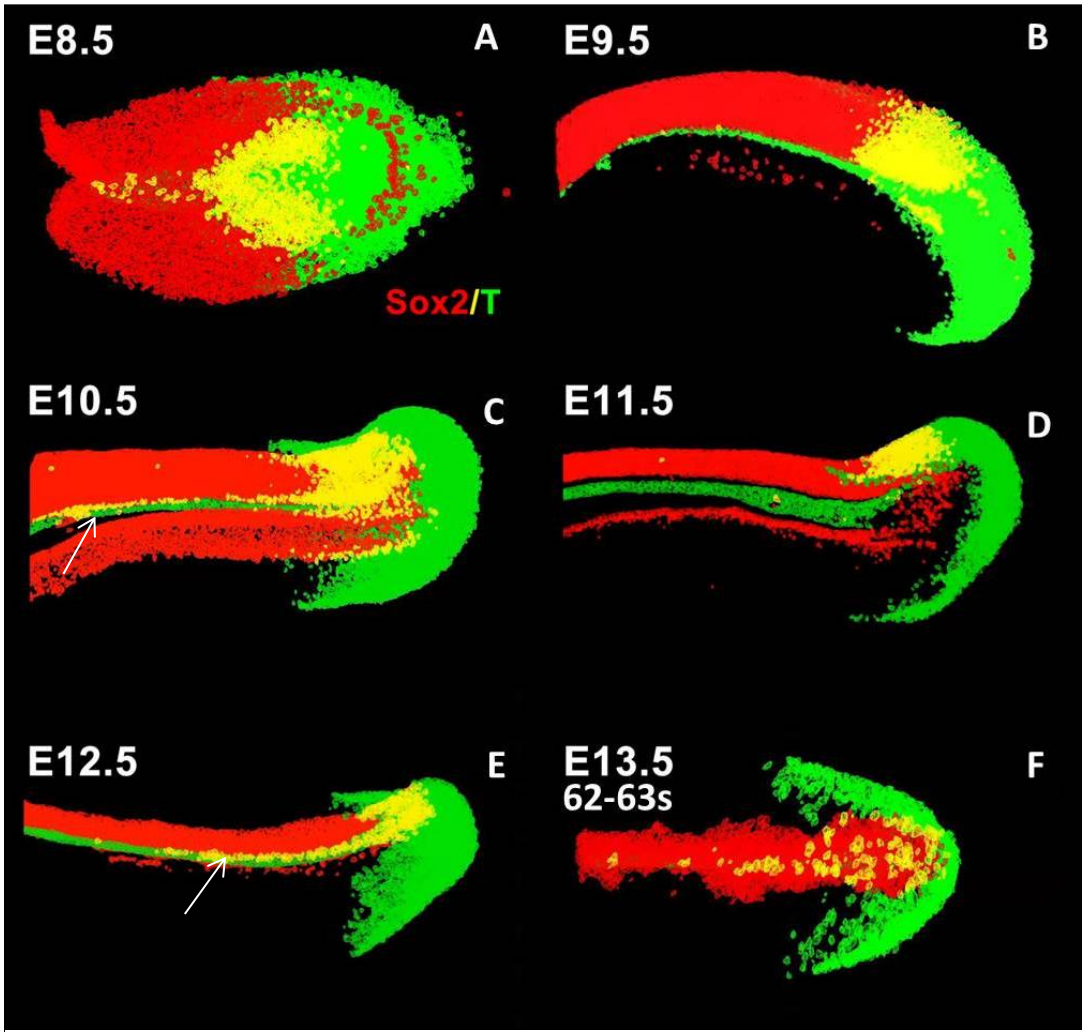

Figure 2. 7 . 3D reconstruction of E8.5 to E13.5 embryos

(A-F) 3D reconstructions of whole-mount immunostained embryos generated from confocal z-stacks, showing T and Sox2 are expressed continuously throughout axis elongation in a similar pattern. Sox2 in red, T in green, $T^{+}Sox2^{+}$ cells in yellow. The white arrows indicate $T^{+}Sox2^{+}$ cells in the anterior notochord. This is probably caused by a segmentation error (see discussion).

2.1.3 Conclusion and discussion

1. T^+Sox2^+ domains overlap extensively with NM potent areas during axis elongation

I used whole-mount immunofluorescence staining and 3D reconstructed images to illustrate the continuity of T^+Sox2^+ cells throughout axis elongation (E8.5-E13.5) and the loss of T^+Sox2^+ cells after the axis is fully formed. At E8.5 T^+Sox2^+ cells are mainly detected in locations containing NM progenitors (the dorsal layer of the NSB and L1-3). From E9.5 to E13.5, T^+Sox2^+ cells also persist in the CNH where the NM progenitors are suggested to be during tail bud stages. Therefore, T^+Sox2^+ domains overlap extensively with NM potent areas in the embryos.

Notably, T/Sox2 coexpression domains are wider than the NM potent regions that have been identified. For example, some T^+Sox2^+ cells are present in the primitive streak midline at E8.5. During tail bud stages (E10.5-E12.5), T^+Sox2^+ cells are also detected in the posterior neural tube and the tail gut. Since T^+Sox2^+ cells spread wider than the identified NM potent regions, it raises the question: are all T^+Sox2^+ cells are equivalent to NM potent cells?

The potency of cells in the very anterior primitive streak (PS1) has been tested. Previous results showed that, while the anterior primitive streak midline at E8.5 (2-5 somites) almost exclusively produced mesoderm, very occasionally neuroectoderm was also colonised when this tissue was grafted into the NSB (Cambray and Wilson, 2007). The low efficiency of neural contribution may therefore result from the low percentage of T^+Sox2^+ cells in the PS1 (Figure 2.1B). Therefore, it is possible that T^+Sox2^+ cells in the single lineage fated areas such as the primitive streak and posterior neural tube may still have the potential to give rise to other lineages when placed in an appropriate environment. However, the potential of the posterior neural tube and tail gut, which also contain T^+Sox2^+ cells has never been investigated, and heterotopic grafts of these tissues to the NSB of E8.5 embryos would be required to investigate whether these cells are able to give rise to both neural and mesodermal tissues.

2. The possible effects of T expression on neural progenitors

According to my staining, there are T^+Sox2^+ cells in the posterior neural tube where the neural tube is separated from the surrounding mesoderm by a fibronectin-rich basal lamina (Figure 2.3B and Figure 2.4B,C). It is very likely that these cells are only fated to be

neuroectoderm. As mentioned in the introduction, fate maps and retrospective clonal analysis indicate that neural progenitors are located in the posterior most neural tissues (Brown and Storey, 2000; Roszko et al., 2007). According to the position of $T^{+}Sox2^{+}$ cells in the neural tube, it is likely that they are neural progenitors. It is known that Sox2 is a marker for neural stem cells and is important for neurogenesis (Ferri et al., 2004; Gomez-Lopez et al., 2011). However, the role of T expression in neural progenitors is still unclear.

A recent study shows that $T^{-/-}$ ESCs can upregulate neural markers such as β-Tubulin, suggesting neural differentiation is not dependent on T expression (Gouti et al., 2014). In WT embryos, cells in the dorsal neural tube show higher mitotic activity than in the ventral region. However, this pattern is absent in embryos heterozygous for the *T* mutation, indicating that T expression may influence the cell proliferation rate in the neural progenitors. (Yanagisawa and Kitamura, 1975). Another possibility is that the additional T expression indicates mesoderm differentiation potential in these neural progenitors. Thus, although T is not required for neural differentiation, it may play a role in modulating cell proliferation or may be required to maintain mesoderm potency of NM progenitors.

3. No $T^{+}Sox2^{+}$ cells in the anterior notochord

Some 3D reconstructed images show a low frequency of $T^{+}Sox2^{+}$ cells in the anterior notochord (yellow cells indicated by white arrow in Figure 2.7C, E). However, as far as is known neither Sox2 transcripts nor protein have been reported in the notochord anterior to the newly formed somite. In my opinion, these $T^{+}Sox2^{+}$ cells apparently present in the anterior notochord may be due to the limitation of the nuclear segmentation software during 3D reconstruction. As mentioned in the materials and methods, our current workstation could not process the large volume of data collected by the confocal microscope. For the 3D reconstruction I first had to scale down the DAPI images for the segmentation, which may have caused an overestimation of the nuclear size in some cells. Therefore, it is possible that in some areas where the neural tube is very close to the notochord, the computed volume of notochord cells may expand to their adjacent neural cells, which results in the mistakenly shown T/Sox2 coexpression in some anterior notochord cells.

4. The role of $T^{+}Sox2^{+}$ cells in the hindgut is unclear

According to the staining, it is clear that both T and Sox2 proteins are expressed in the hindgut (Figure 2.2D, F, 2.3B and 2.3C), where their transcripts have also been detected in a

previous study (Wymeersch, 2011). $T^{+}Sox2^{+}$ cells in the hindgut are unlikely to have either neural or mesodermal differentiation potential since this would imply pluripotency- i.e. differentiation to all three germ layer derivatives in these hindgut cells However pluripotency is undetectable in embryos from early somitogenesis (E8.0) (Osorno et al., 2012). Therefore, T and Sox2 may have a novel function in gut development unrelated to the neuromesodermal progenitor phenotype. One study indicates that Sox2 expression in the gut inhibits differentiation and maintains the plasticity of the primitive gut (Raghoebir et al., 2012). Microarray analysis of gastrulation in sea urchin embryos carrying brachyury mutations has identified a group of endoderm genes which may be a direct target of brachyury. Some of these genes are cytoskeletal modulators or expressed in the archenteron, suggesting brachyury may play a role in gut morphogenesis or be related to its functions (Rast et al., 2002). However, since few studies have been carried out to investigate the functional effects of T or Sox2 in the endoderm, their roles in mouse gut development are still unclear.

2.2 Quantitative analysis of NM progenitors from E8.5 to E13.5

2.2.1 Aims

Several interesting observations arise from examining the T/Sox2 staining images: (1) the levels of Sox2 and T expression appeared to form a reciprocal gradient within the double positive areas: cells in the anterior region expressed higher Sox2, while more posterior cells expressed higher T (Figure 2.1B, 2.2D-F, 2.3B,C and 2.4B-D); (2) T^+Sox2^+ cells appeared to express relatively low levels of both proteins compared with $Sox2^+$ cells in the anterior neural tube and T^+ cells in the tail bud mesoderm (Figure 2.1C, 2.2E, 2.3B and 2.4C); (3) the coexpression domains appeared to reduce in size from E10.5 to E13.5 (Figure 2.7C-F). To further confirm these observations, confocal images were further analysed. Image analysis software was used to determine the relative T and Sox2 expression levels in each cell and to calculate the number of T^+Sox2^+ cells at each developmental stage.

2.2.2 Results

1. T^+Sox2^+ cell numbers peaked at E9.5 and gradually declined until the end of axis elongation

To determine the number of T^+Sox2^+ cells, DAPI nuclear counterstained confocal z-stack images were used to create nuclear volumes in which the average fluorescence intensity of Sox2 and T in each cell could be quantified as described previously (see also the materials and methods charter) (Tsakiridis et al., 2014). Figure 2.8A shows the absolute numbers of T^+Sox2^+ cells at different developmental stages. There was a significant peak at E9.5 and then a gradual reduction afterwards (Figure 2.8A, B). The number of T^+Sox2^+ cells was minimal when the embryos formed 65 somites at E13.5, suggesting a strong correlation between the loss of NM progenitors and the end of axis elongation.

It should be noted that due to the thickness of the samples, very lateral PSM only expressing T was not imaged in E10.5 and E11.5 tail samples. Ventral gut and tissues below it were not imaged in E12.5 and E13.5 samples. All the imaged samples varied in their anterior limits but contained all T^+Sox2^+ areas in the posterior region of the embryos. Therefore, it is difficult to determine the changes of single T^+ or $Sox2^+$ cells in the tail bud during axis elongation based on the images I acquired (Figure 2.8C, D).

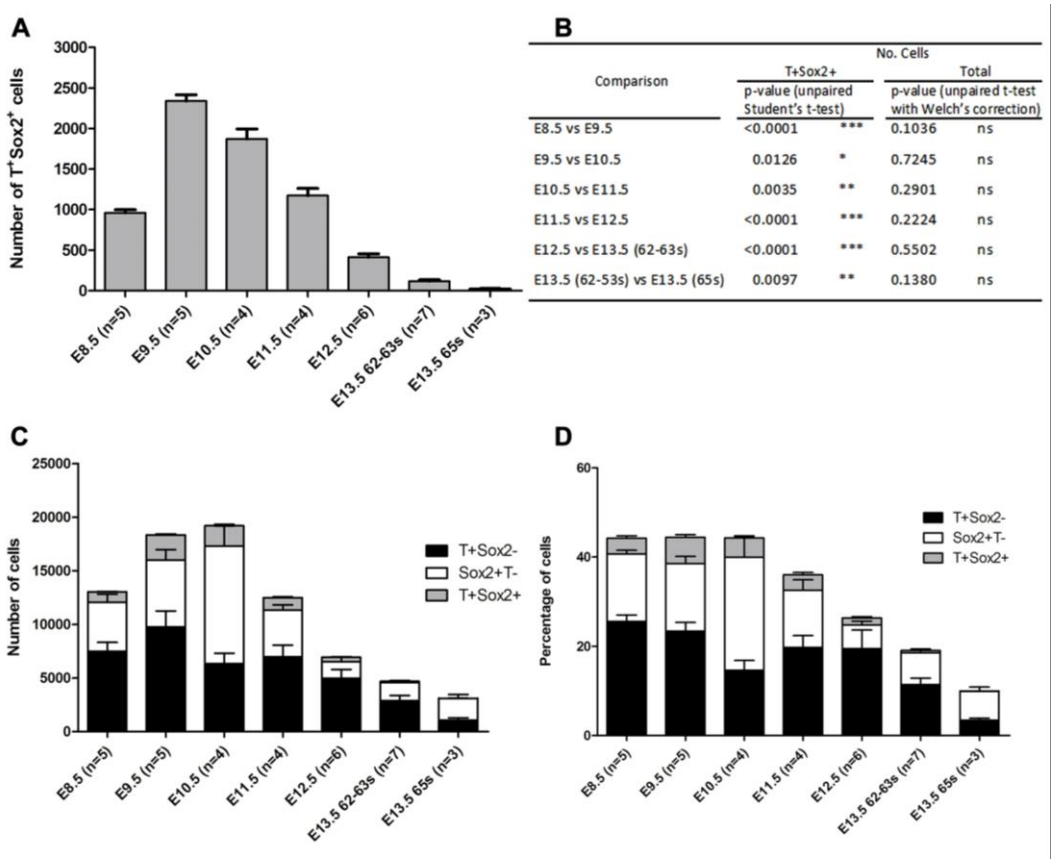

Figure 2. 8 . Quantitative analysis of T^+Sox2^+ cells from E8.5 to E13.5

(A) The absolute numbers of T^+Sox2^+ cells in the posterior of the embryos during axis elongation (mean±s.d.).

(B) Changes in the number of T^+Sox2^+ cells are statistically significant between consecutive stages.

Comparison of the number (C) and the percentage (D) of T^+Sox2^-, $Sox2^+T^-$ and T^+Sox2^+ cells in the posterior regions I imaged. Note: All the imaged samples varied in their anterior limits but contained all T^+Sox2^+ regions in the posterior of the embryos (mean±s.d.). Therefore, no statistical analysis was applied to compare T^+Sox2^- and $Sox2^+T^-$ cells in the images.

2. T^+Sox2^+ cells expressed low levels of both proteins

As mentioned in the materials and methods, the volume of data collected by the confocal microscope was too large for the processing power of the workstation for image analysis. To reduce the data volume, I divided each sample into 2 or 3 subregions for the quantification of T and Sox2 intensity in each cell. The results are shown in the dot plots (Figure 2.9). The majority of T^+Sox2^+ cells expressed relatively low levels of both T and Sox2 proteins compared with the maximum intensity of single T or Sox2 expressing cells in each sample (Figure 2.9). Notably, in the double positive population the levels of T and Sox2 expression appear to be anticorrelated, suggesting there may be a reciprocal inhibition between these two TFs in NM progenitors.

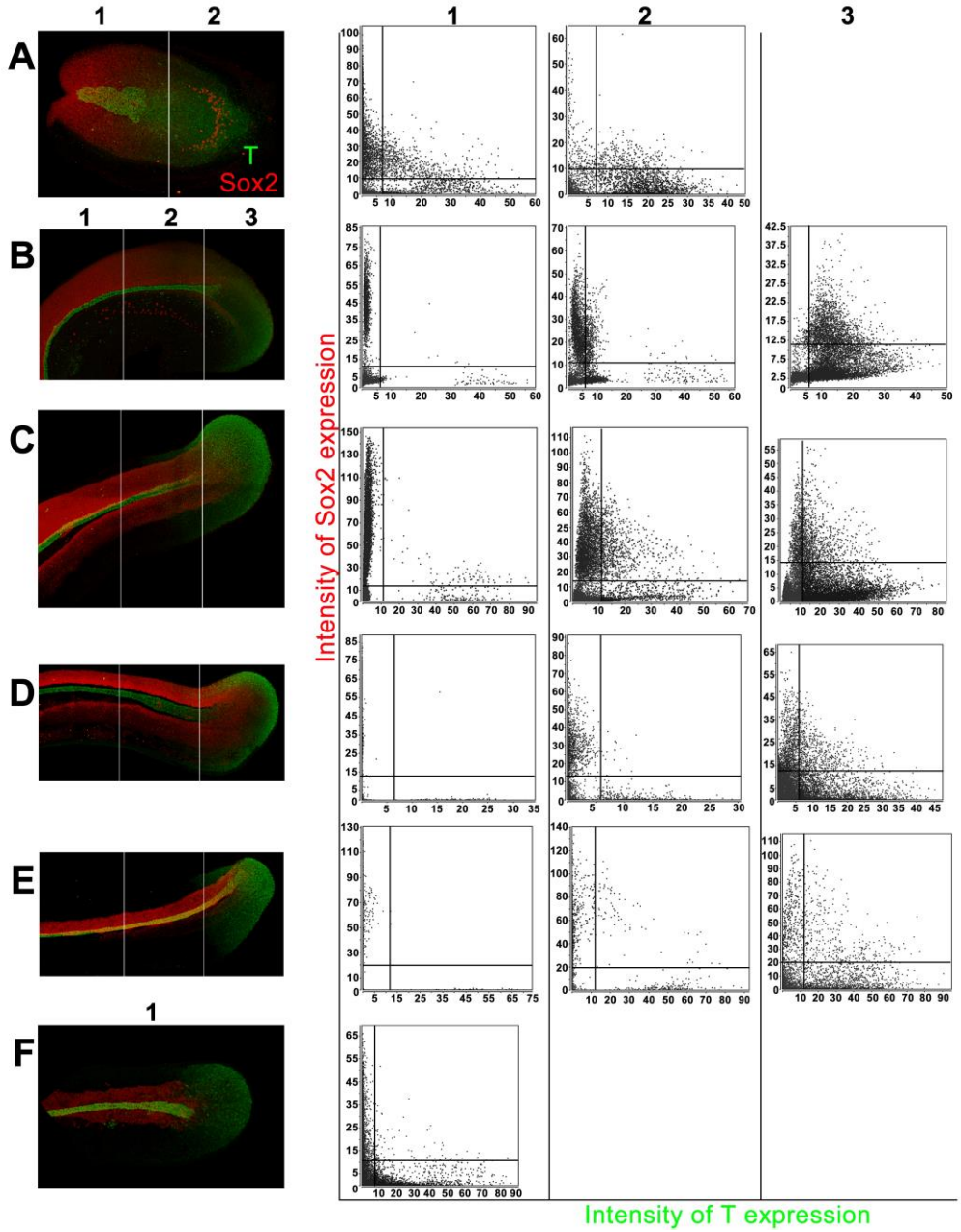

Figure 2. 9 . The levels of T and Sox2 expression in T^+Sox2^+ cells during axis elongation

(A-F left plane) Representative embryos showing T (green) and Sox2(red) expression at each stage.

Generally, a confocal z-stack was cropped into two or three parts for quantitative analysis. (A-F right planes) Dot plots showing T and Sox2 expression levels in all the cells in each part of the confocal images. Note: anticorrelation between high levels of both T and Sox2 expression in T^+Sox2^+ cells.

2.2.3 Conclusion and discussion

1. Reasons for the significant drop in T^+Sox2^+ cell numbers after E9.5

It has been shown that the PSM size increases during early somitogenesis with a peak at about the 30-somite stage and then gradually decreases until the end of somitogenesis (Gomez et al., 2008; Tam, 1986). The size of somites at the time of segmentation varies and also reaches a maximum at E10.5 around 30-35 somite stages (Gomez et al., 2008). The switch from PSM and somite expansion to shrinkage corresponds to the time at which there is a reduction of T^+Sox2^+ cells (Figure 2.8A). Therefore, it is possible that the increase in T^+Sox2^+ cells drives the increase of PSM size, which then results in the enlargement of the somites. During tail bud stages there is no obvious change in the rate of somite formation but there is a drop in the somite size, which would therefore suggest that a smaller number of progenitors is required. The significant reduction of T^+Sox2^+ cell numbers after E9.5 result from (1) apoptosis; (2) a decrease in cell proliferation rate; (3) cell differentiation and exit from the progenitor zone. I will consider each of these in turn.

(1) Apoptosis

Whole-mount TUNEL staining shows that at E9.5 there are localized apoptotic cells in the posterior neuropore (Massa et al., 2009). In this study, I show that cells in this region are coexpressing T and Sox2. Therefore, it is possible that apoptosis is one of the reasons for the drop of T^+Sox2^+ cells from E9.5 to E10.5. However, in the later stages (E10.5-E13.5), apoptotic cells are not specifically located in any T^+Sox2^+ regions (Wymeersch, 2011). Thus, it is unclear whether apoptosis is the causative factor for the further reduction of T^+Sox2^+ cells after E10.5.

(2) A decrease in proliferation rate

Our microarray analysis does not show a significant change of Cyclins and Cyclin-dependent kinases in NM progenitors during axis elongation (Wilson lab, unpublished data). Moreover, the investigation of cell proliferation rate in the mouse tail bud has been previously conducted (Kokubu et al., 2004; Ukita et al., 2009; Wymeersch, 2011). These studies show that cell proliferation in the neural tube, PSM and tail bud mesoderm appears to be constant from E9.5 to E13.5. Although a reduction of cell proliferation rate is detected in the notochord and the tail gut in E12.5 and E13.5 tails (Wymeersch, 2011), no study has reported an obvious reduction of cell proliferation rate in any T^+Sox2^+ regions. Therefore, it

is unlikely that the dramatic drop in T^+Sox2^+ cell numbers depends mainly on a reduction in their cell proliferation rate.

(3) Differentiation

When T^+Sox2^+ cells differentiate to committed lineage progenitors, they have to downregulate one of the TFs. Therefore, the loss of T^+Sox2^+ cells is associated with cell differentiation. Although the factors for inducing differentiation of T^+Sox2^+ cells are not unknown, many studies have shown that Wnt and FGF signals are important for the maintenance of the posterior progenitor zone (see introduction). Moreover, Wnt3a directly regulates T expression via Wnt/β-catenin signalling (Galceran et al., 2001; Yamaguchi et al., 1999b). Therefore, it is possible that downregulation of Wnt and FGF signals favours the differentiation of T^+Sox2^+ cells. Consistent with this hypothesis, our microarray analysis shows an overall reduction of Wnt and FGF signals in E10.5 to E13.5 CNH samples (Wilson lab, unpublished data). It is worth noting that the number of T^+Sox2^+ cells drops after E9.5, while the general reduction of Wnt and FGF signals (including ligands, receptors and targets) in NM progenitors occurs after E10.5. The NM progenitor pool shrinks before the general reduction of Wnt and FGF signals. We tried to identify which gene expression patters correlate with the change of T^+Sox2^+ cells. Unlike other Wnt proteins, the transcripts of *Wnt3a* in NM progenitors start to decrease at E9.5 (Wilson lab, unpublished data). Therefore, it raises the possibility that a decrease in Wnt3a induces the differentiation of T^+Sox2^+ cells from E9.5 to E10.5. An attenuation of Wnt and FGF signalling after E10.5 causes a further reduction of T^+Sox2^+ cells in the tail bud stages.

It has been shown that retinoid signalling plays an important role in the cessation of axis elongation in chick embryos. The onset of *c-Raldh2* expression and RA activity are associated with localized cell death and repression of Fgfs in the chick tail bud, which further leads to the end of axis elongation (Olivera-Martinez et al., 2012; Tenin et al., 2010). Although *Raldh2* transcripts are detected in the mouse tail bud (Tenin et al., 2010), retinoic acid response element (RARE)-$LacZ^+$ cells do not appear in any T^+Sox2^+ regions in the tail bud (E10.5-E13.5) of RA activity reporter mouse embryos. This indicates that there is no endogenous RA activity in the mouse tail bud. This is also consistent with there being no obvious localized cell death detected in the mouse tail bud (Wymeersch, 2011). Moreover, our microarray analysis shows that retinoid signalling reduces in NM progenitors from E8.5 to E10.5 and remains at a similar level in the CNH from E11.5-E13.5 (Wilson lab, unpublished data). Collectively, there is no direct link between retinoid signalling and the

end of axis elongation in mouse embryos. It has also been proposed by Oliver *et al.* that the mechanism for the cessation of axis elongation may differ between mouse and chick embryos. Therefore, the role of retinoid signalling in the reduction of T^+Sox2^+ cells is still unknown.

2. A reciprocal inhibition between Sox2 and T expression

In this study, I showed that T^+Sox2^+ cells expressed lower levels of both TFs compared with $Sox2^+$ cells in the anterior neural tube and T^+ cells in the notochord. In T^+Sox2^+ cells, the levels of T and Sox2 expression appear to be anticorrelated (Figure 2.9A-E). Moreover, it has been previously shown that an ectopic neural tube forms in *T/T* mutants (Yamaguchi et al., 1999b). Also, deletion of both Sox3 and the N1 enhancer of Sox2 resulted in the production of more mesoderm cells from the primitive streak (Yoshida et al., 2014). Therefore, all these results suggest there may be a reciprocal inhibition between Sox2 and T expression in neural vs mesodermal fate choice. Expressing low levels of both TFs in NM progenitors may provide them with the potential to differentiate to neural or/and mesodermal cells.

Variable T and Sox2 levels are observed within the double positive population (Figure 2.9A-F). It is possible that the levels of TF expression correlate with the fate choice of T^+Sox2^+ cells. This is supported by the observation that some subregions, containing cells that recently chose neural or mesodermal fates, show high levels of T or Sox2, but not both (Figure 2.1 B, Figure 2.2 D-F, Figure 2.3 B, C and Figure 2.4 B, C). For example, the posterior neural tube expresses high Sox2 but low T (Figure 2.2D-F). To better illustrate subregions within T^+Sox2^+ domains, the image analysis software will be updated allowing the identification of the location of each cell with the specific T and Sox2 expression levels (G. Blin, personal communication). This would help to further reveal how T and Sox2 expression levels are linked to the fate choices of NM progenitors.

2.3 NM progenitors are not committed at late-streak to early bud stages (E7.5)

2.3.1 Aims

T^+Sox2^+ cells initiate in the dorsal layer of the node at the headfold stage (E8.0) (Wilson lab, unpublished data from F. Wong, Figure 2.10). There are no T^+Sox2^+ cells in the preceding stages including late-streak or bud stages (E7.5) (F. Wong, personal communication). Prospective clonal analysis by labelling a single cell with HRP shows that the derivatives of distal epiblast at LS-EB stages (E7.5) contribute to the dorsal part of the NSB (Forlani et al., 2003), where the NM progenitors reside. It is worth noting that since the precursors for dorsal NSB and L1-3 have not been extensively investigated, so far cells in the distal epiblast at the headfold stage (E7.5) are the only ones that have identified as the precursors of NM progenitors at E8.5. It has been shown that distal epiblast at LS-EB stages (E7.5) expresses Sox2 but not T (Iwafuchi-Doi et al., 2012) (F. Wong, personal communication). In this study, I intended to investigate whether the precursors of NM progenitors are determined before they start to coexpress T and Sox2. To address this question, I aimed to graft distal epiblast at LS-EB stages (E7.5) to the NSB of E8.5 (2-5 somite stage) embryos. However, it is technically difficult to separate the epiblast (dorsal cells) from the cells underneath (ventral cells) by manually dissecting (Figure 1.3A). Therefore, I grafted distal cells (both layers) from LS-EB stage embryos (E7.5) to the NSB of E8.5 (2-5 somite stage) embryos and then assessed their contribution in the host embryos after culture.

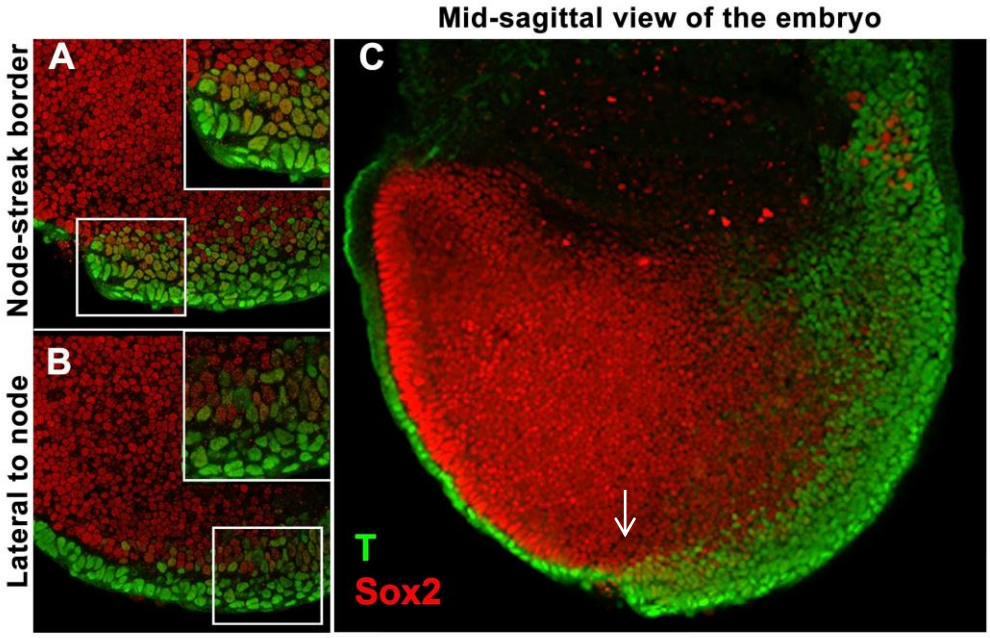

Figure 2.１０. T and Sox2 expression in a headfold stage embryo (E8.0).

Confocal sections of a wholemount immunostained headfold stage embryo. Sox2 in red, T in gree.

(C) Representative sagittal section showing the midline of the embryo. $T^{+}Sox2^{+}$ cells are found in the node areas (arrow).

(A and B) Enlargements of node area in (C). $T^{+}Sox2^{+}$ cells are present in dorsal layer of NSB (A) and are gradually absent from the lateral sides (B). Insets: enlargement of the areas in the white boxes.

This figure is kindly provided by F.Wong.

2.3.2 Results

1. The distal cells at LS-EB stage (E7.5) incorporated efficiently in the notochord at E8.5 NSB

Distal cells were dissected from LS-EB stages AGFP embryos which ubiquitously express green fluorescent protein (GFP) (Figure 2.10A) (Gilchrist et al., 2003). The cells were then grafted to the NSB of E8.5 (2-5 somite stage) wild type embryos (Figure 2.10B), which were cultured ex vivo for 24-48 hours. GFP expression was used to trace the descendants of the graft. It should be noted that both dorsal and ventral layers of the distal region were grafted due to the difficulty of manually separating these two layers. 7 embryos received a graft of distal cells: two embryos were cultured ex vivo for 24 hours, the other 5 embryos for 48 hours. The host embryos generally developed to the 15-19 somite stage after 24 hours in culture (Figure 2.10C), and had reached the 30-35 somite stage after 48 hours (Figure 2.10 D) (Wilson and Beddington, 1996). GFP^{+} cells were observed in 6 out of 7 embryos after

culture. They were mainly in the midline of all host embryos but were absent from the tail bud according to the whole-mount images (Figure 2.10C, D). Images of all recipient embryos can be found in the Appendix I, Sup Figure 2.1. The reason that the other embryo did not contain any GFP^+ cells may be because the graft slipped out from the host during culture. Since no GFP^+ contribution may be due to this technical problem, this embryo was excluded from the analysis.

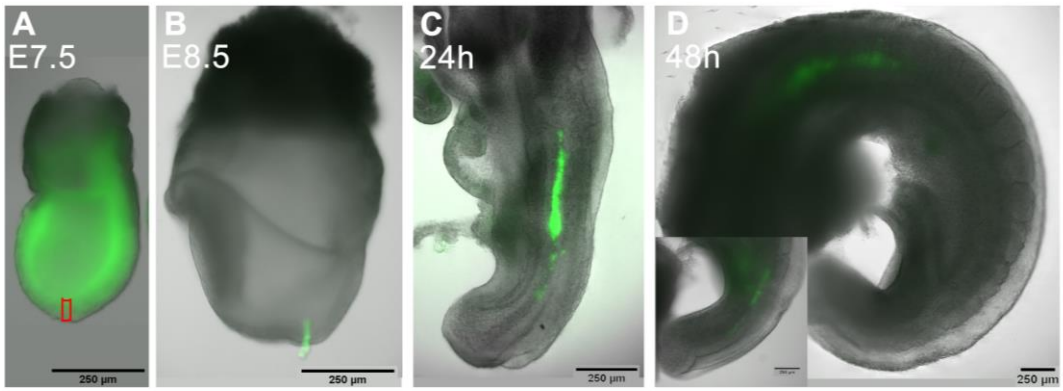

Figure 2.1 1 . Distal cells from the LS-EB stage embryos (E7.5) grafted to the NSB of E8.5 embryos (2-5 somite stage)

(A) Representative AGFP7 embryos at the bud stage (E7.5). Distal cells (red box) were dissected and grafted to the NSB of E8.5 embryos.

(B) Representative E8.5 embryo (2-5 somite stage) grafted with E7.5 distal cells.

(C and D) Example of embryos after 24 (C) and 48 hours (D) culture. Inset: enlargement showing GFP^+ cells in the host tail.

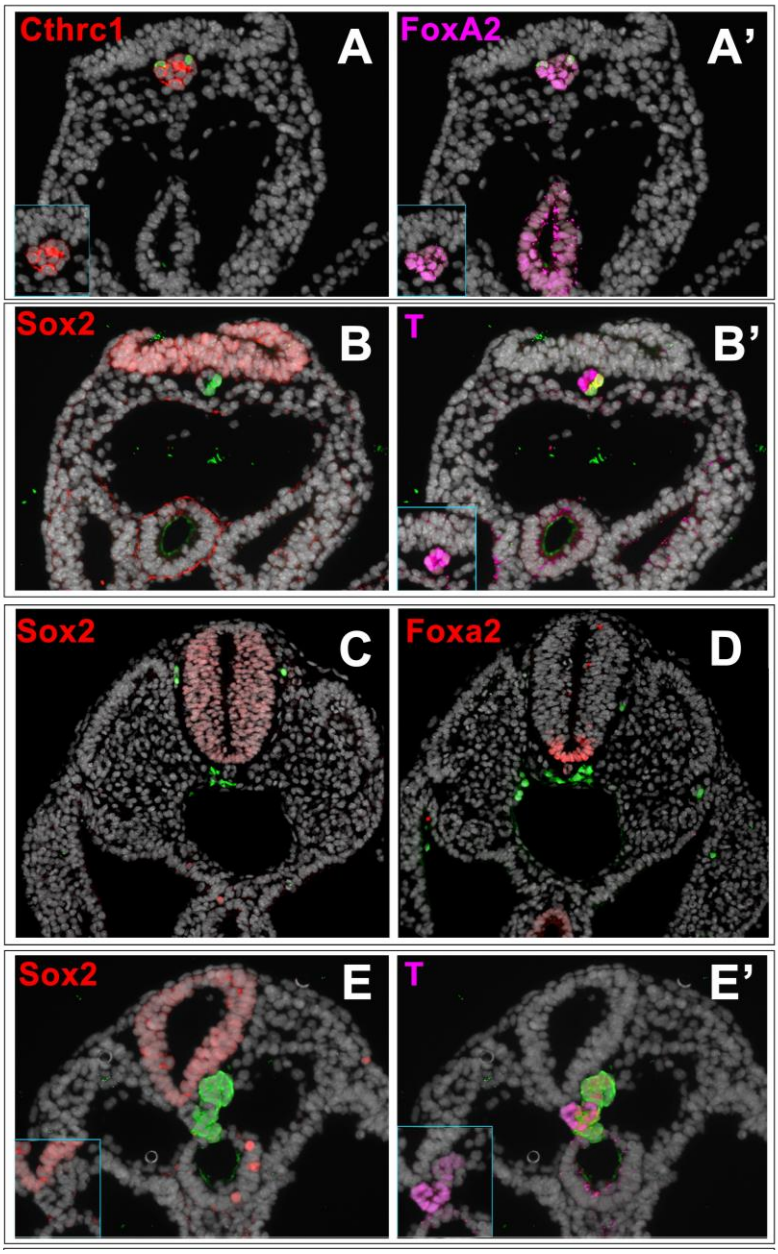

Figure 2.１２. Analysis of the distribution of distal cells from the LS-EB stage (E7.5) in E8.5 embryos

Immunofluorescent staining on sections of host embryos receiving E7.5 distal cells (green) after 24 or 48 hours culture. Grey: DAPI-counterstain. Inserts: enlargement of notochord areas with the removal of green channel.

(A-A') Donor cells in notochord coexpressing Cthrc1 and Foxa2. (B-B') Donor cells in notochord expressing T (B') but not Sox2 (B). (C and D) Donor cells in mesoderm express neither Sox2 (C) nor Foxa2 (D). (E-E') Some donor cells form a clump next to the neural tube ectopically expressing low levels of T but not Sox2. Donor cells in notochord expressing high level of T which is similar to host-derived notochord cells.

To investigate the contribution of donor cells, 4 out of 6 embryos were cryosectioned, of which two embryos were fully scored for the presence of GFP^+ cells in each section. In all 4 examined embryos, GFP^+ cells contributed predominantly in the notochord with an AP extension as seen in the whole-mount images. Some GFP^+ cells were also located in the ventral mesoderm surrounding the notochord in the anterior part of the embryos (Figure 2.11C, D). Notably, neither neural ectoderm nor paraxial mesoderm contribution was detected. Interestingly, all the posterior contribution was restricted to the notochord and ceased anterior to the notochordal plate.

To further assess the cell integration, representative slides were stained. GFP^+ cells in the notochord expressed specific notochord markers: Cthrc1 (Figure 2.11A) (Durmus et al., 2006), Foxa2 (Figure 2.11A') (Uetzmann et al., 2008) and T (Figure 2.11B') (Inman and Downs, 2006). Moreover, GFP^+ cells in the notochord and ventral mesoderm did not express Sox2 which was expressed in the dorsal layer of the tissue originally grafted. Occasionally, GFP^+ cells formed some ectopic structures next to the ventral neural tube, which expressed a low level of T but no Sox2 (Figure 2.11E, E'), suggesting an ectopic notochord. Therefore, these results showed that donor cells predominantly gave rise to the notochord and if incorporated, donor cells were identical to their host-derived immediate neighbours.

2.3.3 Conclusion and discussion

To summarise, when grafted to E8.5 NSB, cells from the distal region of LS-EB stage embryos (E7.5) incorporated efficiently in the notochord with a wide contribution along the AP axis. Some cells were also detected in the ventral mesoderm. However, there was neither neural tube nor paraxial mesoderm contribution, which differs greatly from E8.5 NSB homotopic grafts or L1-3 to NSB heterotopic grafts. Therefore, these results indicate although cells in the distal epiblast at LS-EB stages (E7.5) are the precursors of NM progenitors, they are not equivalent to E8.5 NM progenitors.

1. NM progenitors may not be specified at LS-EB stages (E7.5)

As mentioned previously, there are two cell layers in the distal region of LS-EB stage embryos (E7.5) and their fate has been investigated. The ventral cells predominantly give rise to notochord with some contribution to the adjacent endoderm (Beddington, 1994), whereas the dorsal cells mainly gives rise to neural tissue with a minimal contribution to the mesoderm including notochord (Forlani et al., 2003). Therefore, the distal region I grafted contains both the notochord progenitors (ventral cells) and the precursors of NM progenitors (dorsal cells). Surprisingly, these cells contributed extensively to notochord but to neither the neural tube nor paraxial mesoderm. Since this observation is consistent in all 4 examined embryos, this is unlikely to be caused by only ventral cells rather than both layers being grafted.

The reason that the grafted cells gave rise to neither neural tissues nor paraxial mesoderm could be that either dorsal cells (the precursors of NM progenitors) did not incorporate in E8.5 embryos or they incorporated and gave rise to the notochord in the host embryos. In future, to determine whether dorsal cells could incorporate in E8.5 NSB, we can use DiI to label the epiblast of LS-EB stage embryos (E7.5) and then perform the grafting experiments. Whether dorsal cells can incorporate or not, they will contribute to neither neural tissues nor paraxial mesoderm in E8.5 NSB. This could be because dorsal cells are not specified as NM progenitors. Indeed, the epiblast at E7.5 expresses high pluripotency markers such as Nanog and Oct4 but not T. This raises the hypothesis that coexpressing T and Sox2 may indicate the specification of NM progenitors. We could test this hypothesis by grafting $T^{+}Sox2^{+}$ cells from headfold stage embryos to E8.5 NSB. The incompatibility between distal epiblast at LS-EB stages (E7.5) (dorsal cells) and NM progenitors at E8.5 could also be due to Hox gene expression. It has been shown that cells in the distal region of LS-EB stage embryos (E7.5) do not express any Hox genes but NM progenitors at E8.5 express different Hox

genes (paralogous groups 1-8) (Forlani et al., 2003) (Wilson lab, unpublished data). However, Hox genes are not expressed in the notochord. This may be the reason that cells from the distal region of LS-EB stage embryos (E7.5) mainly contribute to the notochord when grafted into E8.5 embryos.

2. Specification of notochord progenitors at LS-EB stages (E7.5)

Cells in the distal region at LS-EB stages (E7.5) are able to incorporate and contribute to the notochord in E8.5 embryos, indicating that notochord progenitors at LS-EB stages (E7.5) are compatible with those at early somite stages (E8.5). Therefore, it is highly possible that notochord progenitors are already specified at LS-EB stages. A similar observation was also made in chick embryos. Cells in the midline V-portion of Hensen's node at HH4 stage (late PS stage) give rise to floor plate and notochord in both homotopic and heterotopic grafts (Selleck and Stern 1992). Moreover, when grafted into the area opaca of a host embryo, Hensen's node can autonomously generate a well organised notochord (Dias and Schoenwolf, 1990). These experiments indicate that some cells in Hensen’s node are committed notochord progenitors during the mid-gastrulation stage. Notably, in my results although cells from the distal region contribute extensively to the notochord, they do not give rise to the notochordal plate. This raises a possibility that the specified notochord progenitors at LS-EB stages (E7.5) only act as body notochord progenitors. The tail notochord may have other origins.

2.4 The loss of NM progenitors at E14.5

2.4.1 Aims

The disappearance of T^+Sox2^+ cells after the 65 somite stage precisely coincides with the end of axis elongation. It raises a hypothesis that the loss of NM progenitors results in the end of axis elongation. It has been shown that T^+Sox2^+ cells at E12.5 are still retained as long-term axial progenitors and are capable of populating both neural and mesodermal cells in E8.5 NSB (Cambray and Wilson, 2002). Preliminary homotopic grafting experiments show that the descendants of E12.5 NM progenitors (CNH cells) are still present in the host tails after 24 hours culture but are eliminated after 48 hours (Wymeersch, 2011). This indicates that there should be no NM progenitors at E14.5. Despite the presence of a few T^+Sox2^+ cells dispersed in the early E13.5 tail bud, due to the lack of a fluorescent marker for isolating these cells live, it is not known if they are still NM bipotent cells. One critical feature of NM progenitors is that cells at late developmental stages are still able to generate tissues along the axis when placed into a young environment (Wilson et al., 2009). To investigate whether there are still NM progenitors in the early E13.5 tail bud, E13.5 CNH cells were grafted to E8.5 NSB

2.4.2 Results

1. E13.5 CNH proliferated extensively in E8.5 NSB but with only a minor incorporation

A small piece containing the CNH (posterior neural tissue and notochord) was dissected from early E13.5 tails (before 65 somite stage) (as described in Chapter 6: materials and methods) and then grafted to the NSB of E8.5 embryos (2-5 somite stage) (Figure 2.12A, C). 13 wild type embryos received a graft from AGFP embryos: 5 embryos were cultured for 24 hours, the other 8 embryos for 48 hours. In 12 out of 13 embryos GFP^+ cells contributed extensively in the midline but all were absent from the tail bud in the hosts (Table 2.1). Images of all recipient embryos can be found in the Appendix I, Sup Figure 2.2. However, it is difficult to determine the incorporation of donor cells according to the whole-mount images (Figure 3D, 3E). No GFP^+ cells were observed in the other embryo, which was excluded from further analysis.

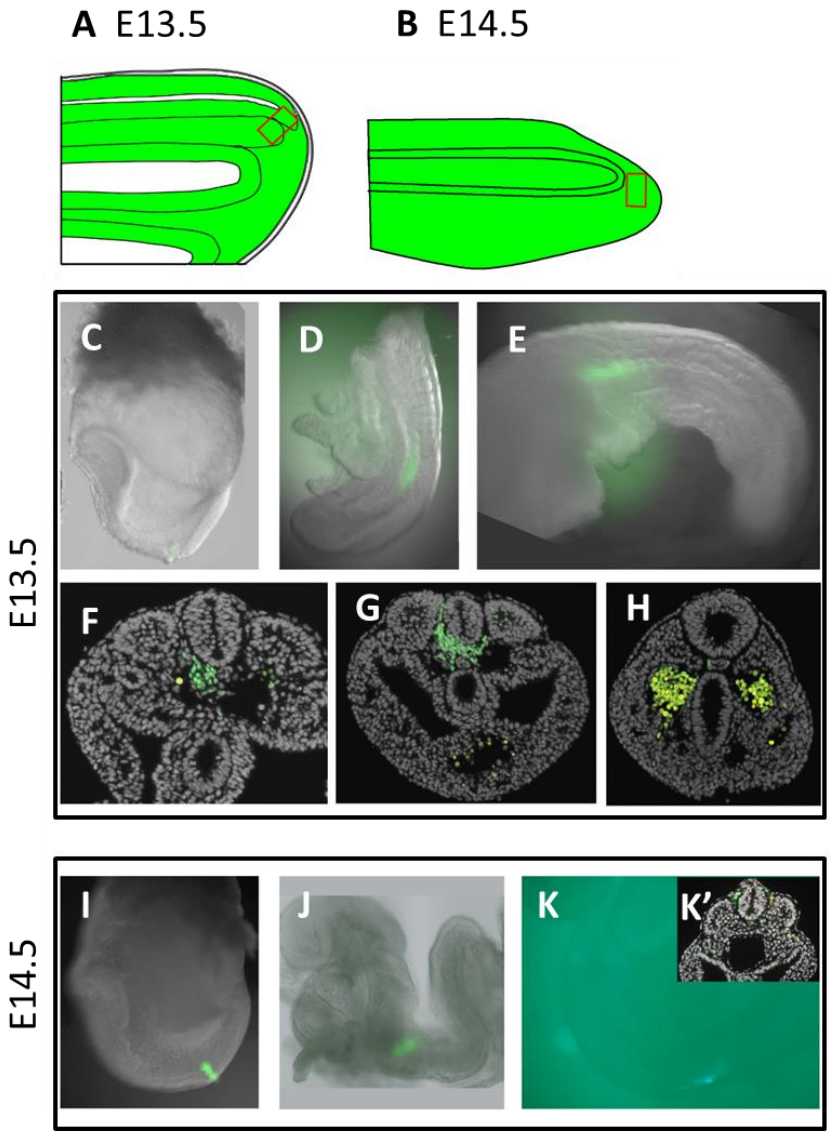

Figure 2.1 3 . Tail bud cells from E13.5 and E14.5 embryos grafted in E8.5

(A and B) Schematic diagrams showing the morphology of tails at E13.5 (62-63 somite stage) and E14.5.

(C) Representative E8.5 embryo grafted with E13.5 CNH cells (red box in A). (D and E) Examples of embryos receiving a graft of E13.5 CNH after 24 (D) and 48 hours (E) culture. (F-H) Section examples showing that the majority of donor cells formed clumps in the host. A few dispersed GFP+ cells were detected in paraxial mesoderm and notochord.

(I) Representative E8.5 embryo grafted with cells from E14.5 tail tip (red box in B). (J and K) Examples of embryos receiving a graft of E14.5 tail tip after 24 (J) and 48 hours (K) culture. Donor cells remained in the graft site without significant proliferation. The bright field image was lost in (K), so only the green channel is shown here. Inset: Example section from the embryo in (K). Donor cells in green. DAPI-counterstain in grey.

Table 2. 1 . Intact embryo assessment of E8.5 embryos grafted with E13.5 CNH and E14.5 tail tip

Experiments	24h culture (No. of embryos with GFP$^+$ cells)	48h culture (No. of embryos with GFP$^+$ cells)
E13.5 CNH to E8.5	5 (5)	8 (7)
E14.5 tail tip to E8.5	2 (1)	6 (1)

To further assess the incorporation, 3 out of 12 embryos were sectioned and fully scored for the presence of all GFP$^+$ cells. In the sections, the majority of GFP$^+$ cells formed clumps underneath the neural tube (Figure 2.12F, G). Notably, most clumps appeared to be mesenchymal self-associated tissues. However, there were some ring-like clumps which resembled an ectopic neural tube or notochord (Figure 2.12F, G). The exact nature of the ectopic tissues requires further verification by immunostaining. Only a few cells appeared to incorporate in the somites (Figure 2.12F), notochord (Figure 2.12H) and the mesenchymal cells between neural tube and somites (Figure 2.12G). The number of GFP$^+$ cells was high in the trunk and gradually decreased in the posterior with mainly notochord contribution at the end (Figure 2.12F-H). Notably, no GFP$^+$ cells were observed either in the neural tube or the CNH of the tail bud, suggesting a restricted potency of E13.5 CNH cells or technically few T$^+$Sox2$^+$ cells were grafted. All sections containing GFP$^+$ cells from two embryos can be found in the Appendix I, Sup Figure 2.3. and 2.4. In summary, E13.5 CNH cells proliferated extensively in E8.5 embryos but only showed minor incorporation in the mesoderm.

2. E14.5 tail tip cells barely proliferated and incorporated in E8.5 NSB

As shown previously (Figure 2.6C, D), at E14.5 most structures in the tail bud, including the CNH, have already disappeared, except for the notochord. Thus, the mesenchymal cells from the most posterior tail tip were dissected (as described in the materials and methods) and grafted to the NSB of E8.5 embryos (Figure 2.12B, I). In total, 8 wild type embryos received a graft from the tail tip of E14.5 AGFP embryos: 2 embryos were cultured for 24 hours, the other 6 embryos for 48 hours. Surprisingly, GFP$^+$ cells were only detected in 2 out of 8 embryos close to the graft site (Figure 2.12J, K and Table 2.1). The single embryo containing GFP$^+$ cells after 48 hours in culture was sectioned and scored for GFP$^+$ cells. GFP$^+$ cells were only detected in 9 consecutive sections (Figure 2.12K'). Collectively, these results show that cells in E14.5 tail tip can only incorporate and/or proliferate poorly in E8.5 embryos, indicating the complete disappearance of NM progenitors at E14.5

2.4.3 Conclusion and discussion

To summarize, although E13.5 CNH proliferated extensively after grafting to the NSB of E8.5 embryos, it incorporated poorly. Thus, it is difficult to determine whether there are still NM progenitors by this stage. Because the descendants of NM progenitors from E12.5 are possibly eliminated at E14.5 and T^+Sox2^+ cells have disappeared in E14.5 tails, I assume that there are definitely no NM progenitors at E14.5. The poor proliferation and incorporation of E14.5 tail tip cells in E8.5 NSB is consistent with this assumption. The obvious contrast between the CNH (E10.5-E13.5) and E14.5 tail tip cells in E8.5 NSB (Table 2.1) indicates that the former are progenitors and the latter are differentiated cells.

1. Reasons for no neural contribution of E13.5 CNH cells in E8.5 NSB

Since the neural tube starts to regress after E13.5, it is not surprising that all NM progenitors might specify as mesoderm progenitors at this stage. This may explain why no neural contribution was observed. Alternatively, our microarray data shows that the general transcripts are quite different between E8.5 NSB and E13.5 CNH, therefore testing the potential of E13.5 CNH by grafting into E8.5 NSB may not be a suitable assay. We may need to find another assay to test the potential of NM progenitors during late tail bud stages. It is also possible that because T^+Sox2^+ cells in E13.5 are dispersed in the posterior neural tube rather than gathered in confined areas as in earlier stages (Figure 2.7), very few T^+Sox2^+ cells were actually grafted to E8.5 NSB. This might lead to the low incorporation of donor cells in the host.

2. Reasons for the non-integrated tissues formed by E13.5 CNH cells

Most of E13.5 CNH cells formed self-adherent clumps that extended along the axis in their host (Figure 2.12F, G). However, it has been shown that 10-20 mesenchymal cells isolated from early E13.5 tail bud, 150-200 μm away from tail tip, were still able to contribute to the somites after being grafted to the primitive streak of E8.5 embryos (Tam and Tan, 1992). This differs from the minor incorporation of E13.5 CNH cells in my grafts. There are several differences between this experiment and mine, which may cause the variations in the incorporation of donor cells. Firstly, the posterior neural sheet and tail gut were completely removed in their experiment to isolate only mesenchymal cells. However, the CNH region I grafted contained the posterior neural sheet and notochord but not many tail bud mesoderm cells. Secondly, the number of donor cells transplanted may differ. The actual number of grafting cells was not checked in my grafts. It is very possible that I grafted a larger number

of cells to E8.5 NSB. In this instance, donor cells may be able to create their own niche in the host, which prevents them fully interacting with the host environment and results in the clump formation. It would be interesting to test whether the clump formation could be avoided by grafting 10-20 cells. Thirdly, the transplanted locations are different. The mesenchymal cells were placed in the primitive streak where there may be more cell movement and cell-cell intercalation compared with NSB. Thus, the donor cells in the primitive streak have more chances to interact with the host, which leads to better incorporation. Finally, the clump formation may indicate a mismatch in developmental status between E13.5 CNH and E8.5 NSB cells. Therefore, a different assay may be required to investigate the in vivo potential of E13.5 CNH.

3. E13.5 CNH cells may not be long-term NM progenitors

My E13.5 CNH to E8.5 NSB grafting results cannot clearly show whether there are still NM progenitors at E13.5 due to most donor cells forming clumps in the hosts. In my opinion, there may be no long-term NM progenitors at E13.5 for the following two reasons. Firstly, E13.5 CNH grafts did not contribute to the neuroectoderm and repopulate CNH areas when grafted to E8.5 NSB, indicating they may have lost their neural differentiation potential and self-renewal capacity. Secondly, when E10.5 CNH cells were transplanted under the kidney capsule, they formed clumps containing both neural and mesodermal derivatives. However, no obvious growth was observed in most E13.5 CNH kidney capsule grafts (unpublished data from Dr. N Cambray), indicating that these cells cannot self-renew and have limited differentiation potential.

As discussed previously, Wnt and FGF signals are important for the maintenance of NM progenitors. A gradual decrease of these signals from E10.5 may be responsible for the reduction of NM progenitors by promoting their differentiation. The expression of some important genes for the maintenance of posterior progenitor zone such as *Wnt3a*, *Fgf8*, *Nkx1.2* and *Cdx2* are undetectable between E12.5 to E13.5. Therefore, it is possible that after E12.5 Wnt and FGF signals reach a threshold where their levels are not able to sustain NM progenitors. This results in the differentiation of all NM progenitors after E12.5 and the loss of NM progenitors at E13.5. The existence of $T^{+}Sox2^{+}$ cells at E13.5 may be due to the delay in turning off transcription factor expression. Therefore, my hypothesis is that due to the extremely low levels of Wnt and FGF signals, NM progenitors are eliminated from the embryos between E12.5 to E13.5.

Chapter 3. Wnt/β-catenin signalling controls the differentiation choice of NM progenitors

3.1 Conditional deletion of β-catenin at E8.5 in whole embryos with ex vivo culture

3.1.1 Aims and experimental approach

Conditional activation or deletion of genes using the Cre/loxP recombination system is a powerful tool to study gene function and track cell fate (reviewed by (Kuhn and Torres, 2002; Metzger and Chambon, 2001). This is achieved by flanking essential genomic sequences with loxP sites ('floxing'). Subsequent crossing of mice containing a floxed allele with mice that express Cre-recombinase under a tissue-specific promoter allows the tissue-specific and/or temporal removal of the floxed sequences.

For external temporal control of Cre activity, a ligand-dependent chimeric Cre recombinase, named Cre-ER^{T2}, has been developed. In this configuration, Cre activity is regulated by fusion to mutated hormone-binding domains of the estrogen receptor, which sequesters Cre outside the nucleus, so there is no recombination of the floxed sequences. However in the presence of the synthetic estrogen receptor ligand 4-hydroxytamoxifen (4-OHT), Cre can rapidly relocate into the nucleus where it directs recombination (reviewed by (Feil et al., 2009).

As mentioned previously, Wnt/β-catenin signalling plays a vital role in early embryo development. However, since there are many Wnt proteins some of which may also activate noncanonical Wnt signalling, a common way to study the Wnt/β-catenin pathway is through manipulation of β-catenin, a nonredundant and essential component in this pathway. *β-catenin*$^{del/del}$ embryos die after implantation due to the failure of mesoderm and AP axis formation (Haegel et al., 1995; Huelsken et al., 2000). To circumvent this early embryonic lethality, a floxed β-catenin mouse strain was created (Brault et al., 2001), which allows the study of β-catenin function in specific cells. In this study, I took advantage of the conditional knockout Cre-ER^{T2} system to investigate the role of β-catenin in axis elongation and NM progenitors.

Two double homozygous mouse strains have been produced in Alexander Medvinsky's group: one is a β-cat floxed homo: sGFP homo, carrying a silent *GFP* gene in *β-catenin*$^{floxed/floxed}$ mutants (Brault et al., 2001; Gilchrist et al., 2003) (Figure 3.1A); the other is β-cat floxed homo: Cre-ER^{T2} homo, ubiquitously expressing Cre-ER^{T2} in *β-catenin*$^{floxed/floxed}$ mutants (Figure 3.1B) (Chambers et al., 2007). These two double homozygous mouse strains were crossed to create *β-catenin* conditional deletion reporter embryos (β-catCKO), in which

the deletion of β-catenin and activation of silent GFP (sGFP) depends on 4-OHT treatment (Figure 3.1 C, 3.2B). Although the 4-OHT inducible Cre-ER^{T2} system has been extensively used in cell culture and in vivo development, it is not clear whether it works with ex vivo culture. To address this question, I cultured β-catCKO embryos in medium with additional 4-OHT then tested the GFP expression and *β-catenin* gene deletion efficiency in these embryos.

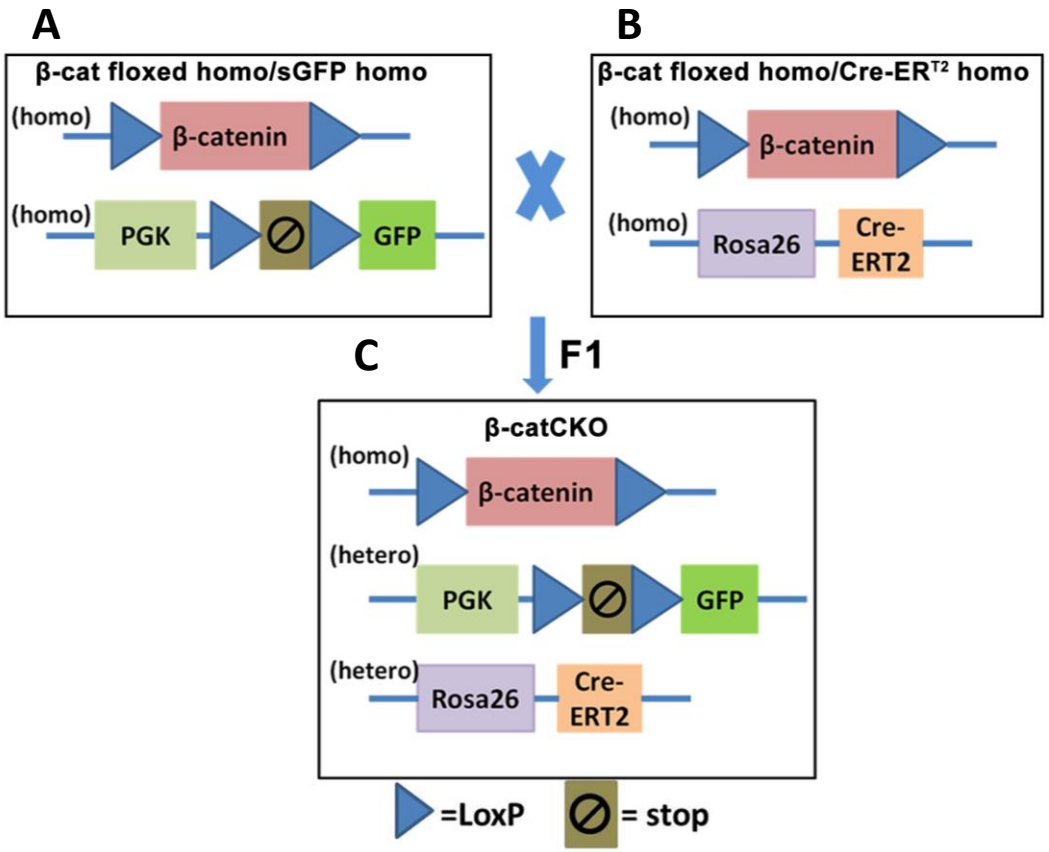

Figure 3.1 . *β-catenin* conditional knockout reporter mice

Schematic representation of the generation β-catenin (β-cat) conditional knockout reporter mice (C) referring to βcatCKO by crossing β-catenin floxed homo/sGFP homo (A) mice with β-catenin floxed homo/ROSA26-CreERT2 homo (B) mice.

3.1.2 Results:

1. Toxicity of 4-OHT on ex vivo culture embryos

Tamoxifen has well-characterised toxic effects on mouse embryos in utero, causing lethality at high doses (Danielian et al., 1998). Moreover, 15 μM 4-OHT is cytotoxic to non-cancerous cell lines after 72 hours treatment (Petinari et al., 2004; Yaacob and Ismail, 2014). To assess the toxicity of 4-OHT on ex vivo cultured embryos, wild type E8.5 (3-6 somites) embryos were dissected from the uterus and cultured in medium supplied with additional 5μM, 7μM and 10μM 4-OHT for 24 hours using 2 embryos for each condition. Embryos exposed to 5μM and 7μM 4-OHT for 24 hours grew well based upon gross morphology and turned at the end of culture. Both embryos exposed to 10μM 4-OHT for 24 hours showed abnormal folding and kinking of the posterior neural tube. Neither of them turned at the end of culture. However, when cultured in the presence of 10μM 4-OHT for only the first 6 or 8 hours, then transferred to 4OHT-free medium, the embryos (two for each condition) turned after 24 hours in culture with normal morphology based on external inspection. Therefore, embryos were cultured in 10μM 4-OHT for 6-8 hours or 5-7μM 4-OHT for 24 hours in subsequent experiments.

2. 4-OHT mediates the reactivation of GFP expression and the deletion of *β-catenin* gene in β-catCKO embryos

E8.5 β-catCKO embryos (3-6 somites) were cultured in 5-7μM 4-OHT for 24 hours or 10μM 4-OHT for 6-8 hours in a total 24 hours culture (Figure 3.1A). The reactivation of GFP expression was first checked under a fluorescent microscope at the end of culture. Even at the lowest dose of 4-OHT (5μM), sGFP was activated in β-catCKO embryos (Figure 3.2B). Embryos were then cut into two parts. The anterior half was kept for genotyping as described or for determining β-catenin protein levels (Figure 3.2 C,D) (Brault et al., 2001). The posterior half was used for whole-mount T/Sox2 immunofluorescence to investigate the effects of β-catenin depletion on NM progenitors.

Genomic DNA PCR shows that all conditions used can mediate *β-catenin* gene recombination in the embryos after 24 hours in culture (Figure 3.2C; *β-catenin*$^{del/del}$ 500bp band). Moreover, a high dose 4-OHT (10μM) for short times (6 or 8 hours) appeared to have higher recombination efficiency than a low dose (5μM) for a long period (24 hours) (Figure 3.2C). Similarly, β-catenin protein also showed the greatest reduction in embryos treated with 10μM 4-OHT for 8 hours (Figure 3.2D). However, it should be noted that although β-

catenin proteins were largely depleted by 24 hours, it is difficult to determine by immunofluorescence what level of residual activity remains. Collectively, these results show that conditional deletion of genes is feasible with ex vivo culture by using the 4-OHT inducible Cre-ER^{T2} system.

3. Abnormalities in the posterior embryos after β-catenin depletion

To investigate the effects of β-catenin depletion on axial elongation and NM progenitors, E8.5 β-catCKO embryos were cultured in 5μM 4-OHT for 24 hours (E9.5 β-catCKO) and then immunostained in whole-mount for T and Sox2. The embryos were examined via a confocal microscope and subsequent 3D image reconstruction. T/Sox2 immunostaining showed that although there were T^+Sox2^+ cells in E9.5 β-catCKO embryos, their distribution was visibly different from E9.5 wild type (WT) embryos (Figure 3.4). In WT embryos, T^+Sox2^+ cells appeared in the CNH and the anterior ectoderm, which is topologically equivalent to the anterior CLE (L1-2) in E8.5 embryos (Figure 3.3A, C), but were absent from the most posterior ectoderm (topologically equivalent to L5 in E8.5 embryos) (Figure 3.3E). In E9.5 β-catCKO embryos, T^+Sox2^+ cells were still present in the CNH and the anterior ectoderm (Figure 3.3B, D) but with an extension to the most posterior ectoderm (Figure 3.3F). The 3D reconstruction images also confirm this observation (Figure 3.4B, D). Moreover, the notochordal plate appeared to deform in E9.5 β-catCKO embryos (Figure 3.3A, B) and the posterior T^+Sox2^- domain containing the tail bud and PSM appeared to be smaller in β-catCKO embryos compared with that in E9.5 WT embryos (Figure 3.4B, D).

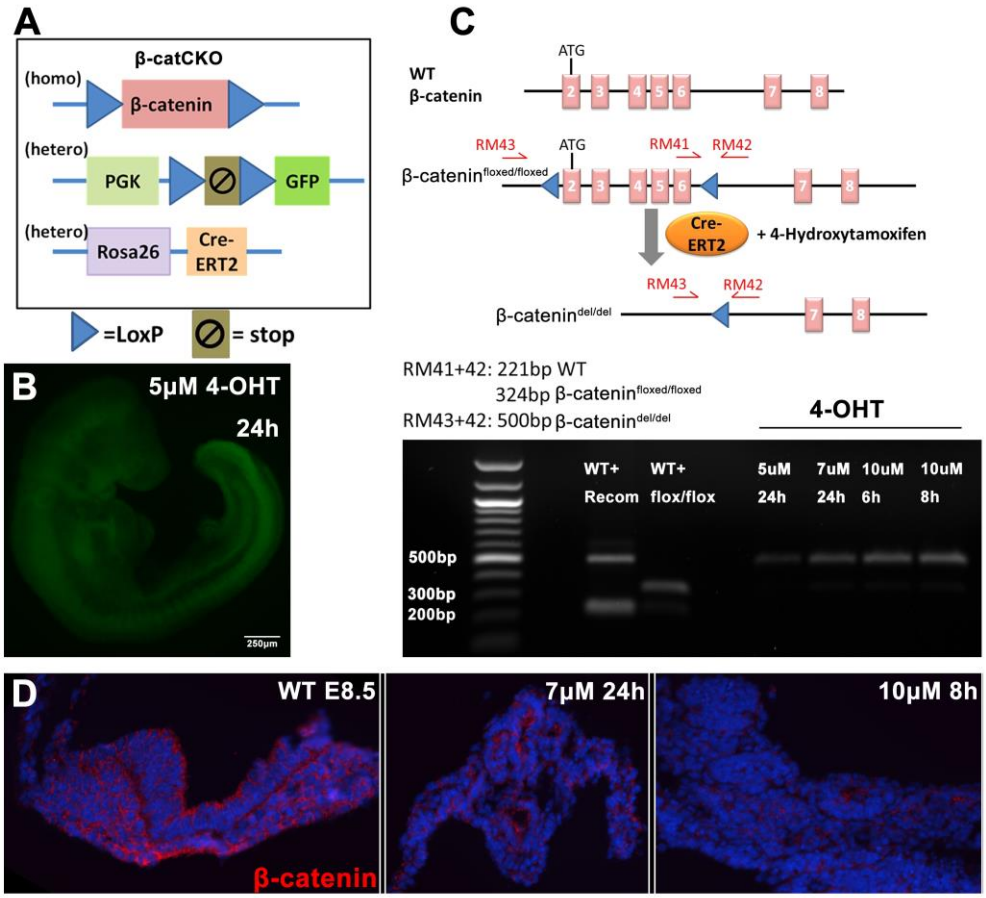

Figure 3. 2 . Optimizing conditional deletion β-catenin in whole embryos with ex vivo culture

(A) Schematic representation of β-catenin conditional knockout reporter embryos (β-catCKO).

(B) After 24 hours cultured with 5μM 4-hydroxytamoxifen (4-OHT), silent GFP is activated in βcatCKO embryos

(C) Different β-catenin alleles and primers used for genotype screening (adapted from (Brault et al., 2001). Agar gel picture showing wild-type (WT), floxed and deleted alleles are identified in the control samples (left two lanes). After a total 24 hours culture, β-catenin floxed bands are faint and β-catenin deleted bands are present in all 4-OHT pulse doses/times treated βcatCKO embryos (right four lanes).

(D) β-catenin immunofluorescence showing the level of β-catenin protein is downregulated in βcatCKO after 4-OHT treatment.

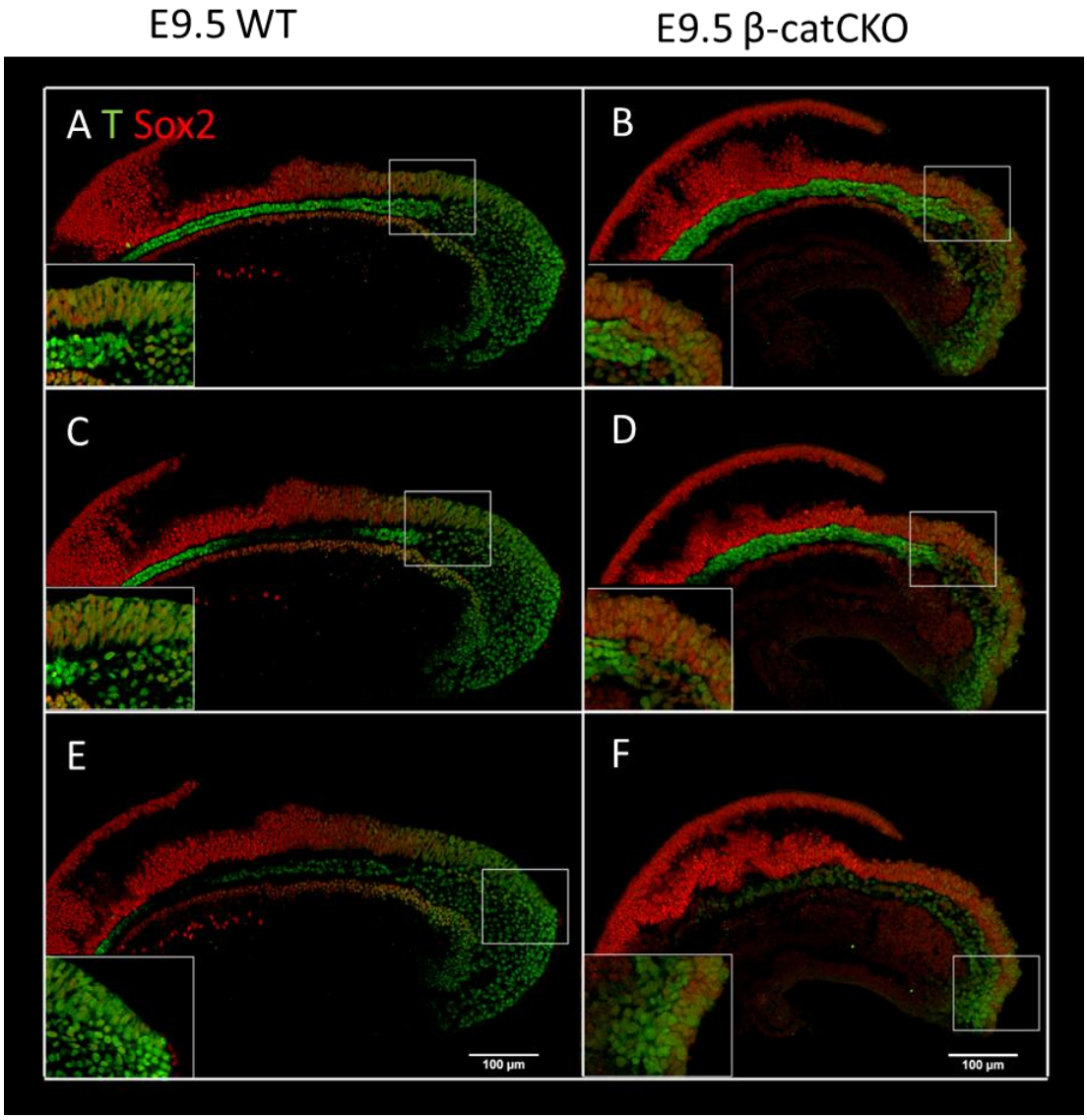

Figure 3. 3 . Comparison of T and Sox2 expression between E9.5 wild-type and βcatCKO embryos

Whole-mount immunofluorescence for T (green) and Sox2 (red). (A,B) Representative sagittal section showing the midline of E9.5 wild type (WT) and β-catCKO embryos. Inset: enlargement of the CNH area

(C, D) Sagittal sections lateral to midline focus on the ectoderm anterior to the CNH, Inset: enlargement of the area in the white box, where it is topological equivalent of anterior caudal lateral epiblast (L1-2) in E8.5 embryos.

(E, F) Sagittal sections lateral to midline focus on the ectoderm posterior to the CNH, Inset: enlargement of the area in the white box, where it is topological equivalent to the most posterior caudal lateral epiblast (L5) in E8.5 embryos.

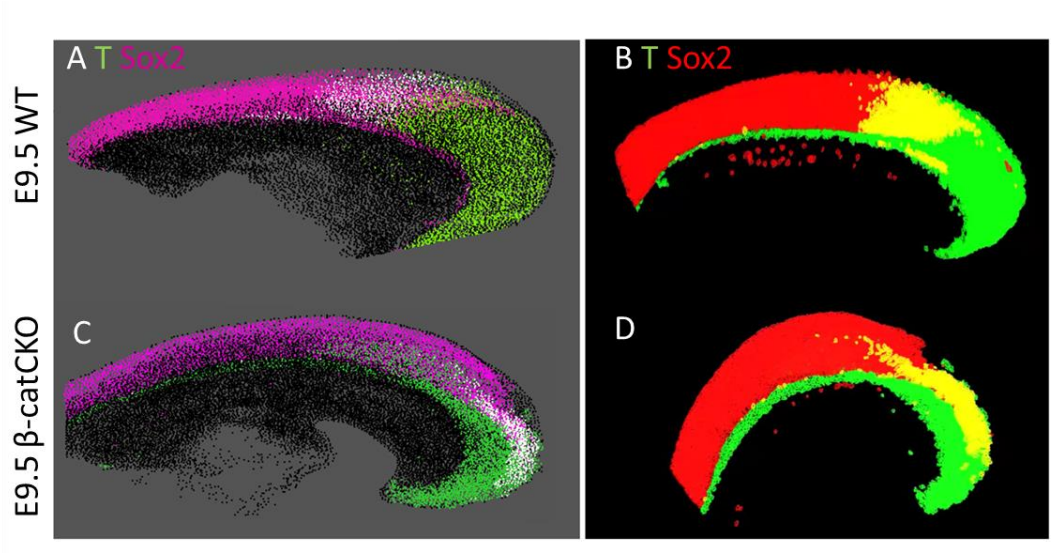

Figure 3. 4 . 3D reconstructed images showing T and Sox2 expression domains in E9.5 wild-type and β-catCKO embryos

Whole mount Immunofluorescent staining for T (green) and Sox2 (red/Magenta). 3D reconstructed images generated from confocal z-stacks showing T and Sox2 expression profiles in each single cell in the posterior region of the embryos. T^+Sox2^+ cells are shown in either white (A and C) or yellow (B and D). Cells do not expressing either T or Sox2 are shown in black

4. A reduction of NM progenitors and posterior mesoderm after β-catenin depletion

To precisely determine the effects of β-catenin depletion on NM progenitors, quantitative analysis of T and Sox2-expressing cells using confocal images was performed as described previously. Compared with E9.5 WT embryos, there was a significant drop in the number of T^+Sox2^- and T^+Sox2^+ (but not $Sox2^+T^-$) cells in E9.5 β-catCKO embryos (Figure 3.5A-C). Interestingly, the number of T^+Sox2^+ cells in E9.5 β-catCKO embryos was not significantly different from E8.5 samples (Figure 3.5A), suggesting that there was no expansion of NM progenitors when Wnt/β-catenin signalling was decreased. The decrease of T^+Sox2^- cells in the posterior region of E9.5 β-catCKO embryos indicates a reduction in the posterior mesoderm, which is consistent with the reduction in the size of the posterior T^+Sox2^- domain (Figure 3.4B,D).

As mentioned previously, the imaged samples varied in their anterior limits. To determine whether any one population was disproportionately affected by this variation, the proportions of each population were also analysed (Figure 3.5D). There was no statistical difference in the percentage of $Sox2^+T^-$ and T^+Sox2^+ cells in E9.5 β-catCKO and WT E9.5 embryos. However, the percentage of T^+Sox2^- cells was still significantly reduced in E9.5 β-catCKO

embryos. Notably, the population of T^+Sox2^- cells in E9.5 β-catCKO embryos was even smaller than that in WT E8.5 (Figure 3.5B, D). The decrease of T^+ cells in β-catCKO embryos is consistent with the previous result showing that T is a direct target of Wnt/β-catenin signalling (Yamaguchi et al., 1999b).

Collectively, these results show that conditional deletion of β-catenin at E8.5 results in the distortion of posterior notochord, the displacement of NM progenitors, and a reduction of NM progenitors and the posterior mesoderm.

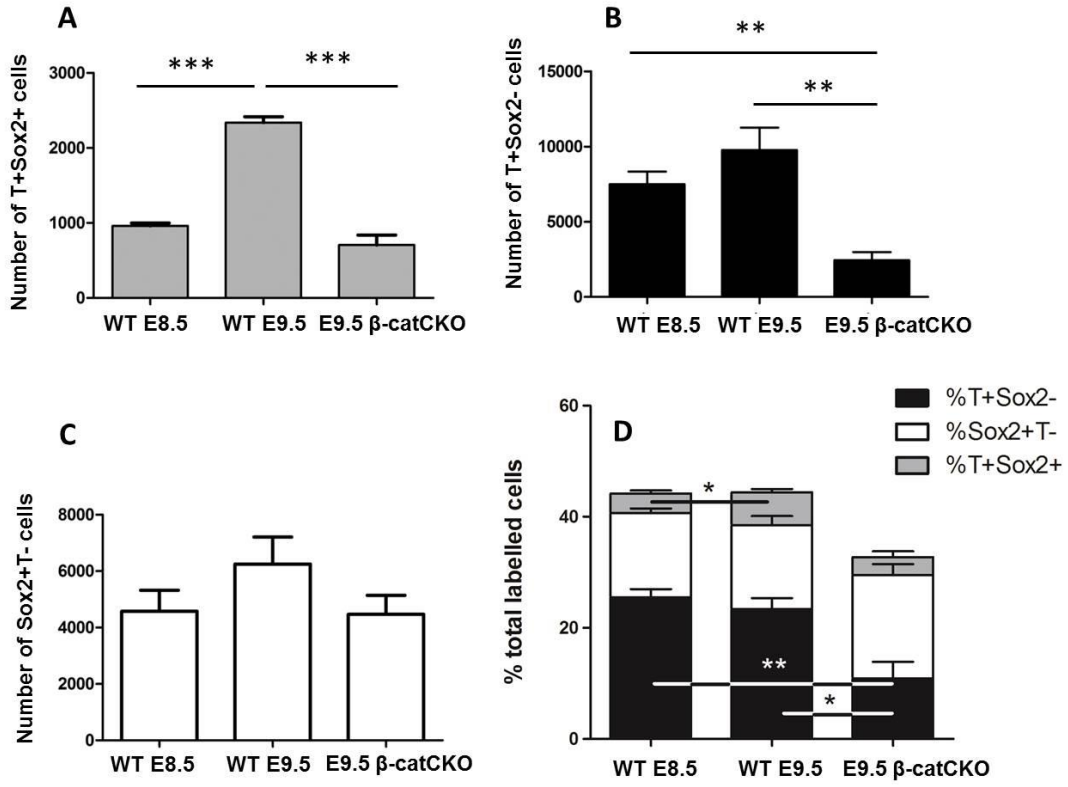

Figure 3. 5 . Quantification of T and Sox2 in cells at the posterior region of wild type and β-catCKO embryos

WT E8.5 (n=5): wild type embryos at 6-8 somite stage; WT E9.5 (n=5); E9.5 βcatCKO (n=5): embryos were dissected at E8.5 and cultured 24h ex vivo in the presence of 5μM 4-OHT .

Error bars: mean±s.d. For T^+Sox2^+ cells an unpaired student's T-test was used to test significant differences. For T^+Sox2^- and $Sox2^+ T^-$ cells, an additional Welsh correction was added to the unpaired student's t-Test to correct for varying anterior limits between samples. *, $0.05 < p \leq 0.1$; **, $0.01 < p \leq 0.005$; ***$p \leq 0.001$.

3.1.3 Conclusion and discussion

In this study, I first showed that it is feasible to conditionally delete genes during ex vivo culture by using 4-OHT inducible Cre-ER^{T2} system. Depletion of β-catenin at E8.5 results in some morphological abnormalities in E9.5 embryos, for example, the distortion of the posterior notochord. It has been shown that notochord cells express high levels of β-catenin and also display high Wnt activity (Ukita et al., 2009). Deletion of β-catenin in Noto expressing cells attenuates posterior notochord development (Ukita et al., 2009). In this experiment the notochord continued to extend during the culture time. This may be a result of the remaining β-catenin protein sustaining the elongation of the notochord for a short time.

E9.5 β-catCKO embryos appeared to show a posterior flexion defect, however, this has not been further investigated in this study. It has been shown that *β-catenin*$^{del/del}$ ES cells do not contribute to endoderm in chimeric embryos, indicating that β-catenin may play a cell autonomous role in endoderm formation (Huelsken et al., 2000). Therefore, the posterior flexion defect in β-catCKO embryos may be due to the arrest of the gut extension. It would be interesting to investigate the role of β-catenin in gut development in future by using a gut-specific inducible Cre transgene or testing endoderm differentiation on *β-catenin* $^{del/del}$ pluripotent cells in vitro.

Taking advantage of our quantification system, I further showed that depleting β-catenin causes a significant decrease in the number of posterior mesoderm (T^+Sox2^- cells) and NM progenitors (T^+Sox2^+ cells) compared to stage-matched controls. A significant reduction of the T expressing population in E9.5 β-catCKO embryos is consistent with the previous finding that T is a direct target of Wnt/β-catenin signalling (Galceran et al., 2001; Yamaguchi et al., 1999b). Notably, the similarity in the number of T^+Sox2^+ cells between E9.5 β-catCKO and WT E8.5 embryos (Figure 3.5 A, D) indicates that continued activity of β-catenin is required for the expansion of NM progenitors.

3.2 β-catenin deletion induces neural differentiation in mesoderm fated NM progenitors

3.2.1 Aims and experimental approach

The conditional deletion experiment indicates that Wnt/β-catenin is important for the expansion of NM progenitors. However, the effects of Wnt/β-catenin on the differentiation of NM progenitors are still not known. A previous study in early zebrafish embryos shows that inhibiting Wnt signalling can divert mesoderm-fated cells towards neural fates. However, it is not clear what type of cells could convert their fate since the perturbations of Wnt signalling were performed on a population of cells whose locations were not known, and not specifically NM progenitors (Martin and Kimelman, 2012). In this experiment, I aimed to investigate whether Wnt/β-catenin signalling can specifically divert mesoderm-fated NM progenitors towards neural fates. To determine whether Wnt/β-catenin signalling plays a cell autonomous role in the fate choice of NM progenitors, I combined the grafting experiment with the 4-OHT inducible Cre-ER^{T2} system, allowing specific deletion of β-catenin in NM progenitors.

3.2.2 Results

1. AGFP L1-3 graft to PS1-2

It has been shown that cells in the PS1-2 are exclusively mesoderm-fated (Cambray and Wilson, 2007). Therefore, this site was chosen to test whether NM progenitors, in a location that should drive them towards mesoderm fates, would change the fate upon β-catenin deletion. Since the fate of NM progenitors has not yet been tested in this location, as a control, L1-3 cells from E8.5 AGFP embryos were dissected and grafted to the PS1-2 of stage matched WT embryos (Figure 3.6A). To control the effects of 4-OHT treatment on grafted cells, grafted embryos were cultured in 10μM 4-OHT for the first 8 hours of a 48-hour culture. All grafts (n=4) incorporated successfully in the axis and contributed extensively to mesoderm bilaterally as far as the tail bud (Figure 3.6B, C and Figure 3.7 A-C) (Table 3.1). Images of all recipient embryos can be found in the Appendix I, Sup Figure 3.1.

Two embryos were further examined by serial cryostat sectioning. One embryo was fully scored for the presence of GFP^+ cells in each section. Donor cells incorporated and differentiated to acquire an identity similar to their host-derived neighbours, as evidenced by GFP^+ cells in the dermomyotome expressing Pax3 (Goulding et al., 1994) (Figure 3.8A).

However, in one case, some GFP^+ cells were found in the posterior neural plate of the CNH together with an unincorporated clump ectopically expressing Sox2 (Figure 3.8B). Occasionally, a similar contribution was observed in PS1 homotopic grafts (Cambray and Wilson, 2007). Therefore, this is not an uncommon behaviour of cells in the anterior primitive streak to contribute to the posterior neural plate of the CNH. Together, these results show that NM progenitors contribute exclusively to mesoderm when placed in the mesoderm-fated PS1-2 area, indicating the differentiation decisions of NM progenitors can be easily influenced by the environment.

2. β-catCKO L1-3 graft to PS1-2

To determine the role of β-catenin specifically in NM progenitors, heterotopic grafting was performed combined with conditional deletion of β-catenin in the grafts during ex vivo culture. NM progenitors were dissected from β-catCKO embryos and then grafted to the PS1-2 region of E8.5 wild type embryos (Figure 3.6A). Embryos were then cultured with 10μM 4-OHT for the first 8 hours of 24 or 48 hours culture. All β-catCKO-derived descendants that underwent Cre-mediated recombination should express GFP at the end of the culture period, allowing tracking of their fate in the host (Figure 3.6E).

11 embryos received a graft of L1-3 cells from E8.5 β-catCKO embryos: one embryo was cultured for 24 hours, the other 10 embryos for 48 hours. 9 out of 11 grafts showed successful incorporation in the whole-mount images (Appendix I, Sup Figure 3.2). The other two embryos only exhibited large unincorporated clumps in the axis and were excluded from further analysis (Table 3.1).

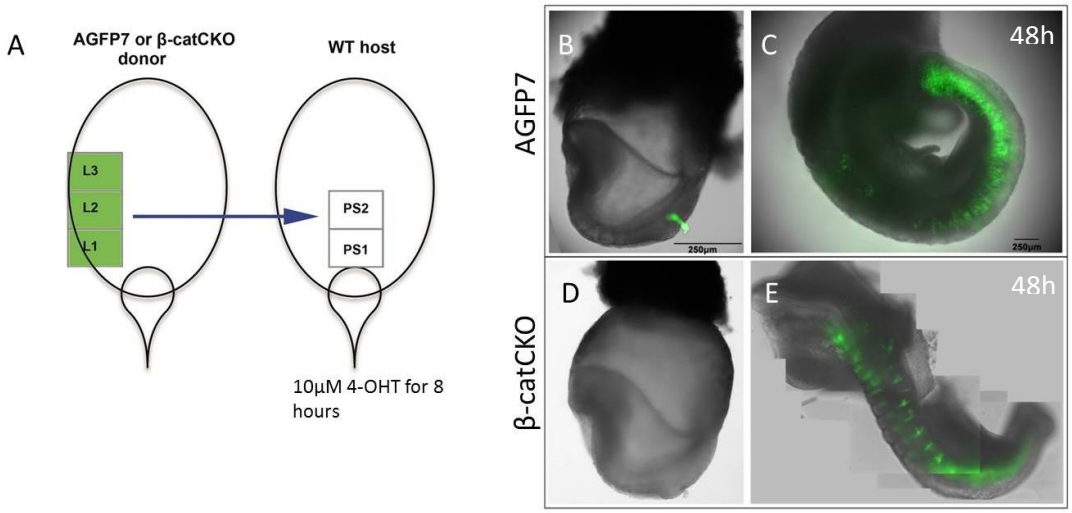

Figure 3. 6 . Conditional deletion of β-catenin in mesoderm fated NM progenitors

(A) Schematic showing the grafting procedure: caudal lateral epibast 1-3 (L1-3) was grafted to the primitive streak 1-2 (PS1-2) region.

(B and D) Representative E8.5 embryos receiving a graft from AGFP and β-catCKO embryos. The culture medium was supplemented for the first 8h with 10μM 4-OHT.

(C) Example of embryos receiving a control graft (AGFP L1-3) after 48 hours culture. Donor cells contribute extensively to the mesoderm in the host embryo.

(E) Example of embryos grafted with β-catCKO L1-3 after 48 hours culture. Donor cells contribute to the paraxial mesoderm anteriorly. However, donor cells are located to the midline posteriorly.

Table 3. 1 . Intact embryo assessment of L1-3 to PS 1-2 and L5 to PS1-3 grafts

Host location		**PS1-2**		**PS1-3**	
Donor origin		**L1-3**		**L5**	
Culture time		**24h**	**48h**	**24h**	**48h**
Donor genotype	**AGFP**	**-**	**4**	**-**	**3**
	β-catCKO	**1**	**10** (2)	**1**	**7** (1)

E8.5 wild type embryos received either AGFP or β-catCKO donor cells and then cultured ex vivo for 24 or 48 hours. The number of embryos exhibiting large unincorporated clumps is shown in brackets.

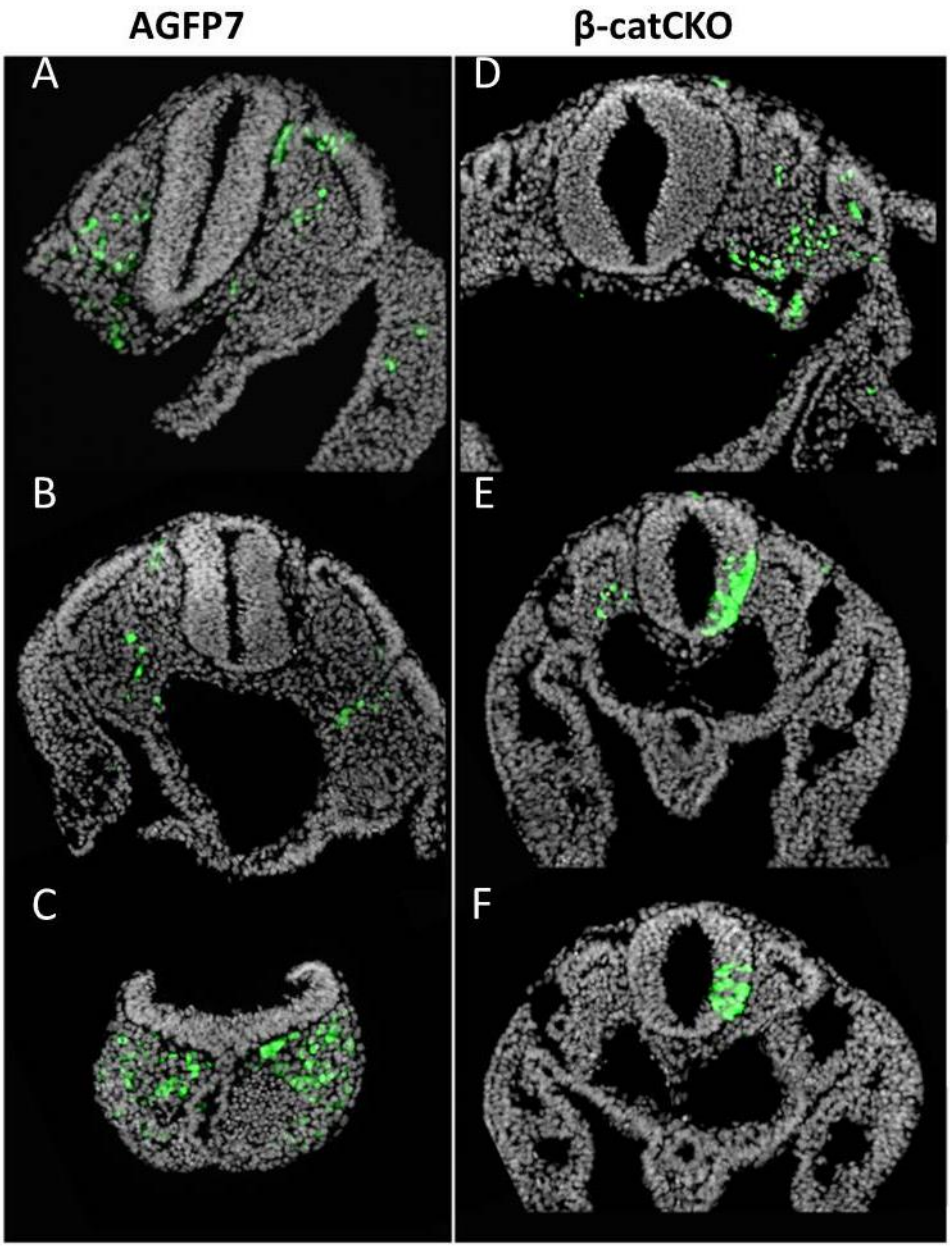

Figure 3. 7 . Analysis of the distribution of L1-3 to PS1-2 grafts

Transverse sections of representative embryos receiving AGFP (A-C) or β-catCKO (D-F) grafts after 48 hours in culture. Green, GFP immunofluorescence; grey, DAPI counterstain.

(A-C) Donor cells contributed extensively to the paraxial mesoderm bilaterally throughout the axis.

(D-F) Donor cells contributed to the paraxial mesoderm anteriorly and the neural tube posteriorly. Donor cells were exclusively in the neural tube in the posterior of the embryo.

All β-catCKO L1-3 grafts showed several well-defined patterns: mesoderm contribution was observed anteriorly, while posteriorly a densely-packed internal strip of GFP^+ cells appeared on or near the midline and continued as far as the tail bud (Figure 3.6E). Three out of 9 embryos were fully scored for the presence of GFP^+ cells in each section (Table 3.1). In all three embryos, GFP^+ cells were exclusively in the mesoderm anteriorly (paraxial and ventral mesoderm), and contributed to both neural tube and mesoderm in mid-trunk sections (Figure 3.7D, E). In posterior sections, GFP^+ cells were exclusively located in the neural tube (Figure 3.7F). A large ectopic neural-like structure was observed in the posteriormost sections of some grafts. To better demonstrate the switch of cell fate in the grafts, all sections containing GFP^+ cells from one embryo are shown in the Appendix I, Sup Figure 3.3.

Representative slides were stained, showing donor cells differentiated to acquire an identity similar to their host-derived neighbours. GFP^+ cells expressed Pax3 in the dermomyotome (Magli et al., 2013) (Figure 3.8C), Sox2 (Avilion et al., 2003) and Pax6 (Ericson et al., 1997) in the neural tube (Figure 3.8D, 8E), and Foxa2 in the floor plate (Sasaki and Hogan, 1993) (Figure 3.8F). These results indicate that NM progenitors without β-catenin are still able to differentiate appropriately into both mesoderm and neuroectoderm in the host.

To more precisely assess β-catenin deletion efficiency in GFP^+ cells, the protein level was determined using two β-catenin antibodies: one generated against amino acids 768-781 of mouse β-catenin which is aimed to detect overall β-catenin present in cells (Cowin, 1994); the other detects the active form of β-catenin which is dephosphorylated on Ser37 or Thr41 (van Noort et al., 2002). Neither total nor active-β-catenin proteins were detectable in the GFP^+ cells, indicating the virtual coincidence of β-catenin depletion and GFP expression (Figure 3.8G-H'). It is important to note that in addition to mediating canonical Wnt signalling, β-catenin is also an important component in the adherens junction (Clevers, 2006; Nelson and Nusse, 2004). Therefore, I tested whether deletion of β-catenin affected cell adhesion in GFP^+ cells. The expression of N-cadherin, a crucial adhesion protein for neural tube development, was not obviously affected in β-catenin deleted GFP^+ cells (Lele et al., 2002). A previous study suggests that plakoglobin may substitute for β-catenin functions in cell adhesion in *β-catenin* $^{del/del}$ embryos (Huelsken et al., 2000). Collectively, these experiments show that β-catenin is important for the neural vs mesoderm fate choice of NM progenitors. When it is absent, NM progenitors differentiate into neuroectoderm even in an environment that provides mesoderm differentiation signals to NM progenitors.

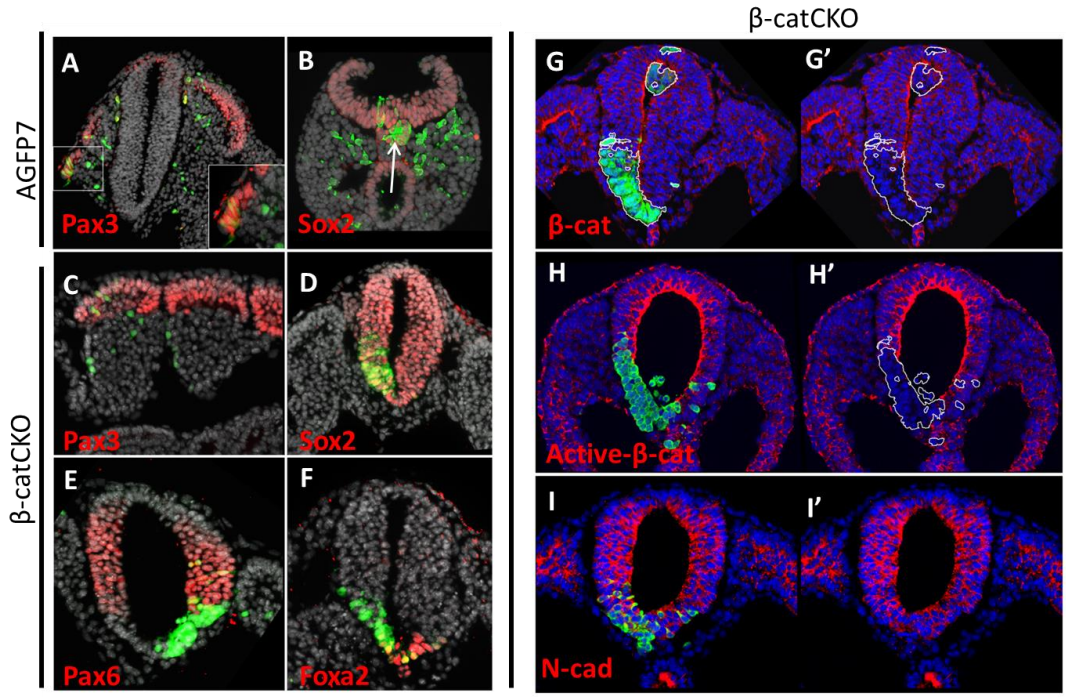

Figure 3. 8 . Analysis of gene expression of L1-3 to PS1-2 grafts

Immunofluorescent staining on the sections of host embryos receiving AGFP or β-catCKO grafts after 48 hours culture. Green: donor cells; Grey or blue: DAPI-counterstain

(A and B) L1-3 AGFP grafts. (A) Pax3, showing donor cells in the dermomyotome. Inset: enlargement of the white square area. (B) Sox2, showing donor cells contribute to the CNH. GFP^+ cells dispersed in the mesoderm do not express Sox2. However, some donor cells form an ectopic clump expressing Sox2 underneath the neural plate indicated by the white arrow.

(C-I) L1-3 β-catCKO grafts. (C) Pax3, showing donor cells in the dermomyotome. (D and F) donor cells in the neural tube expressing Sox2 (D) , Pax6 (E) and Foxa2 (F).

(G and H) β-catenin protein levels were detected by two different antibodies showing overall β-catenin and the active form of β-catenin, respectively. (G' and H') green channel was removed to allow the comparison of β-catenin levels between donor and host cells. White lines outline the position of donor cells.

(I) N-cadherin, showing donor cells can express other adhesion molecule. (I') green channel was removed from (I') for a clearer illustration

3.2.3 Conclusion and discussion

1. Wnt/β-catenin signalling regulates the fate choice of NM progenitors

In this study, I investigated the cell autonomous role of β-catenin on NM progenitors and showed that when NM progenitors were transplanted into mesodermal fated areas, they contributed to mesoderm exclusively. However, conditional deletion of β-catenin in the transplanted NM progenitors resulted in a dramatic conversion of cell fate from mesoderm to neuroectoderm (Figure 3.7). The interchangeability between mesoderm and neuroectoderm has been observed after conditionally inducing Dkk1 (a Wnt inhibitor) in the zebrafish (Martin and Kimelman, 2012). However, there is no direct evidence in mouse embryos to show that cells can switch fate between neural and mesodermal lineages during somitogenesis. This experiment shows for the first time that NM progenitors are able to switch their fate between two lineages according to the intrinsic β-catenin level.

Since β-catenin is a dual function protein, it is not clear if the fate changes depend on Wnt/β-catenin signalling. A previous study shows that ES cells expressing low levels of β-catenin in the ROSA26 locus are able to sustain cell adhesion, but not Wnt signalling. These *ROSA26*$^{\beta/+}$ ES cells display a significant differentiation bias toward neural fates (Rudloff and Kemler, 2012). Moreover, β-catCKO cells in the neural tube express N-cadherin at a similar level as their neighbouring donor derived cells, suggesting other proteins may substitute for the function of β-catenin in cell adhesion. Therefore, it is probably that the fate choice of NM progenitors is regulated by β-catenin via Wnt/β-catenin signalling.

2. Wnt/β-catenin is required cell autonomously for initiating mesodermal fate in NM progenitors but not for further mesoderm differentiation

The anterior mesoderm contribution in β-catCKO grafts may be due to some donor cells migrating away from the primitive streak before β-catenin was downregulated. The successful integration of these β-catCKO cells in the anterior paraxial mesoderm (Figure 3.8C) suggests that deletion of β-catenin may not affect mesodermal differentiation of mesodermal progenitors (this will be further discussed below). In contrast, the later differentiating β-catCKO cells in the primitive streak which had downregulated β-catenin converted to neuroectoderm. This may be because low levels of β-catenin block epithelial-to-mesenchymal transition (EMT) of NM progenitors. Therefore, NM progenitors with low β-catenin levels can only differentiate to neuroectoderm. Collectively, these results indicate that deletion of β-catenin does not affect mesodermal differentiation once cells are

committed to mesodermal lineage but only blocks the initiation of mesodermal fate from NM progenitors.

3. Roles of β-catenin in neural differentiation

In this experiment I show that deletion of β-catenin induces NM progenitors to choose a neural fate. Cells without β-catenin are able to integrate into the neural tube, suggesting that β-catenin may not be required for neural differentiation at least for a short period. However, since the embryos could only be cultured ex vivo for 48 hours, the further development of these *β-catenin* $^{del/del}$ neural cells is not known. Therefore, based on the results of this study the effects of the loss of β-catenin on neural differentiation are not clear.

The role of β-catenin on neural development has been investigated in other studies both in vivo and in vitro. Generally, Wnt/β-catenin signalling is important for neural development since conditional ablation of β-catenin in the neural tube results in a smaller brain in the mutants (Gulacsi and Anderson, 2008; Junghans et al., 2005; Machon et al., 2003; Zechner et al., 2003). Specifically, conditional deletion of β-catenin in the central nervous system does not cause the disappearance of neural stem cells or neural progenitors but affects the expansion of neural progenitors. It has been hypothesised that the lack of neural progenitors in the mutants is due to an increase in cell death rather than the arrest of cell proliferation in *β-catenin* $^{del/del}$ cells (Valenta et al., 2011; Zechner et al., 2003). Moreover, an in vitro clonal differentiation assay in a solid collagen matrix shows that although *β-catenin* $^{del/del}$ neural stem cells display a poor adhesion ability, these cells are still able to differentiate into neurons, glia, astrocytes and oligodendrocytes, suggesting that differentiation proportions are not attenuated in *β-catenin* $^{del/del}$ neural stem cells. However, an increase in cell death is reported when culturing *β-catenin* $^{del/del}$ neural progenitors in vitro (Holowacz et al., 2011). Similarly, I also observed some *β-catenin* $^{del/del}$ donor cells in the neural tube with small, condensed nuclei and an increased number of nuclear body fragments (Figure 3.8G), indicating they are apoptotic cells. Collectively, these results indicate that although β-catenin is not required for the initiation and differentiation of neural progenitors, it is important for their optimal survival.

4. Whether *β-catenin* $^{del/del}$ NM progenitors can contribute to the dorsal neural tube remains unknown

The fate map in the chick embryo shows that cells in the midline region of the posterior neural plate gives rise to the floor plate or the ventral part of the neural tube, whereas cells in the lateral regions contribute to the walls of the neural tube, the roof plate and the neural crest (Catala et al., 1996). The preliminary results from our group also suggest that cells in the very lateral part of the anterior CLE contribute to the dorsal neural tube. In this study, cells were grafted to the midline of the embryos (PS1-2), where they were close to ventral neural tube fated cells. After deletion of β-catenin, the grafts quickly adopted a neural fate similar to their closest neighbours. Therefore, in this experiment *β-catenin* $^{del/del}$ NM progenitors converted their fate to give rise to the ventral but not dorsal neural tube. Currently, it is not clear whether *β-catenin* $^{del/del}$ NM progenitors are able to contribute to the dorsal neural tube. However, since the locations of dorsal neural tube fated cells have been identified, it would be interesting to investigate whether *β-catenin* $^{del/del}$ NM progenitors could give rise to the dorsal neural tube by grafting β-catCKO cells into dorsal neural tube-fated regions.

5. The possible reasons for the formation of unincorporated neural structures in the most posterior region of the host embryos

In all 8 β-catenin grafts, unincorporated neural structures were observed in the most posterior region of the host embryos. This could be the result of excess cells being originally grafted. However, in the control experiment when cells from the AGFP embryos were grafted, an ectopic structure was only observed in one out of four embryos. Since the deletion of β-catenin has been indicated to enhance the self-renewal capacity of neural stem cells, it is possible that too many neural progenitors were generated by *β-catenin* $^{del/del}$ cells. Moreover, the diameter of the neural tube is much smaller in the tail than in the trunk. Therefore, ectopic neural structures are speculated to arise from excess neural fated cells residing in the posterior part of the embryos, which cannot all incorporate into the small tail neural tube.

3.3 β-catenin deletion does not convert mesodermal progenitors (L5 cells) into neuroectoderm

3.3.1 Aims and experimental approach

Since previous experiments have shown that β-catenin deletion switches mesoderm fated NM progenitors to neuroectoderm, it would be interesting to test whether β-catenin deletion can switch mesoderm committed cells to neuroectoderm. The posteriormost CLE (L5) has been considered as a committed mesoderm population for the following reasons: (1) L5 cells only express T but not T/Sox2 (Figure 2.1B); (2) they are fated exclusively for lateral and ventral mesoderm (Cambray and Wilson, 2007); (3) they fail to adopt neural fates when grafted into anterior of the NSB which has been shown to direct L1-3 cells to a neural fate (Wilson lab, unpublished data). To investigate whether the loss of β-catenin could induce mesoderm committed cells to convert their fate to neuroectoderm, a similar experimental approach was applied as previously: L5 cells from β-catCKO embryos were grafted to the mesoderm committed areas of E8.5 WT embryos. β-catenin was deleted in the grafts using the 4-OHT inducible Cre-ER^{T2} system during embryo culture.

3.3.2 Results

1. AGFP L5 graft to PS1-3

As a control, L5 cells dissected from E8.5 AGFP embryos were grafted to the PS1-3 position of stage-matched WT embryos (Figure 3.9A, B). Three embryos were cultured for 48 hours with all grafts demonstrating successful incorporation in the mesoderm throughout the axis (Figure 3.9C) (Table 3,1). Images of all recipient embryos can be found in Appendix I, Sup Figure 3.4. One embryo appeared to only contribute to ventral mesoderm according to the whole-mount images. The other two, which had much wider GFP contribution, were sectioned to determine the cell contribution. GFP^{+} cells integrated extensively in paraxial, ventral and lateral mesoderm bilaterally along the axis with only a few cells in the TBM but not CNH (Figure 3.10A-C). Representative slides were stained, showing that donor cells incorporated and differentiated to acquire an identity similar to their host-derived neighbours, as evidenced by GFP^{+} cells in the ventral and lateral mesoderm expressing pdgfrβ (Figure 3.11A) (Hellstrom et al., 1999).

Four more repeats were done by Dr. F Wymeersch and Prof. V Wilson. Three of them were fully scored by vibratome sections. Similar contribution patterns were observed (Wilson lab,

unpublished data). Together these results show that although L5 cells are fated exclusively for lateral and ventral mesoderm, they are able to differentiate to paraxial mesoderm in response to environmental cues.

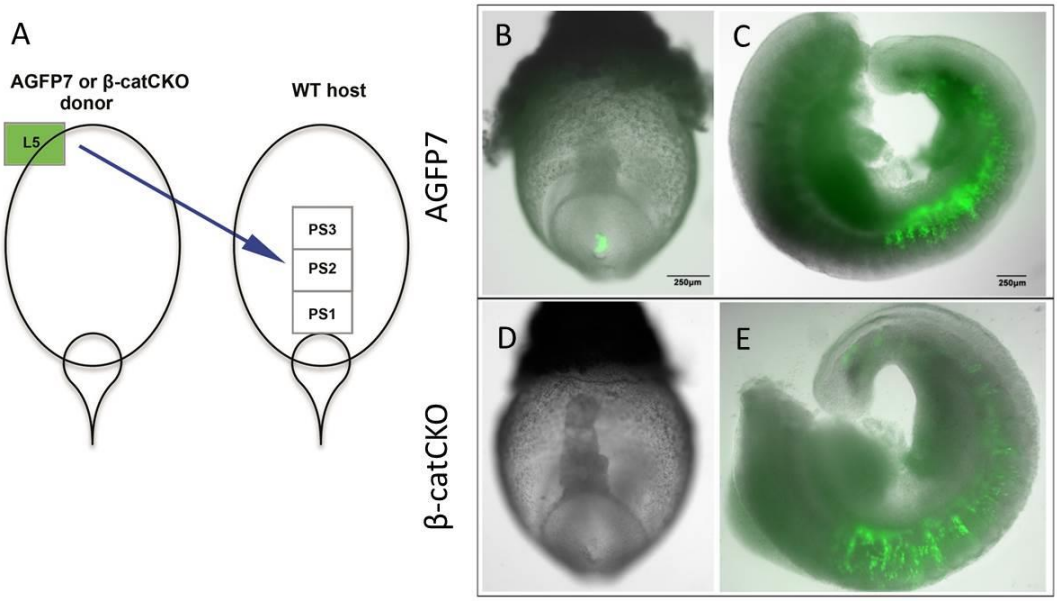

Figure 3. 9 . Conditional deletion of β-catenin in L5 cells

(A) Schematic showing the grafting procedure: caudal lateral epibast 5 (L5) cells were grafted to the primitive streak 1-3 (PS1-3) region.

(B and D) Representative E8.5 embryos receiving a graft from AGFP and β-catCKO embryos. The culture medium was supplemented for the first 8h with 10µM 4-OHT.

(C) Example of embryos receiving a control graft (AGFP L5) after 48 hours culture. Donor cells contributed extensively to the lateral and ventral mesoderm in the host embryo.

(E) Example of embryos grafted with β-catCKO L5 after 48 hours culture. Donor cells contributed extensively to the mesoderm in the host embryo.

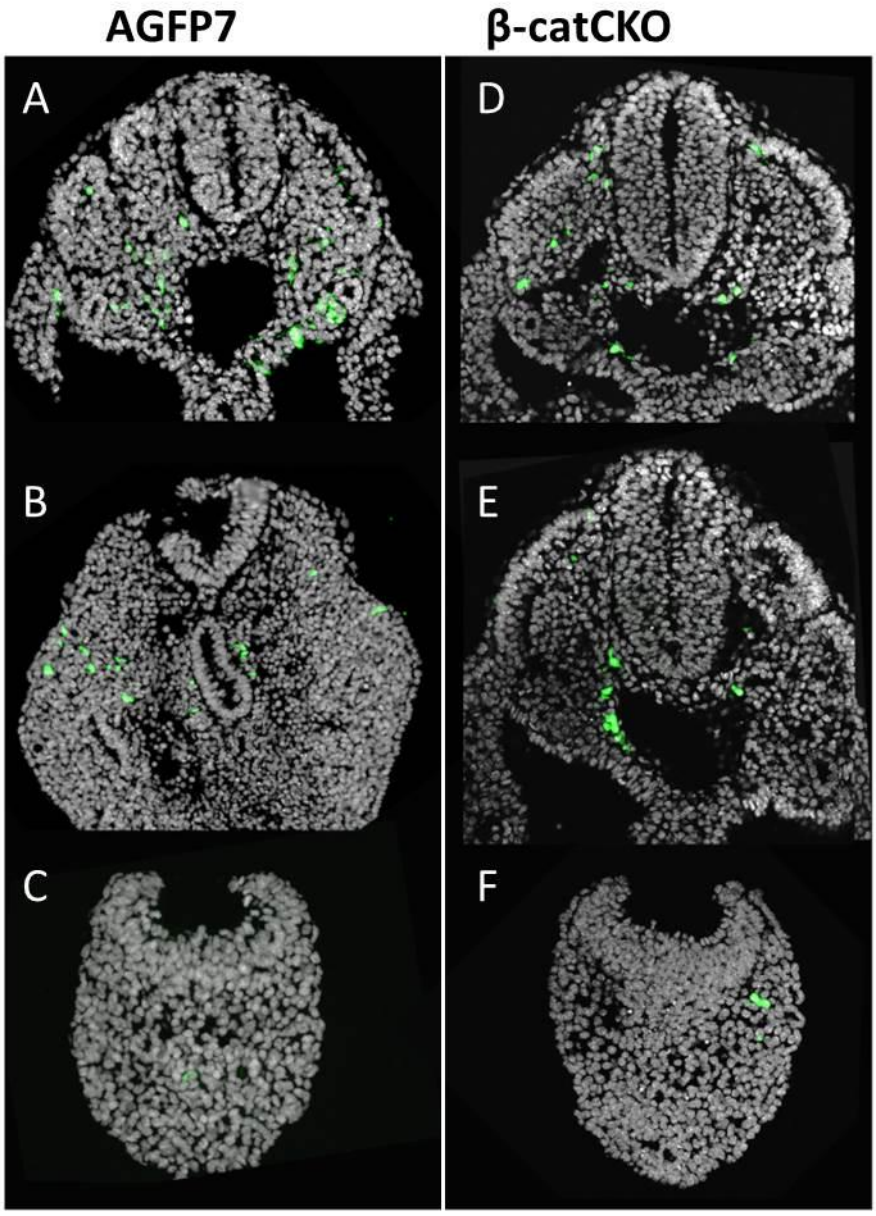

Figure 3.10. Analysis of the distribution of L5 to PS1-3 grafts

Transverse sections of representative embryos receiving AGFP (A-C) or β-catCKO (D-F) grafts after 48 hours in culture. Donor cells (green) continuously contributed extensively to the mesoderm bilaterally throughout the axis. Green, GFP immunofluorescence; grey, DAPI counterstain.

2. β-catCKO L5 graft to PS1-3

To investigate whether deletion of β-catenin is able to switch mesoderm committed L5 cells to neuroectoderm, heterotopic grafting was performed combined with conditional deletion of β-catenin in the grafts during ex vivo culture. L5 cells were dissected from β-catCKO embryos and then grafted to PS1-3 in E8.5 WT embryos (Figure 3.9A, D). Embryos were then cultured with 10μM 4-OHT for the first 8 hours of a 24 or 48-hour culture. The descendants of β-catCKO grafts expressed GFP at the end of culture, allowing tracking of their fate in the host (Figure 3.9E).

8 embryos received a graft of L5 cells from β-catCKO embryos: one was cultured for 24 hours, the other 7 embryos for 48 hours (Table 3.1). 7 out of 8 grafts successfully incorporated in the mesoderm according to the whole-mount images (Figure 3.9E and Appendix I, Sup Figure 3.4). Another embryo only exhibiting unincorporated clumps in the axis was excluded from further analysis.

Similar to the AGFP grafts, GFP^+ cells extensively contributed to the mesoderm in the trunk, with only a few cells in the tail bud (Figure 3.9E). To further determine the distribution of GFP^+ cells, three embryos were sectioned and one was imaged in whole-mount using a confocal microscope. All four embryos showed exclusive contribution to paraxial, ventral and lateral mesoderm but not neuroectoderm (Figure 3.10D-F). Occasionally, small, unincorporated clumps ventral to the neural tube were observed in the posterior sections (Figure 3.11C). However, these small clumps did not express Sox2, T or Foxa2, indicating they are neither neural nor notochord-like structures (Figure 3.11D-F). Although β-catenin levels were much lower in GFP^+ cells compared with their host-derived neighbours (Figure 3.11B), β-catCKO cells still integrated well in the host throughout the AP axis. This suggests that β-catenin may not be required for the further differentiation of mesoderm progenitors. Notably, β-catCKO L5 cells did not contribute to the neural tissue, indicating β-catenin deletion cannot convert mesodermal progenitors into neuroectoderm

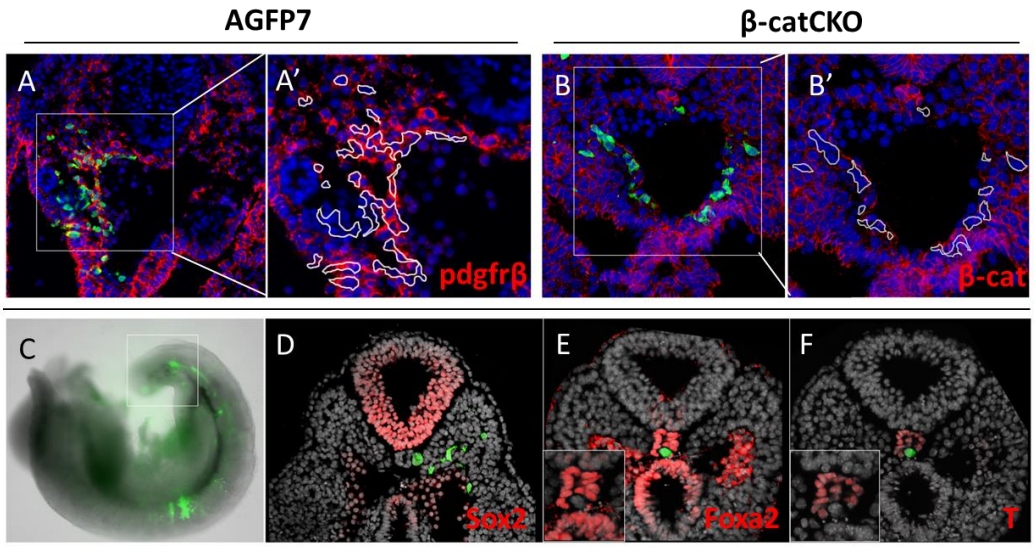

Figure 3.1 1. Analysis of gene expression of L5 to PS1-3 grafts

Immunofluorescence on host embryos receiving an AGFP or β-catCKO graft after 48 hours in culture. Green: donor cells. Grey or blue: DAPI-counterstain.

(A) L5 AGFP grafts. Donor cells in the ventral mesoderm express pdgfrβ. (A') enlargement of the white box in (A). Green channel was removed to allow the comparison of pdgfrβ expression between donor and host cells.

(B-F) L5 β-catCKO grafts. (B) Donor cells express low to undetectable levels of b-catenin compared with the host cells. (B') enlargement of the white box in (B) with the removal of green channel.

(E) Example of embryos receiving a β-catCKO L5 graft which formed small clumps in the tail after 48 hours culture. (D-F) Representative sections from the embryo in (C). Clumps formed by donor cells do not express Sox2 (D), Foxa2 (E) or T (F). Inset: enlargement of the notochord area with the removal of green channel.

3.3.3 Conclusion and discussion

1. Lateral/ventral mesoderm (LVM) and paraxial mesoderm fates are reversible in response to extrinsic cues

As mentioned previously, L5 cells have been considered as a committed mesoderm population. The fate map demonstrates that L5 cells are fated exclusively for LVM (Cambray and Wilson, 2007). In contrast, cells in the anterior of the primitive streak produce paraxial mesoderm. In this study, I showed that when grafted to PS1-3, L5 cells were able to also differentiate into paraxial mesoderm, indicating that early committed mesoderm progenitors still have the potential to differentiate into a range of mesodermal cells in response to environmental cues. According to the microarray analysis from our group, elevated BMP signalling characterises L5 cells compared with PS1, reinforcing previous conclusions that BMP signalling is involved in inducing the LVM but blocking paraxial mesoderm formation. For example, it has been shown in chick that Noggin, a BMP antagonist, can induce paraxial mesoderm formation from lateral plate cells (Tonegawa and Takahashi, 1998). Moreover, mosaic inactivation of Bmpr1a in the epiblast of mouse embryos (Bmpr-MORE) results in ectopic somite formation in the lateral areas (Miura et al., 2006). Furthermore, FGF signalling has been implicated in promoting paraxial mesoderm formation (Ciruna and Rossant, 2001). Inhibition of FGF signalling can partially rescue the abnormal expansion of somites in Bmpr-MORE embryos (Miura et al., 2006). Collectively, these studies indicate that early committed mesoderm progenitors can easily change their fate between LVM and paraxial mesoderm according to the levels of BMP and FGF signalling in the environment.

2. Deletion of β-catenin cannot divert mesodermal committed cells to give rise to neuroectoderm

In this experiment, I showed that L5 cells failed to adopt neural fates even after the deletion of β-catenin, which is sufficient to divert mesoderm to a neural fate in NM progenitors. Moreover, a recent experiment in our group shows that even ectopic expression of Sox2 in L5 cells also does not lead to their integration in the neural tube (Wilson lab, unpublished data). The inability of L5 cells to convert to neuroectoderm indicates that L5 cells are committed mesodermal cells which are a distinct population from NM progenitors. Therefore, it is probable that only NM-potent lineage progenitors can switch between neural and mesodermal fates in response to intrinsic β-catenin levels. It is also consistent with the

previous result that loss of β-catenin cannot convert NM progenitor-derived mesoderm that had migrated away from the primitive streak to a neural fate (Figure 3.10D, E).

3.4 Discussion

Understanding how multipotent cells make their fate decisions in early embryos provides important insights into the in vitro differentiation of particular cell types, which in future may contribute to therapeutic approaches after injury or disease. In this study, I have shown that β-catenin is required in a cell autonomous manner for the initiation of mesoderm fate choice in NM progenitors; in its absence NM progenitors differentiate into neuroectoderm even in mesoderm fated areas. However, loss of β-catenin in mesoderm-committed cells does not appear to affect their ability to undergo mesoderm differentiation.

In mice, some Wnt related mutants such as *Wnt3a*$^{-/-}$, *Tcf1*$^{-/-}$*;Lef1*$^{-/-}$, *T/T* and *Tbx6*$^{-/-}$ embryos, display severe posterior truncations with excessive neural tissues and aberrant mesoderm cells in the posterior region (Chapman and Papaioannou, 1998; Galceran et al., 1999; Yamaguchi et al., 1999b; Yoshikawa et al., 1997). There are two possible interpretations for the phenotype in these mutants: one is that low Wnt signalling promotes the expansion of neural progenitors and inhibits the growth of mesoderm progenitors; the other is low Wnt signalling induces all NM progenitors to take a neural fate. Since I have shown in this study that deletion of β-catenin in committed mesoderm progenitors does not affect their growth and differentiation, it is unlikely that low Wnt signalling would lead to inhibition of the expansion of mesoderm progenitors. In my opinion, low Wnt signalling in these mutants may block the initiation of mesoderm progenitors from NM progenitors by preventing them from undergoing EMT. Subsequently, all these cells are forced to undertake a neural fate, resulting in the accumulation of neural tissues and the loss of mesoderm cells in the posterior.

Because it is known that the attenuation of Wnt signalling induces the neural differentiation of NM progenitors, it would be interesting to investigate which signal triggers mesoderm fate choice of NM progenitors. Few studies in mouse embryos have shown an increase of mesoderm fated cells in the posterior progenitor zone except one recent study showing a thickened primitive streak in *Sox3*$^{-/-}$*; Sox2* $^{\triangle N2/\triangle N2}$ embryos (Yoshida et al., 2014). A study in zebrafish shows that cells in the ventral margin are mainly fated to be mesoderm with some contribution to the spinal cord. Elevating Wnt/β-catenin signalling in these ventral margin cells at the beginning of gastrulation significantly reduces their neural contribution (Martin and Kimelman, 2012). However, according to my preliminary results, enhancing Wnt/β-

catenin signalling in neural fated NM progenitors using a transgenic strain that expresses constitutively active β-catenin does not appear to convert their fate into mesoderm (Data not shown). Therefore, besides enhancing Wnt signalling other factors may be required to induce mesoderm differentiation from NM progenitors.

Since L2-3 are mesoderm fated NM progenitors, comparing their transcription profiles with NSB cells, which are the NM progenitors fated to be both neurectoderm and mesoderm, would provide a clue to this question. However, our microarray data shows no significant transcriptional changes between the dorsal layer of NSB and L1-3. When comparing PS1 with dorsal layer of NSB and L1-3, only two genes, *Tbx6* and *Dll1*, show a significant increase in PS1. According to the immunofluorescence, some cells in the PS1 coexpress T/Sox2 (Figure 2.1B). The previous grafting results show that although PS1 are mesoderm fated cells, occasionally they contribute to neurectoderm when grafted to NSB (Cambray and Wilson, 2007). Therefore, it is likely that there are some NM progenitors in PS1 and the high expression of Tbx6 and Dll1 in this region may indicate the initiation of mesodermal fate choice from NM progenitors.

Tbx6, a member of the T-box family of transcription factors, is expressed in the primitive streak, tail bud, and PSM in mouse embryos. Tbx6 expression is rapidly downregulated as the PSM undergoes segmentation to form somites (Chapman et al., 1996). It has been shown that expression of Tbx6 is essential for the initial specification and correct patterning of posterior somites; in its absence, posterior somites are replaced by ectopic neural structures after the forelimb bud (Chapman and Papaioannou, 1998). These ectopic neural structures express Sox2, Wnt3a and show the activation of Sox2 N1 enhancer (Yoshida et al., 2014). Interestingly, *Tbx6*$^{-/-}$*; Sox2* $^{\triangle N2/\triangle N2}$ embryos fail to express mesoderm and endoderm markers. These observations indicate that Tbx6 expression is important for both inhibition of neural fate choices and specification of mesoderm development. Moreover, it has been indicated that Tbx6 is directly regulated by T expression which is a downstream target of Wnt/β-signalling (Szeto and Kimelman, 2004; Yamaguchi et al., 1999b). Therefore, Tbx6 is also regulated by Wnt/β-signalling. It has been shown that the expression of Dll1, a Notch ligand, is lost in *Tbx6*$^{-/-}$ mutants (Chapman and Papaioannou, 1998; White et al., 2003). Also, Tbx6 and Tcf/Lef factors can bind to Dll1 enhancer (White and Chapman, 2005). Therefore, these results indicate that Tbx6 may directly regulate Dll1 expression.

In my opinion, the important factors for initiating mesoderm development from NM progenitors are combined high Wnt/β-catenin signalling and Tbx6 expression. In NM progenitors only when Wnt/β-signalling activates T and then Tbx6 expression, will they

adopt a mesoderm fate. Later, Tbx6 and Wnt signalling may stimulate Notch signalling through Dll1 to guide mesoderm differentiation of these newly specified mesoderm progenitors.

Chapter 4. In vivo potential of pluripotent stem cells and their derivatives in postimplantation embryos

4.1 In vivo functional equivalence between EpiSCs and epiblast in streak stage embryos (E6.5-E7.5)

4.1.1 Aims

The ability of mESCs to contribute to all cell types in chimeras, including germ cells, by blastocyst injection (Bradley et al., 1984) demonstrates their functional equivalence to preimplantation epiblast cells. However, as described previously, most EpiSCs are unable to contribute to chimeras upon blastocyst injection or morula aggregation (Brons et al., 2007; Tesar et al., 2007). The lack of an in vivo assay for the potency of most EpiSCs raises the issue of whether these cells represent a true in vitro counterpart of an in vivo cell type. Alternatively, EpiSCs derived from postimplantation embryos may be incompatible with the environment of preimplantation embryos. Therefore, to assess the in vivo potential of EpiSCs, these should be challenged with the environment of the postimplantation embryos. In this study, I grafted EpiSCs into streak stage embryos (E6.5-E7.5) which were then cultured ex vivo for 24-48 hours, permitting analysis of cell integration.

The work described in this chapter has been published (Huang et al., 2012; Tsakiridis et al., 2014). For full article see Appendix II. All cell culture work in this chapter was done by Dr. A Tsakiridis and Dr. R Osorno.

4.1.2 Results

1. Verifying grafting and ex vivo embryo culture technique

EpiSCs expressing green fluorescent protein (GFP) were manually scraped from the culture dish and grafted into four sites of E7.5 embryos (early-streak to late-streak stage): mid-anterior (MA), distal (D), mid-posterior (MP), and proximal-posterior (PP) (Figure 4.1A-C). To determine the number of cells that initially grafted into the embryos, four embryos were fixed immediately after grafting and stained with DAPI. The embryos were imaged under a confocal microscope. The number of GFP^+ cells was manually counted. An examination of confocal z-stacks (Figure 4.1C) showed that 10 to 16 cells (n=4, average 12 cells/embryo) were grafted into each embryo.

Two EpiSC lines that ubiquitously express GFP (r04-GFP, derived from E6.5 epiblast, and C2, derived in vitro from mESCs) were injected. Two mESC lines (AGFP7, which

ubiquitously expresses GFP, and TßC44cre6 (Nanog:GFP), which expresses GFP under Nanog regulatory control) were also injected for comparison. Both mESC lines efficiently form chimeras following blastocyst injection (Chambers et al., 2007; Gilchrist et al., 2003). After grafting, embryos were cultured ex vivo and analysed after 24 or 48 hours. The distribution of donor cells was assessed by fluorescence microscopy (Figures 4.1D-F).

A total of 91 embryos received a graft of either EpiSCs or mESCs. Most of them (n = 81) developed normally and contained labelled cells after culture, verifying that the grafting technique is efficient. The remainder either did not contain labelled cells after culture (n = 4) or developed abnormally (n = 6), which were excluded from the analysis. In these 81 embryos, there are 44 embryos grafted with embryo-derived EpiSCs (r04-GFP), 16 with in-vitro-derived EpiSCs (C2), 13 with AGFP7 mESCs, and 8 with TßC44cre6 (Nanog:GFP) mESCs (Figure 4.2A). In addition to Nanog:GFP mESCs, 73 embryos received grafts of cells carrying ubiquitously expressed GFP, 55 of which were analysed after 24 hours in culture, and the remainder analysed after 48 hours culture (Figure 4.2A).

2. The criteria for bona fide chimeras

To describe the distribution of donor cells in the host after culture, embryos were scored for the approximate number of GFP^+ cells that had dispersed from the graft site, and also spread within the host based on the whole-mount fluorescent images (Figures 4.1D-F and Figure 4.3). The results of EpiSC and mESC grafts were compared using the number of dispersed GPF cells and their spread as a semiquantitative assessment of donor cell contribution.

Following culture, an embryo was considered to be a bona fide chimera if the following criteria were met: (1) at least 12 GFP^+ cells had clearly dispersed from the graft site, indicating that donor cells had survived and/ or proliferated in the host; (2) dispersed GFP^+ cells were not restricted to one area and had spread over >1/4 of the embryo's anteroposterior length, indicating robust intermixing with the host cells.

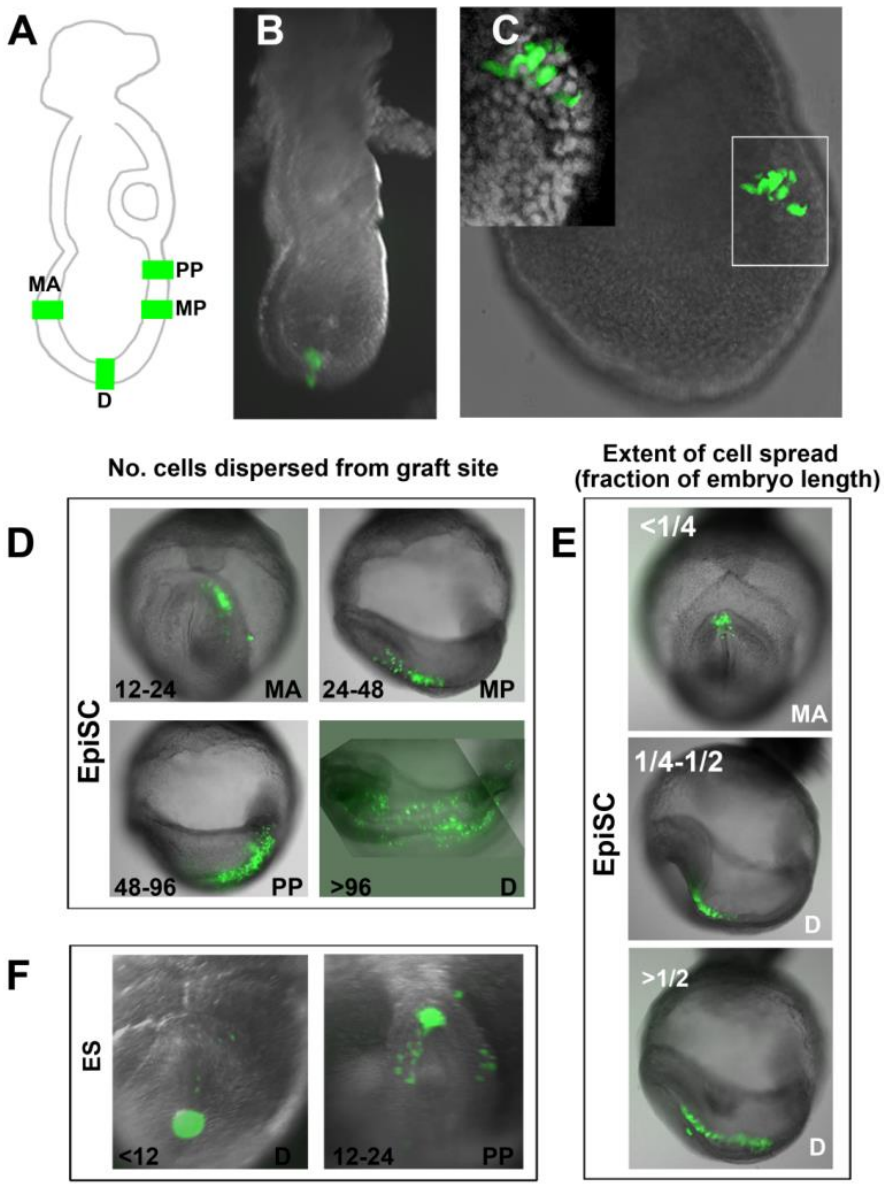

Figure 4. 1 **. Grafting procedure and the distribution of donor cells in host embryos**

(A) Diagram of late-streak embryo, showing graft sites (MA, D, MP, and PP) in the egg cylinder.

(B and C) GFP-labeled cells (green) overlaid on a brightfield or DAPI-counterstained image (C, inset). (B) Embryo-derived EpiSC (r04-GFP) grafted to the D region of a late streak stage embryo (E7.5). (C) Confocal z-stack showing a mid-streak stage embryo (E7.0) with C2 in-vitro derived EpiSC in the MP region. Inset: confocal z-slice showing individual grafted cells.

(D–F) Examples of cell contribution to embryos grafted at indicated sites (lower right of each panel) after culture. Culture period: 24 hours, except for lower right in (D), when it was 48 hours. (D) Embryos with different numbers of dispersed embryo-derived EpiSCs. (E) Embryos with different extents of embryo-derived EpiSC cell spread along the anteroposterior axis. (F) Embryos grafted with ESCs (AGFP7).

MA: mid-anterior; D: distal; MP: mid-posterior; PP: proximal-posterior

3. EpiSCs proliferated extensively in streak stage embryos (E6.5-E7.5)

The profiles of the contributions made by in-vitro and embryo-derived EpiSCs to embryos were similar (Figure 4.2A), and therefore we combined those data in the following analysis (Figures 4.2B-D). Both EpiSC lines incorporated efficiently into the D, MP, and PP regions (Figures 4.2B-D). In the D region, 17 of 18 embryos contained ≥ 12 dispersed GFP^+ cells. GFP^+ cells spread over >1/4 of the embryo's length in 19 of 22 embryos (Figure 4.2C). Similarly, in the MP and PP regions, 21 of 23 embryos contained ≥ 12 dispersed GFP^+ cells, which spread over >1/4 of the embryo's length in all 21 embryos (Figure 4.2D). Hence, the overwhelming majority (82%–91%) of the embryos grafted with EpiSCs in D, MP, and PP regions formed bona fide chimeras (Figures 4.2C, D). Images of all recipient embryos can be found in the Appendix I, Sup Figure 4.1-4.5.

Moreover, after 24 hours in culture, 20 chimeras (74% of those injected in D, MP, and PP regions) contained 24–96 dispersed GFP^+ cells, indicating cell proliferation in the host (Figures 4.2A, C and D). After 48 hours in culture, more than half of the embryos injected into the D, MP and PP regions contained >96 dispersed GFP^+ cells, distributed throughout >1/2 of the embryo's length (Figure 4.2A). Some embryos contained about 300 GFP^+ cells (Figures 4.3), indicating further proliferation and dispersal between 24 and 48 hours. Together, these results suggest that EpiSC readily proliferate and disperse from regions that are in the primitive streak (MP and PP regions) or are recruited there during culture (D region).

EpiSCs that were grafted in the MA region showed less cell dispersal. Just under half (47%) of the embryos contained ≥ 12 dispersed GFP^+ cells after culture. GFP^+ cells extending for >1/4 of the embryo's length were seen in only 20% of the embryos (Figure 4.2A, B). Fate maps indicate that few, if any, cells in the MA region will be recruited to the primitive streak by the mid-streak to late-streak stage (E7.0-E7.5) (Lawson et al., 1991). The primitive streak is a site of extensive cell rearrangement and may provide grafted cells in these regions with a greater opportunity for cell intercalation with the host than cells grafted at the MA site. Alternatively, the high levels of Nodal and FGF signalling in distal and posterior regions of the embryo may favour EpiSCs growth because these pathways are important for EpiSC maintenance.

A

Donor cells	Culture time of embryos	Graft site	Stage of recipients	No.of grafted embryos	Dispersed donor cells					Cell spread		
					<12 cells	12-24 cells	24-48 cells	48-96 cells	>96 cells	<1/4	1/4-1/2	>1/2
Embryo-derived EpiSC (r04-GFP)	24h	MA	M-LS	12	5	7				8	4	
		D	M-LS	8			7	1			6	2
		MP	LS	4	1			3		1	2	1
		PP	M-LS	6	1	1	3	1		1	5	
	48h	D	M-LS	5+(4)			3		2	1+(2)	1+(2)	3
		MP	MS	1			1				1	
		PP	E-MS	4				1	3			4
In vitro derived EpiSC (C2)	24h	MA	MS	3	3					3		
		D	M-LS	5	1	3	1				5	
		MP	MS	4			2	2			3	1
	48h	PP	ES	4				1	3		1	3
ES cells (AGFP7)	24h	D	M-LS	7	7					6	1	
		PP	M-LS	6	3	2	1			5	1	

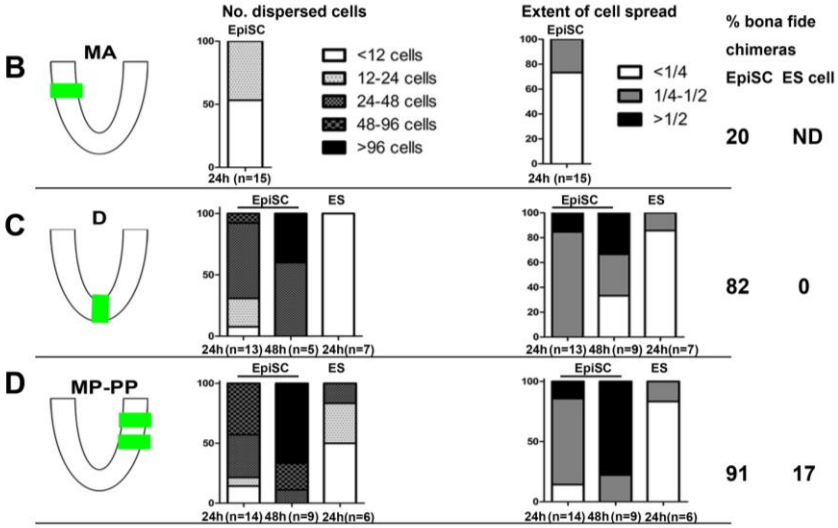

Figure 4. 2 . Analysis of donor cell proliferation and chimera formation rate

(A) List of all grafted embryos. Yellow highlight: ≥50% of embryos fall in the category indicated. Gray type: embryos considered not to be bona fide chimeras.

(B-D) Histograms showing the percentage of embryos for each category of graft containing different numbers of dispersed donor cells and extents of cell spread. The percentage of bona fide chimeras is shown at the right.

Note: cells grafted to the D site of four embryos cultured for 48 hours (brackets) were located internally and consequently only the extent of spread, not the number of dispersed cells,was scored. MA: mid-anterior; D: distal; MP: mid-posterior; PP: proximal-posterior

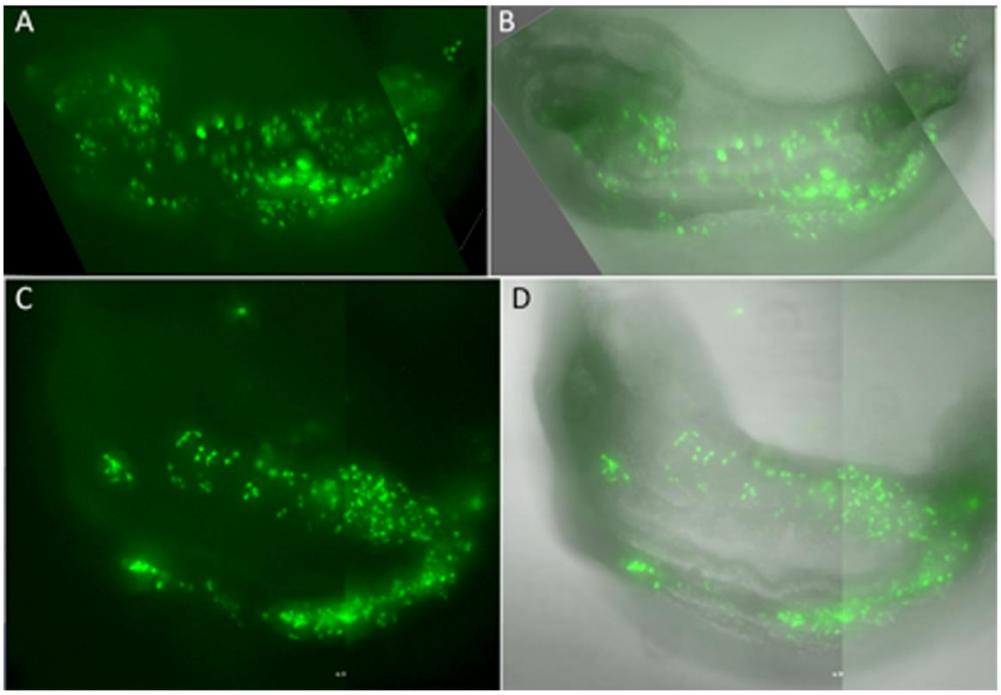

Figure 4. 3 . EpiSCs in host embryos after 48 hours in culture

(A and B) GFP channel (A) and bright field (B) overlay. (B) In vitro-derived EpiSCs (C2) grafted to the proximal-posterior (PP) region of an early streak stage embryo (E6.5) after 48 hours culture.

(C and D) GFP channel (C) and bright field (D) overlay. (D) Embryo-derived EpiSCs (r04-GFP) grafted to the PP region of an early streak stage embryo (E6.5) after 48 hours culture.

4. The successful incorporation and contribution of EpiSCs in bona fide chimeras

To determine whether the dispersed donor cells differentiate to acquire the identity of their immediate host-derived neighbours, cultured embryos were sectioned and assessed for cell integration. Double nuclear and actin filament staining revealed that the morphology of the GFP^+ cells was similar to that of their neighbours (Figure 4.4B). Immunohistochemistry showed that in all assays of somatic lineages (n = 27; Table 4.1), both in-vitro and embryo-derived EpiSC descendants expressed markers characteristic of their host location (Figure 4.4 and Table 4.1). GFP^+ cells express T in the primitive streak and emergent mesoderm (Wilkinson et al., 1990) (Figure 4.4C), Tbx6 in the PSM (Chapman et al., 1996) (Figure 4.4D), AP-2a (Tcfap2a) in the surface ectoderm (Arkell and Beddington, 1997) (Figure 4.4E), Foxa2 in the floor plate and endoderm (Sasaki and Hogan, 1993) (Figures 4.4F, G), and Cdx2 in the allantois and posterior mesoderm (Beck et al., 1995) (Figure 4.4H). It should be noted that T (Wilson et al., 1995), Foxa2 (Dufort et al., 1998), and Cdx2

(Chawengsaksophak et al., 2004) are required for correct differentiation at this stage, and thus failure to express these markers would preclude functional differentiation.

Sox2, which marks not only neurectoderm (Avilion et al., 2003) (Figure 4.4E) but also EpiSCs, was downregulated in the vast majority of EpiSC-derived non-neuroectodermal cells such as surface ectoderm (Figure 4.4E) (five of five assays, comprising three or more sections per assay; Table 4.1). This indicates that dispersed GFP^+ cells lose EpiSC characteristics as they incorporate into the host. Together, these results show that EpiSCs integrate efficiently into all three germ layers of streak stage embryos within 24 hours.

Because morphological integration correlated with functional integration (as verified by marker expression) in all embryos analysed, morphological integration was used as a criterion to score the remaining sectioned embryos (Table 4.1). In all cases, the cellular distribution of dispersed EpiSCs in their host is consistent with the fate map of the epiblast (Table 4.1; Figure 4.5).

Table 4. 1 . Distribution of donor cells in host embryos after culture

Donor cells	Stage of recipients	Graft site	No. of sectioned embryos	No. of embryos with incorporated GFP^+ cells	No. sectioned embryos containing incorporated cells in tissue (No. embryos confirmed/no. tested by immunohistochemistry)					
					Surface ectoderm (AP-2a)	Neural ectoderm (Sox2, Foxa2)	Mesoderm (T, Cdx2, Nkx2.5,Tbx6)	Endoderm (Foxa2)	PS (T)	Allantois (Cdx2, Stella, TNAP)
Embryo-derived EpiSC (r04-GFP)	M-LS	MA	4[a]	3		3	1			
		D	9[a]	9	1(1/1)	8(4/4, 2/2)	8 (2/2, 2/2)		3	1
		MP	3	3	1(1/1)	1(1/1)	1(1)		2(2/2)	2(2/2)
		PP	3	3			3	1	3(2/2)	3(3/3)
	E-MS	PP	4	4		2	4	4	3	2(1/2)
In vitro EpiSC (C2)	M-LS	D	2[b]	2		2	2	2		
		MP	4[a]	4			4(1)	2(2/2)	4(1/1)	4(1/2)
	ES	PP	4	4		1(1/1)	2(1/1, - 2/2)	4	2	
ES cells (AGFP7)	M-LS	D	5[a]	2			2[c]	1(0/1)		
		PP	3	3			1+1[c]		2(0/1[d])	2(0/1 [d])

Brackets: number of sectioned embryos containing GFP cells that expressed the indicated marker/number of embryos tested. For each embryo, three or more sections were tested for immunoreactivity to any one antibody. Staging: ES, early streak; E-MS, early to mid streak; M-LS, mid to late streak.

a: One sectioned embryo contained a small unincorporated clump of cells (three or fewer sections).

b: Both embryos also contained small unincorporated clumps of cells.

c: GFP^+ cells present in three or fewer sections.

d: GFP^+ cells showed ectopic Sox2 and Oct4 expression, and only one cell correctly expressed Cdx2.

MA: mid-anterior; D: distal; MP: mid-posterior; PP: proximal-posterior

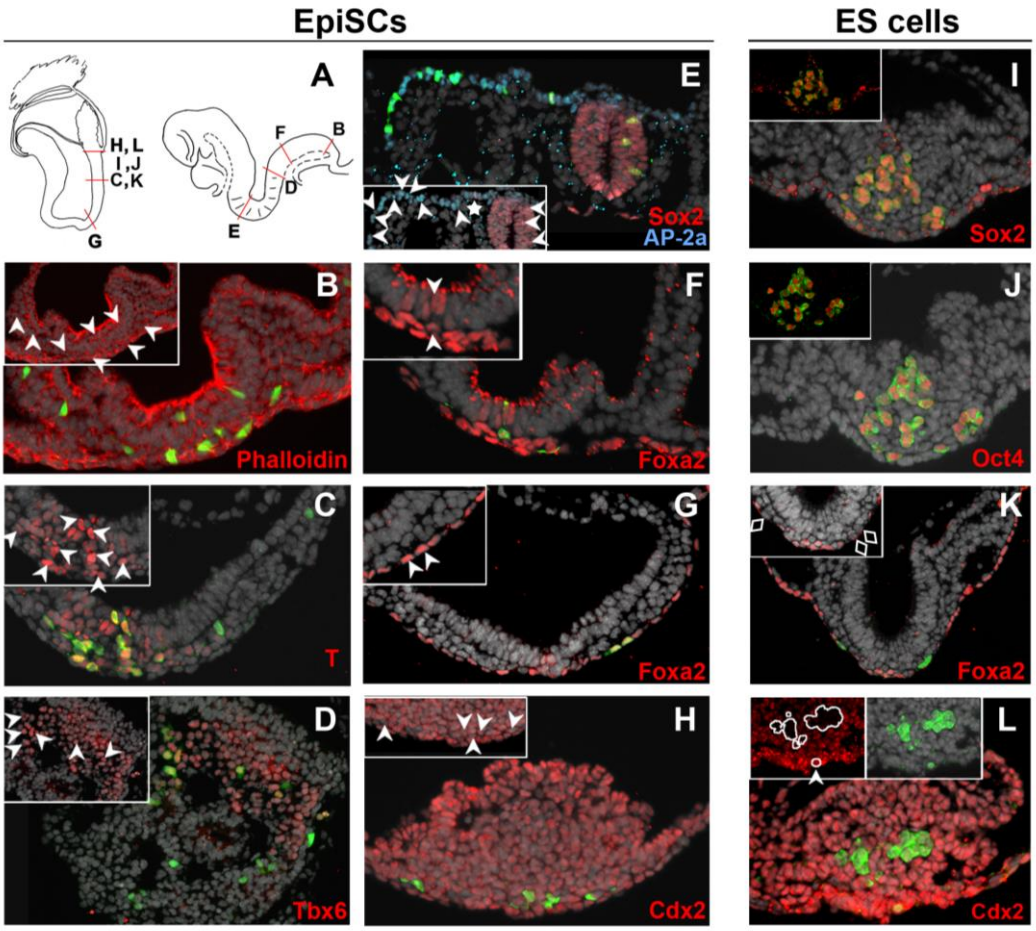

Figure 4. 4 . Analysis of donor cell differentiation in chimeras

(A) Schematic diagrams showing approximate sectioning planes in embryos cultured for 24 hr (left) or 48 hr (right).

(B–L) Specific stains (red/cyan). Insets: position of donor-derived cells with channels removed to allow the comparison of gene expression between donor-derived (green) cells and the host tissue (gray, DAPI counterstain). Arrowheads: donor cells showing correct marker expression.

(B–H) EpiSC grafts. (B) Phalloidin, showing donor cells in the neural groove and mesoderm. (C) T (brachyury), showing donor cells in the primitive streak and paraxial mesoderm. (D) Tbx6, showing donor cells in the PSM. (E) Sox2 (red) and AP-2a (cyan), showing donor cells in the neural tube and surface ectoderm. Asterisk: single cell ectopically expressing Sox2. (F and G) Foxa2, showing donor cells in the floor plate (F) and endoderm (G). (H) Cdx2, showing donor cells in allantois.

(I-L) ESC grafts. (I and J) Donor cells ectopically express Sox2 (M) and (N) Oct4. Inset: nuclear stain removed. (K) Foxa2, showing expression only in host cells. Diamonds: GFP-labeled cells. (L) Cdx2, showing donor cells in allantois do not express posterior marker. A single cell (arrowhead) correctly expresses Cdx2. Left inset: Cdx2 immunofluorescence. White lines outline the position of donor cells. Right inset: position of donor cells.

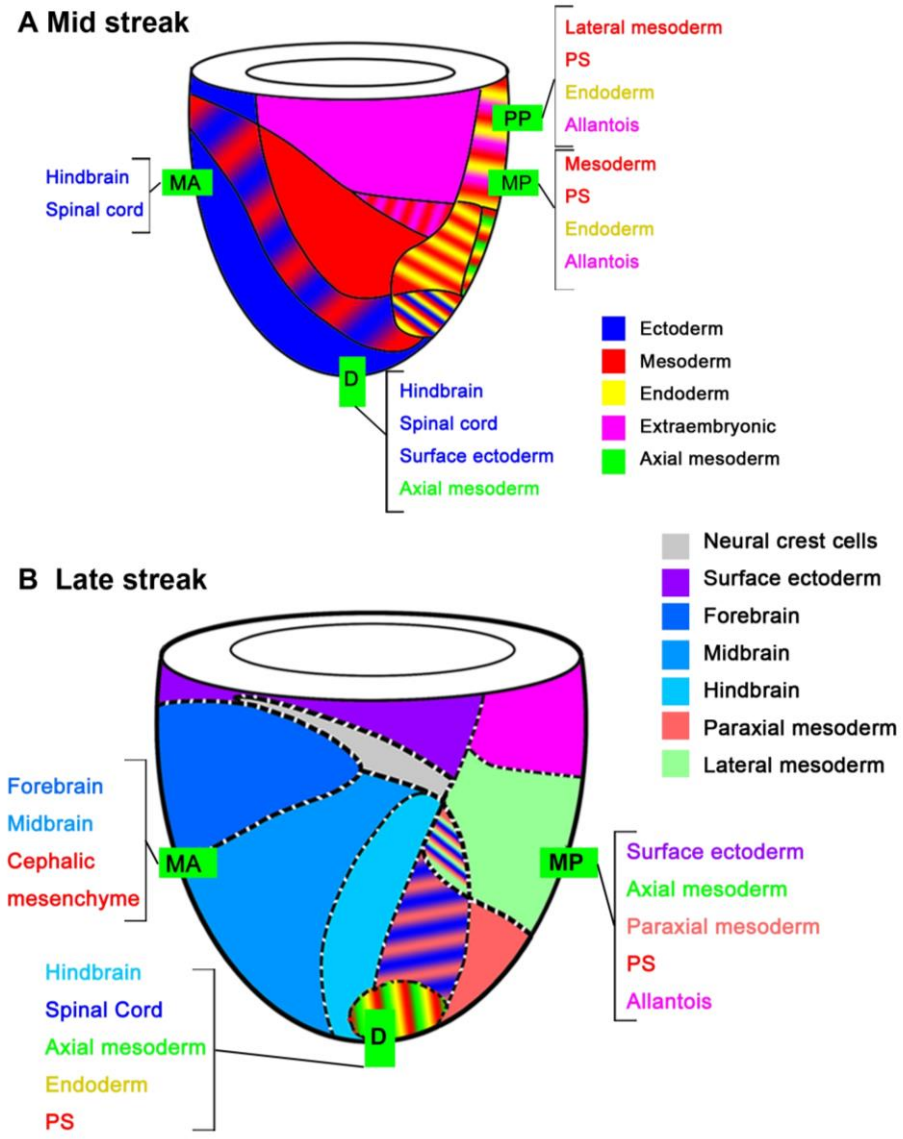

Figure 4. 5 . Comparison of EpiSC tissue colonization with the fate map of the epiblast

(A) Fate map of early-streak-stage epiblast. Note that comprehensive fate maps were not produced specifically for the mid-streak-stage embryo.

(B) Fate map of late-streak-stage epiblast. The tissues colonized by EpiSC are shown next to the graft sites at the appropriate stage.

Text colours match the colour key for the fate maps. Dashed lines indicate domains of predominant fate, rather than absolute lineage boundaries. MA: midanterior; D: distal; MP: mid-posterior; PP: proximal-posterior. The fate maps are adapted from Tam and Behringer (1997).

5. EpiSCs differentiated into functional cell types in bona fide chimeras

To further demonstrate that EpiSCs can form functional cells in chimeric embryos, EpiSCs were grafted into the primitive streak of early-streak stage embryos (E6.5), where cardiac progenitors are present (Kinder et al., 1999). After 48 hours in culture, at which point the heart is beating and required for normal development, GFP^+ cells were observed in the heart of two chimeras (Figure 4.6A; Table 4.1). These cells expressed the cardiomyocyte marker Nkx2.5 (Lints et al., 1993) (Figure 4.6B) at levels comparable to those observed in their neighbours, indicating differentiation of EpiSCs toward cell types with an early functional role.

It was also observed that some donor-derived cells expressed tissue-nonspecific alkaline phosphatase (TNAP) with primordial germ cell (PGC) morphology at the junction between the allantois and posterior primitive streak (Figure 4.6C), which are conventionally designated as PGCs (Ginsburg et al., 1990). Furthermore, donor-derived cells in this location expressed the PGC-specific marker Stella (Saitou et al., 2002) (Figure 4.6D). The specific antibody immunofluorescence of Stella was verified by the detection of $Stella^+$, Nanog:GFP^+ mESCs and $Stella^+$ cells at the base of the allantois in E8.5 Nanog:GFP^+ embryos (Figure 4.6E). Nevertheless, not all GFP^+ cells at the base of the allantois expressed PGC-specific markers (Figure 4.6C, F; Table 4.1), and only two of the seven embryos tested contained any putative PGCs.

6. Grafting excess EpiSCs resulted in clump formation

Occasionally, clumps of cells were observed in sections near the graft site (Table 4.1). Six out of 34 sectioned embryos contained such clumps, two of which were very small, extending over one to two sections. These clumps may represent a subpopulation of EpiSCs that are incapable of integrating into the host embryonic environment, or indicate that contact between EpiSCs and host cells is required to ensure their appropriate differentiation.

In support of the latter possibility, additional grafts containing larger numbers of EpiSCs (>12 cells per embryo, n = 4) was performed. However, this did not result in more extensive chimeras after 24 hours (in all four embryos, 24–48 dispersed cells extended between 1/4 and 1/2 of the embryo length). Instead, all embryos additionally contained partially integrated clumps (Figure 4.7A). Importantly, Sox2 was ectopically expressed at low levels in the centre of the clump but was absent in nearby dispersed cells (Figure 4.7B). This

strongly suggests that the primary influence on EpiSCs differentiation is dispersal from the grafted cell cluster, rather than variations in the abilities of subpopulations to integrate and differentiate. Additionally, unincorporated clumps were previously observed in orthotopic grafts of E7.5 epiblast (Beddington, 1981), indicating that even tissue from an origin equivalent to the host site can fail to incorporate, presumably because there are too many cells to be assimilated by the surrounding host cells.

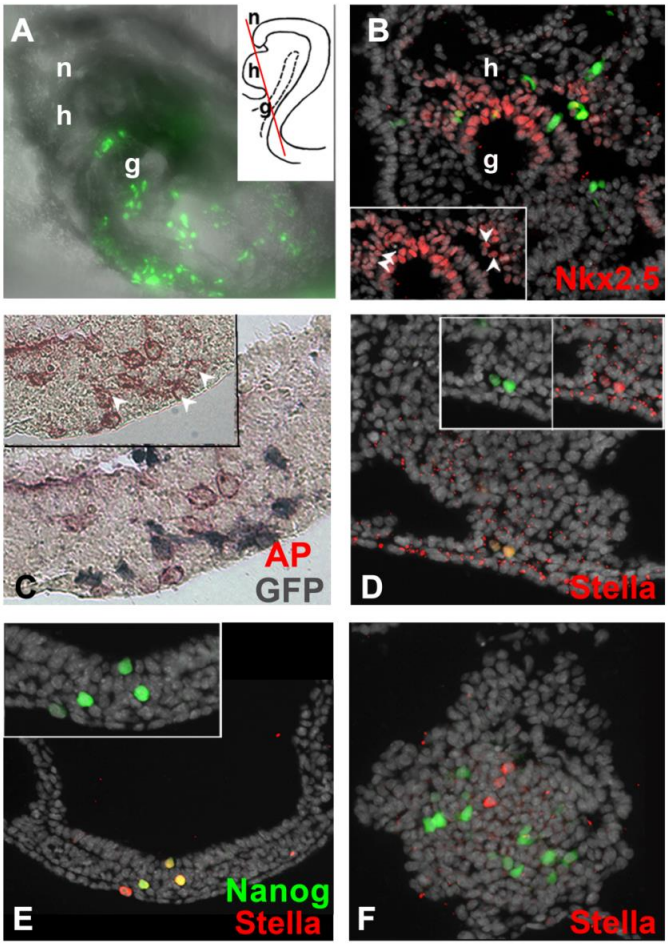

Figure 4. 6 . EpiSCs differentiated into early cardiomyocyte and primordial germ cells (PGCs) in vivo

(A) Frontal view of a 48-hour-cultured, early-streak-stage embryo (E6.5) grafted in the PP region with in vitro-derived EpiSC. Inset: position of section B in this embryo. n, neurectoderm; h, heart; g, gut. (B) Nkx2.5 staining of embryo shown in (A), showing donor cells in the embryonic heart.

(C) Alkaline phosphatase (AP) (red) and GFP immunohistochemistry (gray), showing PGC differentiation. Inset: TNAP staining prior to immunohistochemistry. Arrowheads: $TNAP^{+}/GFP^{+}$ cells with PGC morphology.

(D) Stella staining, showing PGC differentiation. Insets: removal of either the green (GFP) or red (Stella) channel. (E) Stella staining (red) on a transverse section of an E8.5 Nanog:GFP embryo, showing PGCs coexpressing Nanog and Stella. Inset: removal of the red channel (Stella). (F) Stella

staining on a transverse section (MP graft of embryo-derived EpiSC), showing Stella-negative donor cells in the allantois.

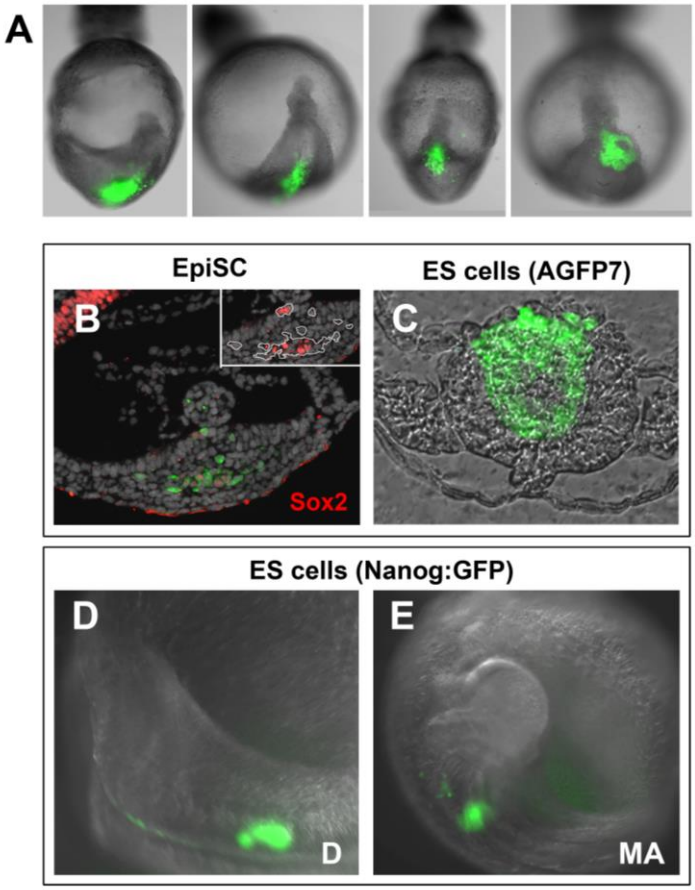

Figure 4. 7 . Unincorporated cell clumps

(A) Four mid-late streak stage embryos (E7.0) grafted with embryo-derived EpiSCs (≥12 cells). The graft sites are shown in the lower right of each panel. Culture period: 24 hr. (B) Sox2 immunofluorescence (red) on a transverse section of the embryo in the last panel of (A). GFP labeled cells are present in the posterior primitive streak, where no Sox2 expression is detectable in the host. Whereas dispersed cells have downregulated Sox2 expression, weak expression is detected in clustered GFP-labeled cells. White lines in the right inset, where the green channel is removed, show the position of donor cells. D: distal; PP: proximal-posterior

(C) Frontal section showing an unincorporated clump in an embryo that received an ESC graft in the D region. (C and D) Examples of embryos grafted with TßC44Cre6 ESCs (Nanog:GFP) after 24 hr culture. Cell clumps in the graft site, as well as some dispersed cells, show ectopic GFP expression, indicating failure to downregulate Nanog:GFP. The graft site for each embryo is shown in the lower-right corner.

4.2 Mouse embryonic stem cells (mESCs) do not incorporate into streak stage embryos (E7.5)

4.2.1 Aims

The efficient integration of EpiSCs in postimplantation but not preimplantation embryos indicates that a match between developmental stage of the cell lines and the host environment is desired for chimaera formation. Although it has been shown that EpiSCs are incompatible with the environment of preimplantation embryos, it is unknown whether pluripotent mESCs can incorporate into postimplantation embryos. To address this issue, I grafted mESCs which can efficiently contribute to chimeras by blastocyst injection to streak stage embryos (E7.5) and then cultured them ex vivo for 24-48 hours. Cell integration was assessed as in the previous experiments.

4.2.2 Results

1. mESCs formed clumps and failed to differentiate in streak stage embryos (E7.5)

mESCs derived from AGFP7 embryos ubiquitously express GFP and can efficiently generate chimeras upon blastocyst injection (Gilchrist et al., 2003). The grafting procedure for mESCs to streak stage embryos (E7.5) is identical to that for EpiSCs described previously. It is surprising that the vast majority of mESC-derived cells typically remained as nonintegrated clumps either in the amniotic cavity or at the graft site (Figures 4.1F, left, and Figure 4.7C). Images of all recipient embryos can be found in the Appendix I, Sup Figure 4.6. Only one of 13 embryos grafted with AGFP7 mESCs contained >12 dispersed donor cells extending >1/4 of the embryo length (Figures 4.1F, right, and Figure 4.2D), suggesting it was a bona fide chimera. However, immunohistochemistry showed that nearly all ES-derived cells ectopically expressed the ESC markers such as Sox2 and Oct4 (Figures 4.4I, J). Moreover, differentiation markers such as Foxa2 and Cdx2 were not upregulated appropriately in the donor-derived cells, except one cell expressing Cdx2 (Figures 4.4K, L; Table 4.1).

2. mESCs failed to downregulate pluripotency marker after grafting

To further test whether ESC-specific gene expression persists in mESC-derived cells after grafting, TßC44cre6 mESCs (Nanog:GFP), which contain a GFP transgene integrated at the Nanog locus of Nanog null mESCs (Chambers et al., 2007), were grafted in the MA, D, and

MP regions of eight E7.5 embryos. It has been previously shown that Nanog is neither required to transit nor to maintain EpiSC pluripotency (Osorno et al., 2012). This cell line can form chimaeras efficiently upon blastocyst injection (Chambers et al., 2007).

Nanog:GFP mESCs should downregulate GFP in somatic tissue, if incorporated into postimplantation embryos, since Nanog expression is restricted to the PGCs by around E8.0 (Hart et al., 2004; Yamaguchi et al., 2005). However, similar to the AGFP7 mESC grafts, Nanog:GFP mESCs generally formed small self-adherent clumps (in 7 out of 8 embryos) after culture (Appendix I, Sup Figure 4.7). One embryo contained apparently dispersed cells at the base of the allantois; because PGCs, like mESCs, express Nanog, this embryo was uninformative. In two out of eight embryos, dispersed GFP^+ cells were also detected distant from the PGC location at the base of the allantois, indicating their failure to downregulate pluripotency markers (Figures 4.7D, E). Thus, unlike EpiSCs, mESCs incorporate very inefficiently into the host, and even when they do, they do not differentiate correctly.

4.3 EpiSCs barely incorporate into E8.5 Embryos

4.3.1 Aims

The pluripotency of the epiblast was originally shown by testing their ability to form teratocarcinomas in adult mice (Diwan and Stevens, 1976). Previous studies have demonstrated that pluripotency is lost in the epiblast between E7.5 to E8.5 (Beddington, 1983; Damjanov et al., 1971). This period of pluripotency loss was recently defined to lie between the headfold stage and the beginning of somitogenesis (E8.0) (Osorno et al., 2012). Moreover, no EpiSC lines can be derived from embryos after somitogenesis begins (Osorno et al., 2012). Although EpiSCs can efficiently incorporate into streak stage embryos (E7.5), their behaviour in somitogenesis stage embryos is still unknown. To better understand the application of pluripotent stem cells, it is important to investigate the behaviour of pluripotent cells among the somatic cells. Therefore, in this study I grafted EpiSCs to E8.5 embryos to assess the potential of pluripotent cells in embryos in which pluripotency is lost.

4.3.2 Results

1. Embryo-derived EpiSCs proliferated but did not incorporate in E8.5 embryos

Both embryo- and in vitro-derived EpiSCs were grafted into the NSB of 2-5 somite stage (E8.5) embryos, where there is a strong inductive influence on grafted cells as describe above. 5 embryos were grafted with embryo-derived EpiSCs (r04-GFP). One was cultured for 24 hours, the other four for 48 hours. Although embryo-derived EpiSCs proliferated extensively in all five recipients (Figures 4.8B), GFP^+ cells appeared to form ectopic clumps rather than incorporating in the host according to the whole-mount images (Appendix I, Sup Figure 4.9). Three out of five embryos were sectioned to analyse the distribution of EpiSC-derived cells in E8.5 embryos (Table 4.2). The majority remained as ectopic neural-like structures, expressing Sox2, Foxa2 but not T (Figure 4.9A-C), and discrete clumps in the medial somite area (Figure 4.9D). However, there were a few dispersed cells observed in the mesoderm, suggesting some incorporation (Figures 4.9E, F).

2. In vitro-derived EpiSCs hardly proliferated in E8.5 embryos

Four embryos were grafted with an in vitro-derived EpiSC line, C2 (Huang et al., 2012). Three were cultured for 24 hours, another one for 48 hours (Table 4.2). Unlike the embryo-derived EpiSC line, in vitro-derived EpiSCs remained in the graft site in three embryos after

culture without clear proliferation signs (Figure 4.8D and Appendix I, Sup Figure 4.8). Only in one embryo cultured for 24 hours did in vitro-derived EpiSCs proliferate along the midline of the embryo (Figure 4.12A-C,). To determine the distribution and incorporation of the EpiSC-derived cells, this embryo was sectioned. Some GFP^+ cells formed an ectopic clump underneath the neural tube (Figure 4.9G). Dispersed GFP^+ cells were detected in notochord and also mesoderm next to the ventral neural tube (Figure 4.9H and Figure 4.12H). GFP^+ cells in notochord expressed appropriate notochord marker such as T, indicating their integration (Figure 4.9H and Figure 4.12G).

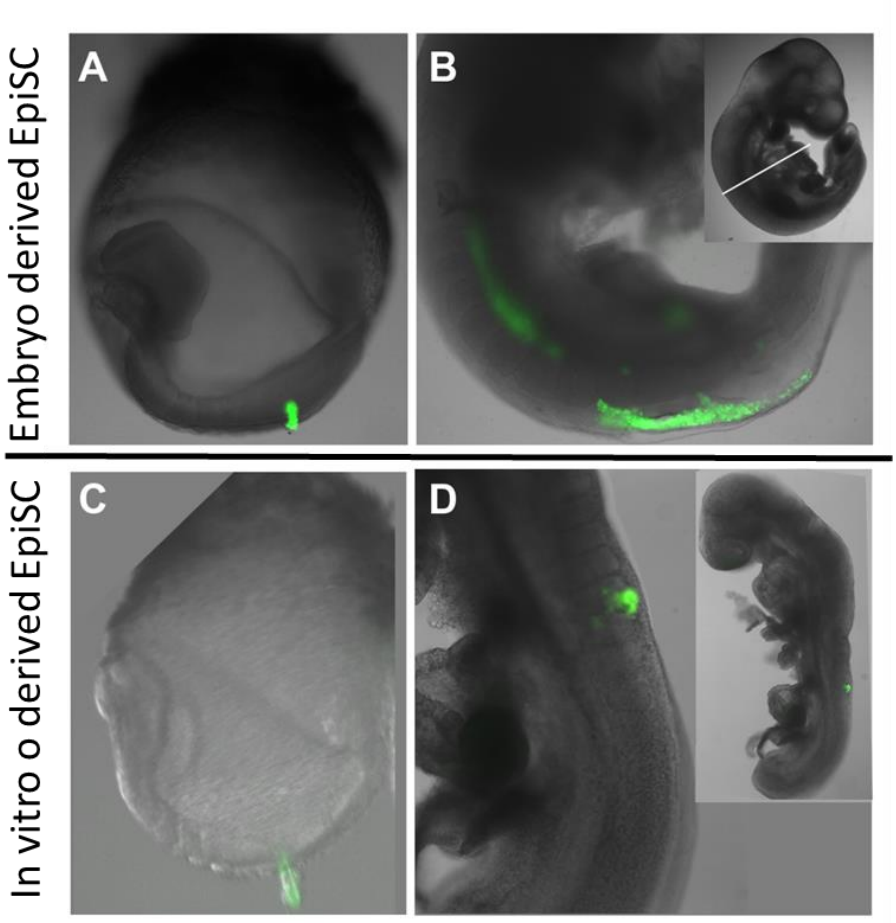

Figure 4. 8 . EpiSCs grafted in E8.5 Embryos

(A and C) Representative E8.5 embryo receiving a graft of embryo and in vitro derived EpiSC in the NSB, respectively

(B) Example of embryo grafted with embryo-derived EpiSCs after 24 hr culture. Aggregated donor cells in the recipient embryo after 48 hr. Inset: whole embryo. White line: only posterior half of embryo shown enlarged.

(D) Example of embryo grafted with in vitro-derived EpiSCs after 24 hr culture Donor cells remain in the graft site after 24 hr culture without significant proliferation. Inset: whole embryo.

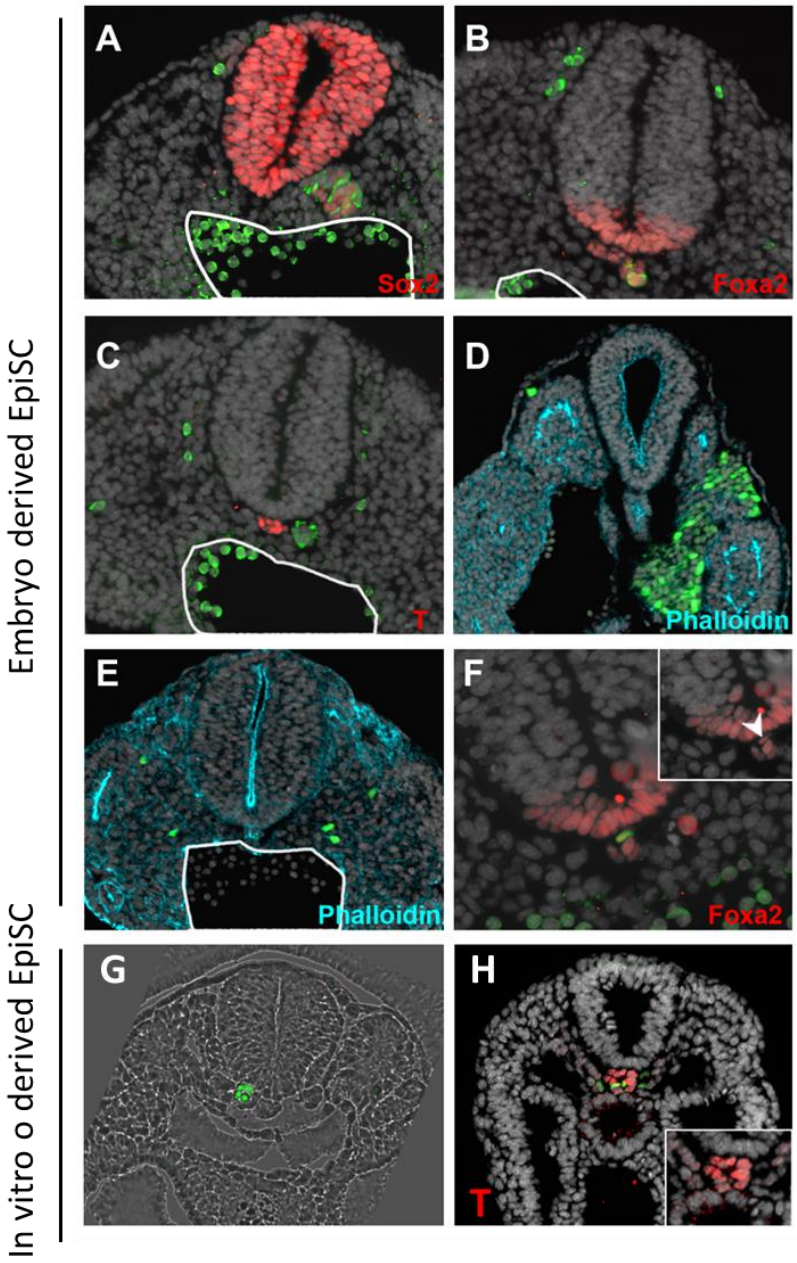

Figure 4. 9 . Analysis of the distribution of EpiSC-derived cells in E8.5 embryos

(A-F) The distribution of embryo-derived EpiSCs in E8.5 embryos. (A-C) Distinct clumps formed by donor cells close to the ventral neural tube express Sox2 (A), Foxa2 (B) but not T (C). (D) Phalloidin staining shows unincorporated cell clumps inserted into somites. (F) Phalloidin staining shows dispersed donor cells in the mesoderm. (H) One Foxa2-expressing donor cell (arrowhead) is present in the notochord. Inset: green (GFP) channel removed.

(G and H) The distribution of in vitro-derived EpiSCs in E8.5 embryos. (G) A small clump formed by donor cells underneath the neural tube. A bright field picture overlaped with GFP channel (H) Dispersed donor cells in the notochord expressing T. Inset: green (GFP) channel removed.

GFP-labeled cells (green) overlaid on a brightfield (G) or DAPI-counterstained image (gray). The boundary of the dorsal aorta (containing highly autofluorescent circulatory blood cells) is indicated by a hand-drawn white line (A, B, C and E).

Table 4. 2 . Intact embryo assessment of E8.5 embryos grafted with EpiSCs and 48h CHI treated EpiSCs

Donor cells	Culture time	No. of grafted embryos (No. of embryos with significant proliferation of donor cells)	No. of sectioned embryos
Embryo derived EpiSC (r04)	24h	1 (1)	1
	48h	4 (4)	2
In vitro derived EpiSC (C2)	24h	3 (1)	1
	48h	1 (0)	0
48h CHI treated C2	24h	5 (5)	3
	48h	6 (5)	3

4.4 Increasing Wnt signalling in EpiSCs blocks anterior neural fate in vivo

4.4.1 Aims

As described in the introduction, stimulation of Wnt signalling in EpiSCs by addition of 3μM CHI, a GSK3β inhibitor, for 48 hours significantly upregulates the transcription of primitive streak-related and Wnt-related genes such as *T, Gsc*, *Fgf8*, *Mesp1, Lhx1* and *Axin2* (Tsakiridis et al., 2014). However, the expression of core pluripotency factors (Oct4, Sox2, and Nanog) is greatly reduced in EpiSCs after 48 hours of CHI treatment, implying that these cells have exited the pluripotent state (Tsakiridis et al., 2014). The transcription levels of anterior neural markers such as *Pou3f1* (Zwart et al., 1996) and *Zic2* (Nagai et al., 1997) are decreased, whereas the expression of posterior neural plate-specific genes such as *Zic3* (Nagai et al., 1997) and *Gbx2* (Li and Joyner, 2001) are increased in 48-hour (h) CHI treated EpiSCs (Tsakiridis et al., 2014). According to their gene expression profile, 48h CHI treated EpiSCs appear to represent cells in the posterior of the embryos from late gastrulation to early somitogenesis. To further investigate which type of in vivo cells 48h CHI treated EpiSCs truly represent, I grafted these cells into both E7.5 and E8.5 embryos and assessed their potency in vivo.

4.4.2 Results

1. 48h CHI treated EpiSCs do not contribute to neurectoderm in streak stage embryos (E7.5)

In vitro-derived EpiSCs (C2) were treated with additional 3μM CHI for 48 hours (Figure 4.15B) and then grafted into two distinct sites of mid to late streak stage embryos (E7.0-E7.5) (Figure 4.10A, B): the distal tip of the embryos (D), where cells produce derivatives of all three germ layers (Figure 4.5), and the middle of the primitive streak (MP), where cells principally give rise to mesoderm and endoderm (Figure 4.5). 11 recipient embryos were cultured for 48 hours, all of which efficiently formed chimeric embryos with many donor-derived cells dispersed from the graft site and widely spread within the host (Appendix I, Sup Figure 4.10). Interestingly, GFP^+ cells appeared to contribute to relatively lateral areas of the embryos, as assessed by fluorescence microscopy after 24 hours of culture (Figure 4.10C).

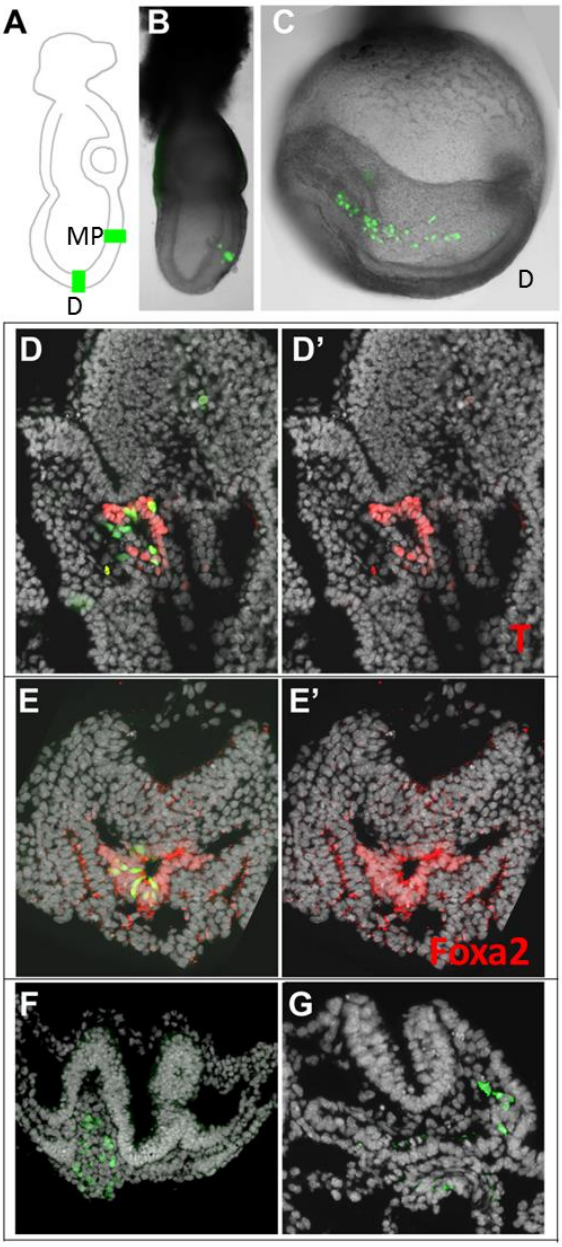

Figure 4.１０. 48h CHI treated EpiSCs (C2) grafted in E7.5 Embryos

(A) Diagram of late-streak embryo, showing graft sites (D and MP) in the egg cylinder. (B) 48h CHI C2 grafted to MP of a late-streak-stage embryo (E7.5). (C) A late-streak stage embryo (E7.5) grafted with 48h CHI C2 in D after 24 hr culture. D: distal; MP: mid-posterior.

(D) T staining showing donor (green) cells in the notochord. (E) Foxa2 staining showing donor cells in the gut. (D' and E') the same images as D and E with green channel removed to allow the comparison of gene expression between donor and host cells. (F) Donor cells in the head mesenchyme. (G) Donor cells in the mesoderm.

A

Donor cells	Embryo ID	stage	position	No of sections	Contribution						
					N	AXM	PLVM	EN	PS	AI	Non Integr
48h CHI C2	Day2 P1 W2 E2	LS	Distal	39			31	8			
	D2 P1 W2 E1	LS	Distal	19			17	7			
	P2 W1 E2	LS	Distal	29			30	0			8
	P2 W2 E5	LS	Distal	25			9	17			10
	D2 P1 W4 E1	MS	MP	30		1	21	12			
	D2 P1 W4 E2	MS-LS	MP	26			23	0			11
	D2 P2 w2 E2	MS-LS	MP	39			12	27			2
	D2 P1 W1 E2	MS-LS	MP	10			9	1			1
	P1 W1 E3	MS-LS	MP	13			8	7			
	P2 W1 E1	MS-LS	MP	45		6	11	40			
	P2 W1 E2	MS-LS	MP	33		1	10	24			
In vitro derived EpiSC (C2)	P2.8	ES	Distal	34			18	33			1
	P2.6	ES	Distal	38		1	37	6			
	P2.5	ES	Distal	53	12	8	45	16	19		
	4.1	LS	Distal	37	11	12	10	22	3		5
	4.2	LS	Distal	36	16	6	13				
	9.1	MS	MP	28		5	24	4	8	4	1
	10.2	MS	MP	40		1	20	17	15	2	
	9.2	MS	MP	31			22	7	13	6	1
	10.1	MS	MP	27		2	21	8	2	9	4

B

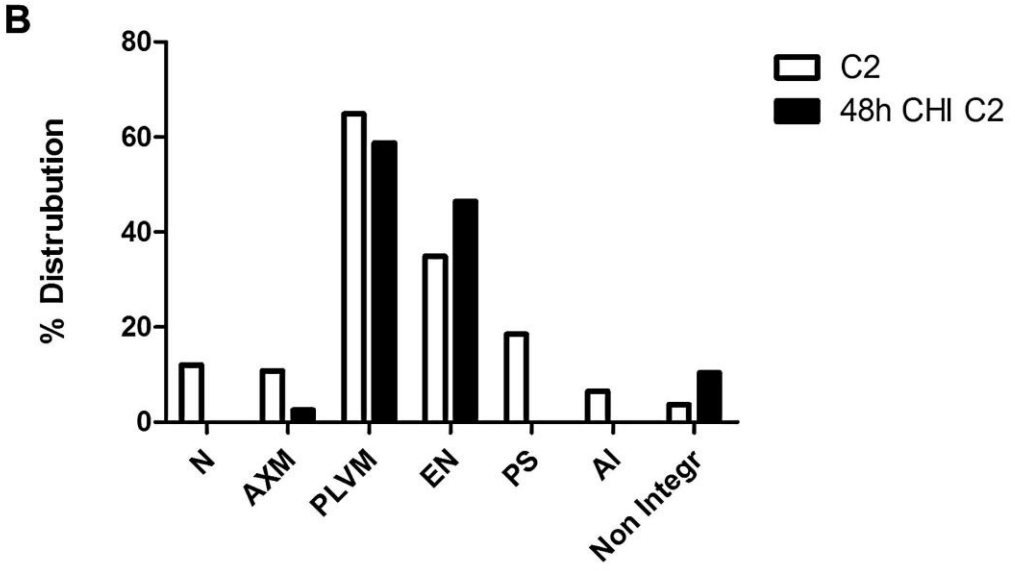

Figure 4.1 1. Distribution of EpiSCs and 48h CHI treated EpiSCs in E7.5 embryos after culture

(A) List of all grafted embryos. All sections with GFP+ cells in each embryo were scored and the number of sections containing GFP cells in each category is shown. (B) A bar graph was made according to table (A). The number of sections in each category was summed up and then divided to the total number of sections with GFP cells.

No of sections: the total number of sections containing GFP+ cells in each embryos.

Stage: ES: early-streak-stage embryo; MS: mid-streak-stage embryo; LS: late-streak-stage embryo;

Abbreviation: MP: mid of the primitive streak; N: neuroectoderm; AXM: axial mesoderm; PLVM: paraxial lateral and ventral mesoderm; EN: endoderm; PS: primitive streak; Al: allantois; Non Integr: non integration clumps

To determine the distribution of the donor-derived cells, embryos were serially sectioned and scored for the distribution of all GFP^+ cells. In total, 324 sections containing GFP^+ cells were found in 11 embryos grafted with 48h CHI treated C2. Previously, 308 sections with GFP^+ cells were found in 9 embryos receiving a graft of untreated C2 (Figure 4.11A). Therefore, similar to EpiSCs, 48h CHI treated EpiSCs proliferated extensively in streak stage embryos (E7.5). Most of 48h CHI treated C2-derived cells were detected in paraxial and/or lateral/ventral mesoderm (PLVM) and endoderm, with 181 sections (59%) and 143 sections (46%) respectively (Figure 4.11B). There is no statistical difference between untreated C2 and 48h CHI treated C2 in their mesoderm and endoderm contribution. However, axial mesoderm contribution in 48h CHI treated C2 was relatively low, in only 3 out of 11 embryos compared with 7 out of 9 embryos grafted with untreated cells (Figure 4.11A). Most strikingly, no neural contribution was detected in all 11 embryos grafted with 48h CHI treated C2 cells, even when grafted into the distal of the embryos, where untreated C2 gave rise to neuroectoderm in three out of five embryos (Figure 4.11A). These results indicate that high Wnt activity in EpiSCs may restrict their potential for neuroectoderm differentiation.

To further test whether the dispersed GFP^+ cells differentiate appropriately in the host, representative slides were stained. Donor cells integrated and acquired an identity similar to their host-derived neighbours, as evidenced by GFP^+ cells in the notochord expressing T (Wilkinson et al., 1990) and in the gut tube expressing Foxa2 (Dufort et al., 1998) (Figure 4.10D, E).

To summarise, these results show that 48h CHI treated EpiSCs are compatible with streak stage embryos (E7.5) in vivo. However, they cannot contribute to neuroectoderm at this stage, suggesting that the pluripotency is compromised after increasing Wnt signalling in EpiSCs.

2. 48h CHI treatment induces EpiSCs to incorporate and contribute to E8.5 embryos

The potency of 48h CHI treated EpiSCs is restricted in E7.5 embryos, suggesting that these cells may be in a more advanced developmental state than EpiSCs. To test this hypothesis, I grafted 48h CHI treated C2 into the NSB of E8.5 embryos. Previous results show that most embryo and in vitro-derived EpiSCs failed to integrate into the NSB of E8.5 embryos (Figure 4.8 and Figure 4.9). However, one embryo grafted with in vitro-derived EpiSCs (C2) exhibited minimal chimerism with donor cells in notochord and ventral mesoderm (Figure 4.12B, G and H). In contrast to untreated EpiSCs, 48h CHI treated C2 cells integrated extensively in E8.5 embryos (Figure 4.12E, F and Table 4.3).

In total, 11 embryos were grafted with 48h CHI treated C2: 5 embryos cultured for 24 hours, the other 6 embryos for 48 hours. Only one out of 11 embryos did not clearly show dispersed donor cells after 48 hours in culture, so this embryo was excluded from further integration analysis (Table 4.3). It should be noted that despite extensive proliferation 48h CHI treated C2 cells did not contribute to the tissues posterior to the hindlimb (Figure 4.12E, F), indicating they do not act as long term progenitors in vivo. Images of all recipient embryos can be found in the Appendix I, Sup Figure 4.11.

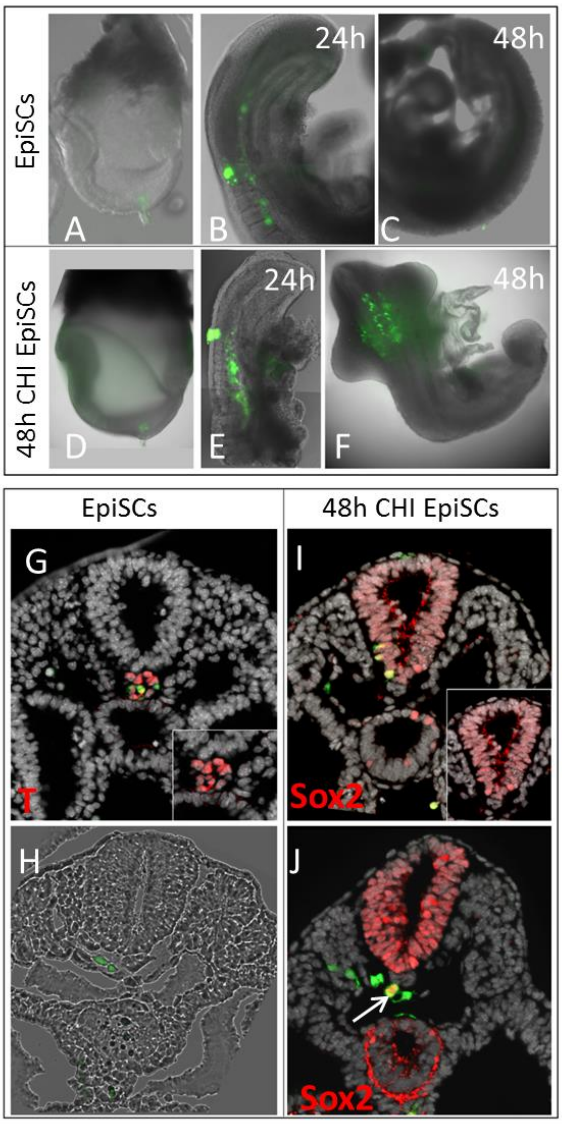

Figure 4.１２. EpiSCs and 48h CHI treated EpiSCs grafted in E8.5 Embryos

(A and D) Representative E8.5 embryos receiving a graft of EpiSCs (C2) and 48h CHI treated EpiSCs (C2), respectively

(B and C) Example of embryos grafted with C2 after 24 and 48 hr culture, respectively.

(E and F) Example of embryos grafted with 48h CHI C2 after 24 and 48 hr culture, respectively

(G and H) Section examples showing the contribution of C2 in E8.5 embryos. Donor cells in the notochord expressing T (G) and in the mesoderm underneath the neural tube (H).

(I and J) Section examples showing the contribution of 48h CHI C2 in E8.5 embryos. Donor cells in the neural tube expressing Sox2 (I). Dispersed donor cells in the mesoderm do express Sox2. However, some donor cells form a small ectopic clump expressing Sox2. This is shown by a white arrow.

Table 4. 3 . The distribution of EpiSCs and 48h CHI treated EpiSCs in E8.5 embryos

Donor cells	Culture period (h)	Embryo ID	Contribution				
			NT	AXM	PXM	V/LM	ectopic structure (clumps)
48h CHI C2	24	48h C2 E1.1 E1	Y	-	Y	Y	Y
		48h C2 E1.1 E2	Y	-	Y	Y	Y
		48h C2 E2.1 T2 E1	-	-	Y	Y	Y
	48	48h C2 E2.2 T3 E1	-	-	Y	Y	-
		48h C2 E2.2 T3 E3	-	-	Y	Y	-
		48h C2 E2.2 T1 E1	-	-	Y	Y	-
In vitro derived EpiSC (C2)	24	C2 E1.1 E1	-	-	-	-	-
		C2 E1.1 E2	-	-	-	-	-
		C2 E1.1 E3	-	Y	-	Y	Y
	48	C2 E1.2 E1	-	-	-	-	-

List of sectioned embryos grafted with C2 and 48h CHI C2. All the sections were examined under a fluorescent microscopy. Y: there are GFP+ cells detected in this category. -: No GFP+ cells were found in this category.

NT: neural tube; AXM: axial mesoderm; PXM: paraxial mesoderm; V/LM: ventral and lateral mesoderm.

To determine the contribution of 48h CHI treated C2 in the hosts, 6 embryos were sectioned and assessed for the distribution of GFP^+ cells. GFP^+ cells predominantly contributed to the mesodermal lineage (Table 4.3). Interestingly, in two recipient embryos, GFP^+ cells were detected in both the neural tube and in the somites (Figure 4.12I, J). This suggests that the elevation of Wnt signalling induces NM potency in EpiSCs. To further assess the correct differentiation of dispersed donor cells in the host embryos, representative slides were stained. The descendants of 48h CHI treated C2 cells integrated and acquired an identity similar to their host-derived neighbours, as evidenced by, GFP^+ cells in the dermomyotome expressing Pax3 (Goulding et al., 1994) and in lateral/ventral mesoderm expressing Snai2 (Sefton et al., 1998) (Figure 4.13B, C). Some GFP^+ cells also differentiated into Pecam1-positive endothelia (Baldwin et al., 1994) (Figure 4.13A). Occasionally, some small ectopic neural-like structures expressing Foxa2 and Sox2 were detected next to the ventral neural tube (Figure 4.12J and 4.13D, D'). No endoderm contribution was detected in these grafts, possibly because the graft site is not ideal for testing endodermal potency in E8.5 embryos. Collectively, these experiments show that enhancing Wnt signalling in EpiSCs by culturing with CHI for 48 hours drives their differentiation into mesoderm and endoderm lineages in

streak stage embryos (E7.5), and mesoderm and posterior neural lineages compatible with early somitogenesis stage embryos (E8.5) (Figure 4.15A).

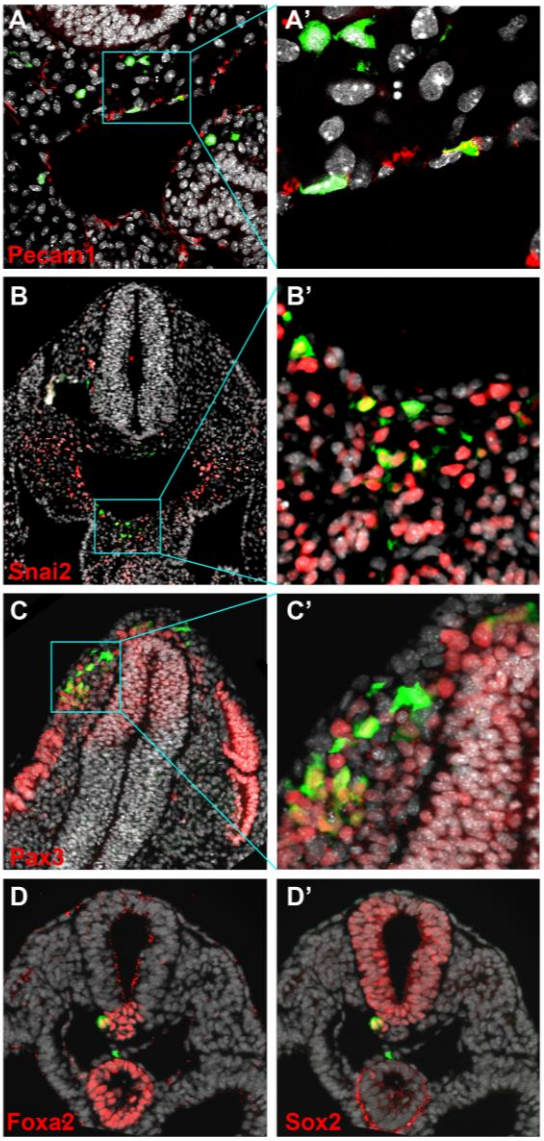

Figure 4.13. Analysis of the distribution of 48h CHI treated EpiSCs (C2) in E8.5 embryos

Section examples showing the contribution of 48h CHI C2 in E8.5 embryos after 24 (D and D') and 48 hr (A-C) culture. Green, GFP immunofluorescence; red, indicated marker immunofluorescence in representative sections after culture; gray, DAPI counterstain.

(A) Donor cells in the dorsal aorta expressing Pecam1. (A') Enlargement of the cyan box in (A). (B) Donor cells in the ventral mesoderm expressing Snai2. (B') enlargement of the cyan box in (B). (C) Donor cells in the dermonyotome expressing Pax3. (C') enlargement of the cyan box in (C). Some donor cells form a small ectopic clump coexpressing Foxa2 (D) and Sox2 (D').

4.5 In vitro differentiated NM progenitors do not successfully incorporate in streak stage embryos (E7.5)

4.5.1 Introduction and aims

As mentioned in previous chapters, NM progenitors are located in the dorsal layer of the NSB and L1-3 at E8.5 and the CNH during tail bud stages. The maximal number of this population is no more than 2500. The inaccessibility of NM progenitors in vivo makes them difficult to study. Since I have shown that EpiSCs represent a true in vitro counterpart of gastrulation epiblast, we can use EpiSCs as a source to generate NM progenitors in vitro to further study their characteristics.

It has been demonstrated that the regions containing NM progenitors show high Wnt and FGF activity. These signals are required for the maintenance of the posterior progenitor zone and axis elongation (see introduction). When EpiSCs were cultured with additional 3μM CHI for 48 hours, 10-20% of the cells coexpressed T and Sox2. Moreover, the previous experiment showed that when grafted to E8.5 embryos, 48h CHI treated EpiSCs contributed to both neuroectoderm and mesoderm in two out of 10 embryos, indicating a small number of NM progenitors may be present. Indeed, a low proportion (around 10%) of $T^{+}Sox2^{+}$ cells were induced in vitro under this condition (Tsakiridis et al., 2014). To improve the induction efficiency, EpiSCs were exposed to a range of CHI, Activin and bFgf concentrations (Gouti et al., 2014). A maximal frequency (up to 70%) of $T^{+}Sox2^{+}$ cell induction resulted from exposing EpiSCs to 3μM CHI and 20ng/ml bFgf for 48 hours.

Besides coexpressing T, Sox2 and trunk Hox genes, other markers for posterior progenitor zone such as *Wnt3a*, *Cdx2* and *Nkx1.2* were also upregulated in these CHI/FGF EpiSCs. By contrast, anterior neural plate and endoderm gene expression was largely absent in these culture conditions (Gouti et al., 2014). Moreover, Nanog expression was undetectable in these cells, which expressed minimal levels of Oct4, suggesting a complete abolishment of pluripotency. The developmental potential of these cells has also been tested in our group by grafting into the NSB of E8.5 mouse embryos. After 48 hours in culture, extensive incorporation of donor-derived cells was observed in all grafts, with 40% of embryos showing both neuroectoderm and mesoderm contribution (Gouti et al., 2014). Collectively, these results indicate that culturing EpiSCs in CHI/FGF for 48 hours results in the induction of NM progenitors in vitro. To further investigate the developmental stage of these in vitro derived NM progenitors (in-vitro NMPs), I grafted them to streak stage embryos (E7.5).

4.5.2 Results

1. In vitro differentiated NM progenitors barely proliferated in streak stage embryos (E7.5)

Embryo-derived EpiSCs (r04) were treated with 3 μM CHI and 20 ng/ml bFgf for 48 hours in the absence of Activin to generate in-vitro NMPs (Figure 4.15B) and then grafted into two distinct sites of mid-streak to early bud stage embryos (E7.0-E7.5) (Figure 4.14 A, B): the distal tip (D) of the embryo and the middle of the primitive streak (MP). 16 recipient embryos were cultured for 24 hours. Most of them (n=13) developed normally and contained a few GFP^+ cells after culture (Appendix I, Sup Figure 4.12 and 4.13). The remainder which either developed abnormally (n=1) or did not contain GFP^+ cells after culture (n=2) were excluded from further analysis.

As shown previously, untreated r04 cells were able to incorporate and proliferate in E7.5 embryos (Figure 4.2A). When grafted to the distal site, r04 cells can contribute to all three germ layers. Also, when grafted to the MP site, they principally produced derivatives of mesoderm and endoderm (Table 4.1). However, when in-vitro NMPs were grafted to streak stage embryos (E7.5), they showed poor proliferation in all 13 host embryos. 8 embryos (LS-EB stages, E7.5) received a graft of in-vitro NMPs in the distal region. Most of them (n=7) exhibited less than 12 dispersed GFP^+ cells and/or some small clumps near the graft site (Figure 4.14C, D and Table 4.4) after 24h culture. The only exception was an embryo containing 12 GFP^+ cells. The other 5 embryos (MS-EB stage, E7.0-E7.5) received a graft of in-vitro NMPs in the MP region. Similar to the distal grafts, few GFP^+ cells were observed in the host (Table 4.4). A small amount of proliferation was detected in two embryos with 20 and 16 GFP^+ cells, respectively (Figure 4.14F, G). However, these GFP^+ cells are relatively restricted to the posterior primitive streak without spreading more than ¼ of the body axis. Since the extent of donor cells was below the threshold we originally used to distinguish bona fide chimeras (Huang et al., 2012), they cannot be considered as bona fide chimeric embryos. Thus, only one out of 13 embryos showed a minor chimerism (with 12 GFP^+ cells), suggesting that in vitro differentiated NM progenitors are incompatible with streak stage embryos (E7.5).

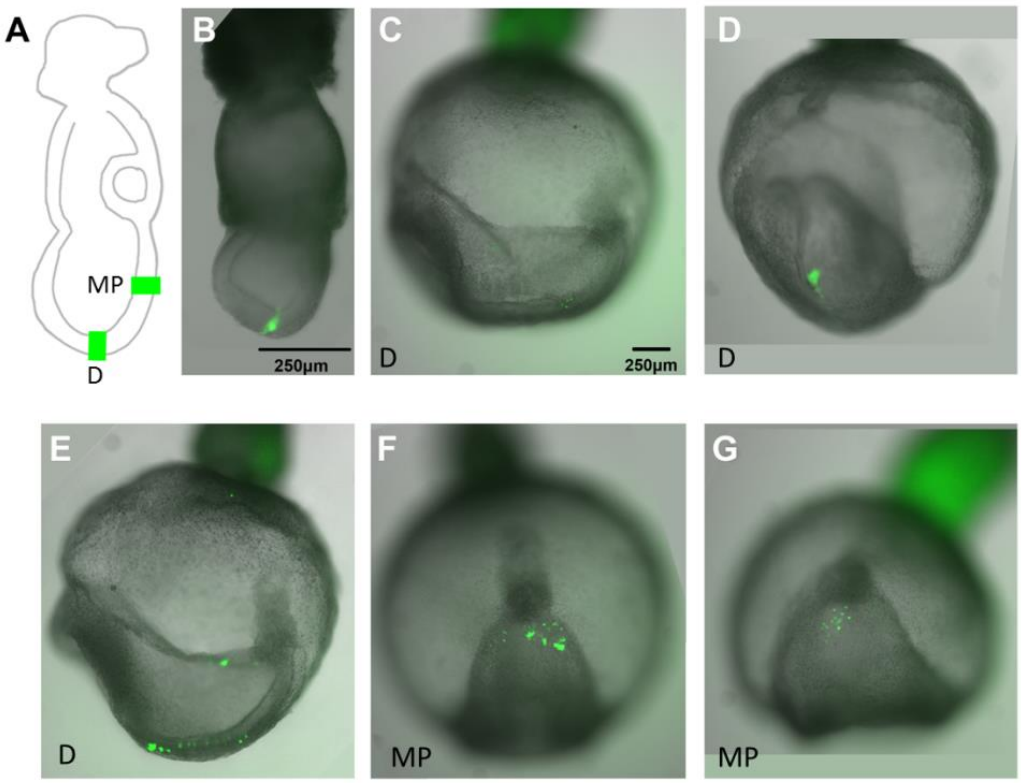

Figure 4.１４. In vitro-derived NM progenitors grafted in E7.5 Embryos

(A) Diagram of late-streak embryo, showing graft sites (D and MP) in the egg cylinder. (B) In vitro-derived NM progneitors grafted to D of a late-streak-stage embryo (E7.5).

(C-G) Examples of cell contribution to embryos grafted at indicated sites (lower left of each panel) after 24 hr culture. (C and G) embryos containing a small number of dispersed donor cells. (D-F): Donor cells not only disperse but also form small clumps in the host. D: distal; MP: mid-posterior;

Table 4. 4 . The number of in vitro differentiated NM in host embryos (E7.0-E7.5) after culture

Embryo ID	Position	stage	No. of dispersed donor cells	No. of small clumps
W3 distal E1	Distal	LS	4	1
W3 distal E2		LS	1	1
W1 distal E1		LS	7	1
W3 distal E1		LS	10	6
W4 distal E1		LS	0	1
W4 distal E2		LS	3	1
W2 distal E1		LSEB	2	2
W2 distal E2		LSEB	8	3
W1 PS E1	MP	MS	12	1
W1 PS E3		LS	10	3
W2 PS E2		LS	8	0
W1 PS E2		LSEB	20	3
W2 PS E1		LSEB	16	0

In vitro differentiated NM progenitors were grafted to D and MP site of E7.5 embryos. The embryos were cultured for 24 hr. The number of dispersed donor cells in the host was manually counted. D: distal; MP: mid-posterior; MS: mid-streak stage; LS: late-streak-stage; LSEB: late-streak to early bud stage.

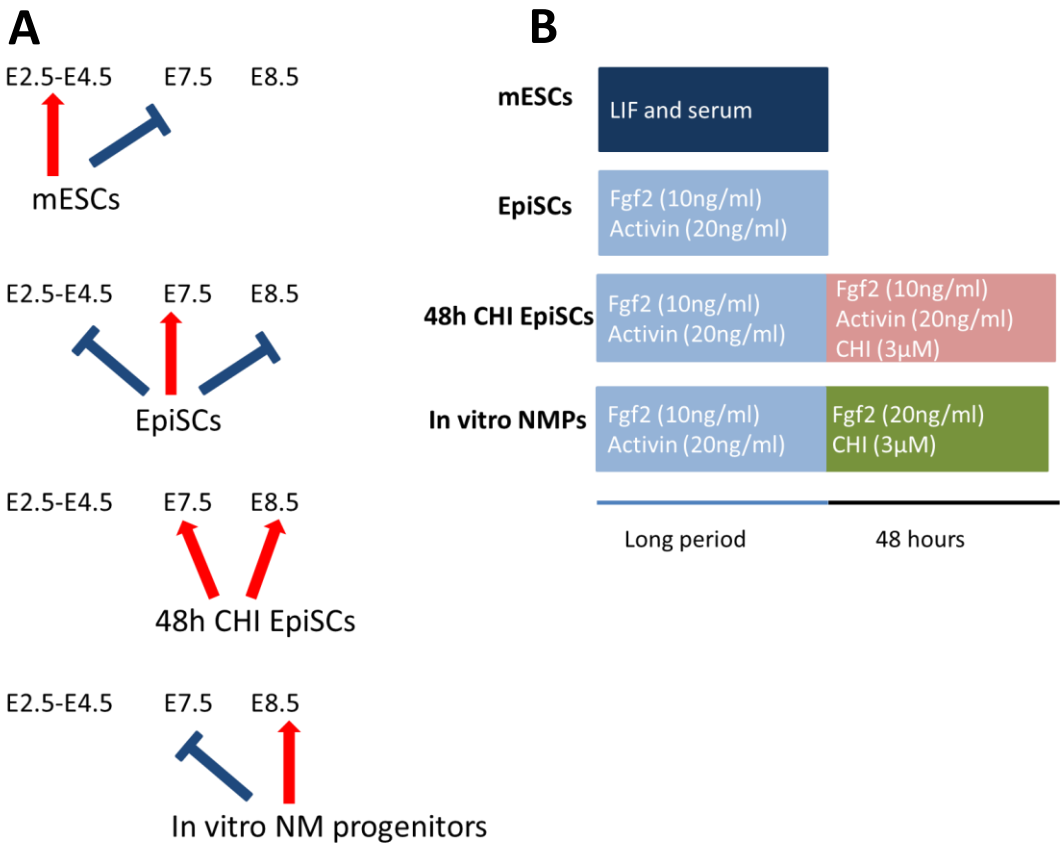

Figure 4.15. A summary of cell incorporation in different stage of mouse embryos

(A) Summary of the grafting experiments in this study combined with results from the literature.

Red arrow: most cells can incorporate at this specific stage. Blue T block: most cells can barely incorporate and proliferate in this specific stage.

(B) Culture conditions for different types cells

4.6 Conclusion and discussion

In this chapter, I show that mESCs, derived from preimplantation embryos, and which show a high efficiency of chimera formation after blastocyst injection are unable to incorporate into postimplantation embryos. However, EpiSCs, which display poor integration in preimplantation embryos (Brons et al., 2007; Tesar et al., 2007), efficiently form chimeras when grafted to streak stage embryos (E7.5). EpiSC integration is severely compromised in E8.5 embryos, indicating that the period of their compatibility with the host embryo corresponds to the timing of the derivation of EpiSC lines (Osorno et al., 2012) (Figure 4.15A). Thus, EpiSCs can be considered functionally equivalent to postimplantation epiblast cells in vivo prior to somitogenesis. These different stages of grafting experiments indicate that the efficient integration of donor cells does not depend primarily on their pluripotency status but on the developmental match between donor and host environment.

The similarity between EpiSCs and the streak stage epiblast suggests that EpiSCs can be used as a physiologically relevant system in vitro to study events during gastrulation and further differentiation of epiblast. Moreover, since EpiSCs are pluripotent cells in a more advanced developmental state compared to mESCs, they have the potential to more easily differentiate into various cell types. Taking advantages of the grafting technique and ex vivo chimera formation assay, we can analyse whether the in vitro-derived cells are equivalent to those cells found in vivo.

Elevation of Wnt signalling in EpiSCs cultured with CHI for 48 hours blocks their neural contribution in streak stage embryos (E7.5) but does not affect their mesoderm and endoderm differentiation. It has been shown that EpiSCs are heterogeneous and contain a neural-like subpopulation (Sox1-GFP). When treated with CHI, this population is considerably reduced. Moreover, the transcription levels of anterior neural markers, e.g., *Pou3f1* and *Zic2*, are also downregulated. Therefore, my grafting result is consistent with these in vitro findings.

Notably, increasing Wnt signalling in EpiSCs leads to their incorporation in E8.5 embryos. 48h CHI C2 contribute to the neural tube in two out of 10 embryos, indicating the enhancing Wnt signalling in EpiSCs may only affect the anterior but not posterior neural differentiation. This raises an interesting question whether 48h CHI treated EpiSCs are pluripotent cells. The pluripotency markers are downregulated but not distinct from in these cells (Tsakiridis et al., 2014). The combined results from E7.5 and E8.5 grafts show that 48h CHI treated EpiSCs

can differentiate into three germ layers. However, these cells may not be pluripotent since their potency has been attenuated.

It has been shown that there is a primitive streak-like subpopulation in EpiSCs which shows high Wnt activity. Moreover, this primitive streak-like subpopulation is significantly increased in 48h CHI treated EpiSCs (50-70%) (Tsakiridis et al., 2014). Since 48h CHI treated EpiSCs can incorporate into both E7.5 and E8.5 embryos, most of them may represent primitive streak cells during bud stage to the beginning of somitogenesis (E7.5-E8.5). Notably, there is 10-20% of 48h CHI treated EpiSCs coexpressing T and Sox2. It has been shown that $T^{+}Sox2^{+}$ cells initiate close to the node at the headfold stage (E8.0) (Figure 2.10, data from F. Wong). Therefore, it is possible that this 10-20% of 48h CHI treated EpiSCs represents $T^{+}Sox2^{+}$ cells in the most anterior region of the primitive streak at the headfold or beginning of somitogenesis stage embryos (E8.0-E8.5).

When grafted to E8.5 embryos, 48h CHI treated EpiSCs contributed to both neuroectoderm and mesoderm in two out of 10 embryos. The low incidence of neural contribution coincides with the low percentage of $T^{+}Sox2^{+}$ cells in 48h CHI treated EpiSCs. If the neural contribution in E8.5 embryos resulted from the $T^{+}Sox2^{+}$ cells, this raises the possibility that these early $T^{+}Sox2^{+}$ cells are already lineage-restricted and perhaps also compatible with those in E8.5 embryos. In chapter 2, I have shown that distal cells (equivalent to the most anterior region of the primitive streak), which express Sox2 but not T at LS-EB stages (E7.5), cannot contribute to neuroectoderm in E8.5 embryos. Taken together, these may indicate that the initiation of $T^{+}Sox2^{+}$ cells marks the appearance of NM progenitors in embryos. However, distal cells at early headfold stage (E8.0) should be grafted into E8.5 NSB in order to assess this proposition. Also, in chapter 2 I show that NM progenitors have been eliminated at E14.5 when there are no $T^{+}Sox2^{+}$ cells in the embryos. Since the presence of NM progenitors corresponds to the coexpression of T and Sox2, these two TFs may be critical for the functions of NM progenitors. Therefore, it would be interesting to further investigate the role of T and Sox2 in NM progenitors by conditional deletion of either gene in in-vitro NMPs.

In this study, I also tested the in vivo potential of in-vitro NMPs. Unlike 48h CHI treated EpiSCs, these cells seldom proliferated in streak stage embryos (E7.5). Although both cell lines can incorporate into E8.5 embryos (Figure 4.15A), their distribution is slightly different. In-vitro NMPs extensively contribute to the paraxial mesoderm (Gouti et al., 2014), while 48h CHI C2-derived cells were often found surrounding the dorsal aorta (Figure 4.13A, B

and Table4.3). It is likely that the different in vivo potentials of these two types of cells result from their culture conditions, in which the major difference is Activin A. Consistent with my observation, Activin has been used in protocols for LVM differentiation (Nostro et al., 2008). Also, nodal is expressed in the LVM during early somitogenesis. Since the LVM contribution of 48h CHI C2 cells in the NSB of E8.5 embryos is not consistent with the fate map of NSB cells, it is possible that there is a subpopulation which represents early LVM progenitors in 48h CHI C2 cells.

The poor proliferation of in-vitro NMPs in streak stage embryos (E7.5) indicates that these cells may be in a more advanced developmental stage compared with the streak stage epiblast. Indeed, the transcription levels of Hox paralogous groups 5-9 are upregulated in these cells. However, since it is a newly generated cell type, a microarray analysis may be required for further investigation.

Chapter 5. Concluding remarks and future perspectives

How cells determine their fate is one of the most challenging problems in developmental biology. Generally speaking both intrinsic and extrinsic factors (cell autonomous and non-cell autonomous signals) are responsible for fate choice. Intrinsic factors generally refer to gene products localised within the cell, such as transcription factors, and number of divisions in the individual cells. Among all these factors, the ones which are critical for specific fate decisions are named intrinsic determinants. Extrinsic factors include cell-cell and cell-matrix contacts, and diffusible factors including morphogens in the extracellular matrix. Similarly, the ones which are sufficient to influence fate choice are called extrinsic determinants. In this thesis, I performed a large number of grafting experiments to find out both intrinsic and extrinsic determinants influencing fate choices in early embryogenesis. By grafting in vitro cultured cells into embryos, I found that each of these in vitro cultured cell types can only incorporate into some regions of the embryos at a specific stage (Figure 4.15). Since in vitro differentiated cells have been widely used in biomedical research and are expected to be used in the clinic in the future, it is important to find out the intrinsic and extrinsic determinants for in vitro cultured cells to incorporate to in vivo.

The presence of intrinsic determinants can be tested by comparing the behaviour of different cell types in the same embryonic environment. To further test the role of specific determinants, wildtype and cells that have been genetically modified for a gene of interest can be compared. It has been shown that EpiSCs are not compatible with preimplantation embryos (Brons et al., 2007; Tesar et al., 2007). However, transiently enhancing E-cadherin expression in the EpiSCs promotes the incorporation of EpiSCs in preimplantation embryos (5% chimera formation efficiency compared to 0.5% in the previous studies) (Ohtsuka et al., 2012). This could be because the overexpression of E-cadherin at the surface leads to a more compatible level of cell adhesion between EpiSCs and ICM. Alternatively, it could be because E-cadherin binds to β-catenin in the cell membrane which then results in the attenuation of Wnt/β-catenin signalling.It has also been shown that inhibiting Wnt signalling in EpiSCs blocks their spontaneous differentiation (Sumi et al., 2013; Tsakiridis et al., 2014). It is thus possible that active Wnt/β-catenin signalling is one of the intrinsic determinants that prevents incorporation in the ICM. The fate switch of the NM progenitors in the anterior primitive streak (Chapter 3) provides a good example showing that β-catenin is one of the intrinsic determinants for mesoderm lineage formation. It has also been shown that intrinsic Notch signalling can regulate the fate choice between the floor plate and notochord in the Hensen's node (Gray and Dale, 2010). Although in mouse embryos there is no direct in vivo evidence showing that NM progenitors can give rise to the notochord, we may be able to test this by inhibiting Notch signalling in in vitro derived NM progenitors.

Extrinsic determinants can be identified by challenging cells with different locations to determine whether they adopt a different fate in vivo, or by adding factors influencing cell differentiation in vitro. In Chapter 3, I show that LVM fated L5 cells can give rise to paraxial mesoderm when placed in the anterior of the primitive streak. This could be because of their responses to different levels of BMP signalling. It has been shown that high levels of BMP signalling promote LVM differentiation in the posterior part of the primitive streak, while lower levels result in paraxial mesoderm formation in the anterior primitive streak (reviewed in (Stern, 2004). From in vitro differentiation, we also know that Wnt signalling is important for increasing a primitive streak-like population in EpiSCs, Nodal signalling is required for initiating mesendodermal cells and Wnt and Fgf signalling is critical to establish NM progenitors from EpiSCs (Gouti et al., 2014; Tsakiridis et al., 2014).

It is worth noting that in different cell types the same intrinsic and extrinsic signals can have different effects. In Chapter 3, I show that β-catenin deletion induces neural differentiation in mesoderm fated NM progenitors. However, this mesoderm-to-neural switch is not observed in mesodermal committed cells. Similarly, the same regulator can have different effects on different cell types. For example, Axin2, one of the key negative regulators of Wnt/β-catenin signalling, inhibits Wnt signalling in the anterior of the embryos but increases Wnt signalling in a specific population in the late primitive streak (Qian et al., 2011). Also, the same signalling pathway can have different roles on different cell types. For example, BMP signalling is also required for both the maintenance of pluripotency in ES cells and mesoderm differentiation in the epiblast. A recent study shows that BMP signalling blocks cell differentiation by maintaining high levels of E-Cadherin and also imposes a posterior identity on undifferentiated epiblast. BMP signalling then promotes mesoderm differentiation of these cells (Malaguti et al., 2013). We also see that mESCs and EpiSCs have different responses to Wnt signalling. It has been shown that enhancing Wnt/β-catenin signalling blocks cell differentiation in mESCs (Miki et al., 2011). We demonstrate that increasing Wnt signalling in EpiSCs induces a primitive streak-like population. Thus a careful analysis of the intrinsic and extrinsic determinants in different cells is vital for predicting the in vivo behaviours of in vitro cultured cells. This would also benefit regenerative therapies and tissue engineering strategies in the future.

Since we have identified some in vitro counterparts of multipotent cells in vivo, we can use them to further investigate to the mechanisms for the restriction of potency during embryogenesis. It is still not clear how cells decide between self-renewal and differentiation. Different mathematical models have been published which try to interpret this event. Lander

and colleagues have tried to predict the behaviour of adult stem cells (Lander et al., 2009). According to their model, the self-renewal and differentiation events in stem cells depend on their replication probability and progression towards differentiation. Also, differentiated cells themselves will negatively feedback on both events. They show that these parameters help to estimate stem cell behaviours in the mammalian olfactory epithelium. Similar principles may also control and coordinate embryo development. By taking advantage of both in vivo and in vitro experiments, it is possible that in the future we would have adequate data to begin to model these parameters and generate a robust model to reveal biological timing mechanisms.

At the end, I would like to list some experiments for Wilson's lab to undertake in future.

1. **Establish a stable notochord progenitor cell line**

Although the notochord is present only in the early embryonic stage in mammalian embryos, it has been shown that the nucleus pulposus of intervertebral discs are derived from notochord cells in mice (McCann et al., 2012). As discussed previously, we know that notochord progenitors are located in the ventral node in mouse embryos. Using microarray analysis our group has identified some genes that are specifically expressed in the ventral node (Wilson lab, unpublished data). Moreover, when grafted to E8.5 NSB, EpiSCs (C2) contribute to the notochord in one out of four embryos, implying there may be a small number of notochord progenitor-like cells existing in C2 cells. A previous study has demonstrated how to differentiate node/notochord-like cells from mouse ESCs (Winzi et al., 2011). Therefore, this study may provide some clues for establishing a stable notochord progenitor cell line either differentiated from EpiSCs or derived from embryonic tissues. Besides acting as nucleus pulposus progenitors, it has been proposed that the ventral node acts as a niche for maintaining NM progenitors. Therefore, the notochord progenitor cell line could be used to as a tool to interrogate both the development of intervertebral disc and the signals for maintaining NM progenitors.

2. **Maintenance of NM progenitors beyond the point of cessation of axis elongation**

Generally, Wnt and FGF signalling are involved in the maintenance of the posterior progenitor zone. A previous study in our group has shown that Fgf8 is necessary for the maintenance of axial progenitors but cannot sustain NM progenitors beyond the end of axis elongation (Wymeersch, 2011). In this study, I show that Wnt/β-catenin signalling is important for the expansion of NM progenitors. Moreover, it has also been demonstrated in another study that increasing Wnt signalling by addition of CHI to tail explant culture induces the ectopic presence of $T^{+}Sox2^{+}$ cells in the tails (Wymeersch, 2011). Therefore, it is worth further investigating whether activation of Wnt signalling in the posterior progenitor zone during the late tail bud stage is able to maintain NM progenitors beyond E13.5. For example E12.5 tails can be cultured with CHI for 24-48h and ectopic $T^{+}Sox2^{+}$ cells can be grafted to E8.5 NSB to assess whether these cells are able to give rise neuroectoderm and mesoderm in a young environment.

3. **The role of $T^{+}Sox2^{+}$ cells for the extension of the hindgut**

The existence of $T^{+}Sox2^{+}$ cells in the posterior of the gut has been found in the early zebrafish, chick and mouse embryos (Martin and Kimelman, 2012; Olivera-Martinez et al.,

2012; Wymeersch, 2011). In this study, I show that $T^{+}Sox2^{+}$ cells persist in the posterior of the hindgut from E9.5 to E13.5. It is likely that these cells act as gut progenitors. However, the role of T or Sox2 in the gut extension has not been extensively studied. Since the coexpression of T and Sox2 in the hindgut is conserved in different species, it is interesting to investigate their role in early gut development. For example, T or Sox2 can be conditionally deleted during in vitro endoderm differentiation to investigate in which period these TFs are required for endoderm formation.

4. Single cell fate map of NM progenitors

Although grafting experiments have identified that the only possible locations of NM fated cells are in the NSB and CLE1, it is still unknown how individual NM progenitors behave in these regions during axis elongation. Moreover, it has been proposed that the pool of axial progenitors may undergo a rearrangement during trunk to tail transition (Tzouanacou et al., 2009). It is likely that there is a subset of NM progenitors that are maintained undifferentiated in a specific subdomain of the NSB and CNH during axis elongation. A possible experimental approach to evaluate these questions could rely on the single cell fate map in NSB and CNH regions. However, it is technically very demanding to graft a single cell. Other techniques such as single cell dye labelling or use of transgenic strains expressing photoconvertible fluorescent proteins to target individual cells could be used instead.

5. Mechanisms for the initiation, maintenance and loss of NM progenitors

As discussed previously, coexpressing T and Sox2 is closely related to the presence of NM progenitors. It is likely that these two TFs play an important role in NM progenitors. Since NM progenitors can be derived from pluripotent stem cells in vitro (Gouti et al., 2014), we can take advantage of these in vitro-derived NM progenitors to investigate the regulatory factors for T and Sox2 expression and the downstream targets of these two TFs to further understand the mechanisms for initiation, maintenance and loss of this population.

Chapter 6: Materials and methods

Materials

Standard molecular biology solutions were made according to Sambrook et al., 1989. All chemicals used were analytical grade and supplied by BDH, Sigma-Aldrich or Life Technologies. Nucleic acid markers 4',6-diamidino-2-phenylindole (DAPI) was supplied by Life Technologies. Laboratory plasticware for growing and plating cells or embryos were supplied by Fischer Scientific. Micropipette for grafting and dissecting were obtained from Harvard Apparatus and Fischer Scientific, respectively. Forceps for dissecting the embryos were obtained from Dumostar. Glasgow Minimal essential medium (GMEM), Dulbecco's Modified Eagle Medium: Nutrient Mixture F-12 (DMEM-F12), Knockout Serum Replacement (KOSR), non-essential aminoacids (NEAA), N2 supplement, B27 supplement, Fetal Calf Serum (FCS), glutamine, sodium pyruvate and penicillin-streptomycin-glutamine (100X) were obtained by Life Technologies. Basic FGF (bFGF) was obtained from R&D Systems. Dulbecco's phosphate buffered saline (PBS), M2 medium and human fibronectin were supplied by Sigma-Aldrich. Rat serum was prepared in-house by Prof. Val Wilson according to Copp and Cockroft, 1990

Solutions

1. 4% paraformaldehyde (PFA): PFA EM grade (Sigma-Aldrich) was dissolved in phosphate buffered saline (PBS) pH 7.4 (Sigma-Aldrich).
2. 6X loading buffer: 0.25% xylene cyanol, 0.25% bromophenol blue, 30% glycerol
3. 15% sucrose (w/v) solution: sucrose (Fischer Scientific) was dissolved in PBS pH7.4
4. 15% sucrose (w/v), 7% gelatin solution: gelatin (Fluka) was dissolved in 15% sucrose solution at 90˚C
5. 50% rat serum culture medium (for E7.5 and E8.5 embryos): 50% heat inactivated rat serum, 50% GMEM, 1% non-essential aminoacids (NEAA), 2mM L-glutamine and 1mM sodium pyruvate, 10,000 I.U/ml penicillin and 10,00 (µg/mL) streptomycin (Copp et al., 1990)
6. 75% rat serum culture medium (for E9.5 embryos): 75% heat inactivated rat serum, 25% GMEM, 1% non-essential aminoacids (NEAA), 2mM L-glutamine and 1mM sodium pyruvate, 10,000 I.U/ml penicillin and 10,00 (µg/mL) streptomycin
7. BABB: 1 benzyl alcohol (Sigma-Aldrich): 2 benzyl benzoate (Sigma-Aldrich)
8. PBST: PBS with 0.1% Triton X-100 (Sigma-Aldrich)

9. Serum blocking buffer: 3% donkey serum (Sigma-Aldrich), 1% *Bovine serum albumin* (BSA) (Sigma-Aldrich) and 0.01% sodium azide (Sigma-Aldrich) in PBST

Methods

Embryology

Maintenance of mice stocks (Mouse husbandry)

All wild type and transgenic mice were housed and bred within the animal unit of the Institute for Stem Cell Research and the MRC Centre for Regenerative Medicine according to the provisions of the Animals (Scientific Procedures) Act (1986). All mice were bred and maintained in a stabilized environment on a 12 hours light/12 hours dark cycle.

Recovery of embryos and dissection

To collect embryos at specific developmental stages, timed matings were set up overnight. Noon on the day of finding a vaginal plug was designated embryonic day 0.5 (E0.5). Embryos were dissected from the uterus in M2 medium (Sigma-Aldrich). The dissection was performed as described (Copp and Cockroft, 1990).

To collect embryos for ex vivo culture, myometrium was carefully torn apart using two pairs of fine forceps. The deciduas were peeled away taking care not to puncture the extraembryonic cavities. Reichert's membrane was then removed by pinching the membrane with forceps and then slowly separating it from the embryo. Before culture, the embryos were checked under a dissecting stereomicroscope to ensure that the yolk sac, amnion and the ectoplacental cone were all intact.

Grafting cells from in vitro culture into embryos

Grafting was performed under a dissecting stereomicroscope using a hand pulled micropipette. Cells were cultured in 6-well plates and then scraped from the plate using a 20-200 μl pipette tip (NICHIRYO). The resulting cell sheets were placed close to the embryos and then drawn into the micropipette by gentle suction. Cells were gently blown out. A small cell clump containing 10-20 cells was sucked into the micropipette again and placed close to the opening of the micropipette (being careful not to suck the cell clump in and out of the micropipette too many times to avoid breaking the clump into smaller pieces). The embryo was held loosely in place with forceps while the micropipette was inserted in the region of

interest to create an opening. Cells were then gently expelled as the micropipette was drawn out of the embryo, leaving a short string of cells lodged in the epiblast (Huang et al., 2012).

Microdissecting subregions from embryos

E7.5 distal cells

E7.5 AGFP embryos (Gilchrist et al., 2003) were carefully staged according to Downs and Davies criteria (Downs and Davies, 1993). LS to EB stage embryos were chosen for further dissection. The embryo was laid sagittally in the dish and two longitudinal cuts were made on either side of the distal region using a fine glass cutting needle. The lateral epiblast was then removed, leaving only a small square of tissue in the middle. This tissue was then divided into two pieces for donor grafting.

E13.5 CNH

The most posterior part of the tail containing at least the 3 most posterior somites was isolated from early E13.5 AGFP embryos with forceps. The CNH was dissected using a fine glass cutting needle. The tail was laid dorsoventrally and a transverse cut was made anterior to the last somites to isolate the tail tip. Two dorsoventral longitudinal cuts were made to remove the PSM. To remove the hindgut, the tissue was placed in sagittal view then cut longitudinally. Where possible, the surface ectoderm on top of the neural tube was trimmed or peeled away. A transverse cut was made at the end of the neural tube and notochord to remove the TBM. The last transverse cut was made anterior to the notochordal plate to isolate the CNH tissue.

E14.5 tail tip

Using forceps, the most posterior part of the tail was isolated intact from E14.5 AGFP embryos. The excess anterior tail tissue was removed using a fine glass cutting needle to isolate the cone-shaped tail tip. Two dorsoventral longitudinal cuts were made to remove the paraxial tissues. The next cut was to remove the ventral half of the tissue. The surface ectoderm covering the dorsal part of the tail tip was trimmed or peeled away. The excess anterior tissue was cut away to isolate a small piece of tissue from the tail tip similar in size to E13.5 CNH.

Ex vivo embryo culture

50% rat serum culture medium was filtered using a 0.45μm filter (Sartorius) and warmed to 37˚C before embryo culture. E7.5 embryos were cultured in static 4-well plates

(NunclonTM). Up to two embryos were cultured per well with 1ml of culture medium. The embryos were cultured in an incubator supplied with 7% CO_2 in air at 37˚C.

Optionally, embryos (developing to 3-4 somite stage after 24h culture) were cultured for a further 24h in fresh 50% rat serum culture medium (0.5ml medium per embryo) in a roller apparatus as described below for culturing E8.5 embryos. However, E7.5 embryos were not cultured longer than 48h ex vivo due to lack of turning.

E8.5 embryos were cultured in 50% rat serum culture medium (one embryo per 1ml medium) in a roller culture apparatus (B.T.C Engineering) supplied with 5% CO_2 in air (BOC) at 37˚C. Alternatively, they could be cultured in a round-bottomed universal tube with a screw cap (Nunc) where the thread was coated with vacuum grease (Baysilone-paste, Bayer) to create an airtight seal. Tubes were gassed with 5% CO_2 in air for 1min. Up to two embryos were cultured per vial. The universals were then placed inside a roller incubator (BTC Engineering) at a slight angle from the horizontal at 37˚C.

After 24 hours in culture, embryo development was checked. Embryos which had undergone turning were cultured for another 24 hours in 75% rat serum culture medium (1ml medium per embryo) in 5% CO2, 40% O2 balance N2 (BOC) at 37˚C. After culture, embryos were dissected in M2 medium (Sigma-Aldrich) for further examination.

Histology

Gelatin embedding and cryostat sectioning

Samples were fixed with 4%PFA for 2 hours to overnight at 4˚C according to the embryonic stage (see Table 6.1). The embedding and sectioning methods were adapted from (Henrique et al., 1995) and optimized by Ron Wilkie. After fixation, samples were washed three times in PBS for 5 min in a shaker followed by a last wash in PBS with 0.1% BSA (Sigma-Aldrich) to prevent samples sticking on tips during transferring. Samples were transferred into 15% sucrose/PBS and left 2 hours to overnight at 4˚C then transferred to a small bijou or 4-well plates in warm 15% sucrose/7% gelatin solution. Samples were incubated at 37˚C for 2-4 hours until the sucrose/gelatin mix had fully penetrated the embryos. Samples were transferred and orientated in the same solution in a mould (Agar Scientific) circled by adhesive tape and parafilm (Pechiney). During orientation in a dissecting microscope, the mould was placed on a Petri dish with ice to allow the sucrose/gelatin solution to set. Samples were then snap frozen in liquid nitrogen. Blocks were stored at -80˚C. Before

sectioning, blocks were transferred to a cryostat chamber (Leica CM1900) to equilibrate for 1-2 hours. Samples were sectioned at 7μm and mounted onto Polysine^{TM} slides (VWR). All the slides were stored at -20˚C.

Table 6. 1 . The optimal time for fixation

Stage of samples	Purpose	Fixation time (at 4˚C)
E8.5	Cryostat section and immunofluorescence	2-4 hours
E8.5	Whole-mount immunofluorescence	2 hours (the fixation time is critical)
E9.5	Cryostat section and immunofluorescence	6 hours-overnight
E9.5	Wholemount immunofluorescent staining	4 hours
E10.5	Cryostat section and immunofluorescent staining	overnight
E10.5-E14.5 tails	Wholemount immunofluorescent staining	2-4 hours
E8.5-E10.5	Immunocytochemistry for GFP using DAB detection	overnight

General immunofluorescent staining on cryostat sections

Slides were thawed at room temperature (RT) for 3min in the dark. The sections were circled with a diamond pen on the back of the slides. Antigen retrieval was performed using 10mM sodium citrate, pH6.0 in the microwave for 15 min (a 5 min cycle: two and a half minutes on full power and stop for two and a half minutes, to keep the temperature below boiling point). Distilled water was added to avoid changes in molarity of the solution during microwaving. Slides were cooled in running water. Individual sections were circled with an ImmEdge TM pen (Vector Laboratories). If no antigen retrieval was needed, gelatin was removed from the sections by microwaving slides in PBS or distilled water for 45 seconds.

Slides were stained and kept in the dark in a humidified box. Sections were permeabilized with 0.1% PBST for 10 min followed by treating with 1M glycine pH7.5 in PBS for 20min to reduce the nonspecific binding (optional). Sections were washed 3 times in PBS 5min

each. Blocking was done for 1 hour at RT in serum blocking buffer or Novocastra protein block (Leica biosystems). All primary antibodies were diluted in the serum blocking buffer and incubated overnight in the dark at RT, followed by 3X 5 min PBS washes. The secondary antibodies were diluted in serum blocking buffer and incubated for 2 hours to overnight in the dark at RT, followed by followed by 3 X 5 min PBS washes, of which the last wash contained 1:1000 DAPI. Slides were mounted in Vectshield (Vector Laboratories). Imaging was conducted within two days. For details on primary and secondary antibodies, see table 6.2 and 6.3.

Table 6. 2 . Primary antibody list

Primary antibody	**Dilution (original conc.)**	**Company and Cat**
Phalloidin-Alexa 647	1:40 (5.35 mg/mL)	Life Technologies (A34051)
Anti-Active β-catenin (Clone: 8E7)	1:1000	Millipore (05-665)
T/Bra	1:400	R&D (AF2085)
Sox2	1:400 (1 mg/ml)	Abcam(ab97959)
Anti-β-catenin, whole antiserum	1:2000	Sigma (C2206)
Anti-PDGF Receptor beta antibody	1:100 (0.084 mg/ml)	Abcam(ab32570)
Anti-CD146 antibody	1:100	Abcam (ab75769)
Anti-CD31	1/1000 (0.1 mg/ml)	Abcam (ab7388)
Anti-GFP antibody	1/800 (10 mg/ml)	Abcam (ab13970)
Anti-SLUG antibody	1/25 (1 mg/ml)	Abcam (ab106077)
Anti-Tbx6 antibody	1/500 (0.3 mg/ml)	Abcam (ab38883)
Anti-CTHRC1 antibody	1/100 (0.2 mg/ml)	Abcam (ab85739)
Anti-Nkx2.5 antibody	1/50 (1 mg/ml)	Abcam (ab35842)
HNF-3β Antibody (M-20)	1/100 (0.2 mg/ml)	Santa Cruz (sc-6554)

Table 6. 3 . Secondary antibody list

Secondary antibody	Dilution (original conc.)	Company and Cat
Donkey anti goat 568	1:1000 (2 mg/ml)	Life Technologies (A-11057)
Donkey anti goat 647	1:1000 (2 mg/ml)	Life Technologies (A-21447)
Donkey anti rabbit 555	1:1000 (2 mg/ml)	Life Technologies (A-31572)
Donkey anti rabbit 647	1:1000 (2 mg/ml)	Life Technologies (A-31573)
Donkey anti mouse IgG 568	1:1000 (2 mg/ml)	Life Technologies (A10037)
Donkey Anti-Chicken IgY H&L (FITC)	1:800 (1 mg/ml)	Abcam (ab63507)
Goat anti mouse HRP	1:2000	Life Technologies (A24512)

Actin Filament staining

After removing gelatin, sections were washed twice in PBS for 5 min and then another 5 min wash in 0.1% PBST. Blocking was done for 30min in PBST with 3% BSA. Phalloidin-Alexa 647 antibody was diluted in the blocking buffer (1:40) and incubated for 30 min in the dark at RT. Slides were mounted and imaged as described below.

Double or triple immunofluorescent staining on cryostat sections

Two or more primary antibodies raised in different host species were used for multicolour immunofluorescent detection. Generally, different proteins were stained sequentially, except T and Sox2 double staining where both primary antibodies were incubated together. Staining was performed as described above.

Active β-catenin staining with Tyramide Signal Amplification (TSA) kit

After removing gelatin, sections were permeabilized with 0.1% PBST for 10 min followed by treating with 3% H_2O_2 for 10min to eliminate endogenous peroxidase activity. 1M glycine pH7.5 in PBS was added to the sections for 20 min to reduce nonspecific binding. Blocking was done for 1 hour at RT in Novocastra protein block. Active β-catenin primary antibody was diluted in the goat serum blocking buffer 1:1000. Sections were incubated with the diluted antibody overnight in the dark at RT, followed by 3 X 5 min PBS washes. The goat anti mouse HRP secondary antibody was diluted in goat serum blocking buffer 1:2000 and incubated for 2 hours in the dark at RT. Direct TSA 568 (PerkinElmer) was diluted 1:50

(dilution buffer was provided in the kit) and incubated for 10min, followed by 3 X 5 min PBS washes, of which the last wash contained 1:1000 DAPI.

Immunofluorescent staining for whole-mount embryos

Samples were fixed with 4% PFA at 4˚C. See Table 6.1 for the fixation time. If desired, samples can be stored in 0.4% PFA in PBS for a few weeks at 4˚C after fixation.

Samples were washed 3 times in 0.1% PBST 30 min each in a shaking incubator, followed by permeabilizing in 0.5% PBST for 30min. Samples were treated with 1M glycine pH7.5 in 0.1% PBST for 30min to reduce unspecific binding followed by 3 X 10 min 0.1% PBST. Blocking was done in serum blocking buffer overnight at 4˚C. Primary antibody was diluted in serum blocking buffer. Samples were incubated with the diluted antibody for 48h in the dark at 4˚C (T and Sox2 primary antibodies were incubated together) followed by at least 3 x 30 min PBST washes. Secondary antibody was diluted in serum blocking buffer and incubated for 48h in the dark at 4˚C (for double staining, two secondary antibodies were incubated together), followed by 3 x 30 min 0.1% PBST washes. Samples were left in DAPI (1:500) at least overnight at 4˚C before imaging.

Imaging

Whole-mount images of embryos or tails were captured by (1) Volocity software (Perkin Elmer) with a digital camera attached a to Zeiss Stemi SV11 dissecting microscope; (2) Nikon software with an EXi Blue TM camera attached to a NIKON NZ100 (NIKON) dissecting microscope; (3) Volocity software with a digital camera attached to an Olympus IX51 inverted microscope (Olympus).

To count the number of grafted GFP^+ cells, E7.5 embryos were imaged using a Leica DM IRE2 inverted confocal microscope (Leica Microsystems) in PBS.

All cryostat sections were imaged using an Olympus BX61 fluorescence compound microscope (Olympus), with an ORCA-R2 monochorme camera (Hamamatsu) driven by Volocity software.

All images were processed using Adobe Photoshop CS4 (Adobe Systems Inc.) and Image J (http://rsbweb.nih.gov/ij/).

Imaging immunofluorescence for T/Sox2 in whole-mount embryos

To reduce light scattering, samples were cleared using BABB solutions before imaging. Samples were first dehydrated through 30%, 50% and 80% methanol 10 min each (the time may vary depending on the size of the samples) in 0.5 eppendorf tubes followed by three 5 min wash in 100% methanol. After dehydration a 50% methanol and 50% BABB mixture was then added to the tube. Samples were then transferred to an Attofluor® Cell Chamber (Life Technologies™) with 100% BABB and finally washed in 100% BABB. Samples were positioned under UV light and imaged using a TCS SPE or SP8 confocal microscope (Leica Microsystems). The same field size was applied to all the tail samples (E10.5-E14.5). For E8.5 and E9.5 samples two sets of z-stake images were taken and stitched together using (Leica Microsystems).

Nuclear segmentation and single cell fluorescence quantification

Confocal images were deconvoluted using Huygens software (Scientific Volume Imaging). The volume of data collected by the confocal microscope was too large for the processing power of the workstation. To reduce data volume, one sample was divided into 2 or 3 adjacent parts for segmentation and quantitative analysis (Figure 6.1C). Results from different parts were summed up at the end.

Firstly, samples were stained with DAPI, a nuclear counterstain, and the images were used for segmentation to create a nuclear volume for each cell

Segmentation methods:

1. To quickly find the segmentation parameters, a small region was cropped from a z-stack of DAPI images and segmented using Farsight 0.4.5 software (http://www.openmicroscopy.org/site/support/bio-formats4/users/farsight/).

2. The def file containing all segmentation parameters was copied and used for the segmentation of the original z-stack DAPI images. The resulting image was named as Nuclei_Segmentation_0, in which each nucleus was labelled with a unique greyscale-based identifier. If desired, gamma correction of DAPI images was applied to enhance weakly fluorescing nuclei.

Secondly, the average pixel intensities in the green (T expression) and red (Sox2 expression) channels of the multichannel images were calculated within each nuclear volume using a Java application developed by Dr. Guillaume Blin within eclipse (www.eclipse.org) (Tsakiridis et al., 2014).

Single cell fluorescence quantification:

1. Internal controls: 4 different regions were cropped from one sample: a $Sox2^{+}T^{-}$ region; a $T^{+}Sox2^{-}$ region; a $T^{+}Sox2^{+}$ region and a $T^{-}Sox2^{-}$ region. They were used to set up the background levels for each channel (Figure 6.1A, B).

2. The background levels were applied to analyse all the whole z-stack images (Figure 6.2 C).

Figure 6. 1 . Flow chart showing single cell fluorescence quantification

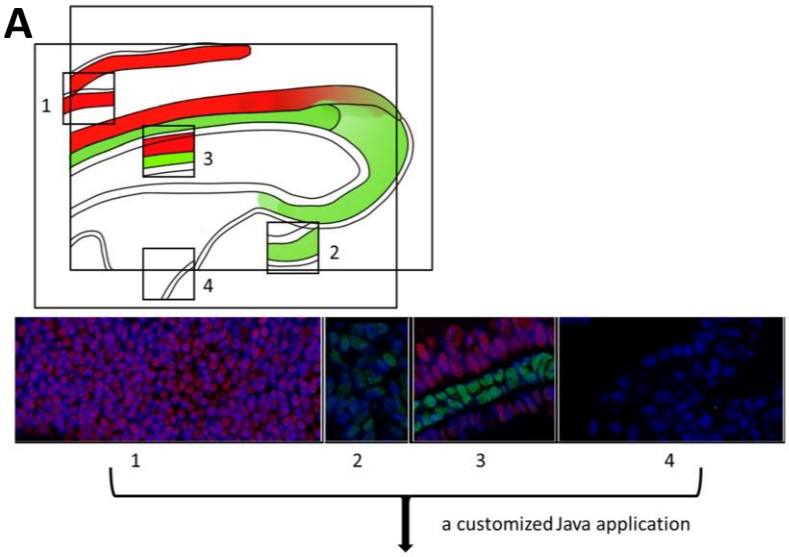

B

Region	Total cell number	No. of Sox2 positive cells	No. of T positive cells	No. of T and Sox2 double positive cells	Per. of T and Sox2 double positive cells
1. Only Sox2 positive region	1466	685	0	0	0
2. Only T positive region	293	0	220	0	0
3. T or Sox2 single region	1745	899	468	10	0.57%
4 double negative region	470	0	0	0	0

a customized Java application

C

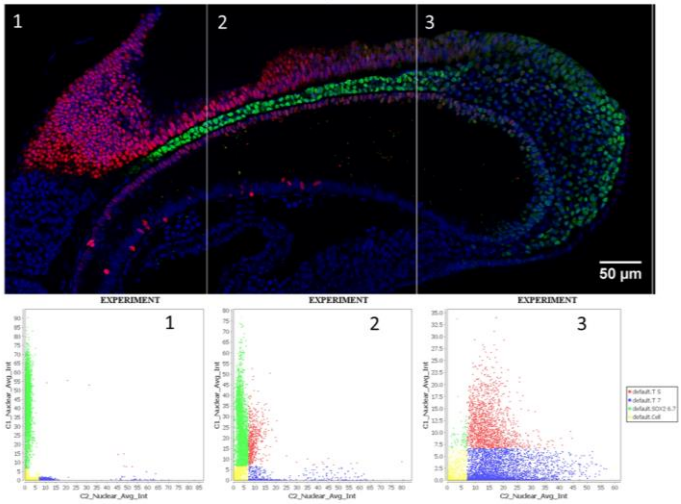

Region	Total cell number	No. of T positive cells	No. of Sox2 positive cells	No. of T and Sox2 double positive cells	% T and Sox2 double positive cells
1	9588	696	3619	8	0
2	12528	2386	3375	561	4.48%
3	10880	7275	1679	1602	14.72%

Molecular biology

Genomic DNA preparation from embryos

TRIzol (Life Technologies) was used to separate genomic DNA, RNA and proteins from embryos according to the manufacturer's instructions. One E9.5 embryo was homogenised in 1 ml TRIzol in a 2ml Eppendorf tube (Ambion) by repeatedly pipetting through a 26 gauge needle. Homogenised samples were incubated for 5 min at RT to allow for complete dissociation of nucleoprotein complexes. 0.2ml of chloroform was added to the sample followed by vigorously shaking the tube by hand for 15 seconds. The sample was incubated at RT for 2-3 min and then centrifuged at no more than 12,000g for 15 min at 4˚C. Phase separation was visible: upper layer (RNA), interphase (DNA) and lower layer (protein and some DNA). The interphase layer was extracted by pipette and used for genotyping.

Polymerase chain reaction (PCR)

DNA was amplified in a 25ul reaction volume using a Taq DNA polymerase kit (Qiagen). PCR master mix was prepared: 1xPCR Buffer, 25mM MgCl2, 40mM dNTPs (10mM each), 1μM primers (0.5μM forward and reverse primer) and 2.5U of Taq DNA polymerase. 5ul of genomic DNA was added to the PCR master mix and the volume adjusted to a total of 25μl with ddH2O. Eppendorf tubes (0.5mL) were used in a GeneAmp® PCR system 9700 (Applied Biosystems).

To detect floxed and/or floxdel β-catenin alleles, 3 primers were used: RM41 (5'AAG GTA GAG TGA TGA AAG TTG TT 3'); RM42 (5'CAC CAT GTC CTC TGT CTA TTC 3'); RM43 (5'TAC ACT ATT GAA TCA CAG GGA CTT 3'). The PCR conditions were as follows: 95˚C 5 min, followed by 35 cycles of: 95˚C for 30 seconds, 59˚C 30 seconds, 72˚C for 1 min. This was followed by a final extension of 10 min at 72˚C. Three products were generated in this PCR: 221 bp for the wild-type allele, 324 bp for the floxed allele and 500 bp for the floxdel allele (Brault et al., 2001).

Agarose gel electrophoresis

PCR products were detected by agarose gel electrophoresis. Agarose (Life Technologies) gels were prepared 1-1.5% w/v with 0.5ug/ml ethidium bromide (Sigma-Aldrich) in 1xTBE running buffer for the visualisation of nucleic acids. Samples were diluted with 6x loading buffer and run at 120 V (Biorad) for the appropriate time. Bands were visualised using a UV

transilluminator (Gene Flash). DNA sizes were estimated by comparison with 100bp ladder (New England Biolab)

ES and EpiSC Cell culture

ES cell culture media

- 500ml - Glasgow minimum essential medium (GMEM) (Sigma-Aldrich, G5154)
- 51ml – Fetal calf serum (FCS) (Life Technologies, 10270-106)
- 5.5ml - 100mM sodium pyruvate (Life Technologies, 11360-039)
- 5.5ml - 200mM L-glutamine (Life Technologies, 25030-024)
- 5.7ml - 100× MEM non-essential amino acids (NEAA) (Life Technologies, 11140-035)
- 570µl - 100mM (1000×) β-mercaptoethanol stock solution (Sigma-Aldrich, M6250)
- 570µl - 100'000U/mL (1000×) LIF supplement

ES cell culture

The flasks or plates were coated with 0.1-0.2% (w/v) gelatin (Sigma-Aldrich) in PBS for more than 10 minutes before use. Frozen ES cells were thawed quickly in a 37°C water bath. Cells were transferred to a 15 ml tube with 5ml ES cell culture medium and then centrifuged at 1000 rpm for 3 min. After the supernatant was aspirated, the cell pellet was suspended in 5 ml ES cell culture medium and transferred to a 6-well plate. Cells were cultured in a 37°C / 7% CO_2 humidified incubator.

Culture medium was changed every 24 or 48 hours. Cells were passaged when they reached 70-80% confluence. Cells were washed with pre-warmed PBS and incubated with 0.025% v/v trypsin (Life Technologies) at 37°C for 1-2 minutes. At least 5 volumes of culture medium were added to block the reaction and the cells were then centrifuged at 1500 rpm for 3 min. Cells were split at least 1:8 at each passage.

EpiSC cell culture media

- 100ml - Dulbecco's modified eagle medium (DMEM) : F12 (Life Technologies, 12634-010)
- 100m l - Neurobasal (Life Technologies, 21103-049)

- 2ml - 100× MEM non-essential amino acids (Life Technologies, 11140-035)
- 2ml - 100× L-glutamine solution (Life Technologies, 25030-024)
- 1ml - 100× N2 supplement (Life Technologies, 17502-048)
- 4ml - 50× B27 supplement (Life Technologies, 17504-044)
- 200µl - 100mM (1000×) β-mercaptoethanol stock solution
- 20ng/mL (final) - Human Activin A (PeproTech, 120-14E)
- 10ng/mL (final) - Human Fgf basic (R&D Systems, 233-FB-025/CF)

EpiSC cell culture

EpiSCs were maintained in Activin/FGF/N2B27 medium and cultured on plates coated with 7.5 µg/ml bovine fibronectin. EpiSCs were cultured in 6-well plates with 3 ml of culture medium per well. Cells were passaged when they reached 70-80% confluence. Cells were washed and treated with 300 µl of pre-warmed 1× accutase solution (Sigma-Aldrich) at 37°C for 5 minutes. At least 10 volumes of N2B27 medium were added to block the reaction and cells were centrifuged at 1500 rpm for 3 minutes. Cells were split at least 1:10 at each passage. Cells were then cultured in a 37°C / 7% CO_2 humidified incubator.

Appendix

I. Images of all grafts

Chapter 2

Sup Figure 2.1: E7.5 distal cells to E8.5 NSB

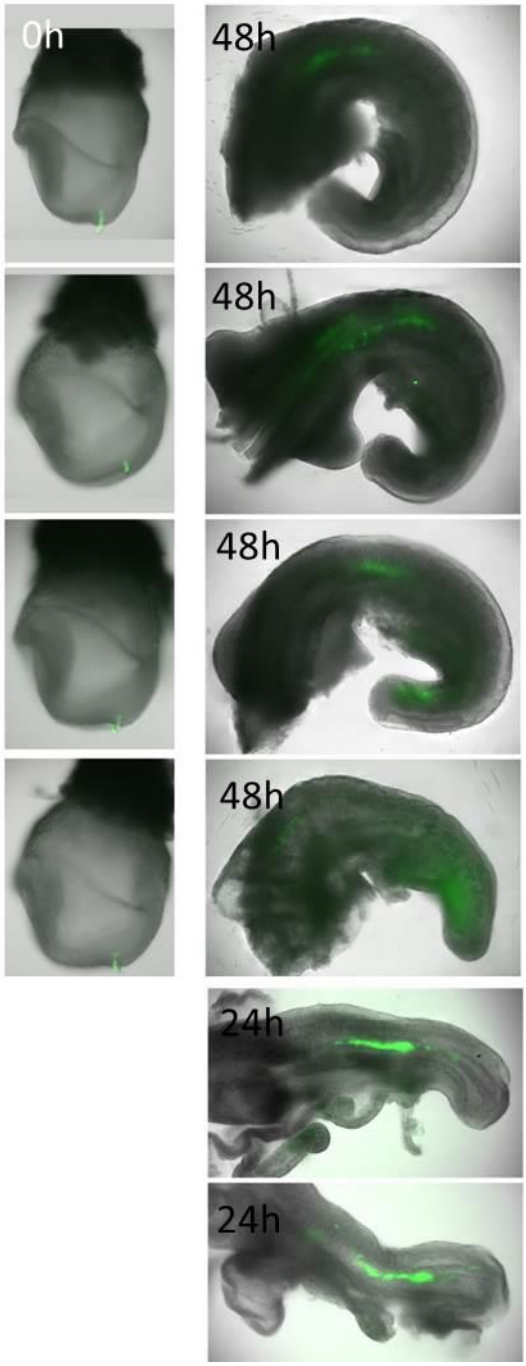

Distal cells from E7.5 AGFP embryos were grafted to the NSB of E8.5 (2-5 somite stage) wild type embryos. In total, 6 embryos recieved a graft. Embryos were imaged before culturing. Four representative embryos are shown after grafting (in the left planes). Two of them were cultured for 24h, the other four for 48h. Note: since two embryos were normally cultured together, the 0h culture images do not correspond to those after culture.

Sup Figure 2.2: E13.5 CNH to E8.5 NSB

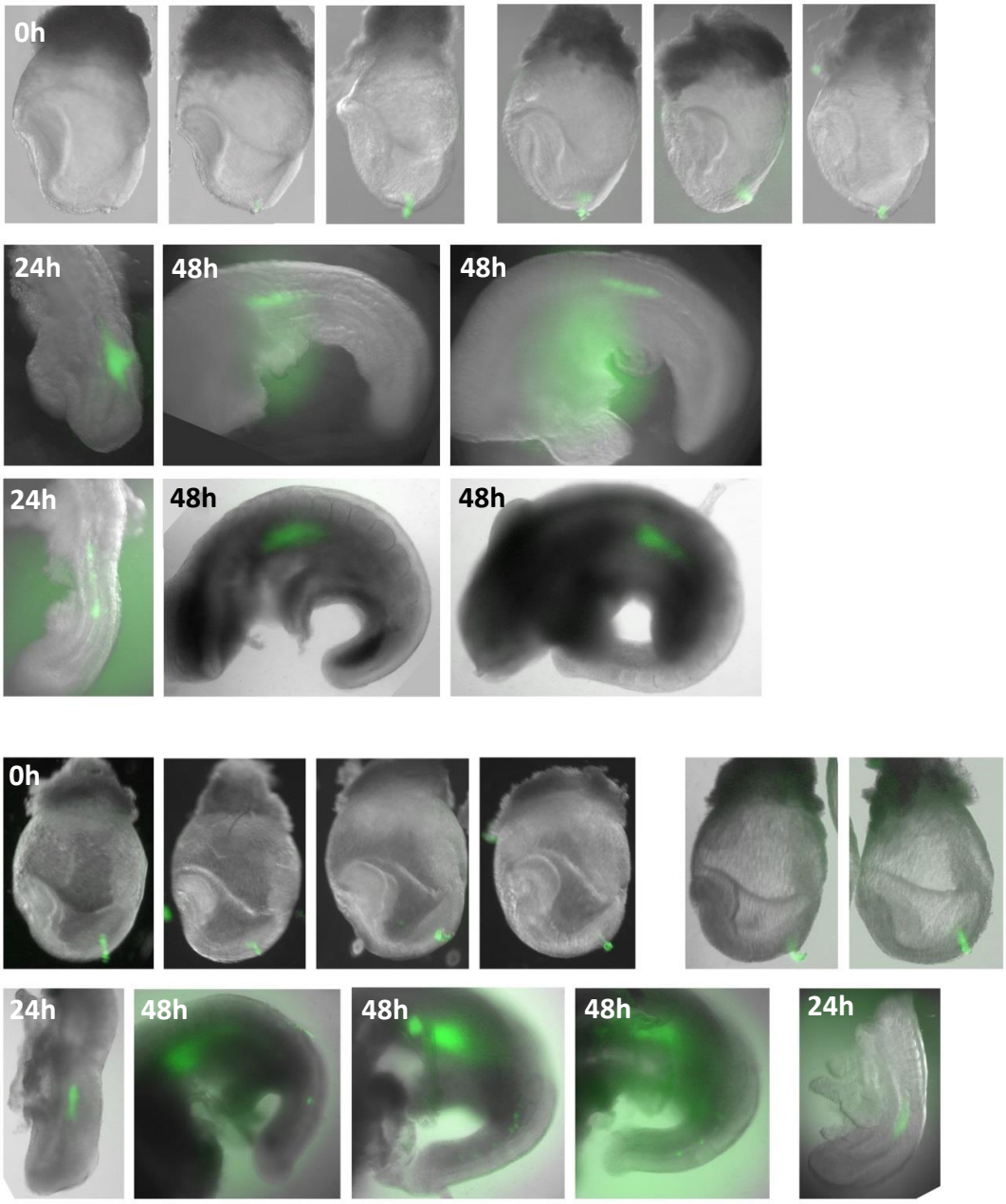

CNH cells from E13.5 AGFP embryos were grafted to the NSB of E8.5 (2-5 somite stage) wild type embryos. In total, 13 embryos recieved a graft and were cultured for 24-48h. 11 representative embryos are shown. Note: since two embryos were normally cultured together, the 0h culture images do not correspond to those after culture.

Sup Figure 2.3: Sections from one E8.5 embryo cultured for 24h after receiving a graft from E13.5 CNH.

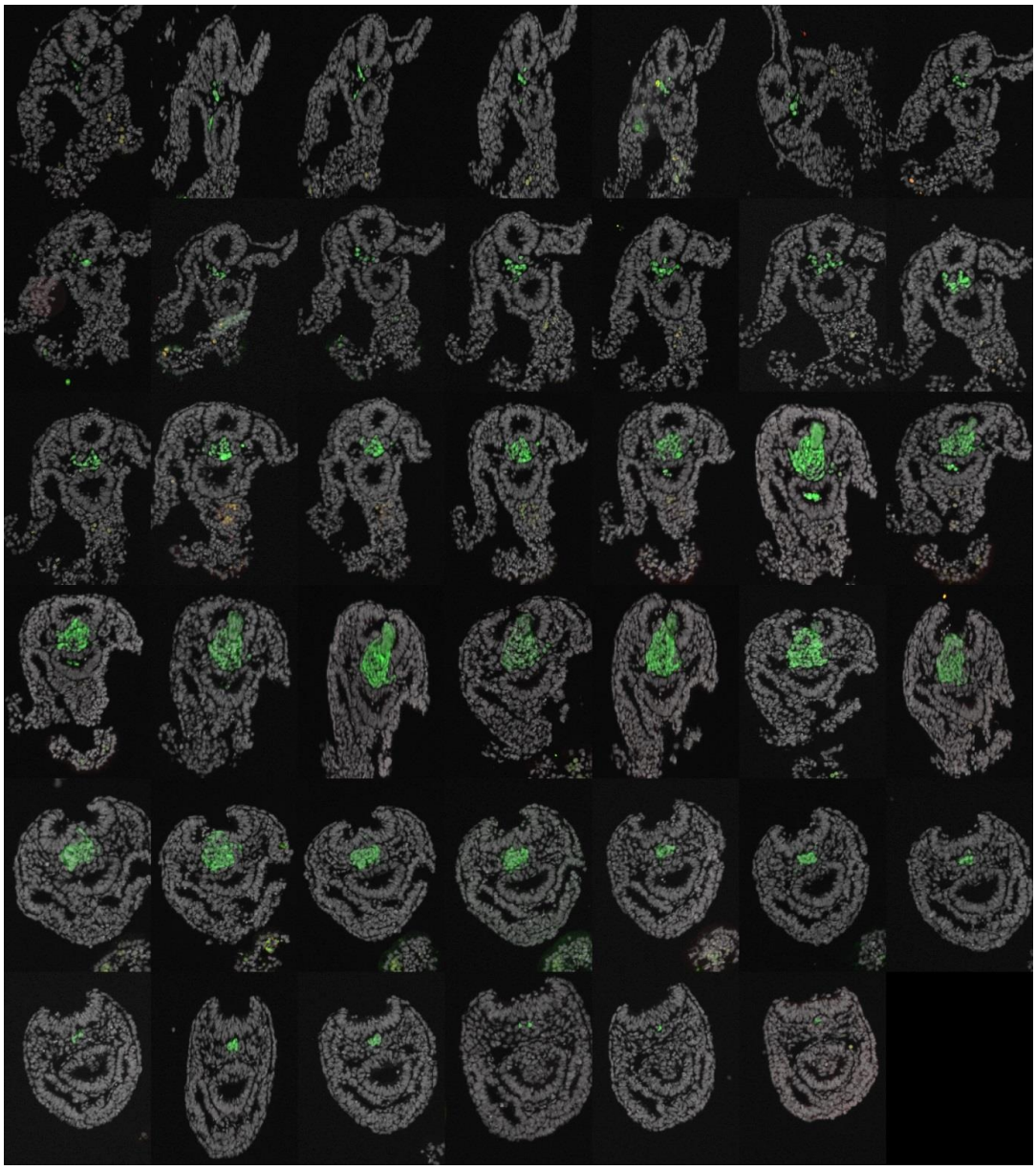

Sup Figure 2.4: Sections from one E8.5 embryo cultured for 48h after receiving a graft from E13.5 CNH.

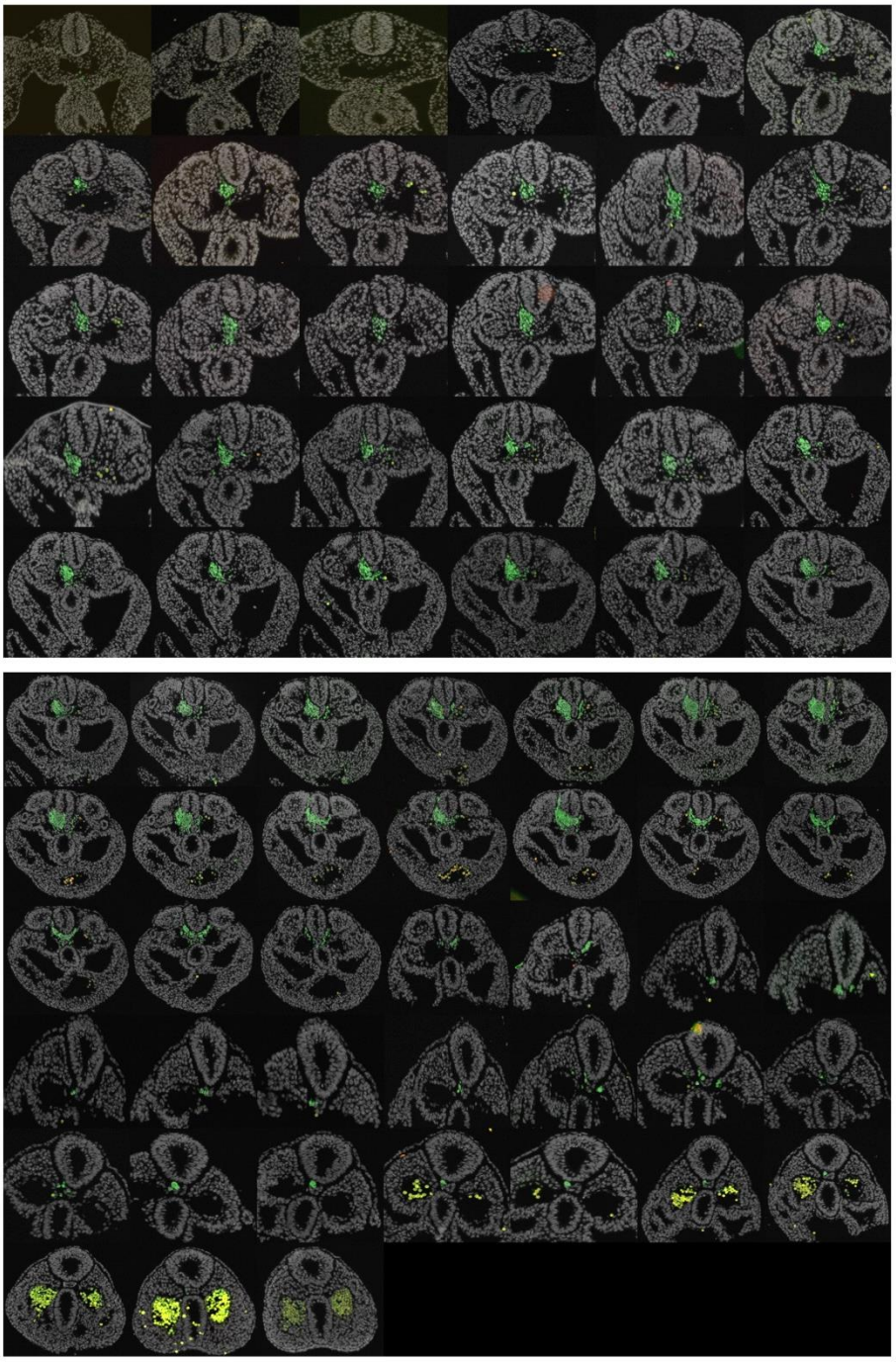

Chapter 3

Sup Figure 3.1: AGFP L1-3 to E8.5 PS1-2

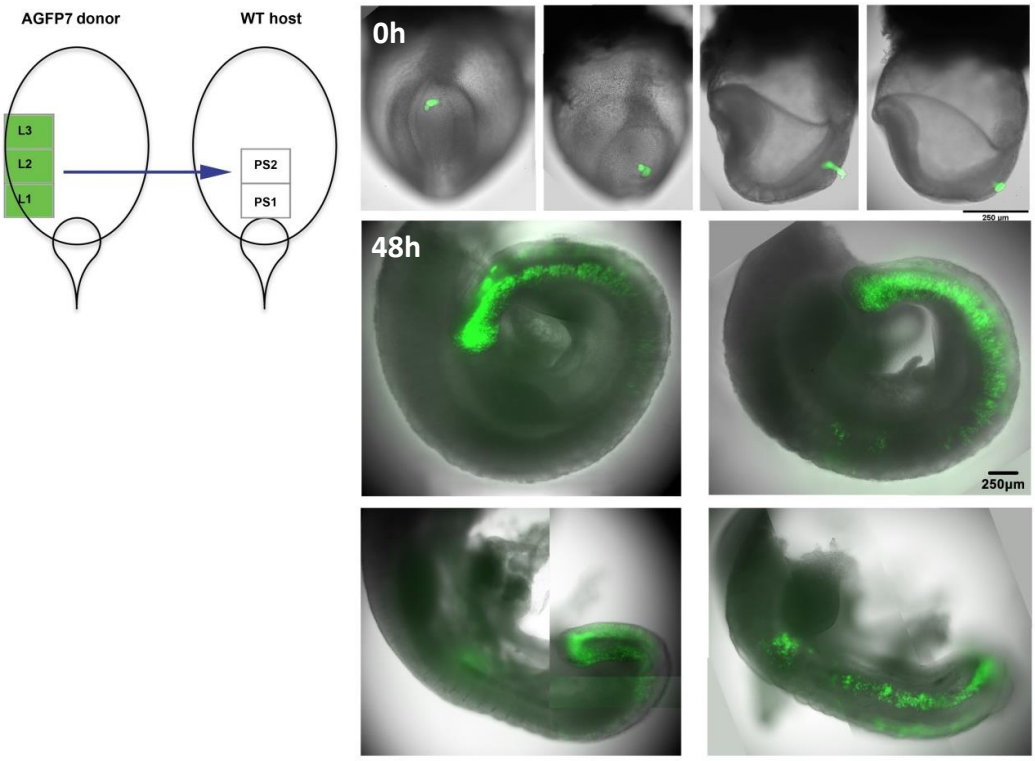

L1-3 cells from E8.5 AGFP embryos were grafted to the PS1-2 of E8.5 (2-5 somite stage) wild type embryos. In total, 4 embryos recieved a graft and were cultured for 48h. Note: since two embryos were normally cultured together, the 0h culture images do not correspond to those after culture.

Sup Figure 3.2: β-catCKO L1-3 to E8.5 PS1-2

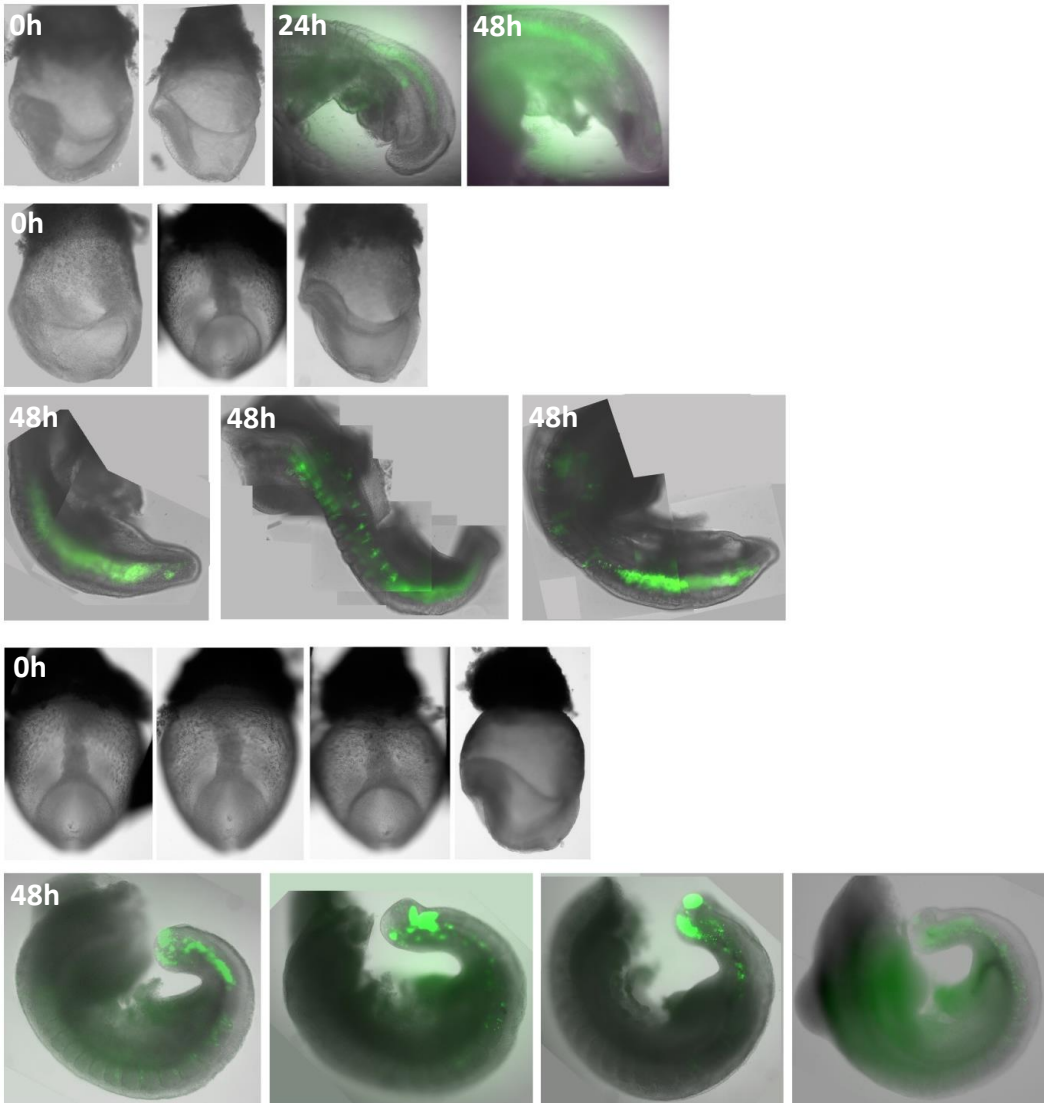

L1-3 cells from E8.5 β-catCKO embryos were grafted to the PS1-2 of E8.5 (2-5 somite stage) wild type embryos. In total, 11 embryos recieved a graft and were cultured for 24-48h. 9 representatives are shown. Note: since two embryos were normally cultured together, the 0h culture images do not correspond to those after culture.

Sup Figure 3.3: Sections from one graft (β-catCKO L1-3 to E8.5 PS1-2)

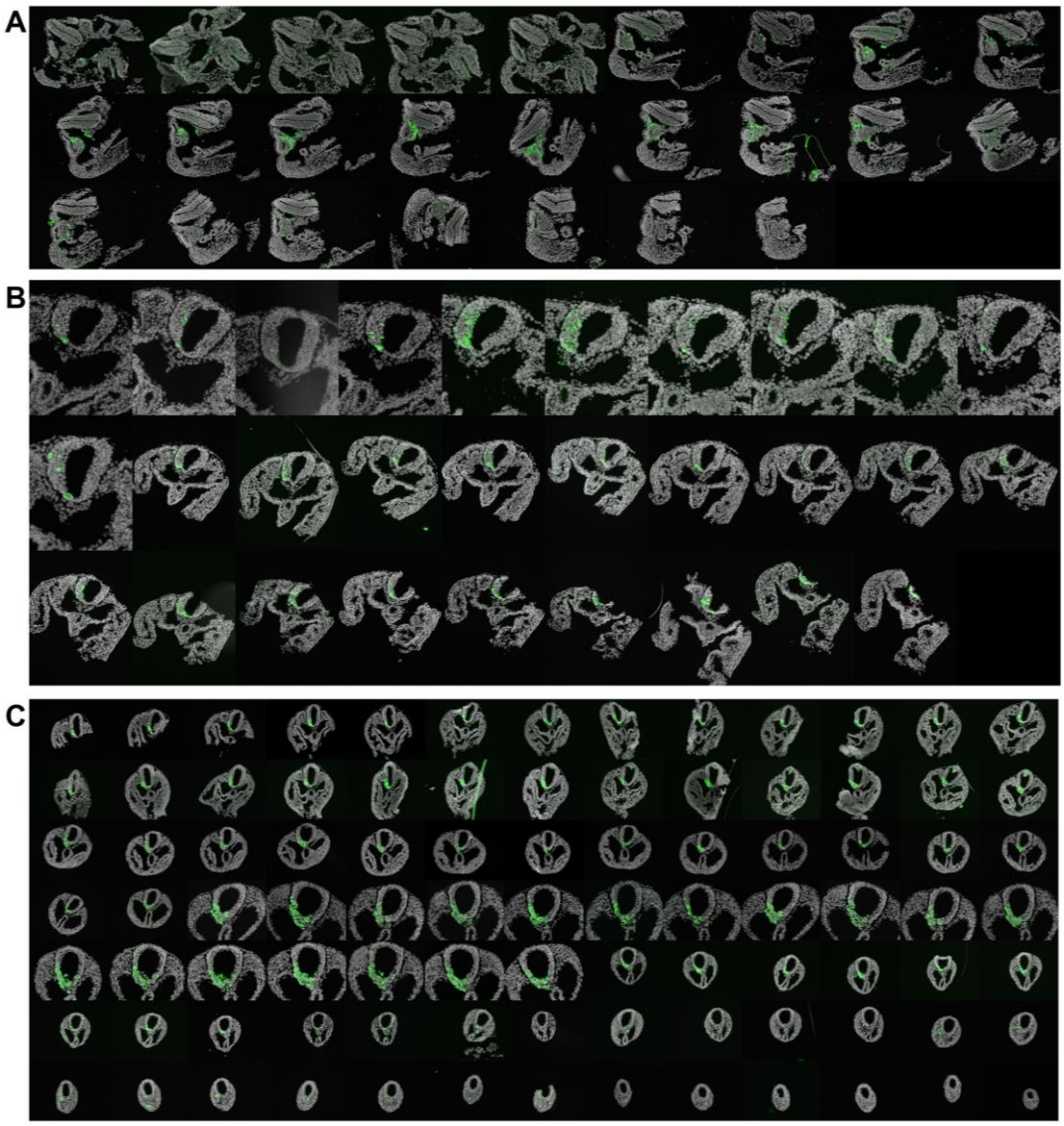

Note: to obtain transverse sections, the embryo was cut into three pieces (A-C). Sections between the adjacent pieces were either destroyed or not intact. This could be the reason that neural and mesoderm contribution does not appear in the same section in this sample. It is also worth noting that some sections were imaged using a higher magnification.

Sup Figure 3.4: L5 to E8.5 PS1-2

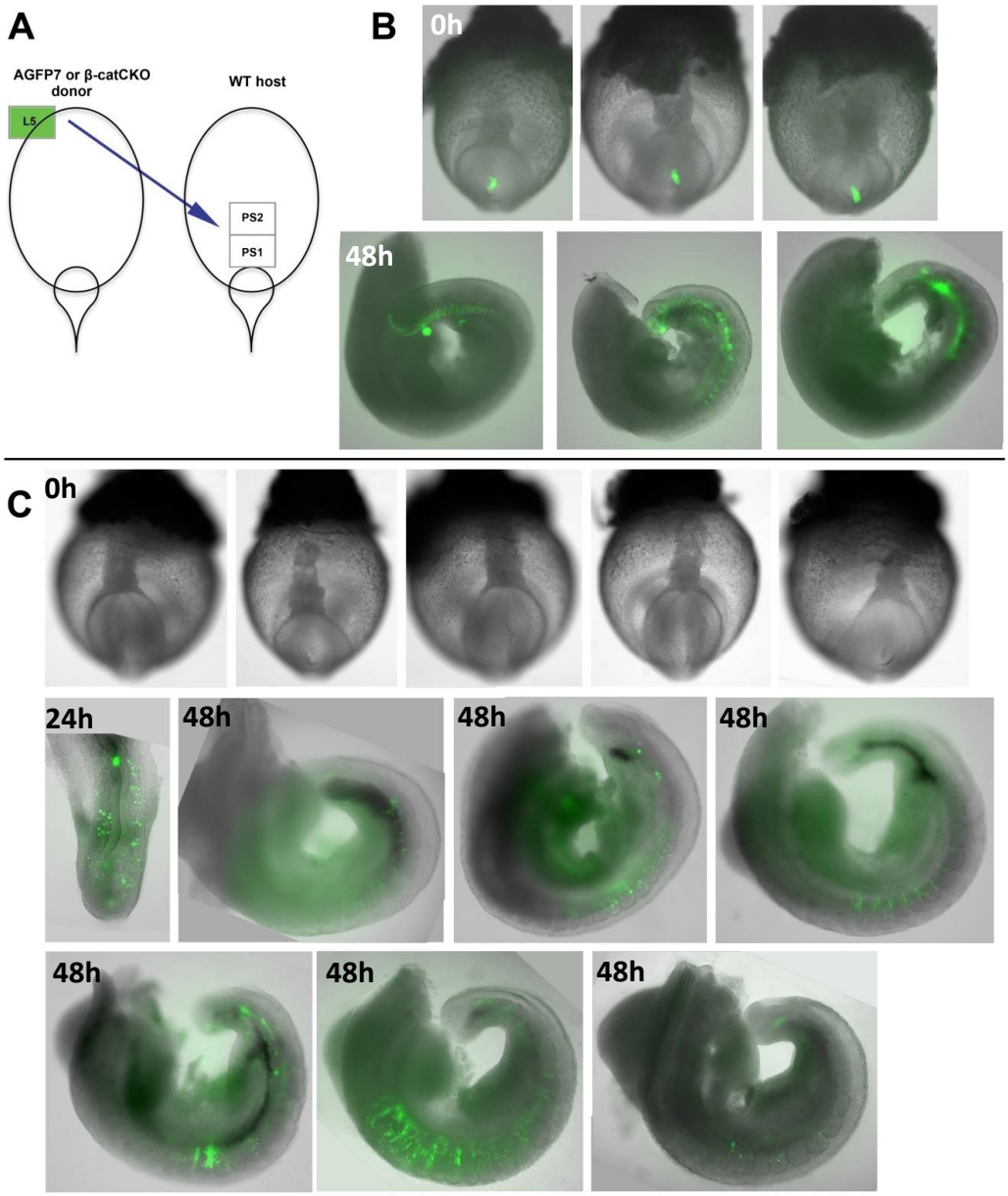

(A) Schematic showing the grafting procedure. (B) L5 cells from AGFP embryos were grafted E8.5 PS1-2. In total, 3 embryos received a graft and were cultured for 48h. (C) L5 cells from β-catCKO embryos were grafted to E8.5 PS1-2. In total, 8 embryos received a graft and were cultured for 24-48h. 7 representatives are shown. Note: since two embryos were normally cultured together, the 0h culture images do not correspond to those after culture.

Chapter 4

Sup Figure 4.1: EpiSCs to the middle of anterior epiblast (MA) after 24h culture

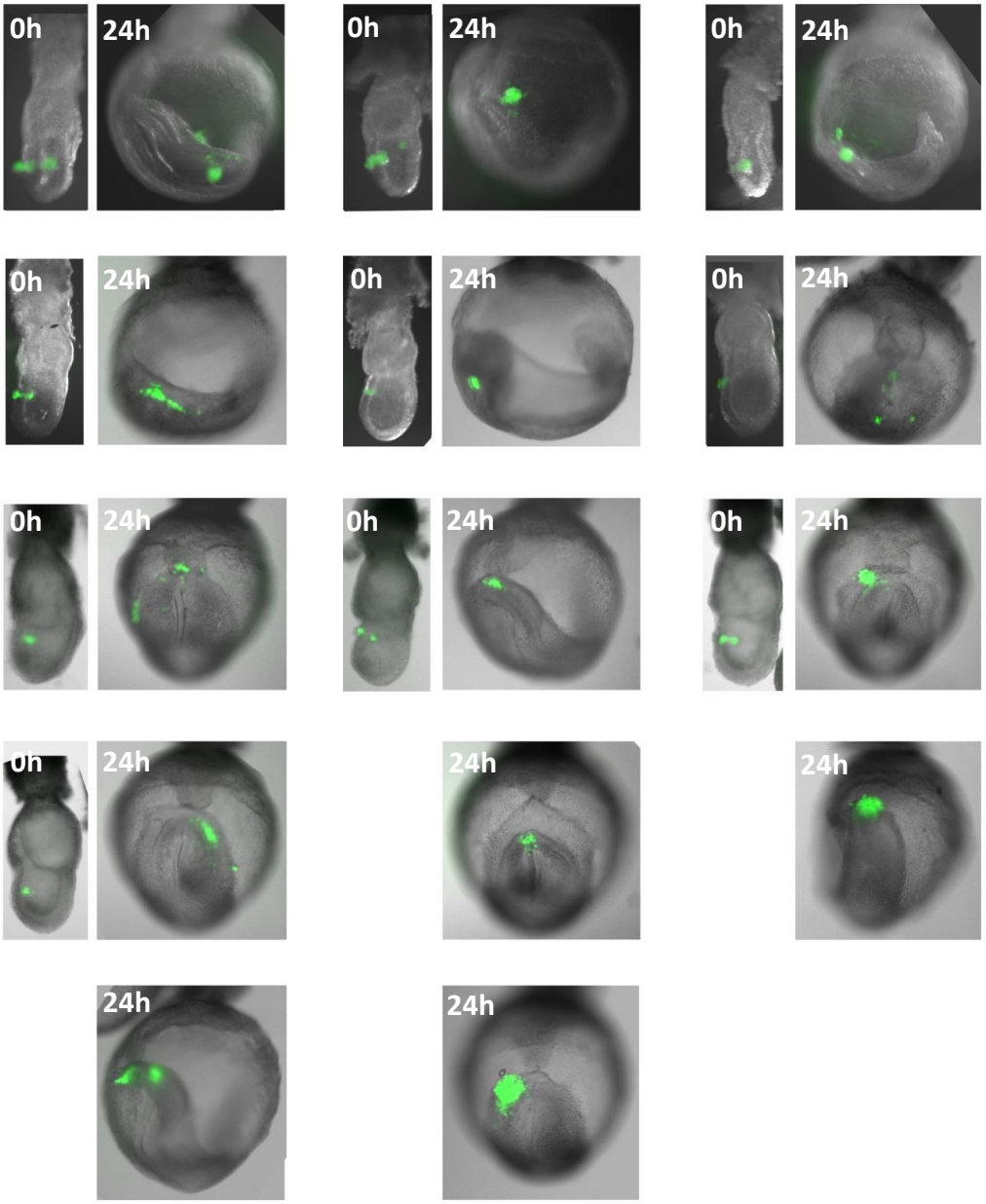

EpiSCs were grafted to the MA site of E7.5 embryos, which were then cultured for 24h. The corresponding 0h images are shown on the left side of 24h cultured embryos. However, in some embryos the 0h images were lost.

Sup Figure 4.2: EpiSCs to the distal region of E7.5 embryos after 24h culture

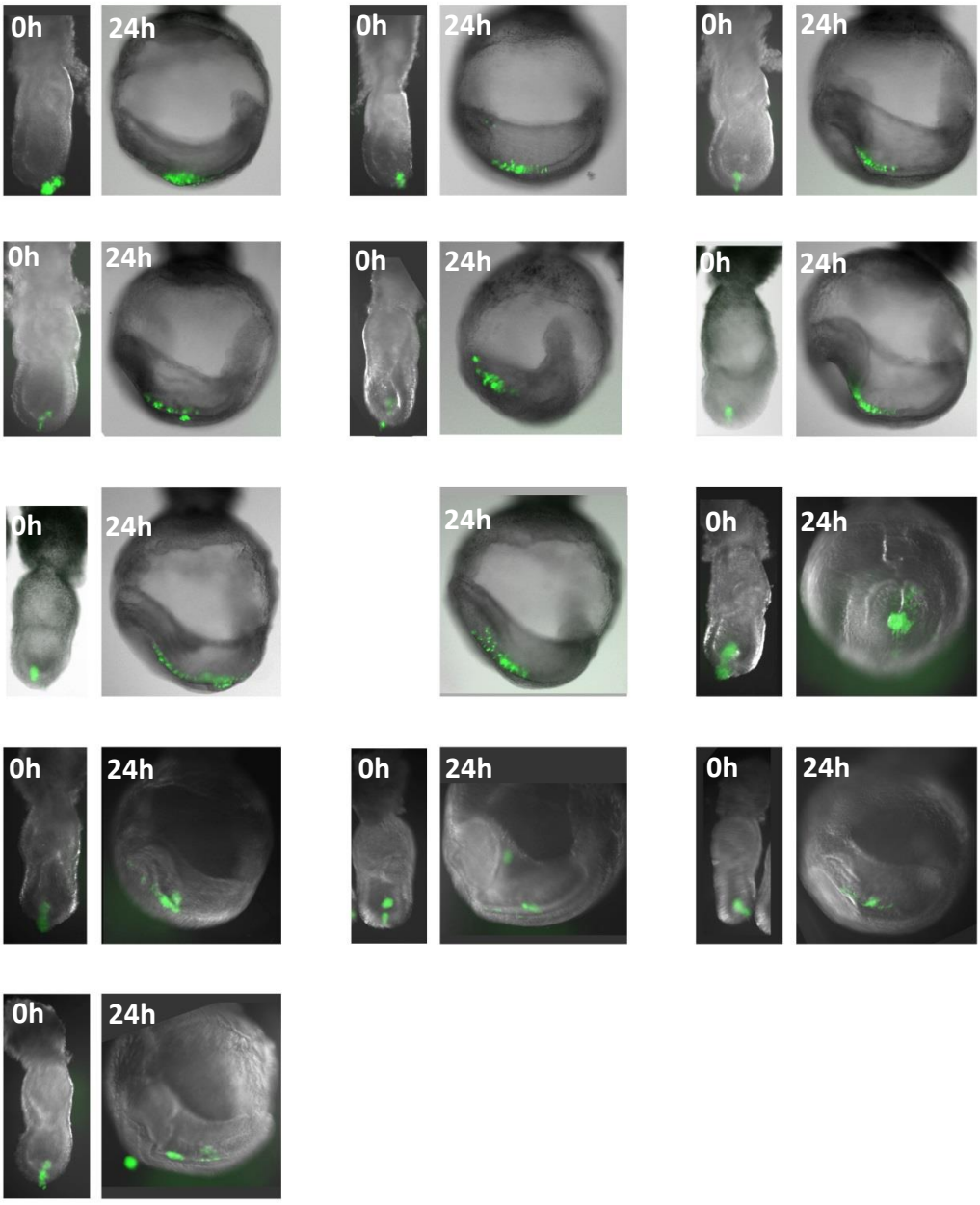

EpiSCs were grafted to the distal region of E7.5 embryos, which were then cultured for 24h. The corresponding 0h images are shown on the left side of 24h cultured embryos. However, 0h image of one embryo was lost.

Sup Figure 4.3: EpiSCs to the distal region of E7.5 embryos after 48h

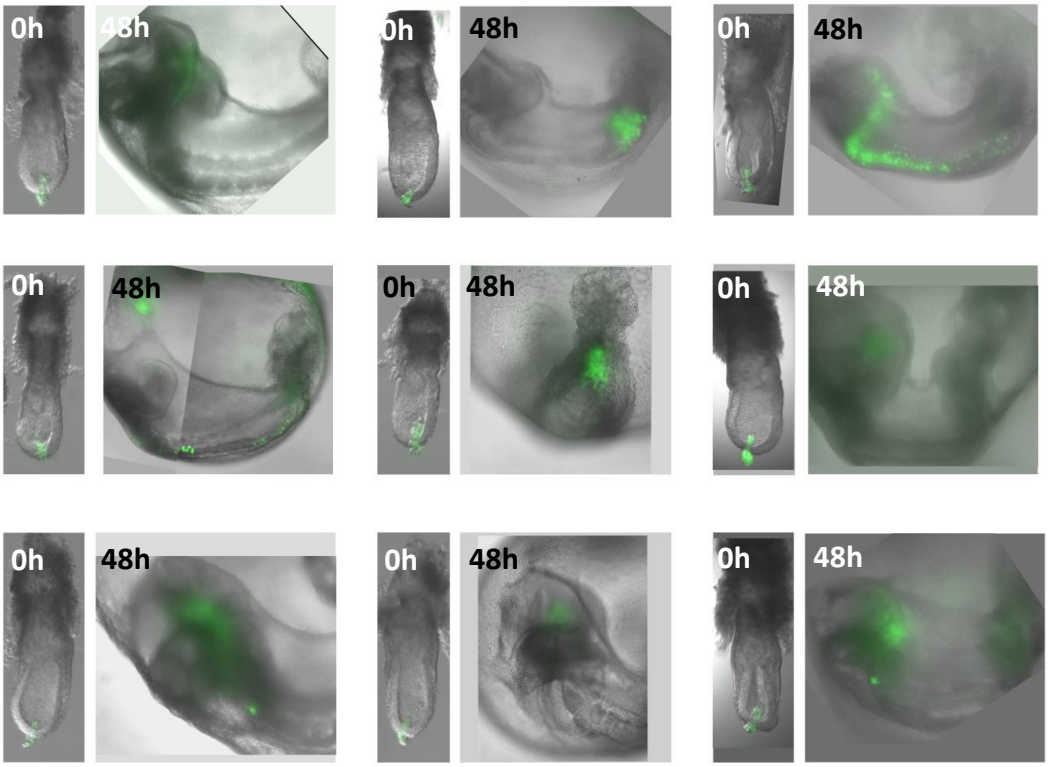

EpiSCs were grafted to the distal region of E7.5 embryos, which were then cultured for 48h. The corresponding 0h images were shown on the left side of 48h cultured embryos.

Sup Figure 4.4: EpiSCs to the middle of the primitive streak (MP) or proximal posterior (PP) of E7.5 embryos after 24h culture

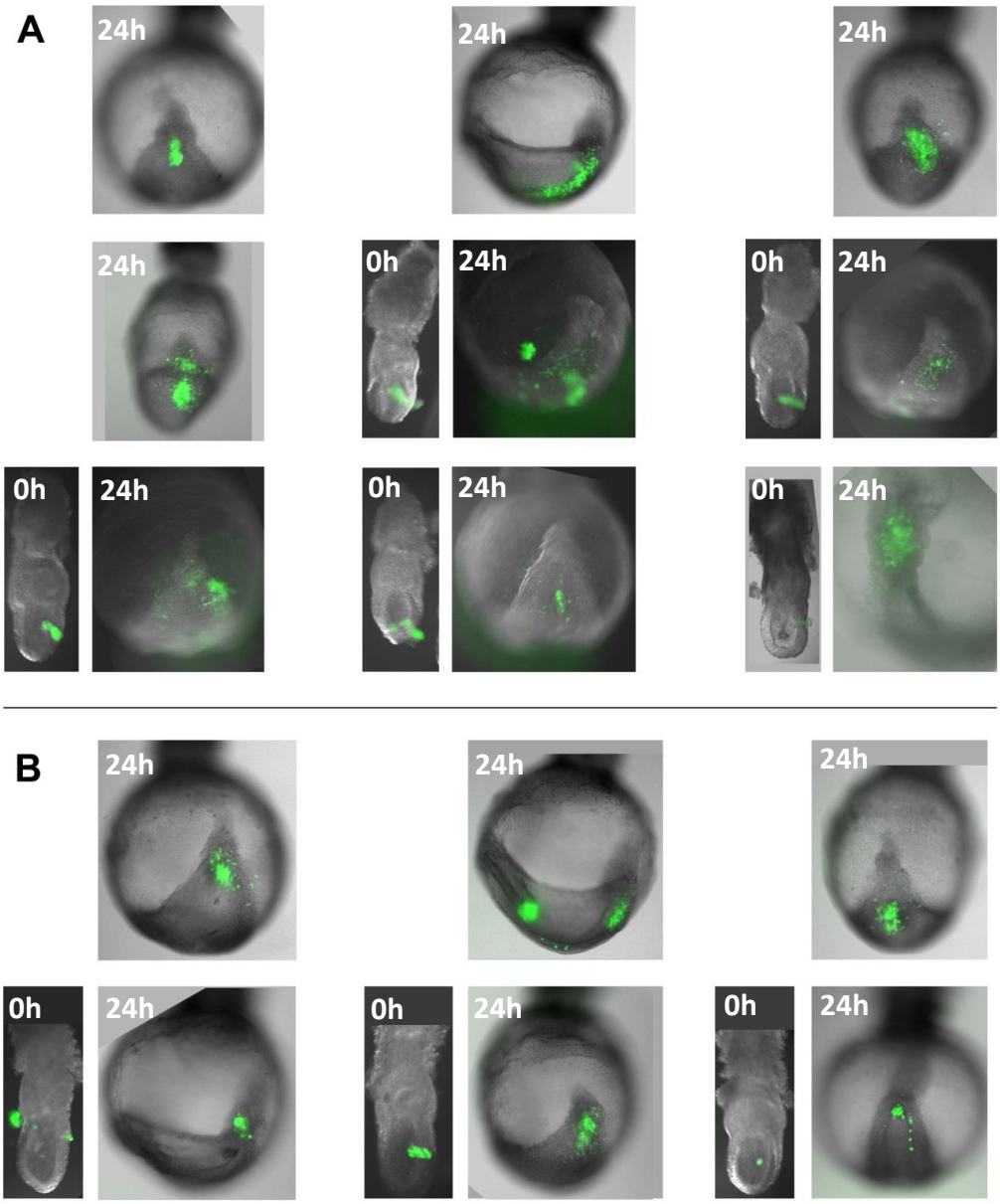

EpiSCs were grafted to the MP (A) or PP (B) site of E7.5 embryos, which were then cultured for 24h. The corresponding 0h images are shown on the left side of 24h cultured embryos. However, 0h images were lost in some embryos.

Sup Figure 4.5: EpiSCs to the proximal posterior (PP) of early streak stage embryos after 48h culture

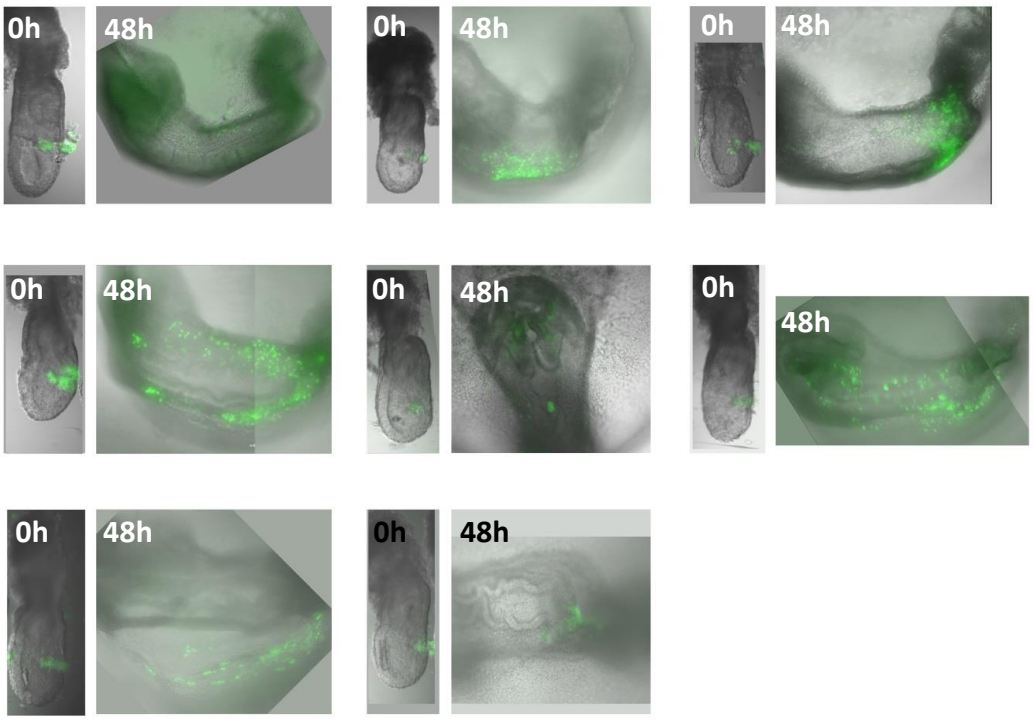

EpiSCs were grafted to the PP site of early streak stage embryos, which were then cultured for 48h. The corresponding 0h images are shown on the left side of 48h cultured embryos.

Sup Figure 4.6: ESCs (AGFP7) to the distal (D) or the middle of the primitive streak (MP) of E7.5 embryos after 24h culture

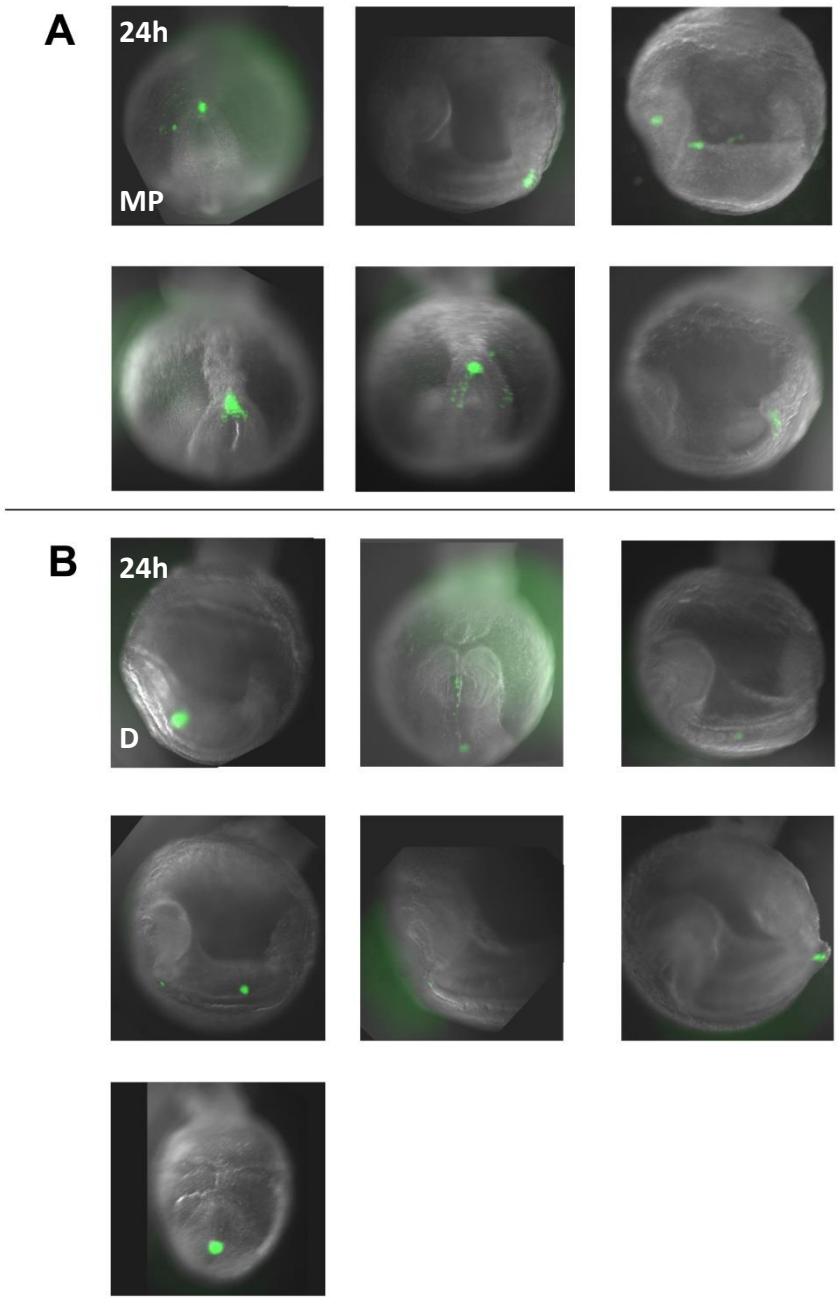

(A) ESCs (AGFP7) were grafted to the MP site of E7.5 embryos. In total, 6 embryos recieved a graft and were cultured for 24h.

(B) ESCs (AGFP7) were grafted to the distal region (D) of E7.5 embryos. In total, 7 embryos recieved a graft and were cultured for 24h.

Sup Figure 4.7: ESCs (Nanog:GFP) to E7.5 embryos after 24h culture

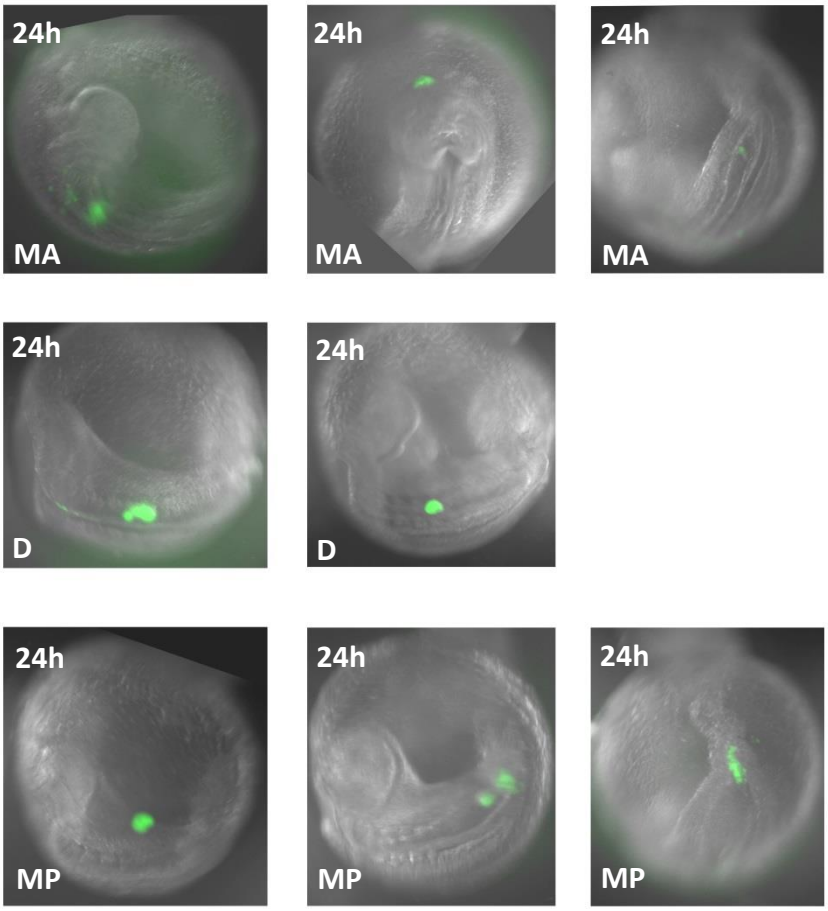

ESCs (Nanog:GFP) were grafted to three different sites of E7.5 embryos. In total, 8 embryos recieved a graft and were cultured for 24h. MA: middle of the anterior epiblast; D distal of the embryos; MP: middle of the primitive streak.

Sup Figure 4.8: EpiSCs (C2) to E8.5 NSB

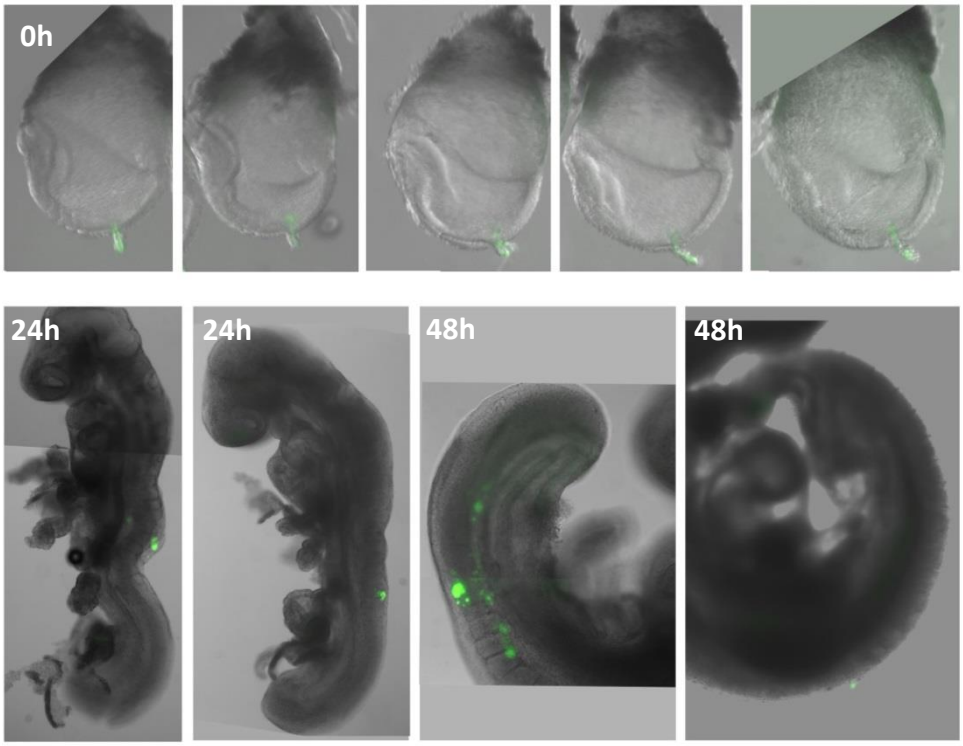

EpiSCs (C2) were grafted to the NSB of E8.5 (2-5 somite stage) wild type embryos. In total, 5 embryos received a graft and were cultured for 24-48h. GFP^+ cells were detected in four embryos after culture. Note: since two embryos were normally cultured together, the 0h culture images do not correspond to those after culture.

Sup Figure 4.9: EpiSCs (0r4) to E8.5 NSB

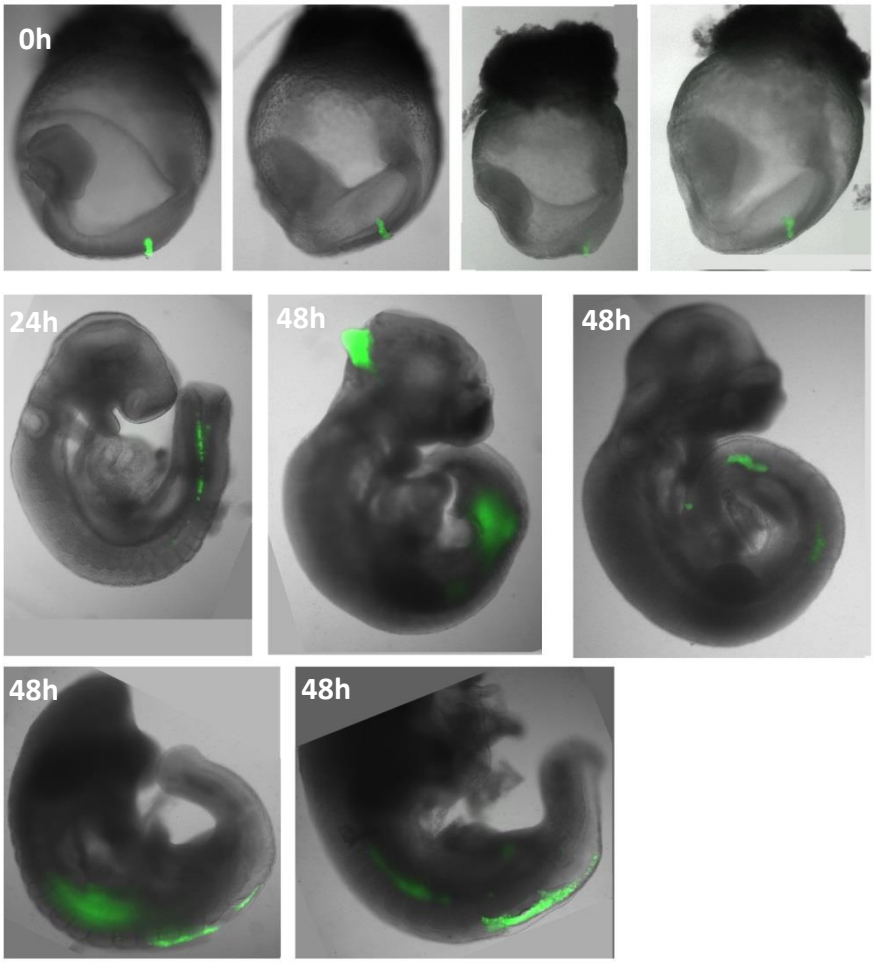

EpiSCs (0r4) were grafted to the NSB of E8.5 (2-5 somite stage) wild type embryos. In total, 5 embryos received a graft and were cultured for 24-48h. In one embryo 0h images were lost. Note: since two embryos were normally cultured together, the 0h culture images do not correspond to those after culture.

Sup Figure 4.10: 48h CHI EpiSCs (C2) to E7.5 embryos

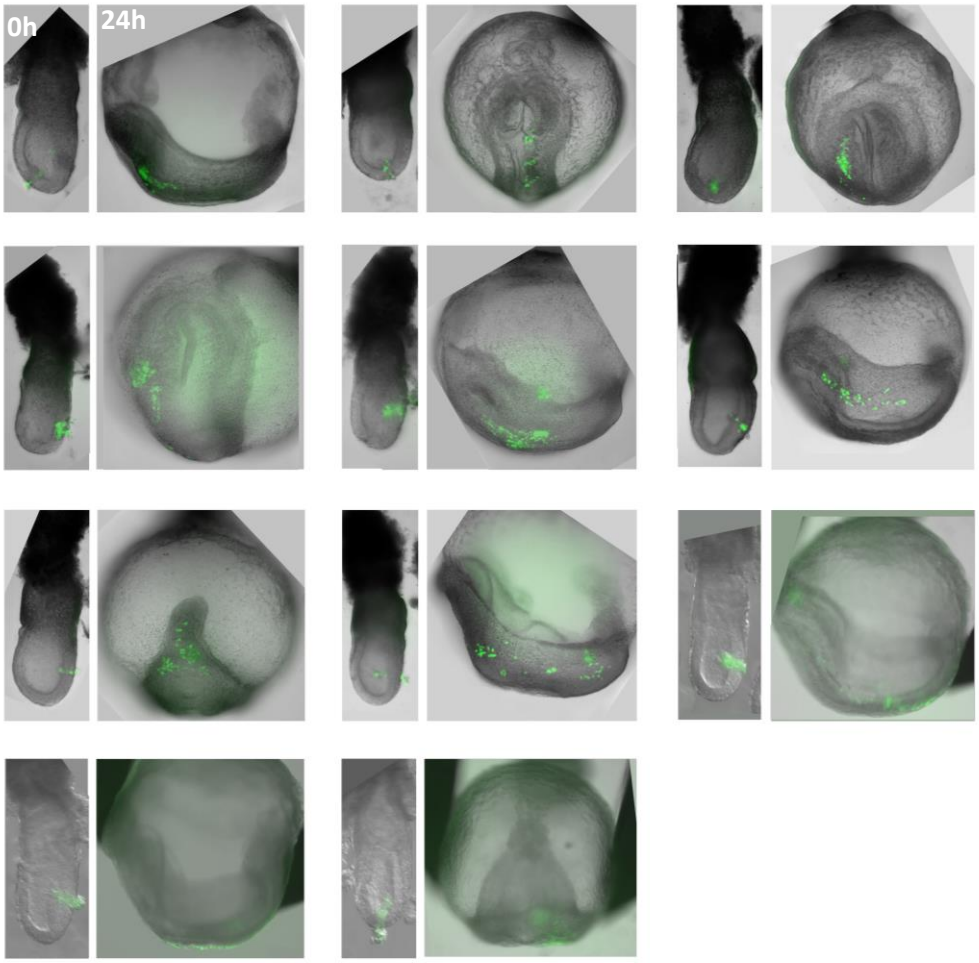

In total, 11 embryos received a graft of 48h CHI EpiSCs (C2) and were cultured for 24h. The graft sites are shown in the corresponding 0h images on the left.

Sup Figure 4.11: 48h CHI EpiSCs (C2) to E8.5 NSB

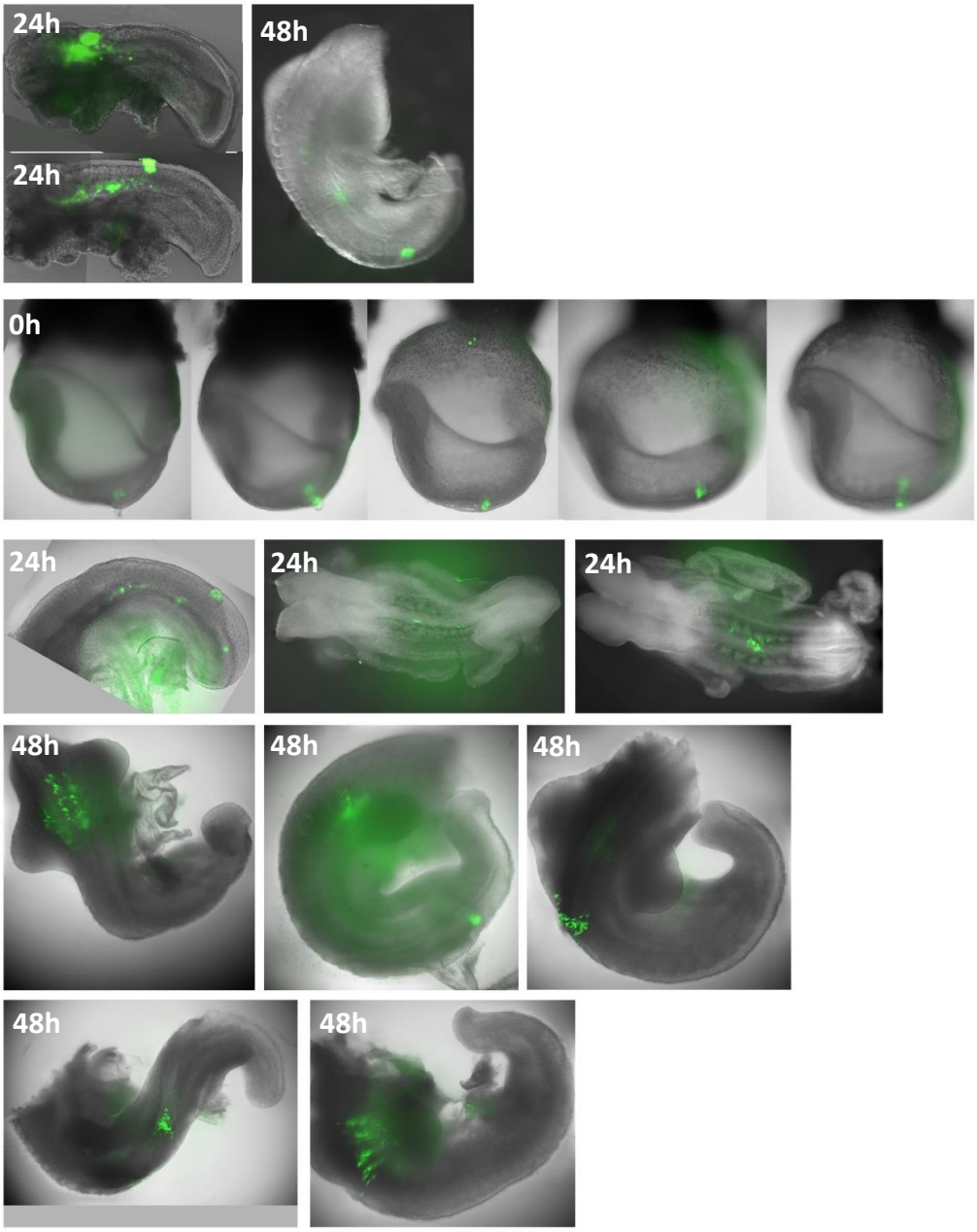

48h CHI EpiSCs (C2) were grafted to the NSB of E8.5 (2-5 somite stage) wild type embryos. In total, 11 embryos received a graft. 5 embryos were cultured for 24h, the other 6 for 48h. 5 representatives are shown after grafting. Note: since two embryos were normally cultured together, the 0h culture images do not correspond to those after culture.

Sup Figure 4.12: In vitro derived NM progenitors (low density) to E7.5 embryos

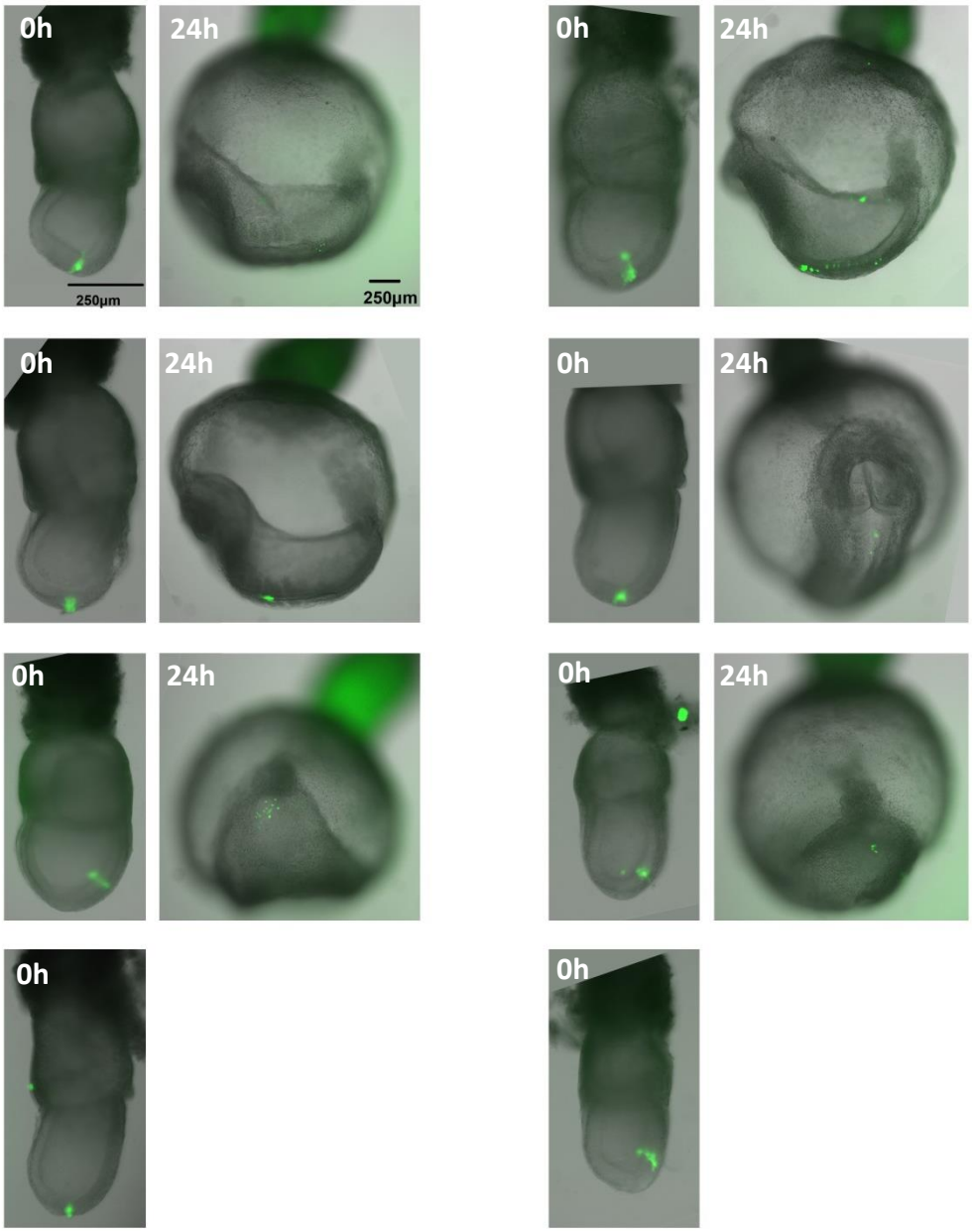

In vitro derived NM progenitors were cultured in a low density and then grafted to E7.5 embryos. In total, 8 embryos received a graft. After 24h culture, only 6 embryos contained a few GFP^+ cells. Their corresponding 0h images were shown on the left. The other two embryos without GPF^+ cells after culture were not shown.

Sup Figure 4.13: In vitro derived NM progenitors (high density) to E7.5 embryos

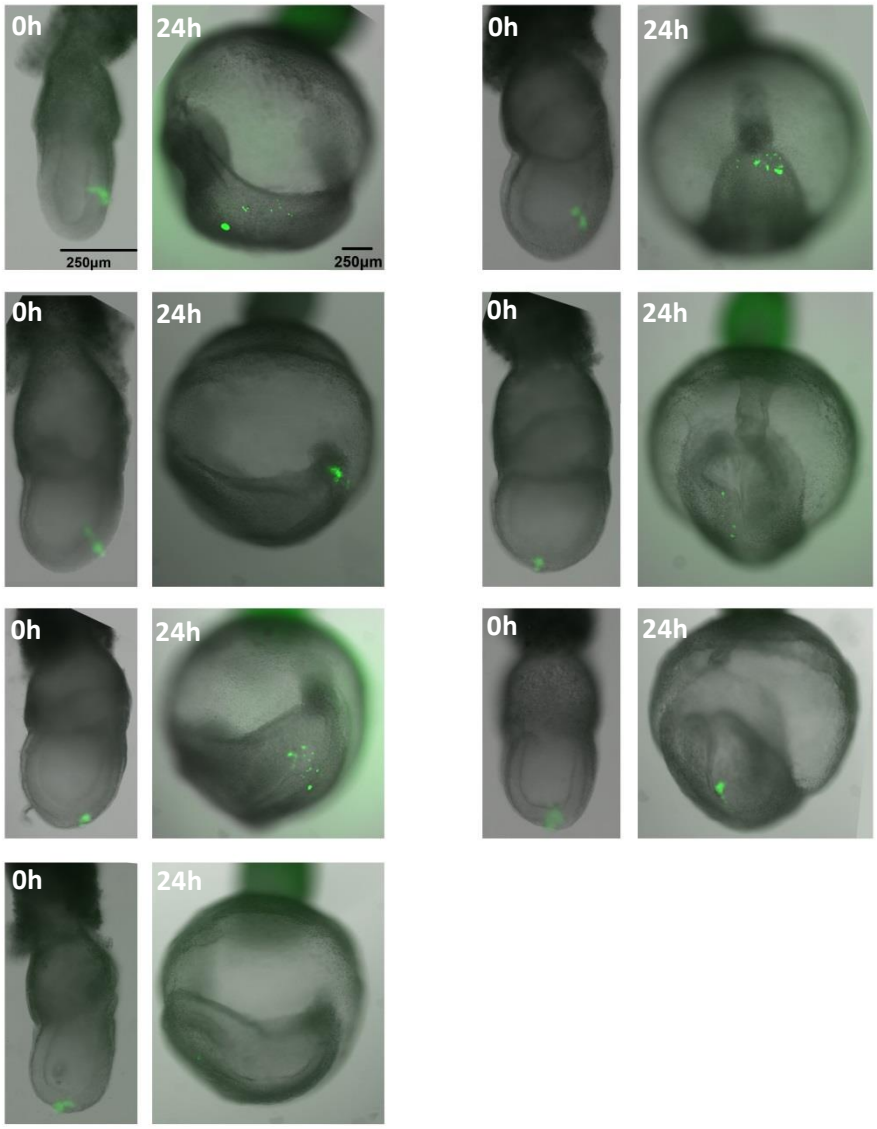

In vitro derived NM progenitors were cultured in a high density and then grafted to E7.5 embryos. In total, 7 embryos received a graft were cultured for 24h. The corresponding 0h images showing the graft sites were displayed on the left.

II. Publication

References

Abdelkhalek, H.B., Beckers, A., Schuster-Gossler, K., Pavlova, M.N., Burkhardt, H., Lickert, H., Rossant, J., Reinhardt, R., Schalkwyk, L.C., Muller, I.*, et al.* (2004). The mouse homeobox gene Not is required for caudal notochord development and affected by the truncate mutation. Genes & development *18*, 1725-1736.

Ang, S.L., and Rossant, J. (1994). HNF-3 beta is essential for node and notochord formation in mouse development. Cell *78*, 561-574.

Arkell, R., and Beddington, R.S. (1997). BMP-7 influences pattern and growth of the developing hindbrain of mouse embryos. Development *124*, 1-12.

Arnold, S.J., and Robertson, E.J. (2009). Making a commitment: cell lineage allocation and axis patterning in the early mouse embryo. Nature reviews Molecular cell biology *10*, 91-103.

Aulehla, A., Wehrle, C., Brand-Saberi, B., Kemler, R., Gossler, A., Kanzler, B., and Herrmann, B.G. (2003). Wnt3a plays a major role in the segmentation clock controlling somitogenesis. Developmental cell *4*, 395-406.

Aulehla, A., Wiegraebe, W., Baubet, V., Wahl, M.B., Deng, C., Taketo, M., Lewandoski, M., and Pourquie, O. (2008). A beta-catenin gradient links the clock and wavefront systems in mouse embryo segmentation. Nature cell biology *10*, 186-193.

Avilion, A.A., Nicolis, S.K., Pevny, L.H., Perez, L., Vivian, N., and Lovell-Badge, R. (2003). Multipotent cell lineages in early mouse development depend on SOX2 function. Genes & development *17*, 126-140.

Baldwin, H.S., Shen, H.M., Yan, H.C., DeLisser, H.M., Chung, A., Mickanin, C., Trask, T., Kirschbaum, N.E., Newman, P.J., Albelda, S.M.*, et al.* (1994). Platelet endothelial cell adhesion molecule-1 (PECAM-1/CD31): alternatively spliced, functionally distinct isoforms expressed during mammalian cardiovascular development. Development *120*, 2539-2553.

Barnes, J.D., Crosby, J.L., Jones, C.M., Wright, C.V., and Hogan, B.L. (1994). Embryonic expression of Lim-1, the mouse homolog of Xenopus Xlim-1, suggests a role in lateral mesoderm differentiation and neurogenesis. Developmental biology *161*, 168-178.

Beck, F., Erler, T., Russell, A., and James, R. (1995). Expression of Cdx-2 in the mouse embryo and placenta: possible role in patterning of the extra-embryonic membranes. Developmental dynamics : an official publication of the American Association of Anatomists *204*, 219-227.

Beddington, R.S. (1982). An autoradiographic analysis of tissue potency in different regions of the embryonic ectoderm during gastrulation in the mouse. Journal of embryology and experimental morphology *69*, 265-285.

Beddington, R.S. (1983). Histogenetic and neoplastic potential of different regions of the mouse embryonic egg cylinder. Journal of embryology and experimental morphology *75*, 189-204.

Beddington, R.S. (1994). Induction of a second neural axis by the mouse node. Development *120*, 613-620.

Beddington, R.S., Rashbass, P., and Wilson, V. (1992). Brachyury--a gene affecting mouse gastrulation and early organogenesis. Dev Suppl, 157-165.

Beddington, S.P. (1981). An autoradiographic analysis of the potency of embryonic ectoderm in the 8th day postimplantation mouse embryo. Journal of embryology and experimental morphology *64*, 87-104.

Bellomo, D., Lander, A., Harragan, I., and Brown, N.A. (1996). Cell proliferation in mammalian gastrulation: the ventral node and notochord are relatively quiescent. Developmental dynamics : an official publication of the American Association of Anatomists *205*, 471-485.

Bernemann, C., Greber, B., Ko, K., Sterneckert, J., Han, D.W., Arauzo-Bravo, M.J., and Scholer, H.R. (2011). Distinct developmental ground states of epiblast stem cell lines determine different pluripotency features. Stem cells *29*, 1496-1503.

Bonnerot, C., and Nicolas, J.F. (1993). Clonal analysis in the intact mouse embryo by intragenic homologous recombination. Comptes rendus de l'Academie des sciences Serie III, Sciences de la vie *316*, 1207-1217.

Bottcher, R.T., and Niehrs, C. (2005). Fibroblast growth factor signaling during early vertebrate development. Endocrine reviews *26*, 63-77.

Bouillet, P., Oulad-Abdelghani, M., Ward, S.J., Bronner, S., Chambon, P., and Dolle, P. (1996). A new mouse member of the Wnt gene family, mWnt-8, is expressed during early embryogenesis and is ectopically induced by retinoic acid. Mechanisms of development *58*, 141-152.

Boulet, A.M., and Capecchi, M.R. (2012). Signaling by FGF4 and FGF8 is required for axial elongation of the mouse embryo. Developmental biology *371*, 235-245.

Bradley, A., Evans, M., Kaufman, M.H., and Robertson, E. (1984). Formation of germ-line chimaeras from embryo-derived teratocarcinoma cell lines. Nature *309*, 255-256.

Brault, V., Moore, R., Kutsch, S., Ishibashi, M., Rowitch, D.H., McMahon, A.P., Sommer, L., Boussadia, O., and Kemler, R. (2001). Inactivation of the beta-catenin gene by Wnt1-Cre-mediated deletion results in dramatic brain malformation and failure of craniofacial development. Development *128*, 1253-1264.

Brennan, J., Norris, D.P., and Robertson, E.J. (2002). Nodal activity in the node governs left-right asymmetry. Genes & development *16*, 2339-2344.

Brons, I.G., Smithers, L.E., Trotter, M.W., Rugg-Gunn, P., Sun, B., Chuva de Sousa Lopes, S.M., Howlett, S.K., Clarkson, A., Ahrlund-Richter, L., Pedersen, R.A*., et al.* (2007). Derivation of pluripotent epiblast stem cells from mammalian embryos. Nature *448*, 191-195.

Brook, F.A., and Gardner, R.L. (1997). The origin and efficient derivation of embryonic stem cells in the mouse. Proceedings of the National Academy of Sciences of the United States of America *94*, 5709-5712.

Brown, J.M., and Storey, K.G. (2000). A region of the vertebrate neural plate in which neighbouring cells can adopt neural or epidermal fates. Current biology : CB *10*, 869-872.

Cambray, N., and Wilson, V. (2002). Axial progenitors with extensive potency are localised to the mouse chordoneural hinge. Development *129*, 4855-4866.

Cambray, N., and Wilson, V. (2007). Two distinct sources for a population of maturing axial progenitors. Development *134*, 2829-2840.

Catala, M., Teillet, M.A., De Robertis, E.M., and Le Douarin, M.L. (1996). A spinal cord fate map in the avian embryo: while regressing, Hensen's node lays down the notochord and floor plate thus joining the spinal cord lateral walls. Development *122*, 2599-2610.

Chambers, I., Silva, J., Colby, D., Nichols, J., Nijmeijer, B., Robertson, M., Vrana, J., Jones, K., Grotewold, L., and Smith, A. (2007). Nanog safeguards pluripotency and mediates germline development. Nature *450*, 1230-1234.

Chapman, D.L., Agulnik, I., Hancock, S., Silver, L.M., and Papaioannou, V.E. (1996). Tbx6, a mouse T-Box gene implicated in paraxial mesoderm formation at gastrulation. Developmental biology *180*, 534-542.

Chapman, D.L., and Papaioannou, V.E. (1998). Three neural tubes in mouse embryos with mutations in the T-box gene Tbx6. Nature *391*, 695-697.

Charrier, J.B., Teillet, M.A., Lapointe, F., and Le Douarin, N.M. (1999). Defining subregions of Hensen's node essential for caudalward movement, midline development and cell survival. Development *126*, 4771-4783.

Chawengsaksophak, K., de Graaff, W., Rossant, J., Deschamps, J., and Beck, F. (2004). Cdx2 is essential for axial elongation in mouse development. Proceedings of the National Academy of Sciences of the United States of America *101*, 7641-7645.

Chenoweth, J.G., McKay, R.D., and Tesar, P.J. (2010). Epiblast stem cells contribute new insight into pluripotency and gastrulation. Development, growth & differentiation *52*, 293-301.

Chia, N.Y., Chan, Y.S., Feng, B., Lu, X., Orlov, Y.L., Moreau, D., Kumar, P., Yang, L., Jiang, J., Lau, M.S., *et al.* (2010). A genome-wide RNAi screen reveals determinants of human embryonic stem cell identity. Nature *468*, 316-320.

Christ, B., Huang, R., and Scaal, M. (2007). Amniote somite derivatives. Developmental dynamics : an official publication of the American Association of Anatomists *236*, 2382-2396.

Ciruna, B., and Rossant, J. (2001). FGF signaling regulates mesoderm cell fate specification and morphogenetic movement at the primitive streak. Developmental cell *1*, 37-49.

Ciruna, B.G., Schwartz, L., Harpal, K., Yamaguchi, T.P., and Rossant, J. (1997). Chimeric analysis of fibroblast growth factor receptor-1 (Fgfr1) function: a role for FGFR1 in morphogenetic movement through the primitive streak. Development *124*, 2829-2841.

Clevers, H. (2006). Wnt/beta-catenin signaling in development and disease. Cell *127*, 469-480.

Collu, G.M., Hidalgo-Sastre, A., and Brennan, K. (2014). Wnt-Notch signalling crosstalk in development and disease. Cellular and molecular life sciences : CMLS *71*, 3553-3567.

Conlon, F.L., and Smith, J.C. (1999). Interference with brachyury function inhibits convergent extension, causes apoptosis, and reveals separate requirements in the FGF and activin signalling pathways. Developmental biology *213*, 85-100.

Copp, A.J., Brook, F.A., Estibeiro, J.P., Shum, A.S., and Cockroft, D.L. (1990). The embryonic development of mammalian neural tube defects. Progress in neurobiology *35*, 363-403.

Copp, A.J., and Cockroft, D.L. (1990). Postimplantation mammalian embryos: a practical approach. Practical Approach Series 69.

Cowin, P. (1994). Unraveling the cytoplasmic interactions of the cadherin superfamily. Proceedings of the National Academy of Sciences of the United States of America *91*, 10759-10761.

Crossley, P.H., and Martin, G.R. (1995). The mouse Fgf8 gene encodes a family of polypeptides and is expressed in regions that direct outgrowth and patterning in the developing embryo. Development *121*, 439-451.

Cunningham, T.J., Zhao, X., and Duester, G. (2011). Uncoupling of retinoic acid signaling from tailbud development before termination of body axis extension. Genesis *49*, 776-783.

Damjanov, I., Solter, D., and Skreb, N. (1971). Enzyme histochemistry of experimental embryo-derived teratocarcinomas. Zeitschrift fur Krebsforschung und klinische Onkologie Cancer research and clinical oncology *76*, 249-256.

Danielian, P.S., Muccino, D., Rowitch, D.H., Michael, S.K., and McMahon, A.P. (1998). Modification of gene activity in mouse embryos in utero by a tamoxifen-inducible form of Cre recombinase. Current biology : CB *8*, 1323-1326.

de la Pompa, J.L., Wakeham, A., Correia, K.M., Samper, E., Brown, S., Aguilera, R.J., Nakano, T., Honjo, T., Mak, T.W., Rossant, J., *et al.* (1997). Conservation of the Notch signalling pathway in mammalian neurogenesis. Development *124*, 1139-1148.

Delfino-Machin, M., Lunn, J.S., Breitkreuz, D.N., Akai, J., and Storey, K.G. (2005). Specification and maintenance of the spinal cord stem zone. Development *132*, 4273-4283.

Dequeant, M.L., and Pourquie, O. (2008). Segmental patterning of the vertebrate embryonic axis. Nature reviews Genetics *9*, 370-382.

Dias, M.S., and Schoenwolf, G.C. (1990). Formation of ectopic neurepithelium in chick blastoderms: age-related capacities for induction and self-differentiation following transplantation of quail Hensen's nodes. The Anatomical record *228*, 437-448.

Diez del Corral, R., Olivera-Martinez, I., Goriely, A., Gale, E., Maden, M., and Storey, K. (2003). Opposing FGF and retinoid pathways control ventral neural pattern, neuronal differentiation, and segmentation during body axis extension. Neuron *40*, 65-79.

Diwan, S.B., and Stevens, L.C. (1976). Development of teratomas from the ectoderm of mouse egg cylinders. Journal of the National Cancer Institute *57*, 937-942.

Dolle, P., Dierich, A., LeMeur, M., Schimmang, T., Schuhbaur, B., Chambon, P., and Duboule, D. (1993). Disruption of the Hoxd-13 gene induces localized heterochrony leading to mice with neotenic limbs. Cell *75*, 431-441.

Downs, K.M., and Davies, T. (1993). Staging of gastrulating mouse embryos by morphological landmarks in the dissecting microscope. Development *118*, 1255-1266.

Dufort, D., Schwartz, L., Harpal, K., and Rossant, J. (1998). The transcription factor HNF3beta is required in visceral endoderm for normal primitive streak morphogenesis. Development *125*, 3015-3025.

Dunty, W.C., Jr., Biris, K.K., Chalamalasetty, R.B., Taketo, M.M., Lewandoski, M., and Yamaguchi, T.P. (2008). Wnt3a/beta-catenin signaling controls posterior body development by coordinating mesoderm formation and segmentation. Development *135*, 85-94.

Dunwoodie, S.L., Clements, M., Sparrow, D.B., Sa, X., Conlon, R.A., and Beddington, R.S. (2002). Axial skeletal defects caused by mutation in the spondylocostal dysplasia/pudgy gene Dll3 are associated with disruption of the segmentation clock within the presomitic mesoderm. Development *129*, 1795-1806.

Durmus, T., LeClair, R.J., Park, K.S., Terzic, A., Yoon, J.K., and Lindner, V. (2006). Expression analysis of the novel gene collagen triple helix repeat containing-1 (Cthrc1). Gene expression patterns : GEP *6*, 935-940.

Durston, A.J., Jansen, H.J., In der Rieden, P., and Hooiveld, M.H. (2011). Hox collinearity - a new perspective. The International journal of developmental biology *55*, 899-908.

Economides, K.D., Zeltser, L., and Capecchi, M.R. (2003). Hoxb13 mutations cause overgrowth of caudal spinal cord and tail vertebrae. Developmental biology *256*, 317-330.

Ericson, J., Rashbass, P., Schedl, A., Brenner-Morton, S., Kawakami, A., van Heyningen, V., Jessell, T.M., and Briscoe, J. (1997). Pax6 controls progenitor cell identity and neuronal fate in response to graded Shh signaling. Cell *90*, 169-180.

Evrard, Y.A., Lun, Y., Aulehla, A., Gan, L., and Johnson, R.L. (1998). lunatic fringe is an essential mediator of somite segmentation and patterning. Nature *394*, 377-381.

Feil, S., Valtcheva, N., and Feil, R. (2009). Inducible Cre mice. Methods in molecular biology *530*, 343-363.

Feldman, B., Poueymirou, W., Papaioannou, V.E., DeChiara, T.M., and Goldfarb, M. (1995). Requirement of FGF-4 for postimplantation mouse development. Science *267*, 246-249.

Ferrer-Vaquer, A., Piliszek, A., Tian, G., Aho, R.J., Dufort, D., and Hadjantonakis, A.K. (2010). A sensitive and bright single-cell resolution live imaging reporter of Wnt/ss-catenin signaling in the mouse. BMC developmental biology *10*, 121.

Ferri, A.L., Cavallaro, M., Braida, D., Di Cristofano, A., Canta, A., Vezzani, A., Ottolenghi, S., Pandolfi, P.P., Sala, M., DeBiasi, S*., et al.* (2004). Sox2 deficiency causes neurodegeneration and impaired neurogenesis in the adult mouse brain. Development *131*, 3805-3819.

Forlani, S., Lawson, K.A., and Deschamps, J. (2003). Acquisition of Hox codes during gastrulation and axial elongation in the mouse embryo. Development *130*, 3807-3819.

Fromental-Ramain, C., Warot, X., Messadecq, N., LeMeur, M., Dolle, P., and Chambon, P. (1996). Hoxa-13 and Hoxd-13 play a crucial role in the patterning of the limb autopod. Development *122*, 2997-3011.

Galceran, J., Farinas, I., Depew, M.J., Clevers, H., and Grosschedl, R. (1999). Wnt3a-/--like phenotype and limb deficiency in Lef1(-/-)Tcf1(-/-) mice. Genes & development *13*, 709-717.

Galceran, J., Hsu, S.C., and Grosschedl, R. (2001). Rescue of a Wnt mutation by an activated form of LEF-1: regulation of maintenance but not initiation of Brachyury expression. Proceedings of the National Academy of Sciences of the United States of America *98*, 8668-8673.

Garcia-Martinez, V., Alvarez, I.S., and Schoenwolf, G.C. (1993). Locations of the ectodermal and nonectodermal subdivisions of the epiblast at stages 3 and 4 of avian gastrulation and neurulation. The Journal of experimental zoology *267*, 431-446.

Garcia-Martinez, V., and Schoenwolf, G.C. (1992). Positional control of mesoderm movement and fate during avian gastrulation and neurulation. Developmental dynamics : an official publication of the American Association of Anatomists *193*, 249-256.

Gardner, R.L. (1998). Contributions of blastocyst micromanipulation to the study of mammalian development. BioEssays : news and reviews in molecular, cellular and developmental biology *20*, 168-180.

Gilchrist, D.S., Ure, J., Hook, L., and Medvinsky, A. (2003). Labeling of hematopoietic stem and progenitor cells in novel activatable EGFP reporter mice. Genesis *36*, 168-176.

Ginsburg, M., Snow, M.H., and McLaren, A. (1990). Primordial germ cells in the mouse embryo during gastrulation. Development *110*, 521-528.

Godwin, A.R., and Capecchi, M.R. (1998). Hoxc13 mutant mice lack external hair. Genes & development *12*, 11-20.

Gofflot, F., Hall, M., and Morriss-Kay, G.M. (1997). Genetic patterning of the developing mouse tail at the time of posterior neuropore closure. Developmental dynamics : an official publication of the American Association of Anatomists *210*, 431-445.

Gomez-Lopez, S., Wiskow, O., Favaro, R., Nicolis, S.K., Price, D.J., Pollard, S.M., and Smith, A. (2011). Sox2 and Pax6 maintain the proliferative and developmental potential of gliogenic neural stem cells In vitro. Glia *59*, 1588-1599.

Gomez, C., Ozbudak, E.M., Wunderlich, J., Baumann, D., Lewis, J., and Pourquie, O. (2008). Control of segment number in vertebrate embryos. Nature *454*, 335-339.

Goulding, M., Lumsden, A., and Paquette, A.J. (1994). Regulation of Pax-3 expression in the dermomyotome and its role in muscle development. Development *120*, 957-971.

Gouti, M., Tsakiridis, A., Wymeersch, F.J., Huang, Y., Kleinjung, J., Wilson, V., and Briscoe, J. (2014). In vitro generation of neuromesodermal progenitors reveals distinct roles for wnt signalling in the specification of spinal cord and paraxial mesoderm identity. PLoS biology *12*, e1001937.

Gray, S.D., and Dale, J.K. (2010). Notch signalling regulates the contribution of progenitor cells from the chick Hensen's node to the floor plate and notochord. Development *137*, 561-568.

Greco, T.L., Takada, S., Newhouse, M.M., McMahon, J.A., McMahon, A.P., and Camper, S.A. (1996). Analysis of the vestigial tail mutation demonstrates that Wnt-3a gene dosage regulates mouse axial development. Genes & development *10*, 313-324.

Gulacsi, A.A., and Anderson, S.A. (2008). Beta-catenin-mediated Wnt signaling regulates neurogenesis in the ventral telencephalon. Nature neuroscience *11*, 1383-1391.

Guo, G., Yang, J., Nichols, J., Hall, J.S., Eyres, I., Mansfield, W., and Smith, A. (2009). Klf4 reverts developmentally programmed restriction of ground state pluripotency. Development *136*, 1063-1069.

Haegel, H., Larue, L., Ohsugi, M., Fedorov, L., Herrenknecht, K., and Kemler, R. (1995). Lack of beta-catenin affects mouse development at gastrulation. Development *121*, 3529-3537.

Hamburger, V., and Hamilton, H.L. (1951). A series of normal stages in the development of the chick embryo. Journal of morphology *88*, 49-92.

Han, D.W., Tapia, N., Joo, J.Y., Greber, B., Arauzo-Bravo, M.J., Bernemann, C., Ko, K., Wu, G., Stehling, M., Do, J.T*., et al.* (2010). Epiblast stem cell subpopulations represent mouse embryos of distinct pregastrulation stages. Cell *143*, 617-627.

Hart, A.H., Hartley, L., Ibrahim, M., and Robb, L. (2004). Identification, cloning and expression analysis of the pluripotency promoting Nanog genes in mouse and human. Developmental dynamics : an official publication of the American Association of Anatomists *230*, 187-198.

Hayashi, K., and Surani, M.A. (2009). Self-renewing epiblast stem cells exhibit continual delineation of germ cells with epigenetic reprogramming in vitro. Development *136*, 3549-3556.

Hebert, J.M., Boyle, M., and Martin, G.R. (1991). mRNA localization studies suggest that murine FGF-5 plays a role in gastrulation. Development *112*, 407-415.

Hellstrom, M., Kalen, M., Lindahl, P., Abramsson, A., and Betsholtz, C. (1999). Role of PDGF-B and PDGFR-beta in recruitment of vascular smooth muscle cells and pericytes during embryonic blood vessel formation in the mouse. Development *126*, 3047-3055.

Henrique, D., Adam, J., Myat, A., Chitnis, A., Lewis, J., and Ish-Horowicz, D. (1995). Expression of a Delta homologue in prospective neurons in the chick. Nature *375*, 787-790.

Herrmann, B.G. (1991). Expression pattern of the Brachyury gene in whole-mount TWis/TWis mutant embryos. Development *113*, 913-917.

Hirata, M., and Hall, B.K. (2000). Temporospatial patterns of apoptosis in chick embryos during the morphogenetic period of development. The International journal of developmental biology *44*, 757-768.

Holowacz, T., Huelsken, J., Dufort, D., and van der Kooy, D. (2011). Neural stem cells are increased after loss of beta-catenin, but neural progenitors undergo cell death. The European journal of neuroscience *33*, 1366-1375.

Huang, Y., Osorno, R., Tsakiridis, A., and Wilson, V. (2012). In Vivo differentiation potential of epiblast stem cells revealed by chimeric embryo formation. Cell reports *2*, 1571-1578.

Huelsken, J., Vogel, R., Brinkmann, V., Erdmann, B., Birchmeier, C., and Birchmeier, W. (2000). Requirement for beta-catenin in anterior-posterior axis formation in mice. The Journal of cell biology *148*, 567-578.

Inman, K.E., and Downs, K.M. (2006). Localization of Brachyury (T) in embryonic and extraembryonic tissues during mouse gastrulation. Gene expression patterns : GEP *6*, 783-793.

Itoh, N., and Ornitz, D.M. (2008). Functional evolutionary history of the mouse Fgf gene family. Developmental dynamics : an official publication of the American Association of Anatomists *237*, 18-27.

Iulianella, A., Beckett, B., Petkovich, M., and Lohnes, D. (1999). A molecular basis for retinoic acid-induced axial truncation. Developmental biology *205*, 33-48.

Iwafuchi-Doi, M., Matsuda, K., Murakami, K., Niwa, H., Tesar, P.J., Aruga, J., Matsuo, I., and Kondoh, H. (2012). Transcriptional regulatory networks in epiblast cells and during anterior neural plate development as modeled in epiblast stem cells. Development *139*, 3926-3937.

Jakuba, C. (2013). Deconstruction of the Presomitic Mesoderm Progenitor Niche through Single-cell Analysis. Doctoral Dissertation University of Connecticut.

Junghans, D., Hack, I., Frotscher, M., Taylor, V., and Kemler, R. (2005). Beta-catenin-mediated cell-adhesion is vital for embryonic forebrain development. Developmental dynamics : an official publication of the American Association of Anatomists *233*, 528-539.

Jurand, A. (1974). Some aspects of the development of the notochord in mouse embryos. Journal of embryology and experimental morphology *32*, 1-33.

Jurberg, A.D., Aires, R., Novoa, A., Rowland, J.E., and Mallo, M. (2014). Compartment-dependent activities of Wnt3a/beta-catenin signaling during vertebrate axial extension. Developmental biology *394*, 253-263.

Kang, M., Piliszek, A., Artus, J., and Hadjantonakis, A.K. (2013). FGF4 is required for lineage restriction and salt-and-pepper distribution of primitive endoderm factors but not their initial expression in the mouse. Development *140*, 267-279.

Kemp, C., Willems, E., Abdo, S., Lambiv, L., and Leyns, L. (2005). Expression of all Wnt genes and their secreted antagonists during mouse blastocyst and postimplantation development. Developmental dynamics : an official publication of the American Association of Anatomists *233*, 1064-1075.

Kinder, S.J., Tsang, T.E., Quinlan, G.A., Hadjantonakis, A.K., Nagy, A., and Tam, P.P. (1999). The orderly allocation of mesodermal cells to the extraembryonic structures and the anteroposterior axis during gastrulation of the mouse embryo. Development *126*, 4691-4701.

Kojima, Y., Kaufman-Francis, K., Studdert, J.B., Steiner, K.A., Power, M.D., Loebel, D.A., Jones, V., Hor, A., de Alencastro, G., Logan, G.J*., et al.* (2014). The transcriptional and functional properties of mouse epiblast stem cells resemble the anterior primitive streak. Cell stem cell *14*, 107-120.

Kokubu, C., Heinzmann, U., Kokubu, T., Sakai, N., Kubota, T., Kawai, M., Wahl, M.B., Galceran, J., Grosschedl, R., Ozono, K*., et al.* (2004). Skeletal defects in ringelschwanz mutant mice reveal that Lrp6 is required for proper somitogenesis and osteogenesis. Development *131*, 5469-5480.

Kondoh, H., and Kamachi, Y. (2010). SOX-partner code for cell specification: Regulatory target selection and underlying molecular mechanisms. The international journal of biochemistry & cell biology *42*, 391-399.

Kopan, R., and Ilagan, M.X. (2009). The canonical Notch signaling pathway: unfolding the activation mechanism. Cell *137*, 216-233.

Kuhn, R., and Torres, R.M. (2002). Cre/loxP recombination system and gene targeting. Methods in molecular biology *180*, 175-204.

Lander, A.D., Gokoffski, K.K., Wan, F.Y., Nie, Q., and Calof, A.L. (2009). Cell lineages and the logic of proliferative control. PLoS biology *7*, e15.

Lawson, K.A., Meneses, J.J., and Pedersen, R.A. (1991). Clonal analysis of epiblast fate during germ layer formation in the mouse embryo. Development *113*, 891-911.

Lele, Z., Folchert, A., Concha, M., Rauch, G.J., Geisler, R., Rosa, F., Wilson, S.W., Hammerschmidt, M., and Bally-Cuif, L. (2002). parachute/n-cadherin is required for morphogenesis and maintained integrity of the zebrafish neural tube. Development *129*, 3281-3294.

Lewis, J., Hanisch, A., and Holder, M. (2009). Notch signaling, the segmentation clock, and the patterning of vertebrate somites. Journal of biology *8*, 44.

Li, J.Y., and Joyner, A.L. (2001). Otx2 and Gbx2 are required for refinement and not induction of mid-hindbrain gene expression. Development *128*, 4979-4991.

Lints, T.J., Parsons, L.M., Hartley, L., Lyons, I., and Harvey, R.P. (1993). Nkx-2.5: a novel murine homeobox gene expressed in early heart progenitor cells and their myogenic descendants. Development *119*, 419-431.

Liu, P., Wakamiya, M., Shea, M.J., Albrecht, U., Behringer, R.R., and Bradley, A. (1999). Requirement for Wnt3 in vertebrate axis formation. Nature genetics *22*, 361-365.

Logan, C.Y., and Nusse, R. (2004). The Wnt signaling pathway in development and disease. Annual review of cell and developmental biology *20*, 781-810.

Lowell, S., Jones, P., Le Roux, I., Dunne, J., and Watt, F.M. (2000). Stimulation of human epidermal differentiation by delta-notch signalling at the boundaries of stem-cell clusters. Current biology : CB *10*, 491-500.

Lu, C.C., Brennan, J., and Robertson, E.J. (2001). From fertilization to gastrulation: axis formation in the mouse embryo. Current opinion in genetics & development *11*, 384-392.

MacDonald, B.T., Tamai, K., and He, X. (2009). Wnt/beta-catenin signaling: components, mechanisms, and diseases. Developmental cell *17*, 9-26.

Machon, O., van den Bout, C.J., Backman, M., Kemler, R., and Krauss, S. (2003). Role of beta-catenin in the developing cortical and hippocampal neuroepithelium. Neuroscience *122*, 129-143.

Magli, A., Schnettler, E., Rinaldi, F., Bremer, P., and Perlingeiro, R.C. (2013). Functional dissection of Pax3 in paraxial mesoderm development and myogenesis. Stem cells *31*, 59-70.

Malaguti, M., Nistor, P.A., Blin, G., Pegg, A., Zhou, X., and Lowell, S. (2013). Bone morphogenic protein signalling suppresses differentiation of pluripotent cells by maintaining expression of E-Cadherin. eLife *2*, e01197.

Mallo, M., Wellik, D.M., and Deschamps, J. (2010). Hox genes and regional patterning of the vertebrate body plan. Developmental biology *344*, 7-15.

Maretto, S., Cordenonsi, M., Dupont, S., Braghetta, P., Broccoli, V., Hassan, A.B., Volpin, D., Bressan, G.M., and Piccolo, S. (2003). Mapping Wnt/beta-catenin signaling during mouse development and in colorectal tumors. Proceedings of the National Academy of Sciences of the United States of America *100*, 3299-3304.

Martin, B.L., and Kimelman, D. (2012). Canonical Wnt signaling dynamically controls multiple stem cell fate decisions during vertebrate body formation. Developmental cell *22*, 223-232.

Maruoka, Y., Ohbayashi, N., Hoshikawa, M., Itoh, N., Hogan, B.L., and Furuta, Y. (1998). Comparison of the expression of three highly related genes, Fgf8, Fgf17 and Fgf18, in the mouse embryo. Mechanisms of development *74*, 175-177.

Massa, V., Savery, D., Ybot-Gonzalez, P., Ferraro, E., Rongvaux, A., Cecconi, F., Flavell, R., Greene, N.D., and Copp, A.J. (2009). Apoptosis is not required for mammalian neural tube closure. Proceedings of the National Academy of Sciences of the United States of America *106*, 8233-8238.

McCann, M.R., Tamplin, O.J., Rossant, J., and Seguin, C.A. (2012). Tracing notochord-derived cells using a Noto-cre mouse: implications for intervertebral disc development. Disease models & mechanisms *5*, 73-82.

McGrew, M.J., Sherman, A., Lillico, S.G., Ellard, F.M., Radcliffe, P.A., Gilhooley, H.J., Mitrophanous, K.A., Cambray, N., Wilson, V., and Sang, H. (2008). Localised axial progenitor cell populations in the avian tail bud are not committed to a posterior Hox identity. Development *135*, 2289-2299.

Metzger, D., and Chambon, P. (2001). Site- and time-specific gene targeting in the mouse. Methods *24*, 71-80.

Miki, T., Yasuda, S.Y., and Kahn, M. (2011). Wnt/beta-catenin signaling in embryonic stem cell self-renewal and somatic cell reprogramming. Stem cell reviews *7*, 836-846.

Miller, J.H. (1992). A Short Course in Bacterial Genetics – A Laboratory Manual and Handbook for Escherichia coli and Related Bacteria. Cold Spring Harbor Laboratory Press *ISBN: 0–87969-349–5*.

Miura, S., Davis, S., Klingensmith, J., and Mishina, Y. (2006). BMP signaling in the epiblast is required for proper recruitment of the prospective paraxial mesoderm and development of the somites. Development *133*, 3767-3775.

Mohamed, O.A., Clarke, H.J., and Dufort, D. (2004). Beta-catenin signaling marks the prospective site of primitive streak formation in the mouse embryo. Developmental dynamics : an official publication of the American Association of Anatomists *231*, 416-424.

Nagai, T., Aruga, J., Takada, S., Gunther, T., Sporle, R., Schughart, K., and Mikoshiba, K. (1997). The expression of the mouse Zic1, Zic2, and Zic3 gene suggests an essential role for Zic genes in body pattern formation. Developmental biology *182*, 299-313.

Naiche, L.A., Holder, N., and Lewandoski, M. (2011). FGF4 and FGF8 comprise the wavefront activity that controls somitogenesis. Proceedings of the National Academy of Sciences of the United States of America *108*, 4018-4023.

Najm, F.J., Chenoweth, J.G., Anderson, P.D., Nadeau, J.H., Redline, R.W., McKay, R.D., and Tesar, P.J. (2011). Isolation of epiblast stem cells from preimplantation mouse embryos. Cell stem cell *8*, 318-325.

Nelson, W.J., and Nusse, R. (2004). Convergence of Wnt, beta-catenin, and cadherin pathways. Science *303*, 1483-1487.

Nichols, J., and Smith, A. (2009). Naive and primed pluripotent states. Cell stem cell *4*, 487-492.

Nichols, J., and Smith, A. (2012). Pluripotency in the embryo and in culture. Cold Spring Harbor perspectives in biology *4*, a008128.

Nicolas, J.F., Mathis, L., Bonnerot, C., and Saurin, W. (1996). Evidence in the mouse for self-renewing stem cells in the formation of a segmented longitudinal structure, the myotome. Development *122*, 2933-2946.

Niederreither, K., McCaffery, P., Drager, U.C., Chambon, P., and Dolle, P. (1997). Restricted expression and retinoic acid-induced downregulation of the retinaldehyde dehydrogenase type 2 (RALDH-2) gene during mouse development. Mechanisms of development *62*, 67-78.

Niederreither, K., Vermot, J., Schuhbaur, B., Chambon, P., and Dolle, P. (2000). Retinoic acid synthesis and hindbrain patterning in the mouse embryo. Development *127*, 75-85.

Nieuwkoop, P.D., Johnen, A.G., and Albers, B. (1985). The epigenetic nature of early chordate development : inductive interaction and competence (Cambridge Cambridgeshire ; New York: Cambridge University Press).

Niswander, L., and Martin, G.R. (1992). Fgf-4 expression during gastrulation, myogenesis, limb and tooth development in the mouse. Development *114*, 755-768.

Norris, D.P., Brennan, J., Bikoff, E.K., and Robertson, E.J. (2002). The Foxh1-dependent autoregulatory enhancer controls the level of Nodal signals in the mouse embryo. Development *129*, 3455-3468.

Nostro, M.C., Cheng, X., Keller, G.M., and Gadue, P. (2008). Wnt, activin, and BMP signaling regulate distinct stages in the developmental pathway from embryonic stem cells to blood. Cell stem cell *2*, 60-71.

Ohinata, Y., Payer, B., O'Carroll, D., Ancelin, K., Ono, Y., Sano, M., Barton, S.C., Obukhanych, T., Nussenzweig, M., Tarakhovsky, A.*, et al.* (2005). Blimp1 is a critical determinant of the germ cell lineage in mice. Nature *436*, 207-213.

Ohtsuka, S., Nishikawa-Torikai, S., and Niwa, H. (2012). E-cadherin promotes incorporation of mouse epiblast stem cells into normal development. PloS one *7*, e45220.

Oka, C., Nakano, T., Wakeham, A., de la Pompa, J.L., Mori, C., Sakai, T., Okazaki, S., Kawaichi, M., Shiota, K., Mak, T.W.*, et al.* (1995). Disruption of the mouse RBP-J kappa gene results in early embryonic death. Development *121*, 3291-3301.

Olivera-Martinez, I., Harada, H., Halley, P.A., and Storey, K.G. (2012). Loss of FGF-dependent mesoderm identity and rise of endogenous retinoid signalling determine cessation of body axis elongation. PLoS biology *10*, e1001415.

Olivera-Martinez, I., and Storey, K.G. (2007). Wnt signals provide a timing mechanism for the FGF-retinoid differentiation switch during vertebrate body axis extension. Development *134*, 2125-2135.

Orsulic, S., Huber, O., Aberle, H., Arnold, S., and Kemler, R. (1999). E-cadherin binding prevents beta-catenin nuclear localization and beta-catenin/LEF-1-mediated transactivation. Journal of cell science *112 (Pt 8)*, 1237-1245.

Osorno, R., and Chambers, I. (2011). Transcription factor heterogeneity and epiblast pluripotency. Philosophical transactions of the Royal Society of London Series B, Biological sciences *366*, 2230-2237.

Osorno, R., Tsakiridis, A., Wong, F., Cambray, N., Economou, C., Wilkie, R., Blin, G., Scotting, P.J., Chambers, I., and Wilson, V. (2012). The developmental dismantling of pluripotency is reversed by ectopic Oct4 expression. Development *139*, 2288-2298.

Parr, B.A., Shea, M.J., Vassileva, G., and McMahon, A.P. (1993). Mouse Wnt genes exhibit discrete domains of expression in the early embryonic CNS and limb buds. Development *119*, 247-261.

Perantoni, A.O., Timofeeva, O., Naillat, F., Richman, C., Pajni-Underwood, S., Wilson, C., Vainio, S., Dove, L.F., and Lewandoski, M. (2005). Inactivation of FGF8 in early mesoderm reveals an essential role in kidney development. Development *132*, 3859-3871.

Perea-Gomez, A., Shawlot, W., Sasaki, H., Behringer, R.R., and Ang, S. (1999). HNF3beta and Lim1 interact in the visceral endoderm to regulate primitive streak formation and anterior-posterior polarity in the mouse embryo. Development *126*, 4499-4511.

Petinari, L., Kohn, L.K., de Carvalho, J.E., and Genari, S.C. (2004). Cytotoxicity of tamoxifen in normal and tumoral cell lines and its ability to induce cellular transformation in vitro. Cell biology international *28*, 531-539.

Petit, A.C., Legue, E., and Nicolas, J.F. (2005). Methods in clonal analysis and applications. Reproduction, nutrition, development *45*, 321-339.

Pfister, S., Steiner, K.A., and Tam, P.P. (2007). Gene expression pattern and progression of embryogenesis in the immediate post-implantation period of mouse development. Gene expression patterns : GEP *7*, 558-573.

Poelmann, R.E. (1981). The head-process and the formation of the definitive endoderm in the mouse embryo. Anatomy and embryology *162*, 41-49.

Popperl, H., Schmidt, C., Wilson, V., Hume, C.R., Dodd, J., Krumlauf, R., and Beddington, R.S. (1997). Misexpression of Cwnt8C in the mouse induces an ectopic embryonic axis and causes a truncation of the anterior neuroectoderm. Development *124*, 2997-3005.

Pourquie, O. (2011). Vertebrate segmentation: from cyclic gene networks to scoliosis. Cell *145*, 650-663.

Psychoyos, D., and Stern, C.D. (1996). Restoration of the organizer after radical ablation of Hensen's node and the anterior primitive streak in the chick embryo. Development *122*, 3263-3273.

Qian, L., Mahaffey, J.P., Alcorn, H.L., and Anderson, K.V. (2011). Tissue-specific roles of Axin2 in the inhibition and activation of Wnt signaling in the mouse embryo. Proceedings of the National Academy of Sciences of the United States of America *108*, 8692-8697.

Raghoebir, L., Bakker, E.R., Mills, J.C., Swagemakers, S., Kempen, M.B., Munck, A.B., Driegen, S., Meijer, D., Grosveld, F., Tibboel, D*., et al.* (2012). SOX2 redirects the developmental fate of the intestinal epithelium toward a premature gastric phenotype. Journal of molecular cell biology *4*, 377-385.

Rashbass, P., Wilson, V., Rosen, B., and Beddington, R.S. (1994). Alterations in gene expression during mesoderm formation and axial patterning in Brachyury (T) embryos. The International journal of developmental biology *38*, 35-44.

Rast, J.P., Cameron, R.A., Poustka, A.J., and Davidson, E.H. (2002). brachyury Target genes in the early sea urchin embryo isolated by differential macroarray screening. Developmental biology *246*, 191-208.

Reaume, A.G., Conlon, R.A., Zirngibl, R., Yamaguchi, T.P., and Rossant, J. (1992). Expression analysis of a Notch homologue in the mouse embryo. Developmental biology *154*, 377-387.

Ribes, V., Le Roux, I., Rhinn, M., Schuhbaur, B., and Dolle, P. (2009). Early mouse caudal development relies on crosstalk between retinoic acid, Shh and Fgf signalling pathways. Development *136*, 665-676.

Richardson, M.K., Allen, S.P., Wright, G.M., Raynaud, A., and Hanken, J. (1998). Somite number and vertebrate evolution. Development *125*, 151-160.

Roelink, H., and Nusse, R. (1991). Expression of two members of the Wnt family during mouse development--restricted temporal and spatial patterns in the developing neural tube. Genes & development *5*, 381-388.

Roszko, I., Faure, P., and Mathis, L. (2007). Stem cell growth becomes predominant while neural plate progenitor pool decreases during spinal cord elongation. Developmental biology *304*, 232-245.

Rudloff, S., and Kemler, R. (2012). Differential requirements for beta-catenin during mouse development. Development *139*, 3711-3721.

Ruiz i Altaba, A., Prezioso, V.R., Darnell, J.E., and Jessell, T.M. (1993). Sequential expression of HNF-3 beta and HNF-3 alpha by embryonic organizing centers: the dorsal lip/node, notochord and floor plate. Mechanisms of development *44*, 91-108.

Saitou, M., Barton, S.C., and Surani, M.A. (2002). A molecular programme for the specification of germ cell fate in mice. Nature *418*, 293-300.

Sasaki, H., and Hogan, B.L. (1993). Differential expression of multiple fork head related genes during gastrulation and axial pattern formation in the mouse embryo. Development *118*, 47-59.

Sefton, M., Sanchez, S., and Nieto, M.A. (1998). Conserved and divergent roles for members of the Snail family of transcription factors in the chick and mouse embryo. Development *125*, 3111-3121.

Selleck, M.A., and Stern, C.D. (1991). Fate mapping and cell lineage analysis of Hensen's node in the chick embryo. Development *112*, 615-626.

Shawlot, W., and Behringer, R.R. (1995). Requirement for Lim1 in head-organizer function. Nature *374*, 425-430.

Shimizu, T., Bae, Y.K., Muraoka, O., and Hibi, M. (2005). Interaction of Wnt and caudal-related genes in zebrafish posterior body formation. Developmental biology *279*, 125-141.

Shum, A.S., Poon, L.L., Tang, W.W., Koide, T., Chan, B.W., Leung, Y.C., Shiroishi, T., and Copp, A.J. (1999). Retinoic acid induces down-regulation of Wnt-3a, apoptosis and diversion of tail bud cells to a neural fate in the mouse embryo. Mechanisms of development *84*, 17-30.

Silva, J., Nichols, J., Theunissen, T.W., Guo, G., van Oosten, A.L., Barrandon, O., Wray, J., Yamanaka, S., Chambers, I., and Smith, A. (2009). Nanog is the gateway to the pluripotent ground state. Cell *138*, 722-737.

Sirbu, I.O., and Duester, G. (2006). Retinoic-acid signalling in node ectoderm and posterior neural plate directs left-right patterning of somitic mesoderm. Nature cell biology *8*, 271-277.

Slusarski, D.C., Corces, V.G., and Moon, R.T. (1997). Interaction of Wnt and a Frizzled homologue triggers G-protein-linked phosphatidylinositol signalling. Nature *390*, 410-413.

Spemann, H., and Mangold, H. (1924). Induction of embryonic primordia by implantation of organizers from a different species. 1923. The International journal of developmental biology *45*, 13-38.

Stern, C.D. (2004). Gastrulation: From Cells to Embryo. Cold Spring Harbor Laboratory Press *42*, 1251-1251.

Stern, M.A.J.S.a.C.D. (1992). Commitment of mesoderm cells in Hensen's node of the chick embryo to notochord and somite. Development *114*, 403-415.

Sulik, K., Dehart, D.B., Iangaki, T., Carson, J.L., Vrablic, T., Gesteland, K., and Schoenwolf, G.C. (1994). Morphogenesis of the murine node and notochordal plate. Developmental dynamics : an official publication of the American Association of Anatomists *201*, 260-278.

Sumi, T., Oki, S., Kitajima, K., and Meno, C. (2013). Epiblast ground state is controlled by canonical Wnt/beta-catenin signaling in the postimplantation mouse embryo and epiblast stem cells. PloS one *8*, e63378.

Sun, X., Meyers, E.N., Lewandoski, M., and Martin, G.R. (1999). Targeted disruption of Fgf8 causes failure of cell migration in the gastrulating mouse embryo. Genes & development *13*, 1834-1846.

Szeto, D.P., and Kimelman, D. (2004). Combinatorial gene regulation by Bmp and Wnt in zebrafish posterior mesoderm formation. Development *131*, 3751-3760.

Takada, S., Stark, K.L., Shea, M.J., Vassileva, G., McMahon, J.A., and McMahon, A.P. (1994). Wnt-3a regulates somite and tailbud formation in the mouse embryo. Genes & development *8*, 174-189.

Takashima, Y., Guo, G., Loos, R., Nichols, J., Ficz, G., Krueger, F., Oxley, D., Santos, F., Clarke, J., Mansfield, W*., et al.* (2014). Resetting transcription factor control circuitry toward ground-state pluripotency in human. Cell *158*, 1254-1269.

Takemoto, T., Uchikawa, M., Yoshida, M., Bell, D.M., Lovell-Badge, R., Papaioannou, V.E., and Kondoh, H. (2011). Tbx6-dependent Sox2 regulation determines neural or mesodermal fate in axial stem cells. Nature *470*, 394-398.

Tam, P.P. (1986). A study of the pattern of prospective somites in the presomitic mesoderm of mouse embryos. Journal of embryology and experimental morphology *92*, 269-285.

Tam, P.P. (1988). The allocation of cells in the presomitic mesoderm during somite segmentation in the mouse embryo. Development *103*, 379-390.

Tam, P.P. (1989). Regionalisation of the mouse embryonic ectoderm: allocation of prospective ectodermal tissues during gastrulation. Development *107*, 55-67.

Tam, P.P., and Beddington, R.S. (1987). The formation of mesodermal tissues in the mouse embryo during gastrulation and early organogenesis. Development *99*, 109-126.

Tam, P.P., and Behringer, R.R. (1997). Mouse gastrulation: the formation of a mammalian body plan. Mechanisms of development *68*, 3-25.

Tam, P.P., and Tan, S.S. (1992). The somitogenetic potential of cells in the primitive streak and the tail bud of the organogenesis-stage mouse embryo. Development *115*, 703-715.

Tenin, G., Wright, D., Ferjentsik, Z., Bone, R., McGrew, M.J., and Maroto, M. (2010). The chick somitogenesis oscillator is arrested before all paraxial mesoderm is segmented into somites. BMC developmental biology *10*, 24.

Teo, A.K., Arnold, S.J., Trotter, M.W., Brown, S., Ang, L.T., Chng, Z., Robertson, E.J., Dunn, N.R., and Vallier, L. (2011). Pluripotency factors regulate definitive endoderm specification through eomesodermin. Genes & development *25*, 238-250.

Tesar, P.J., Chenoweth, J.G., Brook, F.A., Davies, T.J., Evans, E.P., Mack, D.L., Gardner, R.L., and McKay, R.D. (2007). New cell lines from mouse epiblast share defining features with human embryonic stem cells. Nature *448*, 196-199.

Thomson, J.A., Itskovitz-Eldor, J., Shapiro, S.S., Waknitz, M.A., Swiergiel, J.J., Marshall, V.S., and Jones, J.M. (1998). Embryonic stem cell lines derived from human blastocysts. Science *282*, 1145-1147.

Tonegawa, A., and Takahashi, Y. (1998). Somitogenesis controlled by Noggin. Developmental biology *202*, 172-182.

Tsakiridis, A., Huang, Y., Blin, G., Skylaki, S., Wymeersch, F., Osorno, R., Economou, C., Karagianni, E., Zhao, S., Lowell, S*., et al.* (2014). Distinct Wnt-driven primitive streak-like populations reflect in vivo lineage precursors. Development *141*, 1209-1221.

Tsukiyama, T., and Ohinata, Y. (2014). A Modified EpiSC Culture Condition Containing a GSK3 Inhibitor Can Support Germline-Competent Pluripotency in Mice. PloS one *9*, e95329.

Tzouanacou, E., Wegener, A., Wymeersch, F.J., Wilson, V., and Nicolas, J.F. (2009). Redefining the progression of lineage segregations during mammalian embryogenesis by clonal analysis. Developmental cell *17*, 365-376.

Uchikawa, M., Yoshida, M., Iwafuchi-Doi, M., Matsuda, K., Ishida, Y., Takemoto, T., and Kondoh, H. (2011). B1 and B2 Sox gene expression during neural plate development in chicken and mouse embryos: universal versus species-dependent features. Development, growth & differentiation *53*, 761-771.

Uetzmann, L., Burtscher, I., and Lickert, H. (2008). A mouse line expressing Foxa2-driven Cre recombinase in node, notochord, floorplate, and endoderm. Genesis *46*, 515-522.

Ukita, K., Hirahara, S., Oshima, N., Imuta, Y., Yoshimoto, A., Jang, C.W., Oginuma, M., Saga, Y., Behringer, R.R., Kondoh, H*., et al.* (2009). Wnt signaling maintains the notochord fate for progenitor cells and supports the posterior extension of the notochord. Mechanisms of development *126*, 791-803.

Valenta, T., Gay, M., Steiner, S., Draganova, K., Zemke, M., Hoffmans, R., Cinelli, P., Aguet, M., Sommer, L., and Basler, K. (2011). Probing transcription-specific outputs of beta-catenin in vivo. Genes & development *25*, 2631-2643.

van Amerongen, R., and Berns, A. (2006). Knockout mouse models to study Wnt signal transduction. Trends in genetics : TIG *22*, 678-689.

van Noort, M., Meeldijk, J., van der Zee, R., Destree, O., and Clevers, H. (2002). Wnt signaling controls the phosphorylation status of beta-catenin. The Journal of biological chemistry *277*, 17901-17905.

Wahl, M.B., Deng, C., Lewandoski, M., and Pourquie, O. (2007). FGF signaling acts upstream of the NOTCH and WNT signaling pathways to control segmentation clock oscillations in mouse somitogenesis. Development *134*, 4033-4041.

Wellik, D.M., and Capecchi, M.R. (2003). Hox10 and Hox11 genes are required to globally pattern the mammalian skeleton. Science *301*, 363-367.

White, P.H., and Chapman, D.L. (2005). Dll1 is a downstream target of Tbx6 in the paraxial mesoderm. Genesis *42*, 193-202.

White, P.H., Farkas, D.R., McFadden, E.E., and Chapman, D.L. (2003). Defective somite patterning in mouse embryos with reduced levels of Tbx6. Development *130*, 1681-1690.

Wilkinson, D.G., Bhatt, S., and Herrmann, B.G. (1990). Expression pattern of the mouse T gene and its role in mesoderm formation. Nature *343*, 657-659.

Wilson, V., and Beddington, R.S. (1996). Cell fate and morphogenetic movement in the late mouse primitive streak. Mechanisms of development *55*, 79-89.

Wilson, V., Manson, L., Skarnes, W.C., and Beddington, R.S. (1995). The T gene is necessary for normal mesodermal morphogenetic cell movements during gastrulation. Development *121*, 877-886.

Wilson, V., Olivera-Martinez, I., and Storey, K.G. (2009). Stem cells, signals and vertebrate body axis extension. Development *136*, 1591-1604.

Winzi, M.K., Hyttel, P., Dale, J.K., and Serup, P. (2011). Isolation and characterization of node/notochord-like cells from mouse embryonic stem cells. Stem cells and development *20*, 1817-1827.

Wood, H.B., and Episkopou, V. (1999). Comparative expression of the mouse Sox1, Sox2 and Sox3 genes from pre-gastrulation to early somite stages. Mechanisms of development *86*, 197-201.

Wymeersch, t.e.o.a.e.i.m.e.J. (2011). Maintenance and Elimination of Long-term Axial Progenitors in Mouse PhD thesis The University of Edinburgh

Yaacob, N.S., and Ismail, N.F. (2014). Comparison of cytotoxicity and genotoxicity of 4-hydroxytamoxifen in combination with Tualang honey in MCF-7 and MCF-10A cells. BMC complementary and alternative medicine *14*, 106.

Yamada, T., Pfaff, S.L., Edlund, T., and Jessell, T.M. (1993). Control of cell pattern in the neural tube: motor neuron induction by diffusible factors from notochord and floor plate. Cell *73*, 673-686.

Yamada, T., Placzek, M., Tanaka, H., Dodd, J., and Jessell, T.M. (1991). Control of cell pattern in the developing nervous system: polarizing activity of the floor plate and notochord. Cell *64*, 635-647.

Yamaguchi, S., Kimura, H., Tada, M., Nakatsuji, N., and Tada, T. (2005). Nanog expression in mouse germ cell development. Gene expression patterns : GEP *5*, 639-646.

Yamaguchi, T.P., Bradley, A., McMahon, A.P., and Jones, S. (1999a). A Wnt5a pathway underlies outgrowth of multiple structures in the vertebrate embryo. Development *126*, 1211-1223.

Yamaguchi, T.P., Conlon, R.A., and Rossant, J. (1992). Expression of the fibroblast growth factor receptor FGFR-1/flg during gastrulation and segmentation in the mouse embryo. Developmental biology *152*, 75-88.

Yamaguchi, T.P., Takada, S., Yoshikawa, Y., Wu, N., and McMahon, A.P. (1999b). T (Brachyury) is a direct target of Wnt3a during paraxial mesoderm specification. Genes & development *13*, 3185-3190.

Yanagisawa, K.O., Fujimoto, H., and Urushihara, H. (1981). Effects of the brachyury (T) mutation on morphogenetic movement in the mouse embryo. Developmental biology *87*, 242-248.

Yanagisawa, K.O., and Kitamura, K. (1975). Effects of the brachyury (T) mutation on mitotic activity in the neural tube. Developmental biology *47*, 433-438.

Yoshida, M., Uchikawa, M., Rizzoti, K., Lovell-Badge, R., Takemoto, T., and Kondoh, H. (2014). Regulation of mesodermal precursor production by low-level expression of B1 Sox genes in the caudal lateral epiblast. Mechanisms of development *132*, 59-68.

Yoshikawa, Y., Fujimori, T., McMahon, A.P., and Takada, S. (1997). Evidence that absence of Wnt-3a signaling promotes neuralization instead of paraxial mesoderm development in the mouse. Developmental biology *183*, 234-242.

Young, T., Rowland, J.E., van de Ven, C., Bialecka, M., Novoa, A., Carapuco, M., van Nes, J., de Graaff, W., Duluc, I., Freund, J.N.*, et al.* (2009). Cdx and Hox genes differentially regulate posterior axial growth in mammalian embryos. Developmental cell *17*, 516-526.

Zakin, L.D., Mazan, S., Maury, M., Martin, N., Guenet, J.L., and Brulet, P. (1998). Structure and expression of Wnt13, a novel mouse Wnt2 related gene. Mechanisms of development *73*, 107-116.

Zechner, D., Fujita, Y., Hulsken, J., Muller, T., Walther, I., Taketo, M.M., Crenshaw, E.B., 3rd, Birchmeier, W., and Birchmeier, C. (2003). beta-Catenin signals regulate cell growth and the balance between progenitor cell expansion and differentiation in the nervous system. Developmental biology *258*, 406-418.

Zwart, R., Broos, L., Grosveld, G., and Meijer, D. (1996). The restricted expression pattern of the POU factor Oct-6 during early development of the mouse nervous system. Mechanisms of development *54*, 185-194.